

**THE PREDICTION OF SEDIMENT DEPOSITION IN
STORAGE CHAMBERS BASED ON LABORATORY
OBSERVATIONS AND NUMERICAL SIMULATION**

Virginia Ruth Stovin

**This thesis is submitted in part fulfilment of the degree of
Doctor of Philosophy in the Faculty of Engineering**

Department of Civil and Structural Engineering

March 1996

DECLARATION

No portion of the work referred to in the thesis has been submitted in support of an application for another degree or qualification of this or any other university or other institute of learning.

The Prediction of Sediment Deposition in Storage Chambers Based on Laboratory Observations and Numerical Simulation

Virginia Ruth Stovin

SUMMARY

Storage chambers are often incorporated into sewerage systems, where they detain flow that would otherwise spill into urban watercourses. They consequently reduce the pollution load discharged. Sediments deposited in such chambers can be problematic, in that they may reduce the hydraulic efficiency of the system. They also represent a store of pollution.

The original aims of the research were to identify and investigate the geometric and hydraulic aspects of storage chamber design which affect sediment deposition, and to suggest appropriate methods for modelling the sedimentation efficiency.

The initial research phase was concerned with the laboratory scale testing of storage chamber efficiency. Efficiency is a measure of the proportion of the incoming sediment load that settles to the chamber bed. The laboratory system included facilities for continuous sediment input and for the continuous *in-situ* measurement of sediment concentration. Efficiency measurements were made for three chambers with different geometries, and at a range of flowrates. The principal control on chamber efficiency was the inlet velocity, while changes to the internal geometric configuration of the chamber had minimal effect.

Laboratory measurements of the velocity distribution in the model chamber were used to demonstrate that the distribution of sediments on the chamber bed was a function of bed shear stresses, which were estimated from velocity profiles.

The second phase of research focused on the use of computational fluid dynamics, in the form of the Fluent software package, to predict both the distribution of sediment and the chamber efficiency. In addition to the bed shear stress model of sediment deposition, particle tracking techniques were implemented. Ten chamber configurations were assessed using these techniques. It was shown that the length to breadth ratio was the most important geometric parameter, but that overall the efficiency was more dependent on inlet velocity than anything else. Further development of the particle tracking technique was strongly recommended.

DEDICATION

**This thesis is dedicated to the memory of Les Musk,
Lecturer in the School of Geography,
The University of Manchester.**

TABLE OF CONTENTS

| | |
|--|---------------|
| 1. INTRODUCTION | 1 |
| 1.1 BACKGROUND..... | 1 |
| 1.1.1 The Historical Development of Urban Drainage Systems..... | 1 |
| 1.1.2 The Use of Storage..... | 5 |
| 1.1.3 Urban Pollution Management (UPM)..... | 9 |
| 1.2 AIMS | 11 |
| 1.3 STRUCTURE OF THE THESIS..... | 12 |
| 2. LITERATURE REVIEW | 14 |
| 2.1 INTRODUCTION | 14 |
| 2.2 STORAGE TANK DESIGN..... | 15 |
| 2.2.1 Storage Tank Configurations | 15 |
| 2.2.2 Overflow Setting | 16 |
| 2.2.3 Sedimentation and Self-cleansing | 22 |
| 2.3 SEDIMENTS IN SEWERAGE SYSTEMS | 26 |
| 2.3.1 Sources of Sewer Sediments | 26 |
| 2.3.2 Characteristics of Sewer Sediments..... | 26 |
| 2.3.3 Simulation of Sewer Sediments..... | 29 |
| 2.4 MODELLING THE PROCESSES..... | 30 |
| 2.4.1 Introduction..... | 30 |
| 2.4.2 Computational Fluid Dynamics (CFD)..... | 30 |
| 2.4.2.1 Basic Equations | 30 |
| 2.4.2.2 Turbulence..... | 32 |
| 2.4.2.3 Numerical Discretization | 35 |
| 2.4.3 Sediment Transport and Deposition | 36 |
| 2.4.3.1 Introduction..... | 36 |
| 2.4.3.2 The Settlement of Particulate Material..... | 36 |
| 2.4.3.3 The Concept of Critical Bed Shear Stress..... | 38 |
| 2.4.3.4 Other Models of Sediment Transport | 40 |
| 2.4.3.5 Cohesive Sediment Transport | 43 |
| 2.4.4 Modelling Storage Tank Efficiency | 44 |
| 2.4.4.1 Introduction..... | 44 |
| 2.4.4.2 Surface Load Clarification Theory for an Ideal Basin..... | 44 |
| 2.4.4.3 Modelling of Storage Chambers in Urban Drainage Quality Models | 47 |
| 2.4.4.4 Empirical Regression Equations for Basin Efficiency..... | 48 |
| 2.4.4.5 Mathematical Modelling of Sediment Behaviour in Storage Tanks | 50 |
| 2.4.4.6 Implications for Storage Chamber Modelling..... | 54 |

| | |
|--|----------------|
| 3. LABORATORY SET-UP | 56 |
| 3.1 INTRODUCTION | 56 |
| 3.2 THE MODEL CHAMBER | 56 |
| 3.2.1 Configuration | 56 |
| 3.2.2 Water Supply System | 58 |
| 3.2.3 The Control Valve | 61 |
| 3.2.4 Outlet Head/Discharge Relationships | 62 |
| 3.3 THE MODEL SEDIMENT | 64 |
| 3.3.1 Physical Properties | 65 |
| 3.3.2 Sediment Scaling | 67 |
| 3.3.3 Sediment Input System | 68 |
| 3.4 VELOCITY MEASUREMENT | 73 |
| 3.4.1 Miniature Propeller | 75 |
| 3.4.2 Laser Doppler Anemometry | 77 |
| 3.5 CONCLUSIONS | 79 |
| 4. STORAGE CHAMBER EFFICIENCY | 81 |
| 4.1 INTRODUCTION | 81 |
| 4.1.1 Definition of Efficiency | 82 |
| 4.2 LABORATORY INVESTIGATIONS OF EFFICIENCY | 82 |
| 4.2.1 Laboratory Test Program | 82 |
| 4.2.2 The Effect of Flow Variables on Chamber Efficiency | 85 |
| 4.2.3 The Effect of Configuration Variables on Chamber Efficiency | 87 |
| 4.2.4 The Distribution of Sediment | 90 |
| 4.2.4.1 The Effect of Flow Pattern on Sediment Distribution | 92 |
| 4.2.5 Review of the Experimental Procedure | 93 |
| 4.2.5.1 Sediment Mixing in the Inlet | 94 |
| 4.2.5.2 Nephelometer Probe Drift | 94 |
| 4.2.5.3 Probe Reading in the Outflow under Conditions of Low Discharge | 95 |
| 4.2.5.4 Test Regime | 96 |
| 4.3 A COMPARISON OF THEORETICAL AND MODELLED EFFICIENCY | 98 |
| 4.3.1 Introduction | 98 |
| 4.3.2 Results of the Comparisons | 98 |
| 4.3.3 Discussion | 100 |
| 4.4 CONCLUSIONS | 103 |
| 5. THE FLOW FIELD AND SEDIMENT DEPOSITION | 104 |
| 5.1 INTRODUCTION | 104 |
| 5.2 ESTABLISHING THE CRITICAL BED SHEAR STRESS FOR DEPOSITION | 104 |

| | |
|--|----------------|
| 5.2.1 Introduction..... | 104 |
| 5.2.2 The Velocity Distribution | 105 |
| 5.2.3 Sediment Transport and Deposition | 107 |
| 5.2.4 Bed Shear Stress Analysis | 108 |
| 5.3 TIME-VARYING FLOW | 110 |
| 5.3.1 The Velocity Distribution | 110 |
| 5.3.2 Sediment Transport and Deposition | 111 |
| 5.3.3 Bed Shear Stress Analysis | 112 |
| 5.3.4 A Model of Sediment Deposition | 118 |
| 5.4 EFFICIENCY PREDICTION FROM BED SHEAR STRESS ANALYSIS..... | 119 |
| 5.5 THE NEAR-BED VELOCITY DISTRIBUTION | 121 |
| 5.6 CONCLUSIONS..... | 127 |
| 6. FLOW SIMULATIONS | 128 |
| 6.1 INTRODUCTION | 128 |
| 6.2 THE Fluent CFD SOFTWARE | 129 |
| 6.3 THE SIMULATIONS | 130 |
| 6.4 ASSESSMENT OF SIMULATION ACCURACY | 136 |
| 6.4.1 Introduction..... | 136 |
| 6.4.2 A Qualitative Assessment of Simulation Accuracy | 136 |
| 6.4.3 A Quantitative Assessment of Simulation Accuracy | 143 |
| 6.5 DISCUSSION | 146 |
| 6.6 CONCLUSIONS | 147 |
| 7. EFFICIENCY PREDICTION USING FLUENT | 148 |
| 7.1 INTRODUCTION | 148 |
| 7.2 EFFICIENCY PREDICTION BASED ON THE BED SHEAR STRESS DISTRIBUTION | 149 |
| 7.2.1 Introduction..... | 149 |
| 7.2.2 Efficiency Prediction | 150 |
| 7.2.3 Summary | 153 |
| 7.3 PARTICLE TRACKING WITH Fluent..... | 154 |
| 7.3.1 Introduction..... | 154 |
| 7.3.2 Particle Tracking Options..... | 155 |
| 7.3.2.1 Injection Location and Particle Size | 155 |
| 7.3.2.2 Particle Boundary Conditions..... | 156 |
| 7.3.2.3 Stochastic Particle Tracking in Turbulent Flows | 157 |
| 7.3.2.4 Solution Parameters..... | 157 |
| 7.3.2.5 Coupled or Uncoupled Calculations | 158 |
| 7.3.2.6 Limitations | 159 |
| 7.3.3 Optimisation of Efficiency Prediction using Particle Tracking | 159 |

| | |
|--|------------|
| 7.3.3.1 Introduction | 159 |
| 7.3.3.2 Physical Properties | 161 |
| 7.3.3.3 The Number of Simulations | 165 |
| 7.3.3.4 Boundary Conditions | 166 |
| 7.3.3.5 Solution Parameters | 170 |
| 7.3.4 Discussion | 172 |
| 7.3.5 Particle Tracking and Sediment Deposit Location | 172 |
| 7.4 CONCLUSIONS | 174 |
| 7.4.1 A Comparison of Techniques | 174 |
| 7.4.2 Summary Points | 175 |
| 8. EFFICIENCY PREDICTION FOR DIFFERENT CHAMBERS | 177 |
| 8.1 INTRODUCTION | 177 |
| 8.2 CONFIGURATION SELECTION | 177 |
| 8.3 DESCRIPTION OF THE SIMULATION RECORD | 179 |
| 8.3.1 Geometry | 179 |
| 8.3.2 Velocity Distribution | 179 |
| 8.3.3 Particle Tracking | 180 |
| 8.3.4 Efficiency | 180 |
| 8.4 ANALYSIS | 201 |
| 8.4.1 Bed Shear Stress | 201 |
| 8.4.1.1 Length to Breadth Ratio | 201 |
| 8.4.1.2 Longitudinal Gradient | 201 |
| 8.4.1.3 Inlet Surgecharge | 203 |
| 8.4.1.4 Benching and DWF | 203 |
| 8.4.2 Particle Tracking | 203 |
| 8.4.2.1 Length to Breadth Ratio | 203 |
| 8.4.2.2 Longitudinal Gradient | 205 |
| 8.4.2.3 Inlet Surgecharge | 205 |
| 8.4.2.4 Benching and DWF | 205 |
| 8.5 REGRESSION ANALYSIS | 205 |
| 8.6 DISCUSSION | 209 |
| 8.7 CONCLUSIONS | 210 |
| 9. CONCLUSIONS, DISCUSSION AND SUGGESTIONS FOR FURTHER WORK | 212 |
| 9.1 INTRODUCTION | 212 |
| 9.2 CONCLUSIONS | 212 |
| 9.3 DISCUSSION | 215 |
| 9.3.1 Efficiency Results | 216 |

| | |
|---|------------|
| 9.3.2 Design for Self-Cleansing Operation..... | 216 |
| 9.4 SUGGESTIONS FOR FURTHER WORK..... | 217 |
| REFERENCES | 219 |
| APPENDIX A THE FLUENT LINE-PRINT FILE | A-1 |
| APPENDIX B VALIDATION OF THE FLUENT FLOW FIELD SIMULATIONS | B-1 |
| APPENDIX C LABORATORY EFFICIENCY TEST DATA | C-1 |

LIST OF FIGURES

| | | |
|--------------------|---|-----------|
| Figure 1.1 | A typical urban drainage system in the UK | 1 |
| Figure 1.2 | The effect of storage volume on CSO operation | 6 |
| Figure 2.1 | Basic design of a rectangular on-line storage tank | 16 |
| Figure 2.2 | Storage in retention tank during design storm | 19 |
| Figure 2.3 | Development of the boundary layer (after Chow, 1959) | 39 |
| Figure 2.4 | Particle trajectories in an ideal rectangular settling basin | 45 |
| Figure 2.5 | Typical settling velocity analysis curve | 46 |
| Figure 3.1 | The laboratory model chamber | 58 |
| Figure 3.2 | Laboratory set-up | 58 |
| Figure 3.3 | Control valve calibration | 61 |
| Figure 3.4 | Head/discharge relationships for the outlet penstock | 63 |
| Figure 3.5 | Particle size analysis | 66 |
| Figure 3.6 | Settling velocity analysis for the olive stone | 66 |
| Figure 3.7 | Settling velocity comparison | 68 |
| Figure 3.8 | Sediment input and measurement system | 69 |
| Figure 3.9 | The ANALITE nephelometer probe | 71 |
| Figure 3.10 | Grid system used for deposit mapping | 73 |
| Figure 3.11 | Definition sketch for the velocity measurements | 74 |
| Figure 3.12 | Current meter positioning structure | 75 |
| Figure 3.13 | Laser traverse range | 79 |
| Figure 4.1 | Efficiency test regime | 83 |
| Figure 4.2 | Turbidity at the inflow and outflow to the storage chamber | 84 |
| Figure 4.3 | The effect of different flow variables on efficiency | 86 |
| Figure 4.4 | Mean efficiency plots for the storage chambers | 89 |
| Figure 4.5 | Individual efficiency plots for the storage chambers | 90 |
| Figure 4.6 | Sediment distribution on the chamber bed following efficiency tests | 91 |
| Figure 4.7 | Sketch of sediment deposition and flow pattern for the basic chamber at a mean inlet velocity of 0.36 m/s | 92 |
| Figure 4.8 | Sketch of sediment deposition and flow pattern for the chamber with increased length to breadth ratio at a mean inlet velocity of 0.32 m/s | 93 |
| Figure 4.9 | Example turbidity trace | 94 |
| Figure 4.10 | Example turbidity trace | 95 |

| | | |
|-------------|--|-----|
| Figure 4.11 | Example turbidity trace | 96 |
| Figure 5.1 | Steady flow velocity distribution at 0.08 m depth | 106 |
| Figure 5.2 | Bed shear stress distribution, steady flowrate = 15.9 l/s | 109 |
| Figure 5.3 | Time-varying inflow hydrographs | 110 |
| Figure 5.4 | Calculated bed shear stress distribution after 2 minutes of the time-varying inflow hydrograph, HYDRO1 | 113 |
| Figure 5.5 | Calculated bed shear stress distribution after 4 minutes of the time-varying inflow hydrograph, HYDRO1 | 114 |
| Figure 5.6 | Calculated bed shear stress distribution after 6 minutes of the time-varying inflow hydrograph, HYDRO1 | 115 |
| Figure 5.7 | Calculated bed shear stress distribution after 8 minutes of the time-varying inflow hydrograph, HYDRO1 | 116 |
| Figure 5.8 | Calculated bed shear stress distribution after 20 minutes of the time-varying inflow hydrograph, HYDRO1 | 117 |
| Figure 5.9 | Predicted sediment deposition based on calculated shear stress | 119 |
| Figure 5.10 | The relationship between bed sediment coverage and efficiency | 120 |
| Figure 5.11 | Near bed velocity profiles for the slice $Z = 0.875$ m | 123 |
| Figure 5.12 | Near bed velocity profiles for the slice $Z = 0.486$ m | 124 |
| Figure 5.13 | Near bed velocity profiles | 126 |
| Figure 6.1 | FLUENT simulation geometry | 131 |
| Figure 6.2 | Computational grid mapping at the chamber inlet | 132 |
| Figure 6.3 | Initial simulation results for SIM1 | 134 |
| Figure 6.4 | u -velocity contours for SIM1 | 135 |
| Figure 6.5 | Mid-depth velocity vectors for SIM1 | 135 |
| Figure 6.6 | u -velocity contours for SIM2 | 137 |
| Figure 6.7 | Velocity vectors for SIM2 | 138 |
| Figure 6.8 | An example comparison between measured and simulated velocity (Simulation 1, horizontal slice $Y = 0.08$ m) | 139 |
| Figure 6.9 | An example comparison between measured and simulated velocity (Simulation 1, vertical slice $Z = 0.875$ m) | 139 |
| Figure 6.10 | An example of the directional error contour plots presented in Appendix B | 140 |
| Figure 6.11 | Flow comparison for SIM1 | 142 |
| Figure 6.12 | Flow comparison for SIM2 | 142 |

| | | |
|-------------|--|-----|
| Figure 7.1 | Simulated bed shear stress distribution | 150 |
| Figure 7.2 | Bed shear stress distribution calculated from laboratory measurements | 151 |
| Figure 7.3 | Simulated and measured values for the coverage parameter | 151 |
| Figure 7.4 | Efficiency curve derived from simulated C_{BSS} data | 153 |
| Figure 7.5 | Values of the coverage parameter for different values of τ_{cd} | 153 |
| Figure 7.6 | Rosin-Rammler distribution for 150 μm crushed olive stone | 156 |
| Figure 7.7 | Particle tracking efficiency curve compared with the laboratory data | 160 |
| Figure 7.8 | The effect of density changes | 162 |
| Figure 7.9 | Single diameter distributed input test (Test 1) | 163 |
| Figure 7.10 | Discrete injections with the Rosin-Rammler size distribution (Test 2) | 164 |
| Figure 7.11 | Inlet particle injection distribution | 165 |
| Figure 7.12 | The effect of boundary conditions | 167 |
| Figure 7.13 | The effect of a mixed boundary condition at the bed | 169 |
| Figure 7.14 | The effect of the number of time steps | 170 |
| Figure 7.15 | The effect of the step length factor | 171 |
| Figure 7.16 | The effect of the maximum number of wall reflections | 172 |
| Figure 7.17 | Spatial distribution of sediments from particle tracking | 174 |
| Figure 8.1 | Particle distribution in the inlet, looking downstream | 180 |
| Figure 8.2 | Simulation record for TANK | 181 |
| Figure 8.3 | Simulation record for VLNG | 183 |
| Figure 8.4 | Simulation record for LONG | 185 |
| Figure 8.5 | Simulation record for STUB | 187 |
| Figure 8.6 | Simulation record for BEN1 | 189 |
| Figure 8.7 | Simulation record for BEN2 | 191 |
| Figure 8.8 | Simulation record for LGD1 | 193 |
| Figure 8.9 | Simulation record for LGD2 | 195 |
| Figure 8.10 | Simulation record for SUR1 | 197 |
| Figure 8.11 | Simulation record for SUR2 | 199 |
| Figure 8.12 | Efficiency comparison based on bed shear stress analysis | 202 |
| Figure 8.13 | Efficiency comparison based on particle tracking | 202 |

LIST OF PLATES

| | | |
|-------------------|---|------------|
| Plate 1.1 | CSO discharging into an urban watercourse | 3 |
| Plate 1.2 | Modern CSO with bar screen discharging into an urban watercourse | 3 |
| Plate 1.3 | Typical storage chamber sediment deposits | 8 |
| Plate 1.4 | Sediment deposits on chamber benching | 8 |
| | | |
| Plate 3.1 | The laboratory model storage chamber | 57 |
| Plate 3.2 | The laboratory system | 59 |
| Plate 3.3 | The control valves: main supply valve (orange handle) and computer controlled pneumatic valve (green) | 60 |
| Plate 3.4 | HYDRO4 - the control software | 62 |
| Plate 3.5 | Sediment input system: peristaltic pump (left) and constantly mixed suspended sediment reservoir (right) | 70 |
| Plate 3.6 | Nephelometer turbidity probe located in the invert of the outlet pipe | 72 |
| Plate 3.7 | View inside the inlet pipe, showing the tip of the nephelometer probe and the deflector cap | 72 |
| Plate 3.8 | Grid used for sediment input tests - chamber inlet is on the left | 74 |
| Plate 3.9 | Nixon miniature current propeller and system used for support and alignment | 76 |
| Plate 3.10 | Nixon miniature current propeller with cotton thread used for alignment | 76 |
| Plate 3.11 | LDA system mounted on traverse | 80 |
| Plate 3.12 | LDA system angled at 10° to the horizontal to facilitate near bed measurements | 80 |
| | | |
| Plate 4.1 | The laboratory storage chamber with benching at a gradient of 1 in 4, viewed from the outlet | 88 |
| | | |
| Plate 5.1 | Sediment deposition under steady flow conditions | 108 |
| Plate 5.2 | Sediment deposition after 2 minutes of the time-varying inflow hydrograph, HYDRO1 | 113 |
| Plate 5.3 | Sediment deposition after 4 minutes of the time-varying inflow hydrograph, HYDRO1 | 114 |
| Plate 5.4 | Sediment deposition after 6 minutes of the time-varying inflow hydrograph, HYDRO1 | 115 |
| Plate 5.5 | Sediment deposition after 8 minutes of the time-varying inflow | |

| | |
|---|-----|
| hydrograph, HYDRO1 | 116 |
| Plate 5.6 Sediment deposition after 20 minutes of the time-varying inflow hydrograph, HYDRO1 | 117 |
| Plate 5.7 Sediment deposition following the time-varying inflow hydrograph, HYDRO1 | 120 |

LIST OF TABLES

| | | |
|-----------|--|-----|
| Table 2.1 | SDD (1977) design guidelines for storm overflows | 17 |
| Table 2.2 | Characteristics of Littleborough tank sediments | 28 |
| Table 2.3 | Values of the constants in the k - ε turbulence model (after Launder and Spalding, 1974) | 34 |
| Table 3.1 | Orifice depth and area for selected outflow gate positions | 63 |
| Table 3.2 | Head/discharge relationships for the rectangular tank | 64 |
| Table 3.3 | Physical characteristics of 150 μm olive stone sediment | 65 |
| Table 4.1 | Flowrates used in the efficiency tests (l/s) | 83 |
| Table 4.2 | Values of the response time coefficient m | 85 |
| Table 4.3 | Efficiency results for the basic chamber configuration | 86 |
| Table 4.4 | Efficiency results for two variations to the basic chamber configuration | 88 |
| Table 4.5 | A comparison of measured and modelled efficiencies | 101 |
| Table 6.1 | Flow measurement locations | 138 |
| Table 6.2 | Error statistics for SIM1 | 144 |
| Table 6.3 | Error statistics for SIM2 | 145 |
| Table 7.1 | Particle tracking configurations | 160 |
| Table 7.2 | Particle distribution/input location test details | 163 |
| Table 7.3 | Population statistics for the experimental data | 165 |
| Table 7.4 | Comparison of the bed shear stress and particle tracking techniques for efficiency prediction | 175 |
| Table 8.1 | Configurations details of the simulated chambers | 178 |
| Table 8.2 | Application ranges for efficiency equations | 209 |

ACKNOWLEDGEMENTS

Special gratitude is shown to Professor Adrian Saul, whose interest in the field provided a basis for the research, and whose support and advice have been greatly appreciated throughout its duration. His open-mindedness in accepting a Geography graduate into an Engineering discipline was particularly appreciated. Lastly, the author thanks him for his continuous encouragement to publish and to collaborate with researchers; experience which has been of great benefit in the development of her academic career. The author would also like to thank members of Urban Pollution Management Sediment Working Group for their support and encouragement throughout.

The author is indebted to the laboratory assistance provided by Glenn Brawn and his team of technicians in the Water Engineering laboratory at the University of Sheffield. Their excellent workmanship and imaginative problem solving made the practical phase of this research project a pleasure to undertake. In addition, the author would like to express her thanks for the moral support offered to her by many of the staff and students in the Department of Civil and Structural Engineering.

Thanks are also due to Professor Ian Douglas of the School of Geography at the University of Manchester, for providing invaluable support during the author's first few years of postgraduate research.

The author also extends her thanks to the staff of Fluent Europe, in particular Dr. Ferit Boyson, for their support and advice relating to the use of their software.

The support of the Engineering and Physical Sciences Research Council, in funding the research, is also acknowledged.

Finally, the author would like to express her appreciation to her family, and to her husband John, for their patience and encouragement throughout.

NOTATION

| | |
|---------------------------------------|--|
| A | plan area of settling tank |
| A_f | cross sectional area of flow |
| A_{gr} | value of F_{gr} at threshold of movement |
| A_p | cross sectional area of particle normal to the direction of motion |
| B | chamber breadth |
| b | constant |
| c | concentration of sediment at a point |
| c_1, c_2 | constants |
| c_s | constant |
| c_p | specific heat at constant pressure |
| $c_\mu, c_{1\epsilon}, c_{2\epsilon}$ | constants in the k - ϵ turbulence model |
| C_{BSS} | proportion of the chamber bed covered with sediment (estimated from bed shear stress analysis) |
| C_D | drag coefficient |
| C_{in}, C_{out} | sediment concentration in the inflow, outflow |
| C_l | proportion of the chamber bed covered with sediment (laboratory observation) |
| C_{max} | maximum outflow sediment concentration |
| C_t | sediment concentration at time t |
| C_T | total sediment concentration |
| C_v | volumetric sediment concentration |
| d | particle diameter |
| d_{10}, d_{50}, d_n | 10th, 50th, nth percentile of the particle size distribution |
| D | internal pipe diameter |
| D_{DWF} | diameter of the dry weather flow channel |
| D_{gr} | dimensionless grain size |
| E | industrial discharges |
| E_s | internal energy of a system |
| F_{gr} | sediment mobility number |
| g | acceleration due to gravity |
| G_{gr} | non-dimensional transport parameter |
| H | head (flow depth at orifice) |
| H_a | coefficient in Ackers-White |
| I | constant |
| J | constant |

| | |
|-----------------|---|
| k | turbulent kinetic energy |
| k_1 | constant of thermal conductivity |
| k_2 | constant |
| k_h | constant |
| l | mixing length |
| l_m, l_p | characteristic length in model, prototype |
| L | chamber length |
| m | response time coefficient |
| m_a | coefficient in Ackers-White |
| m_R | dimensionless Reynolds number of the laminar boundary layer |
| M_d | mass fraction of particles with diameter greater than d |
| n | short-circuiting constant |
| n_a | coefficient in Ackers-White |
| n_E | constant |
| n_h | constant |
| n_p | population size |
| n_s | sample size |
| n_{sp} | spread parameter |
| p | fluid pressure |
| P | population |
| q | surface overflow rate |
| Q | flow rate |
| Q_c, Q_{cont} | continuation flow rate |
| Q_s | heat energy entering a system by conduction |
| Q_{in} | inflow rate |
| R | hydraulic radius |
| Re | Reynolds number |
| s | specific gravity of sediment |
| s_f | friction slope |
| S_b | transverse slope (benching gradient) |
| S_e | effluent suspended sediment concentration |
| S_i | influent suspended sediment concentration |
| S_l | longitudinal slope |
| t | time |
| t_r | retention time |
| T | temperature |

| | |
|---|---|
| u_0 | shear velocity |
| \bar{u} | mean inlet velocity |
| u, v, w | velocity components in the x, y and z directions |
| u', v', w' | random fluctuating components of velocity in the x, y and z directions |
| $\bar{u}, \bar{v}, \bar{w}$ | mean velocity in the x, y and z directions |
| u_{sim}, u_m | simulated u -velocity, measured u -velocity |
| v_p | particle velocity |
| V | flow velocity |
| V' | velocity at a point |
| V_c | surface loading rate |
| $V_{cr}S$ | critical unit stream power for incipient motion |
| V_l | particle volume |
| V_p | particle settling velocity |
| V_s | suspension settling velocity |
| VS | unit stream power |
| V_t | threshold velocity |
| W | work done by a fluid |
| W_e | effective width of sediment bed |
| x, X | position in the x (streamwise) direction |
| \bar{x} | sample mean |
| X_p | fraction of particles with settling velocity V_p that are removed |
| X_r | fraction of particles with settling velocity V_c that are removed |
| y, Y | position in the y direction (vertical), normal distance from the solid surface |
| y_0 | constant |
| y_f | flow depth |
| z, Z | position in the z (transverse) direction |
| δ | boundary layer thickness |
| δ_0 | thickness of the laminar sublayer |
| Δt | particle tracking time step |
| Δt^* | estimate of time taken for a particle to traverse a control volume |
| ϵ | dissipation rate for k |
| $\epsilon_{10\%}$ | percentage of data points for which the simulation error was within $\pm 10\%$ of the mean inlet velocity |
| $\epsilon_{min}, \epsilon_{mean}, \epsilon_{max}$ | minimum, mean and maximum simulation errors |
| ϵ_s | simulation error |

| | |
|-----------------------------|--|
| η | removal efficiency |
| η_0 | removal efficiency under quiescent conditions |
| η_{BSS} | removal efficiency determined from bed shear stress analysis |
| η_{PT} | removal efficiency determined from particle tracking |
| θ_c | dimensionless critical shear stress |
| κ | von-Kármán constant, usually 0.4 |
| λ | particle tracking step length factor |
| μ | dynamic viscosity |
| μ_p | population mean |
| μ_T | turbulent viscosity |
| ρ | fluid density |
| ρ_s | particle density |
| σ | surface tension |
| $\sigma_k, \sigma_\epsilon$ | diffusion constants in the k - ϵ turbulence model |
| σ_p | standard deviation of a population |
| τ_0 | bed shear stress |
| τ_c | critical bed shear stress |
| τ_{cd} | critical bed shear stress for deposition |
| τ_{ce} | critical bed shear stress erosion |
| τ_y | critical yield stress |
| ν | kinematic viscosity |
| ω | particle settling velocity |

LIST OF ABBREVIATIONS

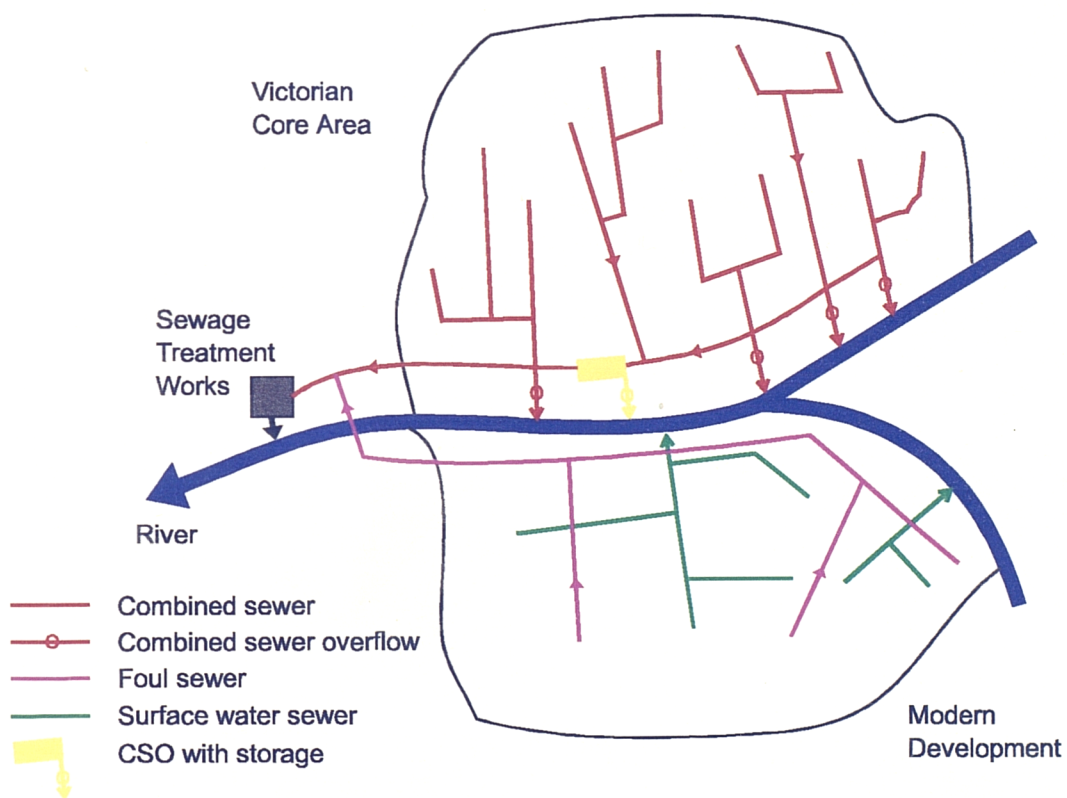
| | |
|---------------|--|
| ATV | The German Water Pollution Control Federation |
| BOD | Biochemical Oxygen Demand |
| BSI | British Standards Institute |
| CEC | Council of the European Communities |
| CFD | Computational Fluid Dynamics |
| CIRIA | The Construction Industry Research and Information Association |
| CSO | Combined Sewer Overflow |
| DHI | Danish Hydraulic Institute |
| DO | Dissolved Oxygen |
| DWF | Dry Weather Flow |
| EPA | (United States) Environmental Protection Agency |
| FFF | First Foul Flush |
| FWR | The Foundation for Water Research |
| IAHR | International Association on Hydraulics Research |
| IAWPRC | International Association on Water Pollution Research and Control |
| LDA | Laser Doppler Anemometry |
| LP | Line Print |
| MHLG | The Ministry of Housing and Local Government |
| RNG | Renormalisation Group |
| RSM | Reynolds Stress Model |
| SDD | The Scottish Development Department |
| SS | Suspended Sediment |
| STW | Sewage Treatment Works |
| TSR | Time Series Rainfall |
| UPM | Urban Pollution Management |
| UWWTD | The (EC) Urban Waste Water Treatment Directive |
| WAA | The Water Authorities Association |
| WRc | The Water Research centre |

1. Introduction

1.1 Background

1.1.1 The Historical Development of Urban Drainage Systems

Figure 1.1 is a schematic plan of the typical drainage system of many towns in the United Kingdom. This plan illustrates the general features of an urban drainage system and the changes in design practice that have occurred over time.



after Crabtree, 1987

Figure 1.1 A typical urban drainage system in the UK

Urban areas in the United Kingdom have historically been drained via combined sewerage systems, which carry both foul sewage from industrial and domestic sources and also surface runoff in times of rainfall. Financial and technical constraints have historically limited the size of sewers and sewage treatment facilities, and this in turn has restricted the amount of sewage that could be carried by the sewerage system and treated by the works. To prevent flooding from these combined sewers, overflows were introduced to pass excess flows directly to a watercourse. It was anticipated that such overflows would only operate in times of rainfall, when the foul sewage was considered to be sufficiently diluted with clean surface water to prevent any adverse impacts on the watercourse.

However, the discharges of many combined sewer overflows (CSOs) are unsatisfactory, in that they detrimentally affect quality in the receiving watercourse. Recently, increased public awareness of environmental problems and the privatisation of the water industry in the UK have highlighted the need to reduce the level of pollution in rivers which is due directly to CSOs.

There are approximately 25,000 CSOs in England and Wales, of which up to one third are unsatisfactory (Morris, 1993). North West Water (1983) believed that some 250 km of their rivers (5% of the total of 5323 km) were unable to achieve their quality objectives because of the effects of CSOs. Of nearly 3,000 overflows, 38% are judged to be operationally unsatisfactory (Sharman, 1994). The problem is so acute in some areas that during heavy rain almost all the flow in the watercourse is storm sewage (Balmforth, 1990). In England and Wales alone the investment required to address the issue of unsatisfactory combined sewer overflows has been identified as £850 million in the 10 years to 2005 (FWR, 1994). Two examples of CSOs discharging into urban water courses are illustrated in Plates 1.1 and 1.2.

Within the European Union a major new directive has been agreed which sets out the common requirements for the construction and operation of sewerage and sewage treatment systems. The EU Urban Waste Water Treatment Directive (UWWTD) (CEC, 1991) requires Member States to ensure that all agglomerations with a population equivalent of 2000 or more are provided with collecting systems. It further states that the design, construction and maintenance of sewage collecting systems should be undertaken with the best technical knowledge, not entailing excessive cost, notably regarding the limitation of pollution of receiving waters due to CSOs.



Plate 1.1 CSO discharging into an urban watercourse



Plate 1.2 Modern CSO with bar screen discharging into an urban watercourse

Historically, three solutions to the problem have been considered (Hedley and King, 1971). These are, firstly, to increase the size of sewers and take all or a greater proportion of the flow to full treatment; secondly, to effectively separate the system of drainage; or thirdly, to provide some storage device at individual overflows. The first of these, namely to construct a combined system without overflows, would clearly be prohibitively expensive except in special circumstances for small drainage areas. The second approach has been adopted in many modern developments. In such a separate system all the foul sewage is passed to treatment via a foul sewer which should have no overflows. The surface drainage is carried via a surface water sewer to a watercourse, as illustrated in Figure 1.1. Several disadvantages to such a system have been identified (Nicoll and McGillivray, 1978):

1. The inherited system would be expensive to replace, and a new combined system is less costly than separate sewers;
2. Urban surface run-off itself contains polluting matter - organic wastes, heavy metals, salts, oil, rubber and litter. Work in Stockholm (Söderlund and Lehtinen, 1972) has suggested that the surface water from modern urban areas is contaminated to the same extent as storm sewage, and has twice the Biochemical Oxygen Demand (BOD) of treated sewage;
3. Wrong connections of foul water into storm sewage drains are frequently made. Nicoll and McGillivray (1978) showed that one wrong connection in 100 could nullify the advantage of a separate system.

Of the traditionally available solutions, the most practical alternative has frequently been to upgrade the existing system, and, in many instances, storage volumes have been incorporated into CSOs.

Before the use of storage is discussed in greater detail, however, it should be noted that several new approaches to the problem of unsatisfactory CSO discharges have been proposed in recent years. Of particular interest are the approaches which involve source control, real-time control and CSO screening.

Source control involves the restriction of inputs to the sewer system, using measures such as permeable pavements (Pratt, 1995) which lead to a reduction in the frequency and magnitude of CSO discharges. Although this approach is most readily employed in new developments, some aspects of the approach may usefully be incorporated into existing systems.

As an alternative to the construction of additional new storage volumes, Geiger (1986) and Sharman (1994) have stressed that better use could be made of existing storage in the sewer systems. In future this may be achieved through the real-time automated operation of in-sewer flow control devices in response to information provided instantaneously from flow monitoring instruments located within the system. The instrumentation and software required for this approach are still under development.

It is also possible to treat the CSO discharges so that they carry a reduced concentration of polluting material. This may be achieved through the use of screens, or through the better design of CSO chambers.

Aspects of all three approaches outlined above are likely to be combined with the use of storage in future attempts to minimise the impacts of CSO discharges on urban water courses.

1.1.2 The Use of Storage

The approach adopted by the WRc/WAA Sewerage Rehabilitation Manual (WRc/WAA, 1994) is that, while existing sewers can only carry a finite maximum rate of flow, a river can only accept a certain maximum amount of storm sewage if its quality objective is to be achieved. Surplus storm sewage must be stored within the sewerage system or diverted elsewhere.

However, the term storage more usually refers to the concept of including an additional volume in the form of an oversized sewer pipe, or a chamber, incorporated into the sewerage system often at the site of a CSO, to be filled with discharge under conditions of high inflow. The incorporation of storage volumes into CSOs improves performance in two ways. Firstly, for a given spill event, the volume of spill is reduced; and secondly, the frequency of spill events is reduced. These effects are illustrated in Figure 1.2.

If storage is to be employed for sewer rehabilitation then a number of complex and conflicting issues need to be considered. For example, the storage volume needs to be sufficiently large to ensure that the frequency and duration of overflow discharges is reduced to a level that enables the receiving watercourse to achieve its quality objectives. On the other hand the upper limit to the volume will be dictated by economic considerations, the availability of land and the capacity of the downstream system to carry and treat the stored sewage. North West Water currently has 200 on-

line and off-line storage/attenuation tanks in the sewer network, ranging in size from 50 m³ to 11,600 m³ and totalling 145,000 m³ (Sharman, 1994).

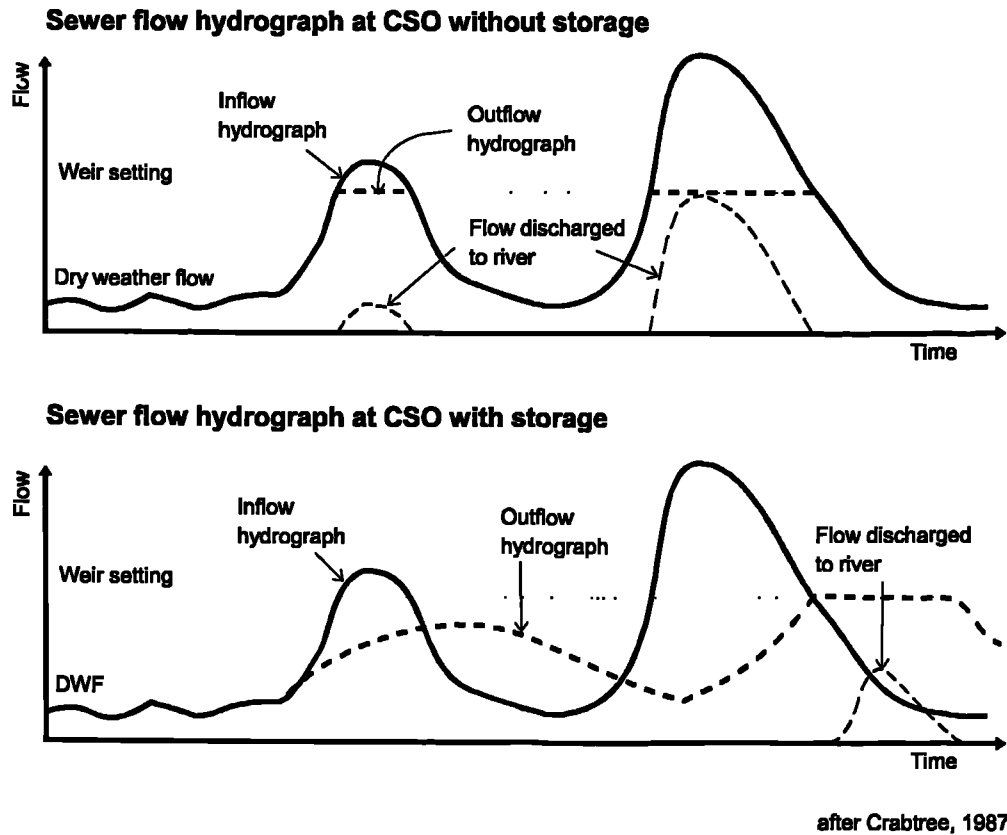


Figure 1.2 The effect of storage volume on CSO operation

Approaches to sizing storage facilities at CSOs have progressed from simple considerations of downstream hydraulic capacity, to methods which account for the temporal variations in storm water quality and attempt to store the worst polluted volumes, and finally, to the catchment quality planning approach, backed up by sophisticated modelling tools, advocated by the UK Urban Pollution Management (UPM) programme.

Yet, whilst storage tanks have frequently provided radical improvements in river quality, the problems that can arise from sediments deposited in such chambers have been comparatively ignored. Flow velocities are greatly reduced on entry to a storage structure, and the hydraulic conditions favour sediment deposition. Deposits of sediments in storage chambers may lead to blockages, surcharging, flooding and premature CSO operation. In addition, the ageing of deposited sediments, and their subsequent resuspension in later storms, can lead to poor quality continuation flow and overflow spilled discharges, and may also lead to odour and septicity problems. It is

therefore important that sediments are not allowed to build up in storage tanks. Typical examples of storage tank deposits are illustrated in Plates 1.3 and 1.4.

It is believed that the chamber geometry is a critical factor in the control of sediment deposition. Two alternative philosophies may be considered in the internal chamber design. The first is to design the tank to maintain self-cleansing operation. The second is to operate the storage facility as a settlement tank with subsequent 'management' of the deposited sediment. Of these two options, the former is currently preferred in the UK. The UPM Manual (FWR, 1994) states that "detention tanks should be designed to be, as far as possible, self-cleansing whilst in operation". Knott and Taylor (1985) produced a review of British and European practice in storage tank design, concluding that a large number of chamber types, with a range of layout and bed shape, were currently in use. They also stated that there were no established design methods for achieving self-cleansing. The deposition of sediment within a storage chamber is a function of the chamber configuration, the flow regime and the nature of the suspended sediments in the flow. The geometric features that are believed to affect sedimentation include: the longitudinal gradient; the length to breadth ratio; the gradient of transverse benching and the presence of a dry weather flow channel. However, quantitative information that explicitly demonstrates the impact of these, and other, parameters is not available. The decisions made by designers are necessarily somewhat subjective.

The first aim of the research described in this thesis was, therefore, to establish guidelines for the design of self-cleansing storage chambers, with the attention initially being focused on the use of laboratory scale model experiments. It is considered that laboratory scale studies provide an important link between full scale observations of sewerage system behaviour, and an understanding of the fundamental processes that control sediment deposition in individual structures. In terms of the self-cleansing operation of storage tanks, Ellis (1992) produced interim design guidelines based on laboratory scale model investigations, and his work has served as a foundation for the work described in this thesis.

Ellis (1992) also highlighted the potential for making use of computational fluid dynamics (CFD) software to address the issue of storage chamber design. Consequently, the second aim of the research was to expand on his preliminary findings, to evaluate the applicability of the software to this type of problem, and to establish procedures for the use of CFD as a design tool.

Plate 1.3 Typical storage chamber sediment deposits



Plate 1.4 Sediment deposits on chamber benching



1.1.3 Urban Pollution Management (UPM)

The previous section illustrates a selection of the issues that led to the initiation of the UPM (Urban Pollution Management) programme of research (Clifforde *et al.*, 1986); the research described herein forms one component of that programme. The intention of the overall UPM research programme was to provide the necessary tools and methodology to allow objective and rational upgrading of deficient sewer systems. The programme was directed towards providing the methodology for the Water Industry to deal with transient river pollution caused by spillage from combined sewers via CSOs.

The design procedure which resulted from the UPM research programme has now been produced, in the form of the UPM Manual (FWR, 1994). The UPM Procedure is a comprehensive planning framework which can be used to identify the appropriate design arrangements for urban wastewater facilities which will protect the legitimate uses of receiving waters under wet weather conditions in a cost effective manner. A fundamental principle of the approach adopted was that it should allow the problem to be tackled in a way which matched realistic environmental expectations with financially achievable demands. It was also recognised that the problem of CSOs should not be tackled in isolation from the rest of the urban wastewater collection and treatment system. The approach of the UPM Procedure is illustrated with reference to the issue of storage chamber design in chapter 2.

The UPM programme has provided a 'tool box' of planning methods which incorporates techniques for modelling rainfall inputs, sewer system flow and quality, wastewater treatment quality and receiving water impacts. Methods with varying degrees of sophistication have been made available and the importance of selecting a level of sophistication in the tools that matches the requirements of the particular problem is stressed.

The requirement for the sewer flow quality model were that it should be capable of replicating the variations in qualitative performance of any given sewer system during any rainfall event and also the cumulative performance over a series of events. This has necessarily included the modelling of processes relevant to sedimentation in storage chambers. Under the UPM Programme the urban drainage quality model MOSQUITO (Modelling of Stormwater Quality Including Tanks and Overflows) has been developed (Moys, 1987). This particular model developed from an existing sewer flow model, WALLRUS. The most recent version of the software is marketed

under the name HydroWorks QM. These models are part of a suite of software packages which is referred to as the Wallingford Procedure and it should be noted that any comments that refer to WALLRUS or MOSQUITO in this thesis may also apply to HydroWorks QM and its successors.

The UPM Procedure does not preclude the use of other quality models with equivalent capabilities. Several similar models have been developed in parallel to the Wallingford Procedure over recent years, of which MOUSE TRAP (MOdelling of Urban SEwer systems - TRAnsport of Pollution) is the most widely used in the UK. MOUSE TRAP was developed by a consortium of European companies and institutions (Crabtree *et al.*, 1994a), and is based around the existing Danish Hydraulic Institute (DHI) MOUSE modelling package for urban sewer systems (DHI, 1994).

Whilst several more modelling packages have been reviewed by Bertrand-Krajewski *et al.* (1993), discussion of urban drainage quality modelling in this thesis will be confined to the Wallingford Procedure and MOUSE TRAP. One further aim of this research was, therefore, to critically evaluate the way in which these models represent storage chambers, and to suggest ways in which the current modelling procedures might be enhanced.

1.2 Aims

The overall objective of the research described in this thesis was to provide a means of predicting the retention efficiency of storage chambers in urban drainage systems.

This objective was divided into a number of specific aims, which are presented below:

1. Assess the importance of flow and geometry parameters on sediment deposition in a laboratory model storage chamber, and comment on the models of efficiency that are currently implemented;
2. Relate the location of sediment deposits in a laboratory model storage chamber to the local hydraulic conditions;
3. Attempt to simulate the laboratory flow patterns and sedimentation phenomena using the computational fluid dynamics (CFD) software FLUENT;
4. Using CFD, evaluate the influence of a range of geometric components on chamber efficiency.

1.3 Structure of the Thesis

Chapter 2 contains a review of the literature on storage tank design, sewer sediments and modelling concepts relating to sediment movement.

The first half of the thesis (chapters 3, 4 and 5) is concerned with the laboratory testing programme. The laboratory system incorporated automatic inflow and sediment input controls, continuous measurement sediment concentration probes, as well as miniature current propeller and a 2D laser doppler anemometry system for velocity measurements. This is described in chapter 3.

The sediment deposition problem can be divided into two components: firstly, estimation of the *quantity* of deposited sediment; and secondly, estimation of the *location* of the sediment deposits.

In order to estimate the quantity of sediment deposited in the laboratory chamber, a system of controlled sediment input and continuous sediment concentration monitoring at the inflow and outflow positions was developed. All the laboratory tests were carried out under steady flow conditions and efficiency was defined as the proportion of the inflow sediment load that was deposited on the chamber bed. Efficiency tests were carried out over a broad range of inflow velocities and the results were compared with several models developed for settling tanks. These investigations are described in chapter 4. The efficiency was also determined for two alternative geometric configurations, although the measurements did not reveal significant differences.

Observations made during the laboratory efficiency experiments suggested that the location of sediments deposited in the chamber was a function of the velocity distribution in the flow field. Laboratory experiments were therefore carried out in order to expand upon this observation. It was shown that the deposition of sediment was a function of the local bed shear stress, and a critical value of bed shear stress at which deposition occurred was identified. It was also demonstrated that changes in the distribution of sediment on the chamber bed under time-varying flow conditions could be predicted using bed shear stress analysis. These measurements and the data analysis are presented in chapter 5. Furthermore, a relationship between the distribution of sediment and the chamber efficiency was identified.

The most important observation arising from the laboratory investigations was that the sedimentation processes occurring in the model chamber were inextricably linked to

the flow field. Consequently, it was suggested that the research would progress more effectively if the laboratory based studies could be replaced by numerical simulations of prototype storage chambers.

In the second half of the thesis (chapters 6, 7 and 8) the use of the computational fluid dynamics (CFD) software FLUENT is discussed. The laboratory experiments showed that the fundamental control on the location of sediment deposits was the flow field. It was also shown that the structure of the flow field was complex and three dimensional. The first task, therefore, was to accurately simulate the flow field that had been measured in the laboratory tank. In chapter 6 the simulation procedure is described and results of the flow field validation are presented. With experience in the use of boundary conditions and the solution procedure, good numerical simulations were produced.

Chapter 7 describes the ways in which the numerical simulation of the model tank was used to predict efficiency. Firstly, bed shear stress distributions were used to predict the location of deposited sediments. These data were also used to predict efficiency, using the calibration between distribution and efficiency described in chapter 5. In addition, stochastic particle tracking was employed to monitor the movement of individual particles and to predict efficiency statistically.

In chapter 8, FLUENT is employed to provide a comparative assessment of the impact of several geometric and hydraulic parameters on chamber performance. These included the length to breadth ratio, the effect of benching, longitudinal slope and level of inlet surcharge. It is demonstrated that the length to breadth ratio is the most critical geometric parameter to impact on sediment deposition, but that the inlet velocity has the greatest impact on performance overall. A regression based chamber efficiency model incorporating these parameters is presented.

Finally, conclusions and suggestions for further work are presented in chapter 9.

2. Literature Review

2.1 Introduction

The historical developments that have resulted in increased usage of storage chambers in urban drainage systems were described in chapter 1. Storage chambers are now regularly constructed as a response to hydraulic problems and as a means of reducing pollution associated with Combined Sewer Overflows (CSOs). Some general observations concerning the configuration and type of existing storage chambers are presented in section 2.2.1, while the various techniques which exist for the selection of chamber volume are discussed in section 2.2.2. Storage chambers inevitably suffer from problems of sediment deposition, and aspects of the internal chamber geometry that are considered important for self-cleansing operation are described in section 2.2.3.

In order to model the behaviour of sewer sediments, it is necessary to understand the origins, physical properties and biochemical characteristics of the material. Section 2.3 therefore contains a review of current knowledge about 'real' sewer sediments.

The main aims of this thesis are to develop an understanding of the processes that control the deposition of sediment in storage chambers, and to build a predictive numerical model based on the FLUENT computational fluid dynamics (CFD) software. Section 2.4 is therefore concerned with the modelling concepts that are relevant to this problem. The principles of hydraulic modelling and CFD are described in section 2.4.2, whilst the transport of cohesive and non cohesive sediments is discussed in section 2.4.3. Although very little modelling work on storage tanks has previously been undertaken, a large body of relevant research can be found in the literature on settling tanks; this is outlined in section 2.4.4.

2.2 Storage Tank Design

2.2.1 Storage Tank Configurations

Storage tanks are sometimes referred to as chambers or basins, and some authors use the words retention or detention in preference to storage. It is therefore appropriate to define the terms, as they will be used in this thesis. The term *basin* refers to large, exposed, naturally formed areas of land used for the above-ground storage of sewage flows. The term *storage tank* or *chamber* will be used to indicate a concrete storage structure which is enclosed underground, and which may be associated with a CSO. *Storm tank* will be used to identify an open-topped concrete tank used at the head of sewage treatment works, whilst *settling tank* refers to a tank used for primary treatment at sewage treatment works.

Knott and Taylor (1985) published a review of British and European practice in storage tank design, concluded that a large number of chamber types, with a range of layout and bed shape, were currently in use. The size of tanks was found to be virtually unlimited with the main restrictions relating to surface site constraints and the existing sewer layout. The greatest proportion of existing tank chambers in the UK and overseas are rectangular. However, kite shaped tanks, circular shaft tanks, storage tunnels and multi component tanks also exist. The use of benching on the chamber floor and the inclusion of single or multiple dry weather flow channels are common but not universal features. In addition, at many overflows some attempt is made to prevent the spillage of floating solids by the installation of scumboards.

There are two general arrangements which may be considered for storage tanks: on-line and off-line. On-line tanks form an integral part of the sewer system, consisting of an enlarged flow section that fills when the inflow exceeds the downstream capacity. Discharge from the tank is controlled by a throttle at the downstream end. An overflow at the inlet caters for rainfall events in excess of the design storm. Usually continuation flow control is achieved via a fixed flow control device, e.g. an orifice or penstock, in which case it must be sized to pass the setting at first spill. As this only occurs when the tank is full, the discharge for most of the operating time will be less than the peak, and consequently, the downstream sewer capacity will be under-utilised. However, the possibility exists for real-time controlled outlets, which respond to flow monitors in the receiving sewer to provide constant discharge irrespective of head.

Off-line tanks are physically separate from the basic system, with the flow entering via a diversion structure when the downstream sewer capacity is exceeded. The stored flows may be returned to the system by gravity where the site allows, or by pumping. Again a CSO is frequently provided on the incoming sewer to relieve flows in excess of the design storm.

A basic design of the rectangular on-line storage tank is shown in Figure 2.1. In this case the circular inflow pipe enters a rectangular section chamber which incorporates a side weir overflow with scumboard, downstream of which there is a large rectangular storage tank and a flow control device.

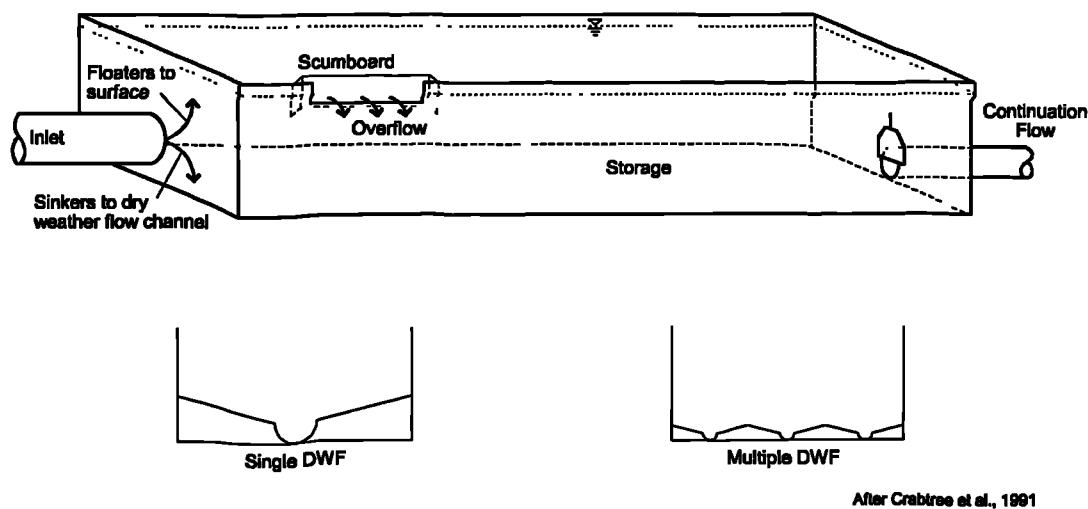


Figure 2.1 Basic design of a rectangular on-line storage tank

2.2.2 Overflow Setting

One of the fundamental design criteria for CSOs is the overflow setting. This is the magnitude of flow within the sewer at which storm sewage begins to pass over the overflow to a watercourse. Traditionally, the CSO setting was based principally upon sewerage criteria by considering the desired or practicable maximum continuation flow in the downstream sewer. This approach led to the establishment of fixed criteria, such as multiples of the dry weather sewer flow (DWF). For example, six times DWF has been commonly used as the desired continuation flow to treatment. The 'Formula A' approach (MHLG, 1970) was an extension of this concept.

'Formula A' is expressed as:-

$$Q_c = DWF + 1360P + 2E \quad (2.1)$$

in which Q_c is the required continuation flow setting, DWF is the dry weather flow in the sewer (litres/day), P is the population and E represents industrial discharges (l/d). In the UK, this is probably the most extensively used criterion for the setting of CSOs (Crabtree, 1987). It is stated as a minimum requirement for new or unsatisfactory CSOs in the AMP2 Guidelines (NRA, 1993).

The practice of allowing spillage to a watercourse once the discharge in the sewer exceeds Formula A or a multiple of the DWF takes no account of the temporal distribution of the polluting matter within the storm flow or the impact of the spilled flow on the receiving watercourse. Later researchers have paid due regard to these factors in their approaches to specifying the overflow setting.

The Rivers Pollution Prevention Sub-Committee of the Scottish Development Department (SDD) (1977) suggested a simple method for calculating the overflow setting based on available dilution in the watercourse. The dilution is based on the dry weather flow of sewage and on the minimum flow in the stream at the discharge point, i.e., the mean daily discharge which is exceeded in the long term for 95% of the time. The guidelines are presented in Table 2.1. The design approach requires an overflow setting equivalent to Formula A plus a storage volume of between 40 litres per head and 120 litres per head depending on the available dilution. Capacities within this range would store between 50% and 80% of the flow that would otherwise be spilled.

Table 2.1 SDD (1977) design guidelines for storm overflows

| Minimum dilution in terms of 95% exceedence mean daily discharge in receiving watercourse and sewage DWF | Approx. percentage of total polluting load of storm sewage spilled from sewer which may be discharged to stream (%) | Type of storm overflow installation |
|--|---|---|
| 8 | 100 | Overflow setting = Formula A, no tank |
| 6 | 75 | Overflow setting = Formula A + 455P, no tank, if sewer capacity available. Alternatively adopt next recommendation. |
| 4 | 50 | Overflow setting = Formula A + tank of capacity 40 l per head. |
| 2 | 25 | Overflow setting = Formula A + tank of capacity 80 l per head. |
| 1 | 12 | Overflow setting = Formula A + tank of capacity 120 l per head. |

This method does not predict the receiving water impact. It only attempts to reduce the impact of the discharge to a lower level which may or may not be acceptable depending on the river's quality objectives and the river's assimilative capacity.

Later approaches have considered not only the total load of pollution passed to the watercourse, but also the temporal distribution of pollutant concentration within the storm event. In particular, a first foul flush (FFF) is frequently observed at CSO outfalls during spill events. The FFF may be defined as the initial period of storm flow during which the concentration of pollutants is significantly higher than those observed during the latter stages of the storm event (Thornton and Saul, 1986). A number of researchers have used the cumulative load/cumulative flow volume curve, to define a foul flush as occurring when the curve has an initial slope greater than the 45° equilibrium line (Geiger, 1986). In some cases, the volume and load in the first flush has been defined by the point of maximum divergence between the cumulative load and the cumulative flow (Gupta and Saul, 1994).

Foul flushes are not observed universally, nor are they always observed within the same sewer for different events. In large catchments their distinctive shape may be lost (Stotz and Krauth, 1986). Thornton and Saul (1986), for example, identified a distinct FFF of suspended solids and chemical oxygen demand in 75 percent of sampled storm events monitored at the downstream end of a combined sewer system in North West England. Ashley *et al.* (1992) reported a first and second flush of suspended solids for the main Dundee interceptor sewer during storm conditions.

Where a first flush occurs, storage tanks can be designed to capture the flush, allowing the flows with lower concentrations to enter the river during the later stages of the storm. At the same time, the required storage volume is lower than would be necessary to store the same volume of pollutants in the case of a constant pollutant concentration for the same total load.

The occurrence of foul flushes is usually attributed to the washout of previously deposited sediment. However, Ackers *et al.* (1968) attributed the FFF to the initiation of a flood wave by the storm water which moves at a greater velocity than the dry weather flow sewage which was in the system prior to the storm event. Consequently, the toe of the advancing flood wave consists of undiluted foul flow which it has overtaken. In addition, increased velocities at the front of the wave cause pipe wall deposits which may have accumulated in the preceding period to be scoured and resuspended.

They therefore presented a design methodology for storm sewage overflows incorporating storage where the size of the tank was a function of the volume of dry-weather flow overtaken by the toe of the advancing storm wave. Design charts for rectangular and circular section tanks were produced, and these have been used successfully in many locations in North West England.

Hedley and King (1971) observed that the major part of the pollution load carried by storm sewage was carried either in solution, or very fine suspension, and could not, therefore, be retained within the sewerage system by the settling processes occurring at a conventional overflow structure. Observations of temporal variations in storm sewage quality at a full scale installation near Birmingham suggested that the FFF had generally passed before the peak flow in the sewer was reached, which in turn, due to attenuation in the particular system considered, usually occurred prior to the time of concentration. They suggested therefore that the storage volume should be equivalent to the excess volume of the rising limb of a design storm hydrograph above continuation flow (Figure 2.2).

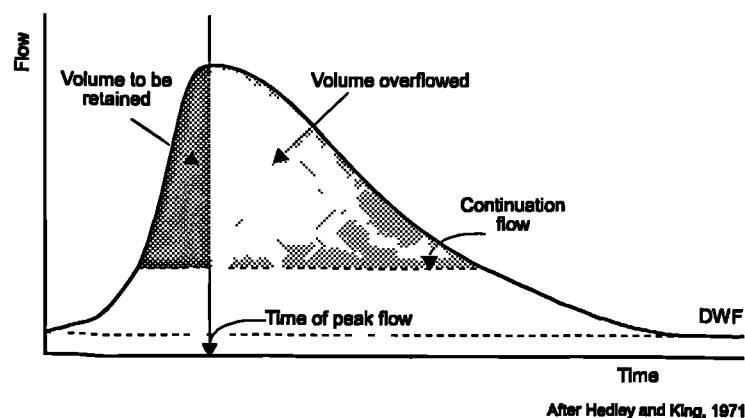


Figure 2.2 Storage in retention tank during design storm

The time axis in Figure 2.2 might typically represent a period of up to three or four hours. The suggested return frequency of the design storm was a function of the size and quality of the receiving stream, ranging from six months for a small stream to an overflow frequency of 10 times per year for large rivers.

In Continental Europe, it is common practice to design the size of the tank based on the storage of a rainfall amount falling on the impervious area of the catchment. Typically 1.5 mm to 4.0 mm may be used for design purposes which gives a volume of storage equivalent to 15-40 m³/hectare of impervious area. This design philosophy

was based on the recommendations of Krauth (1973) in which an estimate was made that 90% of the pollutant material could be stored by this method.

As part of the UK UPM programme, dynamic models are increasingly used to estimate the appropriate size of storage volumes. Volumes are calculated not only on sewer performance criteria, but with consideration for the assimilative capacity and quality objectives of the receiving watercourse. The hydraulic performance of any proposed structure may be evaluated using a sewer flow model, e.g. WALLRUS, and a number of alternative procedures have been employed to predict quality.

QUALSOC (Quality Impacts of Storm Overflows: Consent Procedure) is an extended version of Formula A which uses a mass balance technique to model the effect of varying the overflow setting on the concentration of a specified pollutant in the downstream river. Usually the water quality parameter used is the maximum acceptable concentration of BOD (Biochemical Oxygen Demand) (Morris, 1992).

The CARP (Comparative Acceptable River Pollution) procedure has been used to calculate acceptable CSO spill loads to individual river reaches by comparing the pattern of load input rate per event with a reach which, whilst significantly affected, is not considered to be unacceptably polluted by CSO inputs, i.e. attains its designated quality objectives despite CSO spills. The use of a comparison of input rates is only valid for rivers with similar characteristics.

A recent example of this approach was the methodology adopted in the Littleborough sewer rehabilitation work (Davis and Parkinson, 1990). One CSO with storage was designed to replace eight smaller, unsatisfactory overflows. On the basis of the Hedley and King (1971) approach, the appropriate tank volume to store 25% of the demihydrograph from a 90 minute duration storm with a return period of 2 years was 2800 m³. Instead, using the CARP procedure, a volume of 1500 m³ was selected, actually allowing for a reduction in construction costs. Post constructional monitoring of river quality has totally justified this approach (Davis and Crabtree, 1991).

One major problem with CARP is the difficulty of identifying a range of acceptable reaches with which to compare and validate the method (Morris, 1992). Both QUALSOC and CARP are unable to deal with time-varying pollutant concentrations, such as the FFF.

A simplified model (SIMPOL) has also been developed for use as a planning tool in the UPM Programme (FWR, 1994). In SIMPOL the sewer system is represented as a series of tanks, through which storm flows and pollutants are routed. When calibrated

against a more sophisticated model, SIMPOL may be used to assess a number of alternative solutions rapidly. Without calibration, and using only basic catchment data, SIMPOL provides an alternative to the SDD method or CARP, outlined above. The approach adopted in SIMPOL is similar to a storm tank model presented by Lessard and Beck (1991). Their model produced dynamic predictions of flow and quality, which enabled overflow control strategies to be evaluated.

The most comprehensive approach to deciding on the CSO setting is to model the water quality in the sewerage system using deterministic urban drainage quality models, such as MOUSE TRAP and MOSQUITO, along with dynamic river impact models (e.g. MIKE11), to ensure that the occurrence of pollution concentration levels is within defined limits. The projected river quality impacts may be assessed against river quality standards for intermittent discharges. The Fundamental Intermittent Standards are expressed in terms of dissolved oxygen (DO) and un-ionised ammonia, as it is these determinands which have the most direct effects on the health of fish and invertebrates (FWR, 1994). These standards are expressed in terms of concentration/duration thresholds for a range of return periods. For example, a DO concentration of 4.0 mg/l for one hour may not be exceeded more than once a month, while the same concentration lasting six hours must not be exceeded more than annually (FWR, 1994).

The traditional approach to the use of sewer flow models has embodied the concept of design storms of standard profile and of a return period equal to the frequency with which exceedence of hydraulic capacity could be tolerated. While such design rainfalls represent extreme events they give little indication of the day to day performance of the sewerage system. To assess the performance and polluting impact of CSOs, the magnitude, frequency and duration of spills are required over a long time period, such as a typical year. Appropriate annual rainfall series, termed Time Series Rainfall (TSR) have been statistically synthesised for regions of the UK.

The sewer quality models developed as part of the UPM programme have been designed to provide an accurate representation of system performance under wet weather conditions. These models, used with appropriate rainfall inputs (such as TSR) enable storage chamber sizing to be based accurately on an integrated assessment of rainfall characteristics, sewer flow, pollutant transfer processes and river quality objectives.

The UPM Manual (FWR, 1994) recommends that the urban catchment population, the flatness of the catchment and the extent to which the discharges interact with those of

the sewage treatment works (STW) should be taken into account when identifying the type of modelling procedure appropriate for a particular sewer system. For example, for a catchment population below 20,000 and no significant interaction with the STW a simple model such as SIMPOL would be sufficient. However, for a larger population, with a flat catchment a more detailed model (e.g. MOSQUITO) would be recommended.

The German Water Pollution Control Federation (ATV) has produced guidelines (A128, ATV (1991)) for stormwater detention tanks. These closely mirror the UPM approach, in that tank sizing may be based on the simplified design method which was described earlier, but detailed long term simulations are required for more complex or environmentally sensitive situations (Pecher, 1992). In addition, it is required that no overflow discharge should occur at a dilution lower than 1 part wastewater to 7 parts rainfall runoff.

Approaches to sizing storage facilities at CSOs have therefore progressed from simple considerations of downstream hydraulic capacity, to methods which account for the temporal variations in storm water quality and attempt to store the worst polluted volumes, and finally, to the catchment-wide quality planning approach, backed up by sophisticated modelling tools, advocated by the UPM programme.

2.2.3 Sedimentation and Self-cleansing

When tanks are full or partially full, sewage is moving at velocities which are extremely low (<0.1 m/s) and it is inevitable that sedimentation will occur (Roebuck, 1989). Equally, the longitudinal and transverse components of velocity are insufficient to create any significant flushing of these sediments into the DWF channel. Consequently a thin layer of sediments may be uniformly deposited on the benching at the end of each storm event. Local deposits also occur at regions of low velocity. Where these deposits accumulate they begin to reduce the hydraulic efficiency of the tank, and may result in blockages, surcharging, flooding and premature overflow operation. In addition, tank deposits are highly organic and their pollutant potential may increase with age. They therefore represent a store of pollutants with consequent increased threat to water quality, and risk of odour problems. It is clearly important that sediments are not allowed to build up in storage tanks.

Cant (1991) suggested that very few tanks suffer from severe siltation leading to reduced storage volume and blocked outlets. Existing tanks were found to typically

contain 50 mm of sediment spread throughout the tank with local build up in corners, against columns, or near the outlets.

Two alternative philosophies have been considered in the design of storage tanks. The first is to design the tank to maintain self-cleansing operation. The second is to operate the storage facility as a settlement tank with subsequent 'management' of the deposited sediment. The former designs are biased towards major capital investment with low revenue expenditure, whereas tanks designed to the latter concept have a specific maintenance element and incur an ongoing revenue cost although the initial capital investment may be comparatively lower. In the UK the former approach is currently favoured. The UPM manual (FWR, 1994) states that "detention tanks should be designed to be, as far as possible, self cleansing whilst in operation".

Roebuck (1989) presented a simple decision-making matrix for the selection of appropriate methods for removing sediments in storage chambers. At one extreme, he suggested that in situations where sedimentation was not likely to be severe and generous falls were available the tank should be designed to achieve self-cleansing conditions. On the other hand, for large ($>3000 \text{ m}^3$) tanks with severe sedimentation problems, he recommended the installation of permanently fixed cleaning equipment.

CIRIA (1987) suggested that 'self-cleansing' could be interpreted in two ways - either that sediment is not deposited at any time, or that over a long period of time there is no build up of sediment. Such a definition allows for the fact that sewerage structures are subjected to periods in dry weather when sediment deposition is likely, but that high flows are frequent enough to flush out any such deposits. In tanks which are designed to be self-cleansing, the main problem is to provide storage and effective separation of gross and suspended solids without incurring the penalty of poor self-cleansing and associated high maintenance costs.

It is interesting to note that in Germany (Geiger, 1986) greater emphasis appears to be placed on the operation of detention tanks as effective settling basins, while the requirement for self-cleansing operation has received little attention.

Tank and benching design have a considerable bearing on the ability of the structure to achieve self cleansing operation. The internal configuration must either control flow within the tank such that any sediment deposited on the benching during a storm is washed into the DWF channel as flow in the tank subsides, or such that deposited material is scoured from the benching as the DWF channel is overtopped by flows in a subsequent filling. Knott and Taylor (1985) stated that there were no established

design methods for achieving self cleansing. However, in a recent laboratory model study undertaken to assess the fine sediment retention efficiency of rectangular on-line storage tanks of different geometric configuration (Ellis, 1992), the following conclusions were made:

1. The self-cleansing operation requires high near bed flow velocity;
2. The hydraulic filling process is critical;
3. A DWF channel is essential;
4. A single DWF channel is preferable;
5. The longitudinal slope of the DWF channel should be as steep as practically possible;
6. Transverse benching towards the DWF channel should be included but the gradient of this benching is not critical;
7. A drop in invert to create supercritical flow in the DWF channel is an advantage;
8. Long narrow tanks are preferable;
9. The tank width should not exceed 4m;
10. Maintenance criteria are major design considerations.

Knott and Taylor (1985) recommended the use of longitudinal gradients between 1 in 25 and 1 in 100, and that transverse benching gradients of 1 in 3 be used for off-line tanks, and between 1 in 4 and 1 in 10 be used for on-line tanks. They also stated the importance of minimising obstructions at invert level as experience shows that deposits may accumulate downstream of access ladders, safety protection etc.

Roebuck (1989) suggested that the minimum criteria for self-cleansing conditions were a longitudinal gradient of 1 in 100 and a central DWF channel with flow velocities of 1.5 m/s. The recommendations for benching slope were dependent upon tank geometry: 1 in 2 for an off-line tank sewer; 1 in 5 for an on line tank sewer; and 1 in 10 for a storage tank.

Balmforth (1990) concluded that to prevent the accumulation of solids on the floor of the chamber, benching sloping at between 1 in 12 and 1 in 4 should be provided. The dry-weather flow channel should be semi-circular and at least 300 mm in diameter. A small ramp at the inlet is preferable to flaring, and a longitudinal slope of 1 in 50 should be provided if possible.

Hedley and Lockley (1978) examined the performance of three different retention tanks built in Birmingham between 1972 and 1974. Assessment of the hydraulic

performance suggested that they all performed more effectively than anticipated from design criteria. However, other design aspects were less impressive. One tank, at Coldbath, had been divided into three compartments, with spill into the second and third tanks only occurring during large storms. The intention was that by confining storage on the majority of occasions to one compartment only, maintenance requirements for the other two compartments would be minimised. In addition, they hoped that the emptying process would keep the tank clean. Because the tank was filled with increasingly cleaner sewage during a storm, and because it emptied in the reverse order to that in which it filled, it was hoped that the tank would be swept out by progressively cleaner sewage from the upper compartments as it drained.

In practice, however, all compartments contained deposited sludge, and the tank's performance was judged no better than a single compartment tank. The use of sewage to flush tanks was unsatisfactory. UPC plastic copolymer coatings used on the tank surfaces exhibited problems of blistering. Steep ridges and furrows which had been installed to aid self-cleansing did not produce cleaner surfaces and made subsequent inspections and maintenance more difficult.

Geiger (1986) presented details of a Swiss storage chamber which was divided into two sections. One part of the basin filled at the beginning of an event, catching a first foul flush when one was present. The second part only filled once the first part was filled and functioned like a settling tank. Aside from its effectiveness in pollution control, the subdivision into two parts eased maintenance requirements, as for smaller events only the first portion was filled. Geiger (1986) suggested that this type of chamber represented an optimum solution to the twin objectives of retaining the first flush and enabling treatment by settling. He did not cite self-cleansing operation as a design consideration.

Knott and Taylor (1985) pointed out that mechanical cleaning devices may be incorporated to ensure that sediments do not accumulate. In Continental Europe, automatic or manually controlled mechanical cleaning equipment is favoured, particularly in off-line tanks. Reliable and effective flushing mechanisms are available and used confidently. These include tipping cisterns, sprays and air entraining pumps.

These observations clearly indicate the historical prominence of trial-and-error judgements in storage tank design, and highlight the need for a more rigorous scientific appraisal of the subject. In particular, urban drainage quality models must be able to represent the effect that tank geometry has on sedimentation if river quality impacts are to be modelled realistically.

2.3 Sediments In Sewerage Systems

2.3.1 Sources of Sewer Sediments

CIRIA (1987) produced a list of sediment sources, in decreasing order of importance:

1. Winter gritting operations;
2. Road surfacing materials and roadworks;
3. Ingress of surrounding ground;
4. Industrial / Commercial processes;
5. Construction work;
6. Flooding;
7. Sediment provided by run-off from impervious areas;
8. Domestic sewage;
9. Soil eroded from pervious areas;
10. Windblown sand.

Once sediments have entered the sewer system they interact, and a combined sewer sediment is formed. It is the characteristics of this resulting sediment which are relevant to the sedimentation processes that occur in storage tanks.

2.3.2 Characteristics of Sewer Sediments

The First International Workshop on Sewer Sediments, which was organised by the 'Real Sewer Sediments' Task Group of the IAWPRC/IAHR Joint Committee on Urban Storm Drainage, took place in Brussels, in September, 1991. The research presented at that workshop (Verbanck, 1992a) represented a review of the state of current knowledge in Europe concerning the origin, occurrence and behaviour of sediments in sewer systems. At the conference, several researchers presented field data on sediment characteristics (Ashley and Crabtree, 1992; Chebbo and Bachoc, 1992; Laplace *et al.*, 1992; Michelbach and Wöhrle, 1992; Verbanck, 1992b) from which it was clear that sediment characteristics vary widely, both within a single study area and between different regions.

The mean particle size of suspended sediment appeared to be in the range 1-100 μm , while for deposited sediments the size distributions were generally found to lie between 500 and 5000 μm . CIRIA (1994) have recently suggested a value of $d_{50} = 40 \mu\text{m}$ to represent typical sanitary sediments in suspension, and 60 μm for stormwater

solids. In the case of settling velocity, values typically lay between 0.1 and 1.0 mm/s, although Michelbach and Wöhrle (1992) reported a mean value of around 60 mm/s for suspended sediments in combined sewage. Ashley and Crabtree (1992) suggested that it was not possible to accurately measure the settling characteristics of sewage particulates using currently available techniques. Sewage particles are constantly changing in character. For example, *flocculation* results in particles clustering together to form larger aggregates, or *flocs*. On the other hand particle aggregates may be broken up through a process termed *disaggregation*. This means that it is very difficult to obtain a representative sample for analysis. Ashley and Crabtree (1992) also demonstrated that the nature of the experimental procedure used for the settling velocity analysis could significantly affect the results. This was clearly illustrated with reference to a laboratory and an in-situ analysis carried out on the same sample.

Chebbo and Bachoc (1992) suggested that the mean density of suspended sediments in combined sewers was 2000 kg/m³.

A major input of the UPM Research Programme has been the assimilation of data describing the nature and behaviour of sediments found in combined sewers, for incorporation into sewer flow quality simulation models such as MOSQUITO. A five category classification of types of combined sewer sediments has been produced (Crabtree, 1988). The categories are:

- TYPE A Coarse, Predominantly granular mineral material found in the invert of pipes;
- TYPE B Similar in composition to Type A but concreted by the addition of mineral cements, fats and tars;
- TYPE C Mobile, fine grained, largely organic sludges found in quiescent zones;
- TYPE D Organic pipe wall slimes and zoogloal biofilms;
- TYPE E Fine grained organic and mineral deposits found in storage tanks.

Clearly it is Type E sediments which are of interest for storage tank design. Type E sediments were found to largely comprise sand sized particles, with a mean wet bulk density of 1460 kg/m³, and an average organic content of 22%. Sample variability was broad, a factor which was attributed to differences in tank design and operation. Samples with a high organic content were found in tanks with long retention times, while samples with a low organic content and composed of mainly fine grained mineral matter were found in tanks in which the retention time was short. However spatial

variability in sediment characteristics within a single tank may also be large, as the following example illustrates.

In a recent survey of sediment deposits in the Littleborough storage tank (Brownbill, 1992), 11 samples were analysed for physical and chemical properties. Deposit depths ranged from 10 to 150 mm, and from slurry to sand in texture. Pollutant concentrations varied widely (Table 2.2), and the three most highly polluted samples corresponded to locations in the side channels in the tank. The least polluted samples were collected closer to the central dry weather channel. The results of this particular study suggested that the distribution of different types of sediment deposit on the chamber bed was a function of the geometry of the tank and the flow patterns that developed within the tank.

Table 2.2 Characteristics of Littleborough tank sediments

| Property | Mean | Range |
|----------------------------------|------|-------------|
| BOD (g/kg dry weight) | 34.9 | 1.6 - 160.8 |
| COD (g/kg dry weight) | 167 | 44 - 442 |
| Ammonia (g/kg dry weight) | 0.19 | 0.02 - 0.85 |
| pH | 6.5 | 6.3 - 6.7 |
| Loss on Drying (%) | 70.3 | 34.9 - 88.6 |
| Volatiles (%) | 23.6 | 5.8 - 42.9 |
| Bulk Density (g/m ³) | 1141 | 1034 - 1382 |
| Particle Size Distribution | | |
| d ₁₀ (microns) | 23 | 16 - 35 |
| d ₅₀ (microns) | 100 | 80 - 150 |
| d ₉₀ (microns) | 380 | 200 - 900 |

Many of the small particles in sewage are *cohesive*, that is, they carry an electrostatic charge which facilitates bonding between them. In sewer sediments of all sizes the presence of organic materials and chemicals may enable *cementation* and *agglutination* between particles to occur. These processes all tend to increase the resistance of the deposited sediment to erosion, and have led to the description of most sewer sediments as having *cohesive-like* properties. After deposition from suspension, sewer sediments *consolidate*. This is accompanied by physio-chemical changes resulting from the break-up of flocs or aggregates and consequent rearrangement of the inter-particle bonds. It has been suggested that the bed density and the critical shear required for entrainment increase with time (Ashley *et al.*, 1992).

The critical yield stress of a deposited cohesive material may be assessed via rheological characterisation. Work has been carried out at Swansea University (Williams *et al.*, 1989) to determine the critical yield stress (τ_y) of sediment samples using applied stress rheometry. The critical yield stress is defined as the stress corresponding to a yield point at which the transition from elastic to plastic deformation occurs. This marks the onset of structural failure, or thixotropic breakdown. Values of τ_y for type E sediments varied from 25 to $>800 \text{ N/m}^2$. All samples exhibited a significant degree of cohesion, and were all classed as non-Newtonian materials which exhibited elastico-viscous behaviour.

2.3.3 Simulation of Sewer Sediments

In order to represent sewer sediments in laboratory experiments, previous researchers have used particles of bakelite, polythene, polystyrene and other materials. These were not really representative of sewage particulate. Sharpe and Kirkbride (1959) used weighted wooden beads wherein the basis for calibration was generally the specific gravity of the particles, although Halliwell and Saul (1980) suggested that it is the terminal velocities which should be modelled if anything approaching dynamic similarity is to be achieved.

Research into synthetic sediments which might mimic the behaviour of real sewer sediments for use in laboratory scale studies has been carried out at the University of Newcastle Upon Tyne. Crabtree *et al.* (1989) reported testing of sand mixed with a variety of cohesive additives. Kaolinite-sand mixtures did not behave as a composite sediment bed when subjected to shear, whereas the presence of grease or oil caused a great deal of air bubble formation near the bed, and even a small degree of petroleum jelly made the sediment highly cohesive. Other characteristics of such sediments differed markedly from real sewer sediments. Sediments composed of mixtures of a synthetic clay gel (Laponite RD and water) and sand were identified as rheologically suitable analogues for combined sewer sediment deposits. Small additions of the cohesive material were shown to increase the critical shear stresses dramatically (around 10 times), when compared with those of equivalent non-cohesive sediments.

Ellis (1992) examined a number of crushed and powdered wood products for their ability to replicate the behaviour of sewer sediments in a laboratory situation. He noted that when crushed olive stone was input into a hydraulic scale model chamber, the location and depth of deposition compared well with that observed in a full scale chamber.

2.4 Modelling the Processes

2.4.1 Introduction

Solutions to problems in hydraulic engineering are commonly obtained by constructing models and deriving answers to the imposed questions by interpreting the results from the models. These models can be either physical (laboratory) models that represent a scaled (and usually simplified) version of the 'real' construction, or mathematical models that are solved using numerical methods. Simple, empirically based regression analysis and three dimensional computational fluid dynamics (CFD) represent the two extremes of mathematical models that might be used.

Computational fluid dynamics can be described as the use of computers to produce information about the ways in which fluids flow in given situations (Shaw, 1992). In the last few years the importance of numerical simulations for research work in hydraulic engineering has steadily grown. This development has arisen from the fact that, over the last few years, many commercial CFD packages have been produced, and the availability of computers sufficiently powerful to run them has risen dramatically. Indeed, it is now feasible for numerical simulations to be undertaken as part of a routine design exercise.

Although not mutually exclusive, it is often assumed that a numerical simulation of a storage chamber comprises two parts, the hydraulic simulation and the sediment transport model. Thus, the following review addresses hydraulic modelling and sediment transport modelling in turn. It should be noted that the literature on sediment transport is extensive and only material considered to be of direct relevance to the settlement and deposition of fine sewer sediment in storage chambers is therefore discussed.

Section 2.4.4 describes the development of storage tank modelling, from regression based analysis of full-scale data up to present day techniques of numerical simulation.

2.4.2 Computational Fluid Dynamics (CFD)

2.4.2.1 Basic Equations

The basis of any CFD model lies in finding a flow field that obeys the three basic laws of mechanics. These are:

1. Conservation of mass;
2. Conservation of momentum;
3. Conservation of energy.

Two-dimensional forms of the equations are presented here for clarity, but these may readily be extended into their three-dimensional forms. The general forms of these equations and their derivations may be found in most general fluid dynamics texts, for example Chadwick and Morfett (1993) or Abbot and Basco (1989).

The principle of the conservation of mass states that matter can be neither created nor destroyed. The increase in mass within the control volume is equal to the mass inflow minus the mass outflow through the control surface. For incompressible flow, the continuity equation is expressed by:

$$\frac{\partial u}{\partial x} + \frac{\partial v}{\partial y} = 0 \quad (2.2)$$

in which u and v represent the velocity components in the x - and y -directions respectively.

The equations for the conservation of momentum are derived from Newton's Second Law of Motion. The vector sum of all external forces acting on the control volume is equal to the sum of the total rate of change of momentum of mass within the control volume and the rate of flux of momentum through the control surface.

$$\rho \frac{\partial u}{\partial t} + \rho u \frac{\partial u}{\partial x} + \rho v \frac{\partial u}{\partial y} = -\frac{\partial p}{\partial x} + \frac{\partial}{\partial x} \left(\mu \frac{\partial u}{\partial x} \right) + \frac{\partial}{\partial y} \left(\mu \frac{\partial u}{\partial y} \right) \quad (2.3)$$

$$\rho \frac{\partial v}{\partial t} + \rho u \frac{\partial v}{\partial x} + \rho v \frac{\partial v}{\partial y} = -\frac{\partial p}{\partial y} + \frac{\partial}{\partial x} \left(\mu \frac{\partial v}{\partial x} \right) + \frac{\partial}{\partial y} \left(\mu \frac{\partial v}{\partial y} \right) \quad (2.4)$$

where ρ is the fluid density, t is time, p is the fluid pressure and μ is the viscosity.

Equations 2.3 and 2.4 describe the conservation of momentum in the flow and are often known as the momentum equations or the Navier Stokes equations. The terms on the left hand side of each of these equations come from an acceleration term, the second and third terms being the convection terms; whereas the right side terms come from the pressure gradient in the flow and the effects of viscosity.

For low speed flow without heat transfer, the equations governing the conservation of mass and momentum can be used to describe the flow. When it is necessary to

account for the flow of heat through a liquid, this is achieved through the use of an energy equation derived from the first law of thermodynamics. The first law of thermodynamics is given by:

$$\frac{dQ_s}{dt} = \frac{dE_s}{dt} + \frac{dW}{dt} \quad (2.5)$$

where Q_s is the heat energy entering the system by conduction, E_s is the internal energy of the system and W is the work done by the fluid. The equation for the transport of temperature through the domain is:

$$\begin{aligned} \left(\frac{\partial T}{\partial t} + u \frac{\partial T}{\partial x} + v \frac{\partial T}{\partial y} \right) = \frac{k_t}{\rho c_p} \left(\frac{\partial^2 T}{\partial x^2} + \frac{\partial^2 T}{\partial y^2} \right) + \\ \frac{\mu}{\rho c_p} \left[2 \left(\frac{\partial u}{\partial x} \right)^2 + 2 \left(\frac{\partial v}{\partial y} \right)^2 + \left(\frac{\partial u}{\partial y} + \frac{\partial v}{\partial x} \right) \right] \end{aligned} \quad (2.6)$$

in which T is the fluid temperature, k_t is the constant of thermal conductivity of the fluid and c_p is the specific heat at constant pressure (Shaw, 1992).

2.4.2.2 Turbulence

In turbulent flow the fluid particles move in irregular paths, causing an exchange of momentum from one portion of the fluid to another. In laminar flow fluid particles move along smooth paths in laminas, or layers, with one layer gliding smoothly over an adjacent layer. In most natural and engineered channels the flow regime is turbulent.

Most engineering models of turbulent flow assume that the velocity at a given point in space and a given time can be made up of the superposition of the mean velocity \bar{u} , and a random fluctuating component, u' . The intensity of turbulence is the ratio $\frac{\sqrt{\bar{u}'^2}}{\bar{u}}$. Mathematically the instantaneous velocity component u can be described as:

$$u = \bar{u} + u' \quad (2.7)$$

Substituting this, and the equivalent expression for the second velocity component v into the continuity equation and then integrating with time gives the time averaged continuity equation for turbulent flows:

$$\frac{\partial \bar{u}}{\partial x} + \frac{\partial \bar{v}}{\partial y} = 0 \quad (2.8)$$

Making a similar substitution into the momentum equation does not produce such a convenient result. The convection terms are non-linear terms; that is they are the products of velocity components and the derivatives of velocity components. When Equation 2.7 is substituted into the momentum equations, the convection terms generate terms for some of the products of the fluctuating components and the integral over time of these products is not zero. For example, the momentum equation in the x -direction becomes:

$$\rho \frac{\partial \bar{u}}{\partial t} + \rho \bar{u} \frac{\partial \bar{u}}{\partial x} + \rho \bar{v} \frac{\partial \bar{u}}{\partial y} = -\frac{\partial p}{\partial x} + \frac{\partial}{\partial x} \left(\mu \frac{\partial \bar{u}}{\partial x} \right) + \frac{\partial}{\partial y} \left(\mu \frac{\partial \bar{u}}{\partial y} \right) - \rho \overline{\frac{\partial u'^2}{\partial x}} - \rho \overline{\frac{\partial (u'v')}{\partial y}} \quad (2.9)$$

The last two terms on the right hand side of Equation 2.9 are known as Reynolds Stresses. It is these additional terms that are modelled to account for the effects of turbulence.

Except in very simple flow situations, these modified equations cannot be solved directly. They can only be solved when approximations for the Reynolds Stresses are made. One way of simplifying the equations is to treat the additional terms as viscous stresses produced by the turbulence in the flow. Thus:

$$\text{Reynolds Stress} = \frac{\partial}{\partial x} \left(\mu_r \frac{\partial \bar{u}}{\partial x} \right) + \frac{\partial}{\partial y} \left(\mu_r \frac{\partial \bar{u}}{\partial y} \right) \quad (2.10)$$

where μ_r is an additional viscosity due to turbulence. The momentum equation therefore becomes:

$$\rho \frac{\partial \bar{u}}{\partial t} + \rho \bar{u} \frac{\partial \bar{u}}{\partial x} + \rho \bar{v} \frac{\partial \bar{u}}{\partial y} = -\frac{\partial p}{\partial x} + \frac{\partial}{\partial x} \left((\mu + \mu_r) \frac{\partial \bar{u}}{\partial x} \right) + \frac{\partial}{\partial y} \left((\mu + \mu_r) \frac{\partial \bar{u}}{\partial y} \right) \quad (2.11)$$

It is then necessary to find μ_r from the other flow variables. There are various ways of doing this and these include the following:

1. Mixing length arguments

μ_r is expressed as a function of density, a length scale in the flow and the local mean flow velocity. Typically, this relationship is given as

$$\mu_T = \rho c_\mu l^2 \left(\frac{\partial \tilde{u}}{\partial y} + \frac{\partial \tilde{v}}{\partial x} \right) \quad (2.12)$$

where c_μ is some constant that needs to be determined experimentally together with the length scale, l .

2. Simple partial differential equation models

Equations similar to the momentum equation can be derived that describe the distribution of the turbulent kinetic energy k and the distribution of the dissipation rate of k , ϵ . The transport equations for k and ϵ are complex partial differential equations, but some of the terms in the equations are often replaced by empirically derived constants. These simplified equations may then be solved computationally. If the mixing length l is known then only the equation for k needs to be solved. The additional viscosity due to turbulence can be found from

$$\mu_T = \rho c_\mu k^{1/2} l \quad (2.13)$$

This method is known as a one-equation turbulence model. If l is not known then the transport equations for both k and ϵ must be solved, and

$$\mu_T = \rho c_\mu \frac{k^2}{\epsilon} \quad (2.14)$$

This so-called k - ϵ two-equation turbulence model is commonly used in computational fluid dynamics. Some five empirically derived constants are used with this model. These are c_μ , which was introduced in equation 2.12, $c_{1\epsilon}$, $c_{2\epsilon}$, and the diffusion constants σ_k and σ_ϵ . The values recommended by Launder and Spalding (1974) are given in Table 2.3.

Table 2.3 Values of the constants in the k - ϵ turbulence model (after Launder and Spalding, 1974)

| c_μ | $c_{1\epsilon}$ | $c_{2\epsilon}$ | σ_k | σ_ϵ |
|---------|-----------------|-----------------|------------|-------------------|
| 0.09 | 1.44 | 1.92 | 1.0 | 1.3 |

Another modelling approach is to try to find values for the Reynolds Stresses themselves. The advantage of doing this over the methods mentioned previously is

that those methods give a single additional viscosity, whereas the direct modelling of the stress terms allows the effects of turbulence to vary in the three co-ordinate directions. One and two equation turbulence models give isotropic turbulence values. Algebraic stress models and Reynolds Stress models allow the stresses to be modelled directly.

2.4.2.3 Numerical Discretization

The equations governing the motion of fluids are partial differential equations. In order to solve them computationally, numerical discretization is carried out to obtain the numerical analogues of the equations. The three major numerical discretization techniques are: finite difference; finite element and finite volume. Examples of the way in which each of these techniques would be applied to transform a simple partial differential equation into its numerical analogue are not described here as they are adequately described in several texts, for example Shaw (1992).

The finite difference method is based on the use of so-called Taylor series to build a library of equations that describe the derivatives of a variable as the differences between the values of the variable at various points in space or time.

In the finite element method the domain over which the partial differential equations applies is split into a finite number of sub-domains known as elements. Over each element a simple variation of the dependent variable is assumed and this piecewise description is used to build up a picture of how the variables vary over the whole domain.

The finite volume method is similar in some ways to the finite difference method. Essentially, the governing partial differential equations are converted into numerical form by a physically based transformation of the equations. For example, the momentum equation can be considered as a series of fluxes into a volume of fluid, together with a source term which is the pressure gradient.

The relative merits of each of these techniques are discussed by Shaw (1992) and Abbot and Basco (1989). These texts also provide detailed information on solution procedures, meshing, the definition of boundary conditions and numerous other aspects of CFD modelling. These issues are discussed fully in chapters 6 and 7, in the context of the current research project.

2.4.3 Sediment Transport and Deposition

2.4.3.1 Introduction

Sediment movement in any hydraulic system is usually considered to consist of three phases: erosion; transport; and deposition. Sediment movement is initiated by entrainment or erosion, particles are then transported either as suspended or bed load, and finally sediment is deposited once the transport capacity of the flow has been exceeded or is reduced.

At the inflow of a storage tank the flow velocity, and hence the transport capacity of the flow, is dramatically reduced, both as a result of the increased width, and due to downstream flow control, and storage tanks are consequently a predominantly depositional environment. In modelling storage tanks, therefore, the most important processes to understand are those which control the settlement and deposition of suspended sediment in the flow, and these processes are described in detail in section 2.4.3.2.

However, self-cleansing may be achieved through the reentrainment of deposited sediments, and consideration will also be given, in section 2.4.3.3, to the processes of sediment erosion and transport. The process of consolidation, the effects of which may significantly effect erosion processes, is also considered in this context.

2.4.3.2 The Settlement of Particulate Material

The settling of discrete, non flocculating particles can be analysed by means of the classic laws of sedimentation formed by Newton and Stokes. Newton's law yields the terminal particle velocity by equating the gravitational force of the particle with the frictional resistance, or drag. The gravitational force is given by:

$$\text{Gravitational force} = (\rho_p - \rho)gV_i \quad (2.15)$$

where ρ_p is the particle density, ρ is the density of fluid, g is the acceleration due to gravity and V_i is the particle volume.

The frictional drag force depends on the particle velocity, fluid density, fluid viscosity, and particle diameter and the drag coefficient C_D (dimensionless) and is defined by Equation 2.16.

$$\text{Frictional drag force} = \frac{C_D A_p \rho v_p^2}{2} \quad (2.16)$$

where A_p is the cross sectional area of particle at right angles to v_p , and v_p is the particle velocity.

Equating the gravitational force with the frictional drag force for spherical particles yields Newton's law:

$$\omega = \left[\frac{4g(\rho_s - \rho)d}{3C_D \rho} \right]^{1/2} \quad (2.17)$$

where ω is the particle terminal velocity and d is the particle diameter.

The drag coefficient takes on different values depending on whether the flow regime surrounding the particle is laminar or turbulent, and therefore may be expressed in terms of the Reynolds number (Re):

$$C_D = \frac{24}{\text{Re}} + \frac{3}{\sqrt{\text{Re}}} + 0.34 \quad (2.18)$$

For Reynolds numbers less than 0.3, the first term in Equation 2.18 predominates, and substitution of this drag term into Equation 2.17 yields Stokes' law:

$$\omega = \frac{g(\rho_s - \rho)d^2}{18\mu} \quad (2.19)$$

where μ is the fluid viscosity.

Equation 2.19 describes the fall velocity of discrete spherical particles in still water and it is applicable when particles settle as individual entities, and there is no significant interaction with neighbouring particles. In a dilute suspension of particles flocculation may occur. Flocculation refers to particles that coalesce, and in so doing increase in mass and settle at a faster rate. This process is particularly important when particles in the flow are cohesive, as some sewer sediments are. Flocculation may also be enhanced by turbulence in the flow, as this increases the likelihood of particles coming into contact with one another. Under other flow conditions, however, turbulence may cause large particles to break up.

At higher concentrations of the suspended sediment inter-particle forces are sufficient to hinder the settling of neighbouring particles. The particles tend to remain in fixed positions with respect to each other, and the mass of particles settles as a unit. A solids-liquid interface develops at the top of the settling mass. This is referred to as hindered settling.

The effects of settling in flowing fluids are discussed in the context of settling tank models, beginning at section 2.4.4.2.

2.4.3.3 The Concept of Critical Bed Shear Stress

Historically, theories of sediment transport have assumed that a critical bed shear stress τ_c must be exceeded to initiate particle movement. Such a critical shear stress is referred to as the incipient (threshold) motion condition, below which the particles will be at rest.

It is convenient to relate incipient motion to easily measured time-averaged properties of the whole flow, such as mean bed shear stress ($\tau_0 = \rho g R s_f$) or velocity. Hjulström (1935) produced an empirical threshold curve that related the entrainment velocity to sediment diameter. The curve predicted that the lowest threshold mean velocity occurred for well sorted 0.2 - 0.5 mm sands, while higher critical velocities were needed to entrain larger, heavier gravel and pebbles and the smaller cohesive clays.

The mean bed shear stress criterion of Shields (1936) recognised that critical bed shear increases with particle size, but also depends on the roughness of the bed. A dimensionless critical shear stress θ_c , was defined as:

$$\theta_c = \tau_c / (\rho_s - \rho) g d \quad (2.20)$$

The critical bed shear stress was found to be a function of the grain Reynolds number.

Where the mean bed shear stress is inappropriate, it is possible to calculate local bed shear stress from the velocity distribution in the turbulent boundary layer. The approach outlined below was applied by Ellis (1992) to predict the distribution of bed shear stresses in a laboratory model storage chamber.

When water enters a channel, the velocity distribution across the channel section, owing to the presence of boundary roughness, will vary with the distance over which the water travels in the channel, as shown in Figure 2.3.

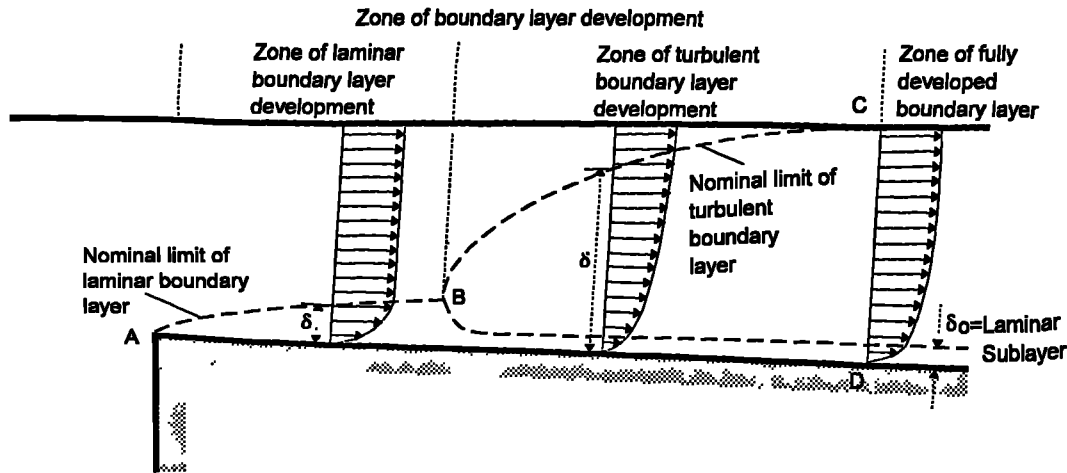


Figure 2.3 Development of the boundary layer (after Chow, 1959)

In the channel, the effect on the velocity distribution due to boundary roughness is indicated by the line ABC. Outside the surface represented by ABC the velocity distribution is practically uniform. The region inside ABC is known as the boundary layer and its thickness is designated by δ . A common definition is that the thickness δ is the magnitude of the normal distance from the boundary surface at which the velocity is equal to 99% of the free stream velocity, which the velocity distribution curve in the boundary layer approaches asymptotically. At the beginning of the flow in the channel the flow is entirely laminar and a laminar boundary layer is developed along the channel surface, as shown by the curve AB. The velocity distribution in the layer is approximately parabolic. As the water travels further along the channel, the flow in the boundary layer will eventually change to turbulent (point B). Downstream from B a turbulent boundary layer is developed; the velocity distribution in this layer is approximately logarithmic.

The surface of the bed is composed of irregular peaks and valleys. The effective height of the irregularities forming the roughness elements is termed the roughness height. Roughness heights range from 1×10^{-5} m for polished glass, up to 0.1 m or more for a natural river bed. If the roughness height is less than a certain fraction of the thickness of the laminar sublayer, the surface irregularities will be so small that all roughness elements will be entirely submerged in the laminar sublayer. This is termed an hydraulically smooth surface. If the roughness height is greater than the critical value, then the roughness elements will extend their effects beyond the laminar sublayer and disturb the flow in the channel. The surface is then said to be hydraulically rough.

The Prandtl-von-Kármán universal velocity distribution law describes the logarithmic velocity profile in the turbulent boundary layer:

$$u = \frac{1}{\kappa} u_0 \ln \left(\frac{y}{y_0} \right) \quad (2.21)$$

in which u is the velocity, κ represents the von-Kármán constant, y is the normal distance from the solid surface, y_0 is a constant and u_0 is the shear velocity. Von-Kármán (1930) showed that the value of κ may be taken to be 0.4, but Vanoni (1946) and Einstein and Chein (1955) suggested that, based on experimental results, κ decreased with an increase in the suspended sediment concentration. However, Coleman (1981) demonstrated that such a change in the value of κ could be attributed to a misinterpretation of the experimental data, and that κ was essentially constant over a range of flow conditions from those with no sediment in suspension to those carrying a near capacity load. κ is therefore generally assumed to be 0.4.

For a smooth surface the constant y_0 depends solely on the shear velocity and the kinematic viscosity (ν):

$$y_0 = \frac{m_R \nu}{u_0} \quad (2.22)$$

where m_R represents the dimensionless Reynolds number of the laminar boundary layer and is equal to about 1/9 for smooth surfaces.

Substituting Equation 2.22 for y_0 in Equation 2.21, and using $\kappa = 0.4$:

$$u = 2.5 u_0 \ln \frac{9 y u_0}{\nu} \quad (2.23)$$

Equation 2.23 gives the velocity distribution in turbulent flows over a smooth surface.

The bed shear stress, τ_0 , may then be calculated from the bed shear velocity using:

$$\tau_0 = \rho u_0^2 \quad (2.24)$$

where ρ is the density of the liquid.

2.4.3.4 Other Models of Sediment Transport

In the previous section it was suggested that the initiation of sediment transport (or the onset of deposition) is dependent on the bed shear stress. It should be noted that

several authors have rejected the concept of a critical tractive force, largely because of the lack of any standardised definition. The definition of the critical force has varied from a value of bottom stress at which the value of the extrapolated transport rate was zero (Shields, 1936), to the point where movement was first detected visually, and even to a stress at which general movement was observed. Some of the most significant alternatives to the critical bed shear stress concept are outlined below.

Einstein (1942) introduced the concept that bed load transport is governed by the laws of probability. He developed a theoretical bed load transport formula based on the probability that, at a given point on the bed, the lifting force required to overcome the weight of the particle has been generated. This was the first bed load formula which did not involve critical shear, or equivalent.

Yang (1973) approached the problem using the concept of unit stream power, which he defined as the time rate of potential energy expenditure per unit weight of water in an alluvial channel. He described the total sediment concentration as a function of dimensionless effective unit stream power, as follows

$$\log C_T = I + J \log \left(\frac{VS}{\omega} - \frac{V_{*c} S'}{\omega} \right) \quad (2.25)$$

in which C_T is the total sediment concentration in ppm, VS is the unit stream power, $V_{*c} S'$ is the critical unit stream power required at the incipient motion and I and J are constants. For a wide variety of field data, values of I ranged from 4.2 to 5.7, and values of J fell between 0.82 and 2.03. However, Yang also demonstrated that I and J might be derived from fluid and sediment properties.

CIRIA (1994) reviewed a number of sediment transport formulae in an attempt to identify the most suitable ones for the purpose of modelling sediment movement in sewer pipes. In all the equations considered the sediment concentration was expressed as a function of the mean flow velocity, the characteristics of the pipe and the characteristics of the sediment. They compared all the formulae with laboratory data, concluding that the data were best approximated by an equation derived from May *et al.* (1989). The resulting equation, connecting the volumetric sediment concentration, C_v , and the flow velocity, V , at the limit of deposition was:

$$C_v = 3.03 \times 10^{-2} \left(\frac{D^2}{A_f} \right) \left(\frac{d}{D} \right)^{0.6} \left(1 - \frac{V_t}{V} \right)^4 \left(\frac{V^2}{g(s-1)D} \right)^{1.5} \quad (2.26)$$

in which D represented the internal pipe diameter, A_f was the cross sectional area of flow, d was the sediment diameter, g represented acceleration due to gravity and s represented the specific gravity of the sediment. The threshold velocity (V_t) was given by:

$$V_t = 0.125\sqrt{g(s-1)d}\left(\frac{y_f}{d}\right)^{0.47} \quad (2.27)$$

in which y_f is the depth of flow relative to the pipe invert.

The sediment transport equations most widely implemented in current urban drainage quality models are those of Ackers and White (1973), and their subsequent modified forms (Ackers, 1984). The equations are presented below, in the form given by CIRIA (1994).

The rate of sediment movement (C_v) is expressed in terms of the non-dimensional transport parameter:

$$G_{gr} = \left(\frac{C_v R}{d}\right) \left(\frac{A_f}{W_e R}\right)^{1-n_a} \left(\frac{u_o}{V}\right)^{n_a} \quad (2.28)$$

in which R represents the hydraulic radius of flow, W_e represents the effective width of the sediment bed, u_o represents the shear velocity and n_a is a coefficient. All other parameters follow the notation given for Equations 2.26 and 2.27 above.

G_{gr} depends on the mobility of the sediment given by the parameter:

$$F_{gr} = \frac{u_o^{n_a}}{\sqrt{g(s-1)d}} \frac{V^{1-n_a}}{[\sqrt{32} \log_{10}(12R/d)]^{1-n_a}} \quad (2.29)$$

The transport and mobility parameters are connected by the equation:

$$G_{gr} = H_a \left(\frac{F_{gr} - A_{gr}}{A_{gr}} \right)^{m_a} \quad (2.30)$$

where A_{gr} is the value of the mobility parameter at the threshold of movement and m_a and H_a are coefficients. The various coefficients in the above equations are related to the dimensionless grain size:

$$D_{gr} = \left(g \frac{(s-1)}{\nu^2} \right)^{1/3} d \quad (2.31)$$

2.4.3.5 Cohesive Sediment Transport

These sediment transport formulae have been developed for non-cohesive sediments. However, it was suggested in section 2.3.2 that sewer sediments exhibit cohesive-like properties. The movement of cohesive sediments is therefore discussed below.

Extensive research into cohesive sediment behaviour has been carried out in the context of coastal and estuarine environments. For examples of sediment transport models that apply to cohesive sediments refer to Delo (1988) and Parchure and Mehta (1985). Effects of flocculation, deposition, consolidation, erosion and slump of sediment were incorporated into a three-dimensional numerical cohesive sediment transport model developed by Nicholson and O'Connor (1986). The model was applied to Grangemouth Harbour, part of which is subjected to heavy siltation, and accurate predictions of average monthly deposition were obtained.

Clearly, the effects of cohesive-like behaviour and consolidation need to be included in a sewer sediment transport model. Crabtree *et al.* (1991) proposed a two phase system for the transport, deposition and erosion of sewer sediments, whereby there is:

1. Transport and deposition of 'clean' sediments using conventional non-cohesive sediment transport theory related to particle settling velocity and bed shear stress conditions during dry weather flows; and
2. Post depositional changes (consolidation, biological action) which lead to the development of a 'dirty' cohesive sediment bed. This will require the use of cohesive sediment transport theory to predict erosion of the bed by the higher bed shear stresses associated with storm flows.

In the light of this recommendation, and given that the thesis was primarily concerned with the process of sediment deposition in storage chambers, further examination of the literature on cohesive sediment transport models was not undertaken.

2.4.4 Modelling Storage Tank Efficiency

2.4.4.1 Introduction

Storage chambers are in many respects similar to the settling tanks used at treatment works to clarify the sewage. Many models of settling tank performance have been developed, and these include theoretically based formulae, regression based methods, and, more recently, mathematical simulation of the dynamic processes.

The measure of a settling tank's performance has been termed its removal efficiency, η , and this has been defined as the proportion of the inflow load that is settled to the chamber bed. The removal efficiency (η) is the proportion of the inflow suspended sediment (SS) that is deposited in the settling basin:

$$\eta = \frac{S_i - S_e}{S_i} \quad (2.32)$$

where S_i and S_e represent the influent and effluent suspended sediment concentration.

2.4.4.2 Surface Load Clarification Theory for an Ideal Basin

The theory was originally developed by Hazen (1904), and expanded upon by Camp (1946), who defined an ideal rectangular continuous flow settling basin as having the following characteristics:

1. The direction of flow is horizontal and the velocity is the same in all parts of the settling zone (hence, each particle of water is assumed to remain in the settling zone for a time equal to the detention period - namely, the volume of the settling zone divided by the discharge rate);
2. The concentration of suspended particles of each size is the same at all points in the vertical cross section at the inlet end of the settling zone;
3. A particle is removed from suspension when it reaches the bottom of the settling zone.

Any particle settling in a moving liquid will move in a direction and at a velocity, with reference to the basin, which is the vector sum of its own settling velocity and the velocity of the surrounding liquid. In an ideal rectangular basin the paths of all discrete particles will be straight lines, and all particles with the same settling velocity will move in parallel paths.

In the design of settling tanks, the usual procedure is to select a particle with a terminal velocity V_c and to design the basin so that all particles that have a terminal velocity equal to or greater than V_c will be removed. The rate, Q , at which clarified water is produced is then

$$Q = AV_c \quad (2.33)$$

where A is the surface area of the basin.

V_c represents the overflow rate, or surface loading rate, in cubic metres per square metre surface area per day. Particles that have a fall velocity of less than V_c will not all be removed during the time provided for settling. Assuming that the particles of various sizes are uniformly distributed over the entire depth of the basin at the inlet, it can be seen from an analysis of the particle trajectory in Figure 2.4 that particles with a settling velocity less than V_c will be removed in the ratio:

$$X_r = \frac{V_p}{V_c} \quad (2.34)$$

where X_r is the fraction of the particles with settling velocity V_p that are removed.

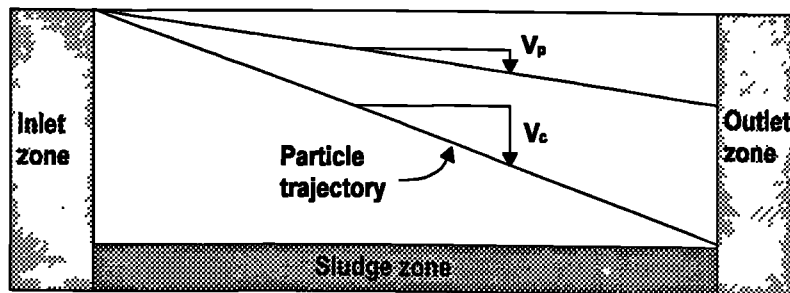


Figure 2.4 Particle trajectories in an ideal rectangular settling basin

In a typical suspension of particulate matter, a large gradation of particle sizes occurs. To determine the efficiency of removal for a given settling time, it is necessary to consider the entire range of settling velocities present in the system, by means of the settling velocity curve (Figure 2.5).

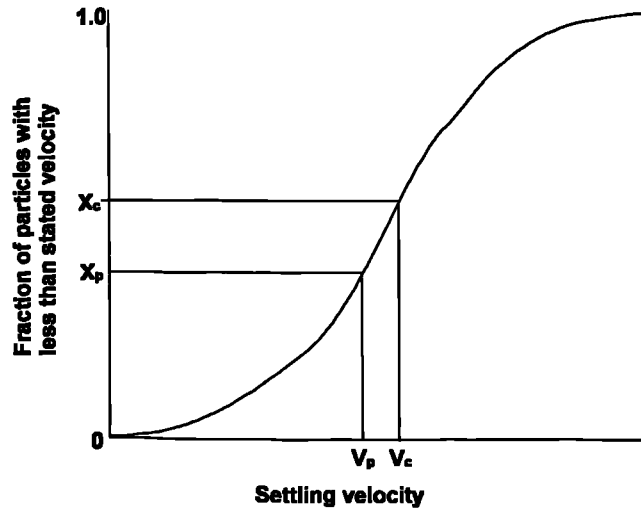


Figure 2.5 Typical settling velocity analysis curve

The total fraction of particles removed is given by

$$\text{Fraction removed} = (1 - X_c) + \int_0^{X_c} \frac{V_p}{V_c} dx \quad (2.35)$$

Ideal settling basin theory leads to two important conclusions (Camp, 1946):

1. For any given discharge, the removal is a function of the surface area and is independent of the depth of the basin, or, the removal is a function of the overflow rate, and, for a given discharge is independent of the detention period;
2. The concentration of suspended matter at any cross section in the settling zone increases with the depth below the surface, and decreases with the proximity of the cross section to the outlet end of the basin.

If an average settling velocity (V_s) is assumed for the suspension, then according to surface load theory the removal efficiency (η) for quiescent conditions is given by:

$$\eta = \frac{V_s}{Q/A} \quad (2.36)$$

However, this expression is only valid under uniform, steady and laminar flow conditions. The EPA (1986) proposed the following methodology to estimate sediment removal under dynamic conditions:

$$\eta = 1 - \left(1 + \frac{1}{n} \frac{V_s}{Q/A} \right)^{-n} \quad (2.37)$$

where n is a turbulence or short circuiting constant that is used to indicate the settling performance of the pond:

- $n = 1$, for poor performance;
- $n = 3$, good performance;
- $n > 5$, very good performance;
- $n = \infty$, ideal performance.

2.4.4.3 Modelling of Storage Chambers in Urban Drainage Quality Models

Both the urban drainage quality models described in chapter 1, MOSQUITO and MOUSE TRAP, model sedimentation in storage chambers using forms of ideal settling theory.

In MOUSE TRAP, the removal of sediments in tanks is described as a function of settling velocity, inflow discharge and surface area, that is, it is determined using surface overflow rate theory, making use of the EPA (1986) formula (DHI, 1994). Once settled the sediments are removed and taken out of the computations. No morphological modelling of the sediment takes place of the deposited sediment, and it is not possible to resuspend this sediment. MOUSE TRAP allows weir and basin efficiencies to be defined. The removal of sediments in overflow structures is described by a removal efficiency factor. The efficiency factor may be modelled as either a constant, a function of discharge, or a complex function of discharge, flow split and CSO type.

MOSQUITO also implements surface overflow rate theory, but only to the extent that separation of sediments at the overflow weir is modelled (Osborne and Shamash, 1993). With MOSQUITO, all of the settled sediment is assumed to be discharged through the chamber and on to treatment and not to remain on the floor of the ancillary structure. Therefore there is no attempt to model the deposition efficiency of the chamber. The model allows the user to input efficiency factors to determine how the sediments and pollutants in suspension are split between the continuation flow and the overflow.

Sensitivity testing of MOSQUITO, carried out by Gent *et al.* (1994), showed that the effect of altering the efficiency factor was significant. Changing the efficiency from 0

to 0.25 decreased the mass spilled by 91% due to the decrease in the concentration of sediment in the spill. The deposition efficiency of the chamber and the separation efficiency of the overflow weir are clearly fundamental to the sediment transport modelling, but there is very little guidance as to the selection of appropriate values. The need for better data in this respect was highlighted in a recent review of UPM modelling tools (Crabtree *et al.*, 1994b).

2.4.4.4 Empirical Regression Equations for Basin Efficiency

Many empirically derived models for the removal efficiency of a settling basin have related basin performance exponentially to the surface overflow rate, using equations of the form:

$$\eta = \eta_0 e^{-c_s q} \quad (2.38)$$

where η is the removal efficiency for SS, η_0 is the removal efficiency for SS under quiescent conditions, q is the surface overflow rate and c_s is a constant.

Smith (1969), for example, produced values of $\eta_0 = 0.82$ and $c_s = 0.0088$ respectively. Tebbutt and Christoulas (1975) demonstrated that this type of relationship could be applied to several sets of data, but with wide-ranging values for both η_0 and c_s . They suggested that the values of η_0 and c_s reflected differences in the SS concentration, the nature of the solids and their size distribution, flocculation and temperature, and concluded that universal values of η_0 and c_s were likely to be unobtainable.

Most other workers have suggested that both hydraulic loading and initial SS concentration can affect removal efficiency. The total SS is of relevance since flocculation will be more significant at higher SS levels. It is also possible that higher SS concentrations contain a greater proportion of settleable solids and there is some evidence that for sewage in the UK there is a fairly constant non-settleable SS concentration of around 150 - 200 mg/l (Tebbutt and Christoulas, 1975).

Data from a number of full-scale plants was examined by Escritt (1956) who derived a relationship relating effluent SS to retention time and inflow SS with the aid of constants depending upon the tank design, the nature of the suspension and other, unspecified, factors. His model took the form:

$$S_e = \frac{S_i}{c_1 t_r^{n_2} \log S_i} \quad (2.39)$$

where t_r is the retention time (hours), $n_E = 1/c_2 \log S_i$, c_1 is a constant, approximately 1.1 and c_2 is a constant, approximately 10. Equation 2.39 may be rearranged to give efficiency:

$$\eta = -\frac{1}{c_1 t_r^{n_E} \log S_i} \quad (2.40)$$

The relationship published by CIRIA (1973) was developed from the analysis of data obtained from a number of large sewage works in the London area and which covered retention times of 2-10 hours.

$$\eta = (0.00043 S_i + 0.51)(1 - e^{-0.7 t_r}) \quad (2.41)$$

When used in the CIRIA optimising model the maximum value of the first bracket in Equation 2.41 is limited to 0.90 to prevent removal efficiencies in excess of this value which was considered to be a practical limit.

Tebbutt and Christoulas (1975) incorporated the suspended solids concentration into Equation 2.38, and suggested that the regression should take the form

$$\eta = \eta_0 e^{-[(b/S_i) + c_s q]} \quad (2.42)$$

where b is a constant.

They suggested that values of $\eta_0 = 0.955$, $b = 265$ and $c_s = 0.0021$ fitted pilot plant data in the range 200 - 600 mg/l. They concluded that the effect of hydraulic loading was small when compared with inflow SS.

In contrast, Garde *et al.* (1990) have recently suggested that the influent suspended sediment concentration is not of significance, and that the efficiency is instead a function of the basin geometry and the ratio ω/u_0 , that is, the particle settling velocity, ω , divided by the shear velocity in the settling basin, u_0 . u_0 represented the mean shear derived from the bed slope. They derived the relationship

$$\eta = \eta_0 (1 - e^{-k_2 L/y_f}) \quad (2.43)$$

where y_f is the depth of flow, L is the length of the settling basin and k_2 and η_0 are constants related graphically to ω/u_0 .

The regression based models described above are based on sediment removal relationships which are derived empirically, from observed influent and effluent data. Nevertheless, the utilisation of these models on different systems, or configurations, or both, is always susceptible to concern about their applicability. Models derived from a mathematical understanding of the processes occurring within a settling tank have the advantage of allowing detailed simulation of performance and have the facility to vary the physical configuration in order to study the performance under alternative conditions. Numerical models of settling tank performance are described in the following section.

2.4.4.5 Mathematical Modelling of Sediment Behaviour in Storage Tanks

The first hydraulic models for settling basins were presented by Dobbins (1944) and Camp (1946). Although the models were based on the assumptions of ideal settling basin theory, turbulence terms were included.

Dobbins (1944), presented a general turbulent settling equation for the two-dimensional case corresponding to the condition of steady uniform flow in the central region of a wide channel, in the form

$$V' \frac{\delta c}{\delta x} = \epsilon_y \frac{\delta^2 c}{\delta y^2} + \left(\omega + \frac{\delta \epsilon_y}{\delta y} \right) \frac{\delta c}{\delta y} + \epsilon_x \frac{\delta^2 c}{\delta x^2} \quad (2.44)$$

in which V' is the velocity at a point, ϵ is the kinematic turbulence coefficient, ω is the settling velocity of the particulate, c is the concentration of sediment in suspension at a point, x is the horizontal distance in the direction of flow and y is the elevation above the surface of the bed material. Although a numerical solution to Equation 2.44 was presented, it required too many simplifications to be generally applicable.

Later approaches have rejected the concept of the ideal basin and recognised the need to compute the flow field (if only in two dimensions). More importantly, computational resources have developed to such an extent that complex numerical models could be solved without recourse to undue simplification.

Larsen (1977) probably made the most significant contribution to the science since Hazen, initially through extensive field measurements of point velocity and concentration. Previous field measurement programmes had been restricted to tracer studies that yielded concentration versus time curves at the outlet. His work included the development of an ultrasonic current meter that operated at velocities from

0.062 m/s upwards and at sediment concentrations of up to 2 kg/m³. He examined seven different settling basins, observing that the flow at the inlet was generally three dimensional, and that the main settling zone was characterised by a bottom current zone and a return current zone, rather than by ideal settling tank flow.

Larsen's second important contribution was to put forward the idea of using a mathematical model to describe settling basin behaviour and to enable comparisons of different geometries to be made. He claimed that "only the boundary geometry is reasonably simple". Nevertheless, he presented a simplified two-dimensional model of the settling zone which yielded promising results, concluding that only a two-phase (i.e. fluid and particulate) three dimensional model could produce optimum solutions.

Takamatsu *et al.* (1974) developed a dispersion model based on the hydrodynamics of fluid flow in a clarifier, assuming no stratification. They considered the scouring of deposited material to be one of the most important factors affecting settling basin efficiency. The overflow rate theory ignores the effects of scouring of deposit on the design depth of a sedimentation basin. They showed that optimal depth and surface area do exist for a rectangular clarifier and how these could be found in actual design practice. Unfortunately their technique was too cumbersome to be accepted in actual design practice (Alarie *et al.*, 1980).

Shiba and Inoue (1975) extended the work and presented a series of simple relationships that could be easily used and understood. They reduced the unsteady state diffusion equation for sediment particles (of Takamatsu *et al.*, 1974) from a three-dimensional distributed parameter form to a simple, one-dimensional lumped-parameter equation. Empirical relationships, based on studies of a scale model rectangular clarifier, were developed to relate a scouring parameter to a longitudinal turbulent diffusion coefficient that was related to local fluid velocity. Although several numerical examples were considered, no empirical observations were presented in support of the model.

Using a similar approach to Shiba and Inoue, Alarie *et al.* (1980) developed a simulation model for circular settling tanks. Their model was tested against suspended sediment concentration data derived from two identical primary clarifiers operating in parallel at the Waterloo Water Pollution Control Plant. They selected an hourly sampling rate in order to reflect the short term dynamic response of clarifiers in real time. Sediment settling characteristics were determined for four influent sediment types, and the appropriate velocity then applied to the model. Reasonable results were obtained from the simulation. However, they found the selection of four groups

insufficient to describe the huge range of short term temporal fluctuations in influent quality, and concluded that this inadequacy accounted for the small deficiencies observed in their simulation. Their model predictions were shown to improve upon those made by a selection of regression models that included those of Smith (1969) and Tebbutt and Christoulas (1975).

Imam *et al.* (1983) developed a two dimensional finite difference numerical model to simulate the settling of discrete particles in a rectangular clarifier operating under neutral density conditions. The model was divided into a hydrodynamic submodel and a transport submodel, as they believed that the solids concentrations in primary clarifiers were low enough to justify decoupling the solid and liquid phase simulations. The velocity profiles predicted by the hydrodynamic submodel compared favourably with a laboratory model tank in which velocity measurements were made using an LDA system. The model also predicted eddy sizes effectively. A constant eddy viscosity turbulence model was used and validation of the sediment transport model, using dye tests, suggested that improved results would have been obtained if a more sophisticated turbulence model (k - ϵ , for example) had been used. Other authors, including Schamber and Larock (1981) and Celik *et al.* (1985) implemented the two equation k - ϵ turbulence model in their clarifier simulations.

In the numerical model presented by Stamou *et al.* (1989) the flow was approximated to be steady, two-dimensional, of single phase character and unaffected by density currents. The flowfield was then used as input to a suspended sediment transport model. However, the model was an improvement over previous numerical models because it employed the k - ϵ turbulence model which allowed a more realistic prediction of the velocity and turbulence diffusivity distribution, and also because it accounted for differential sizing by solving concentration equations for individual fractions of different particle sizes. Model predictions of the flow and sediment concentration were compared with field measurements made in the primary settling tank of the wastewater treatment plant in Sarnia, Ontario. Although very good predictions for the suspended solids concentration field and the removal efficiency were obtained, it was suggested that better predictions of the flow field would require three-dimensional simulation.

Ostendorf (1986) presented a simple, approximate, hydraulic model that bypassed computer based numerical simulation and did not address the issue of sediment transport. Instead, the inlet, settling and outlet zones were characterised as turbulent jet, uniform and converging flow fields respectively. Using existing analytical

solutions and turbulent jet data, he generated a composite, independently calibrated set of velocity profiles in the three zones that compared favourably with real data. He suggested that the turbulence intensity was attributable to the inlet jet and not generated by bottom and wall friction, as suggested by Takamatsu *et al.*, (1974).

McCorquodale *et al.* (1988) experimentally studied the effect of geometry on the hydraulics of rectangular settling tanks in the absence of density currents and suspended solids. They used LDA to measure turbulent velocities in 13 different tank configurations, also concluding that the major hydraulic processes in rectangular clarifiers could be represented by relatively simple jet mixing concepts.

Sediment driven density currents result when the fraction of suspended solids in the influent is sufficiently high to cause this inflow bulk fluid to flow as a bottom current under the less dense clarified fluid. Larsen (1977) found sediment driven density currents to be the distinguishing feature of his flow measurements in secondary clarifiers at sewage treatment plants. In this case the suspended sediment concentration of influent activated sludge varied between 0.86 and 5.0 kg/m³. The flow of density currents into natural lakes and reservoirs has been modelled extensively. The earliest numerical model capable of predicting these sediment-induced density currents for flow conditions in a typical secondary clarifier was presented by DeVantier and Larock (1987). The formation of a strong bottom current and a free surface return current were correctly predicted and the predicted sediment concentrations convincingly reproduced the sediment concentration profiles found by Larsen (1977).

In order to provide detailed measurements of the flow field characteristics in settling tanks, Lyn and Rodi (1990) used a two channel laser doppler system to monitor the mean flow and turbulence characteristics at the entrance of a model rectangular settling tank. They commented that LDA, with its relatively high spatial resolution and its ability to handle high turbulence and reverse flows is especially appropriate for the study of the hydraulic properties of settling tanks without suspensions. They examined the effect of one and two-sided deflectors placed in the path of the inlet stream with flow conditions of constant depth and discharge. Flow through curves for both types of deflector were shifted to the right, when compared with the case with no deflector, indicating increased hydraulic efficiency. Although the flow through curves for both types of deflector were similar, flow and recirculation patterns differed markedly. Of particular relevance is the fact that three dimensional effects were strong and exhibited a complex vertical as well as a complex plan flow structure.

2.4.4.6 Implications for Storage Chamber Modelling

Although it is clear that many parallels exist between settling tanks and storage chambers, there are several important differences that need to be considered:

1. Inlet velocities are generally lower in settling tanks, and hence the levels of turbulence are far lower;
2. Settling tanks are usually geometrically far simpler than storage chambers - although it is clear that the flow patterns in both are three dimensional in character;
3. Flows into settling tanks are relatively constant in time, while the inflows into storage chambers are highly transient. Lessard and Beck (1991) suggested that four modes of behaviour for an off-line storage tank could be identified: fill; draw; dynamic sedimentation and quiescent settling. On-line chambers are subject to the full range of flows, from low dry weather flows up to storm events.

The comparisons listed above imply that some caution should be used in transferring settling tank models to storage chambers. Despite these reservations, the above discussion concerning the numerical modelling of settling tanks has highlighted several points which are of direct relevance to the task of modelling storage tanks. These are:

1. Both field and laboratory studies have shown that the flow fields are complex and three dimensional. Surface overflow theory is an oversimplification and accurate modelling of the flow field is essential for valid efficiency prediction;
2. The techniques of computational fluid dynamics have successfully been applied to predict the flow fields;
3. Sophisticated turbulence models (such as k- ϵ) are essential for accurate simulations; constant eddy viscosity models are insufficient;
4. Where the influent suspended sediment concentrations are high, then the effects of density-driven flows must be considered. In practice this means that the solution of the hydrodynamic and sediment transport equations must be coupled;
5. The transport of sediments is better modelled where a range of size fractions can be considered.

This substantial body of research would clearly form an excellent basis from which to develop a numerical model for storage chamber performance. Equally, as the intention

in this thesis is not to develop an application specific numerical model, but to investigate the possibilities of applying generic CFD software to storage chamber design, the discussion presented above provides a foundation for this research.

3. Laboratory Set-Up

3.1 Introduction

As the main elements of the laboratory system were similar for several of the experiments described in later chapters, it is appropriate to describe the whole system at this point. Details of the specific testing programmes, and of alterations to the set-up described here are given where appropriate. In section 3.2 the basic chamber configuration is described in full, along with detail of the flow control facility, and the outflow penstock control. Section 3.3 is concerned with the model sediment, its properties, the method of input and the laboratory measurement of its concentration. The techniques that were used to measure the velocity distribution in the chamber are detailed in section 3.4.

3.2 The Model Chamber

3.2.1 Configuration

Plate 3.1 shows the model chamber which was constructed from clear perspex, and had internal dimensions 2.0 m long by 0.972 m wide and 0.47 m deep. In later experiments the chamber depth was increased to 1 m, as shown in Figure 3.1. The base of the chamber was horizontal and the inverts of both the inlet and outlet pipes were level with the chamber base. The inlet was 0.19 m in diameter, while the outlet diameter was 0.15 m.

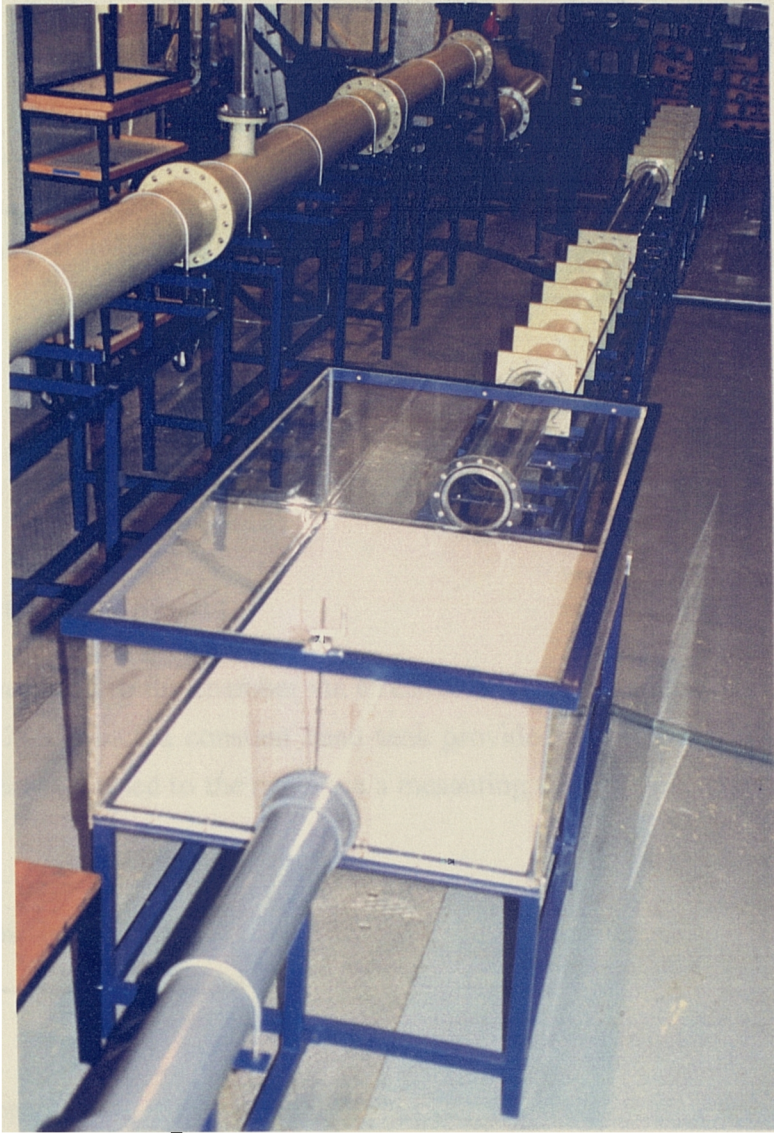


Plate 3.1 The laboratory model storage chamber

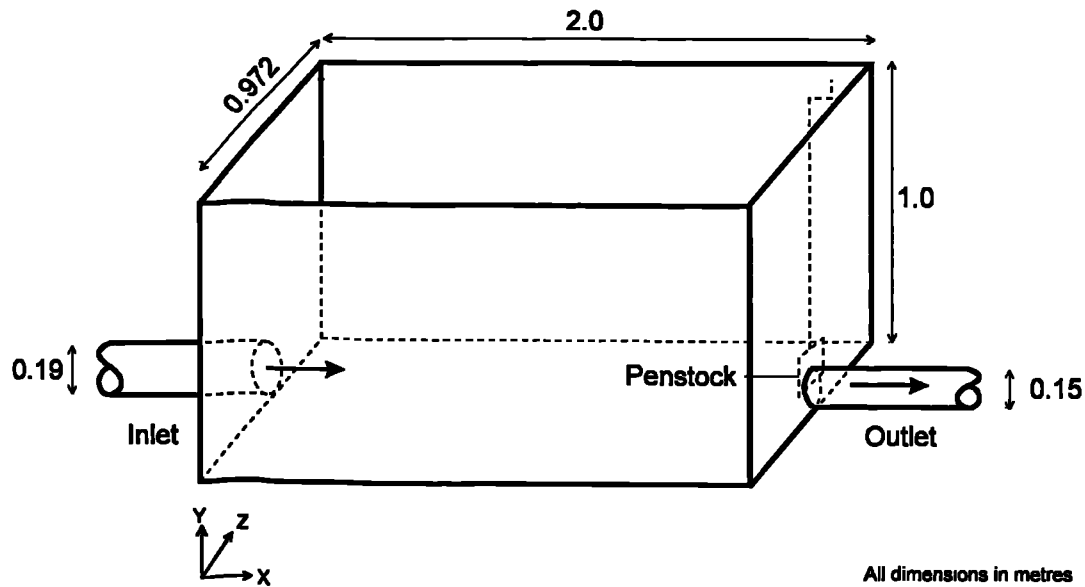


Figure 3.1 The laboratory model chamber

3.2.2 Water Supply System

Water was supplied to the chamber via a recirculating system, illustrated in Figure 3.2 and Plate 3.2, in which a constant head tank provided the inflow to the model, with the waste being returned to the sump via a measuring tank.

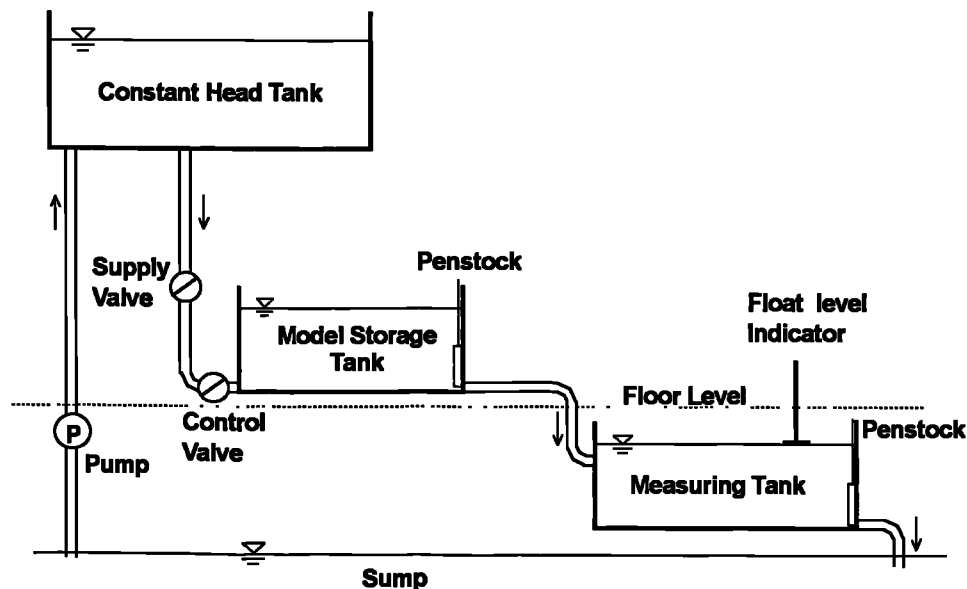


Figure 3.2 Laboratory set-up



Plate 3.2 The laboratory system

In Plate 3.2 the constant head tank is coloured light grey and situated centrally at the top of the picture. The dark grey pipe which leads from this tank and passes horizontally right across the picture carries the inflow to the model chamber. As the supply pipe drops vertically to the laboratory floor, the supply valve (orange handle) and the control valve (green) may be seen. The model chamber appears in the foreground of the picture. The measuring tank is located beneath the laboratory floor and is therefore not visible in the photograph.

The measuring tank was used to estimate the flowrate volumetrically. When the outlet to the measuring tank was closed, the water level rose, pushing upwards a float housed in a stilling pond. The top of the float was visible above floor level, and the

rate at which it rose, given that the plan area of the measuring tank was known, was used to determine the flowrate.

From the measuring tank, water passed down into the sump, from which a pump continuously recharged the volume of the header tank. The system was capable of supplying a maximum of 60 l/s. Flow from the header tank to the experimental chamber was controlled via two butterfly valves, a manually operated main supply valve and a Fisher controls pneumatically operated 150 mm control valve. Both valves are shown in Plate 3.3. In all the laboratory experiments the main supply valve was fully opened and the flow into the chamber was regulated using the control valve.

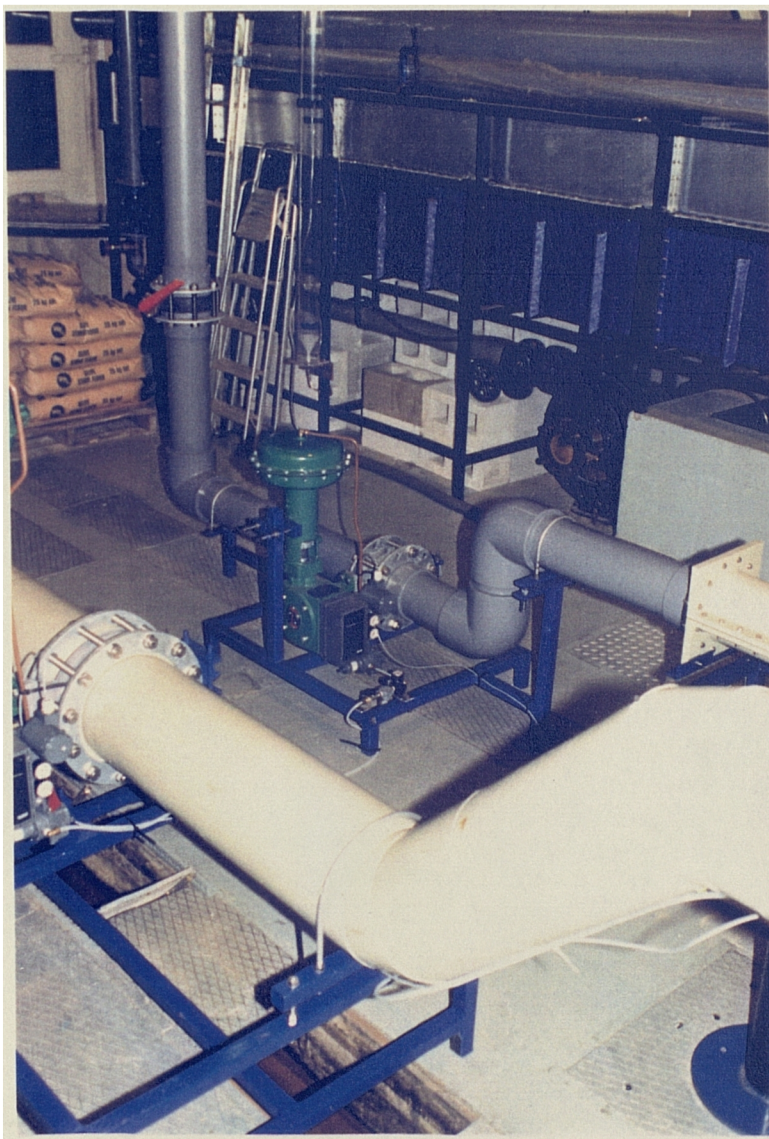


Plate 3.3 The control valves: main supply valve (orange handle) and computer controlled pneumatic valve (green)

3.2.3 The Control Valve

Dedicated computer software was used with the laboratory chamber for both real time control of inputs, such as flow or sediment, and for the real time logging of data supplied by external monitors, for example, turbidity probes.

To operate the control valve, the software produced a digital signal which was converted via a digital to analogue converter card in the computer into the current supplied to the valve. The valve was completely shut at a current of 4 mA, and 100% open at 20 mA.

In order to use the software to control the flow of water into the model chamber, it was necessary to establish a calibration relationship between the degree of valve opening (the signal from the computer) and the resultant discharge. This was achieved by opening the control valve in small stepped increments, starting from 0% open, and measuring the flowrate at each step, until the maximum required discharge, or 100% open had been reached. Because the valve characteristically supplied a slightly lower flowrate for a given position when it was being closed to that supplied during the opening stages, the calibration procedure was completed with measurements made at regular stages as the valve was being closed. With a butterfly valve, a certain amount of movement must occur before any flow actually passes through it. For the valve used in this study, flow was only detected once the valve opening exceeded 5%. A typical calibration curve, of percentage valve opening against flowrate is given in Figure 3.3.

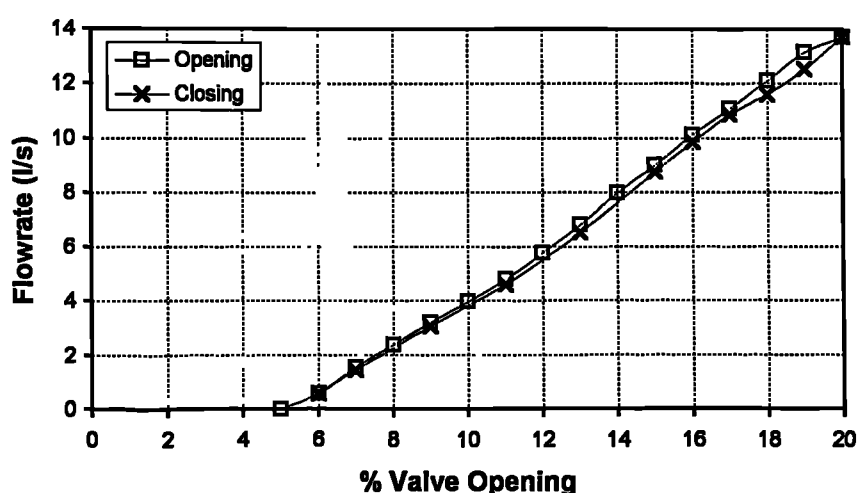


Figure 3.3 Control valve calibration

The calibration relationship was stored for future use, making it possible then simply to select a flowrate, or a time-varying inflow hydrograph, which the software then converted into an appropriate analogue signal to the valve. In Plate 3.4 a typical screen display from the HYDRO4 control software is illustrated. In this particular case two valves are being controlled to deliver a time-varying flow into the chamber.

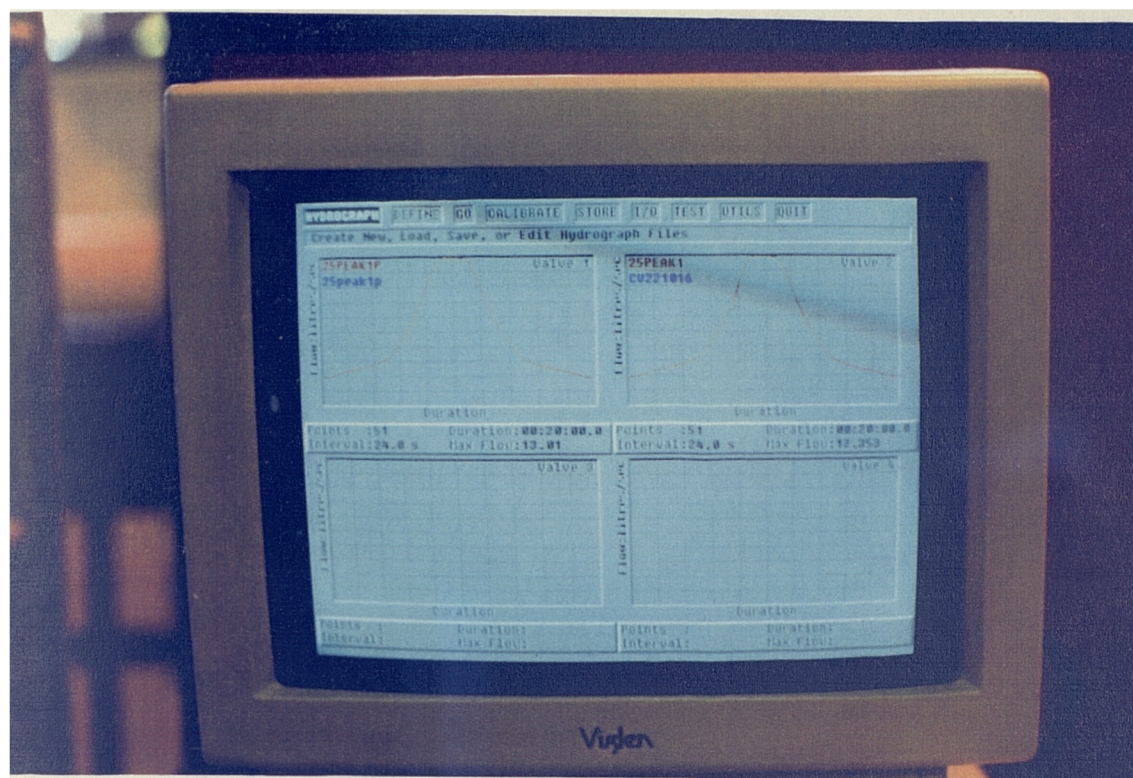


Plate 3.4 HYDRO4 - the control software

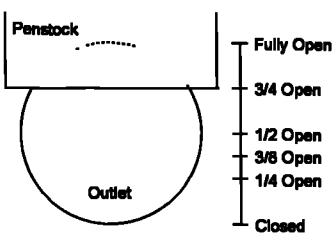
3.2.4 Outlet Head/Discharge Relationships

In addition to real-time control of the inflow to the model chamber, it was possible to adjust the outflow penstock to control outflow discharge. The size of the outlet was adjusted using a rectangular perspex penstock gate. In addition to fully open and fully closed, four penstock positions were selected. The orifice height and area for each position is given in Table 3.1.

The relationship between the depth of flow in the storage chamber and the outflow discharge was established for each of these penstock positions. Each was derived from a series of steady flow tests, in which head and flowrate were measured. For each increment in the flow setting the depth of flow in the chamber was allowed to equilibrate for several minutes in order to ensure that the flow was steady, i.e., inflow and outflow were equal. Head of water above the base of the chamber was measured

using a Vernier point gauge. This was positioned on the central chamber axis, two thirds of the distance downstream from the chamber inlet. Flow measurements were made using the measuring tank, as described above. For each outlet gate position, a series of regression relationships were identified, corresponding to different discharge conditions, and these are illustrated in Figure 3.4.

Table 3.1 Orifice depth and area for selected outflow gate positions

| Outflow Gate Positions | Gate Position | Depth (mm) | Area (mm ²) | % Open |
|---|---------------|------------|-------------------------|--------|
|  | Open | 150.0 | 17672 | 100.0 |
| | 3/4 Open | 112.5 | 14217 | 80.4 |
| | 1/2 Open | 75.0 | 8836 | 50.0 |
| | 3/8 Open | 56.3 | 6053 | 34.3 |
| | 1/4 Open | 37.5 | 3455 | 19.6 |
| | Closed | | | |

When the head in the chamber was below the bottom of the gate free discharge occurred. This was described by a power law equation of the form

$$Q = k_h H^{n_h} \quad (3.1)$$

where Q is the flowrate, H represents head, and k_h and n_h are constants.

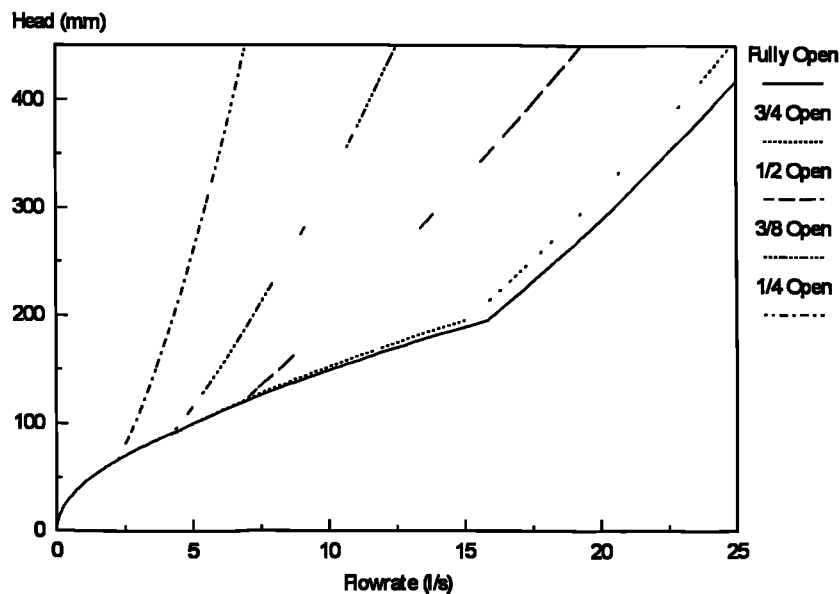


Figure 3.4 Head/discharge relationships for the outlet penstock

Once the head in the chamber exceeded the outlet depth a second power law equation was established, and this was different for each outlet condition. As expected, a decrease in outlet area resulted in a steeper curve. A transition zone between the two curves, of exponential form, was evident in the case of a 1/2 open or smaller outlet. However, for clarity this is not illustrated in Figure 3.4.

Table 3.2 Head/discharge relationships for the rectangular tank

| | Outlet Gate Positions | | | | |
|------------|-----------------------|-----------|-------------|-------------|--------------|
| | Fully Open | 3/4 Open | 1/2 Open | 3/8 Open | 1/4 Open |
| Head (m) | 0 - 0.1 | 0 - 0.1 | 0 - 0.09 | 0 - 0.08 | 0 - 0.065 |
| k_h | 0.765 | 0.765 | 0.765 | 0.765 | 0.765 |
| n_h | 2.152 | 2.152 | 2.152 | 2.152 | 2.152 |
| Transition | - | - | 0.09 - 0.15 | 0.08 - 0.13 | 0.065 - 0.11 |
| Head (m) | 0.1 - 0.2 | 0.1 - 0.2 | 0.15 + | 0.13 + | 0.11 + |
| k_h | 0.258 | 0.212 | 0.0358 | 0.0213 | 0.0111 |
| n_h | 1.709 | 1.624 | 0.778 | 0.673 | 0.592 |
| Head (m) | 0.2 + | 0.2 + | - | - | - |
| k_h | 0.0419 | 0.040 | - | - | - |
| n_h | 0.597 | 0.598 | - | - | - |

Finally, a third relationship was observed in the fully opened and 3/4 open cases. This arose at flowrates greater than about 15 l/s, when the outlet was completely drowned. The equations which describe the relationships are given in Table 3.2. Interpolation between the five sets of equations enabled the outlet penstock to be positioned correctly to obtain a desired depth of flow in the chamber for a given inflow.

3.3 The Model Sediment

It was necessary to find a material for use in the model study that was physically representative of full scale sewer sediments. The selection of an appropriate sediment for the model tests was based on the findings of Ellis (1992). He noted that when crushed olive stone was input into a hydraulic scale model chamber, the location and depth of deposition compared well to that observed in a full scale chamber. Hence, 150 μm crushed olive stone was selected as the model sediment. The properties of this material were further examined to establish the appropriateness or otherwise of using it to represent full scale sediments.

3.3.1 Physical Properties

The physical properties of the olive stone are summarised in Table 3.3, and the techniques used in the assessment are described below.

Moisture content was determined for the sediment dried to 50°C from room temperature, and was found to be 10.6%. Subsequent wetting and drying of sediment at 50°C did not alter the final weight of the dry sediment. However, during the drying process regular mixing of the sediment was required to prevent crust formation. Due to the highly organic nature of the olive stone, burning and weight loss occurred if drying was carried out at temperatures above 80°C.

Table 3.3 Physical characteristics of 150 µm olive stone sediment

| Size fraction | Diameter (µm) | Stokes' settling velocity (m/s) | Specific density (kg/l) |
|-----------------|---------------|---------------------------------|-------------------------|
| d ₂₀ | 28 | 1.94 x 10 ⁻⁴ | } 1.453 |
| d ₅₀ | 47 | 5.45 x 10 ⁻⁴ | |
| d ₈₀ | 88 | 1.91 x 10 ⁻³ | |

Specific Density was determined using the density bottle (small pycnometer) method (BS 1377 (BSI, 1990)), and was found to be 1.453 kg/l for undried olive stone, and 1.495 kg/l for sediment that had been dried at 50°C. In this study, all experiments were undertaken using undried olive stone - thus the relevant density was 1.453 kg/l.

The particle size distribution was determined for undried olive stone using a Coulter Counter. It is important to note that the label '150 µm' actually refers to material with a d₅₀ of 47 µm, and that 150 µm corresponds to the upper limit of the particle size range. In Figure 3.5 the olive stone is compared with suspended sediments from the CSO discharges at Littleborough, with sediment deposits found on the chamber benching, and with natural river sediments (Brownbill, 1992). The olive stone has a narrower particle size range than any of the river or sewer sediments. At the finer end of the distribution the olive stone characteristics are comparable to the natural suspended sediments; however the coarsest olive stone particles are an order of magnitude smaller than the coarsest suspended sediments. However, the olive stone was noticeably more coarse than the river muds and china clay which have been used in other studies. Torfs (1995) used two types of clay as 'artificial' cohesive material:

kaolinite (China clay) and a brown pottery clay that mainly consisted of montmorillonite. For these sediments, nearly 100% and 70% respectively of the particles were finer than 20 μm .

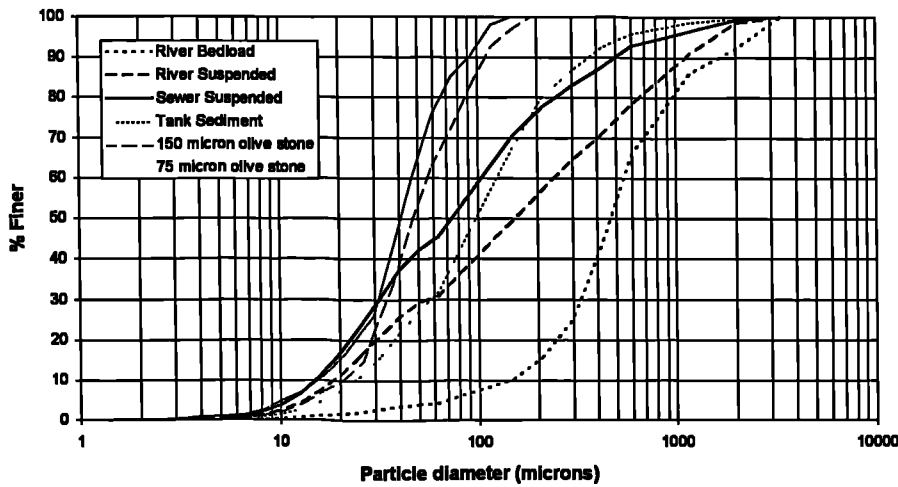


Figure 3.5 Particle size analysis

The settling velocity was estimated from Stokes' law for each of the size categories used in the particle size analysis.

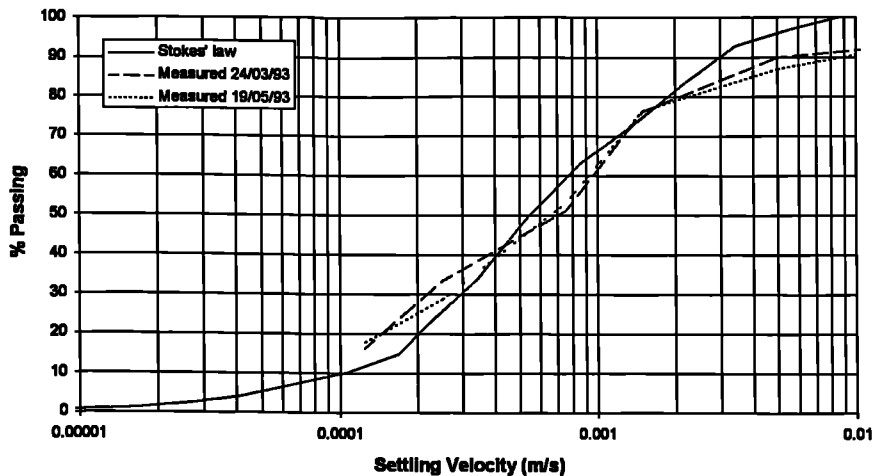


Figure 3.6 Settling velocity analysis for the olive stone

The proceedings of the International Conference on Sewer Solids - Characteristics, Movement, Effects and Control (Ashley, 1995) detailed a number of studies which focused on the measurement of settling velocity. It was evident that a range of techniques are currently in use, but that there is a lack of comparability between them and limited confidence in the physical significance of any of the current techniques. The need to develop a unified approach to the measurement of settling velocity was highlighted as a priority area for future research. With the reservations expressed above in mind, laboratory settling velocity analysis on the olive stone was carried out

by researchers at the University of Abertay, Dundee (formerly Dundee Institute of Technology). The Dundee Institute of Technology/Aston University measurement technique was employed. This is based on the Scottish Development Department (SDD, 1980) approach, and a full description may be found in Arthur (in press).

The laboratory settling velocity measurements suggested a very similar distribution to that which had been calculated through the use of Stokes' law. The two sets of measurements correspond to different batches of olive stone. Settling tests were also carried out at the Catholic University of Leuven, where it was noted that the settling behaviour of the olive stone differed from that of china clay or river muds. Normally the bed level approached a maximum asymptotically over a period of several minutes, and the supernatant liquid clarified. With the olive stone, however, the bed level reached a maximum depth after approximately 5 minutes but further consolidation in the sediment bed was observed over the next few minutes. At the same time, a certain fraction of the olive stone never settled, and the supernatant liquid remained cloudy. Tebbutt and Christoulas (1975) commented that an unsettleable fraction commonly exists in sewage suspensions.

3.3.2 Sediment Scaling

In the following section it is shown that the olive stone sediment is an appropriate scale equivalent of the sediments found in full scale storage tanks.

The difficulties associated with hydraulic scale models are usually concerned with the requirements for geometric, kinematic and dynamic similarity and to reproduce the Reynolds, Weber and Froude numbers simultaneously. For all practical purposes it is impossible to do so, and the engineering solution is usually to use models of such a scale that the important forces involved are accurately reproduced while the secondary forces are only approximately scaled. In the case of storage chambers the free surface gravitational forces are much more important than those due to viscosity (provided that the Reynolds number of the flow is well into the turbulent flow range) and surface tension. It is therefore appropriate to adopt Froudian scaling.

In their consideration of storm sewage overflow efficiency, Halliwell and Saul (1980) argued that the characteristics of the particle can be defined by its diameter and effective density within the fluid, or alternatively by its terminal velocity and its diameter. With respect to the movement of particles, they concluded that the fundamental parameter to model was the settling velocity, ω . For velocity, the Froudian scale relation is expressed by:

$$\left(l_m/l_p\right)^{1/2} \quad (3.2)$$

where l is the characteristic length and the subscripts m and p refer to the model and the prototype respectively. The laboratory chamber may be considered to be a 1:15 scale model of a typical full scale chamber. In this case, therefore, it is required that the settling velocity of the model sediment should be $1/3.87$ of the full scale sediment.

The measurement of settling velocity was discussed in chapter 2, and the inadequacies of the Stokes' velocity were demonstrated. In the case of the olive stone, however, it has been shown that the Stokes' velocity did in fact give a good approximation to the settling velocity measured in a laboratory settling column. The particle size distributions for sediments found in the Littleborough chamber were presented by Brownbill (1992), but settling velocity measurements were not available for these sediments. As a consequence the Stokes' settling velocity distribution was calculated from the particle size distribution with an assumed average density of 1500 kg/m^3 .

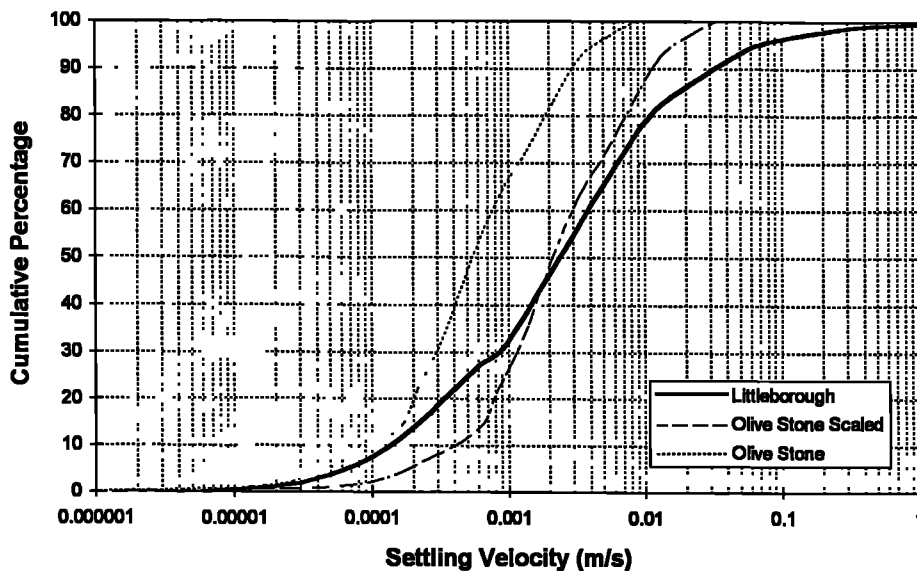


Figure 3.7 Settling velocity comparison

Figure 3.7 shows that when the settling velocity for the olive stone was scaled up the distribution was narrower, but the mean value very closely matched the field data. It was concluded that the olive stone could be used as a laboratory scale representation of the sediments found in full scale chambers.

3.3.3 Sediment Input System

Initially sediment was introduced into the model chamber by means of a series of cups filled with suspended sediment that were poured manually into the input pipe. The

disadvantages of this system were that a very uneven temporal distribution in inflow sediment concentration resulted, and that both preparation and input were time consuming. In order to represent suspended sediment concentrations observed in reality in the inflow to the model chamber, a controlled system of sediment input was developed. This comprised three elements: a completely mixed concentrated suspended sediment reservoir; a variable speed peristaltic pump; and the sediment input pipe in the inlet pipe of the model. These items are described in detail below, and the complete sediment input and monitoring system is illustrated in Figure 3.8 and Plate 3.5.

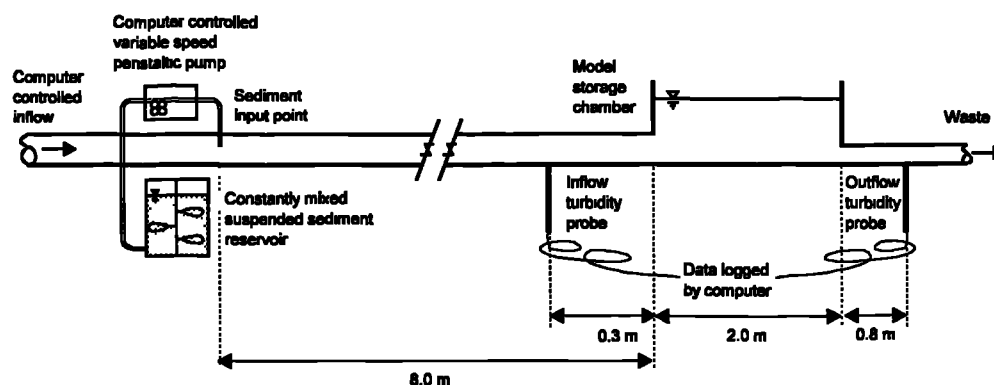


Figure 3.8 Sediment input and measurement system

The sediment reservoir consisted of a perspex cylindrical container, with a capacity of 20 litres. A concentrated mix of olive stone in water (up to 400 g/l) was placed in the container, and continuous mixing was ensured by three paddles fixed to a motor-driven rotating central shaft. The sediment mix was drawn from the reservoir via a small tube inserted into the container side.

A miniature variable speed peristaltic pump (Watson Marlow model no. 503U) was used to transfer the sediments from the reservoir into the laboratory model. The pumping speed was controlled by computer, in exactly the same manner as the flow control, and it was shown that the calibration relationship between output signal and pump speed was unaffected by the sediment concentration in the reservoir, for the range 0 to 400 g/l. In the same way that time-varying flow hydrographs could be defined, time-varying pumping rates were defined to simulate constant concentration, constant load or a first foul flush effect in the sediment input. The sediment concentrations used in the tests were representative of those monitored in full scale tanks (Thornton and Saul, 1986).

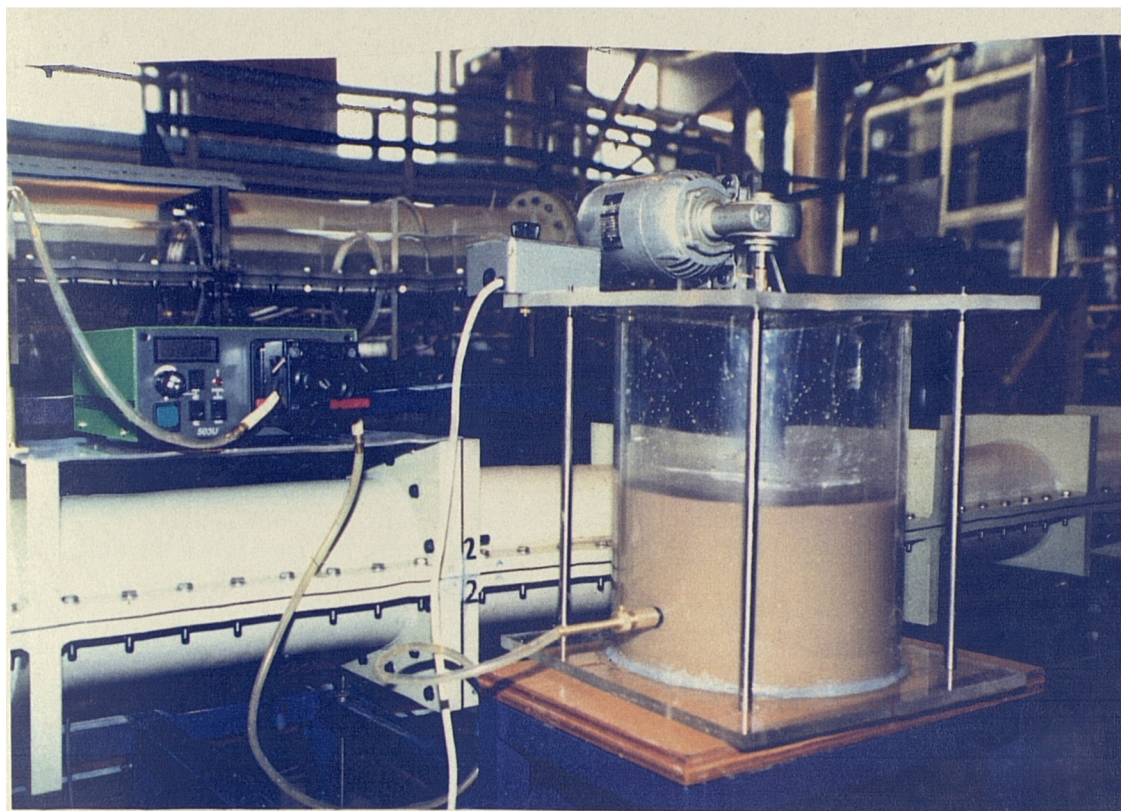


Plate 3.5 Sediment input system: peristaltic pump (left) and constantly mixed suspended sediment reservoir (right)

In order to ensure that sediments entering the model chamber were fully mixed within the inflow, the sediment input point was located 8 m, or 25 D, upstream from the model inlet. Input was via a brass tube inserted vertically into the inlet pipe. The tube had a sealed end, and the suspension was passed instead through six small holes drilled into its downstream facing side.

During sediment input tests the flow was not passed from the chamber into the sump tank for recirculation. Instead, the measuring tank penstock was closed and the flow was pumped to waste. The sump tank was recharged with fresh water. This prevented the sump water from becoming contaminated with olive stone

In order to estimate the concentration of sediment in suspension, continuous measurements of turbidity were made at both the inlet and outlet using ANALITE nephelometer probes. Turbidity is the optical property that causes light to be scattered and absorbed rather than transmitted in straight lines through a sample. This scattering and absorption is caused by particles suspended in the sample media. The scattered light level is proportional to the particulate concentrations and can be measured by an electronic photodetector. With the ANALITE process the scattered light is picked up at 180°. The measurement technique is termed nephelometry and turbidity is measured in Nephelometric Turbidity Units (NTU). Although the actual

measurement of turbidity is a function of the suspended sediment concentration, it may also be affected by other factors that include the particle's size, shape, composition and refractive index. There is therefore no absolute conversion from NTU to mg/l, although the relationship between the concentration of suspended sediment and the measured NTU may be established for a particular experimental set-up.

The main advantages of the ANALITE probes for this type of application is that they are virtually non-intrusive and that the measurements may be logged by means of a continuous output voltage. Each probe was positioned vertically in the base of the pipe and a deflector cap was attached to the probe tip to protect against reflections. In Plate 3.6 the nephelometer probe positioned in the outlet pipe is illustrated, while Plate 3.7 shows the probe located in the inlet pipe, viewed from inside the model chamber. Figure 3.9 shows that the measuring volume was confined to a column above the probe tip, approximately 8 mm in diameter and 25 mm deep.

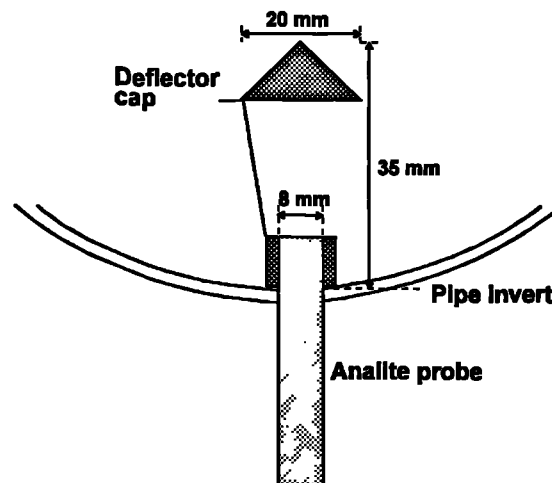


Figure 3.9 The ANALITE nephelometer probe

In order for the turbidity measurements to be representative of the sediment concentration in the whole pipe it was clearly necessary to ensure that the sediments were fully mixed in the flow. In the inlet pipe it was anticipated that adequate mixing would be ensured through the location of the sediment input point some 8 m upstream from the chamber inlet. It was also expected that the high flow velocity at the outlet would ensure that the flow sampled by the outlet probe would be well mixed.

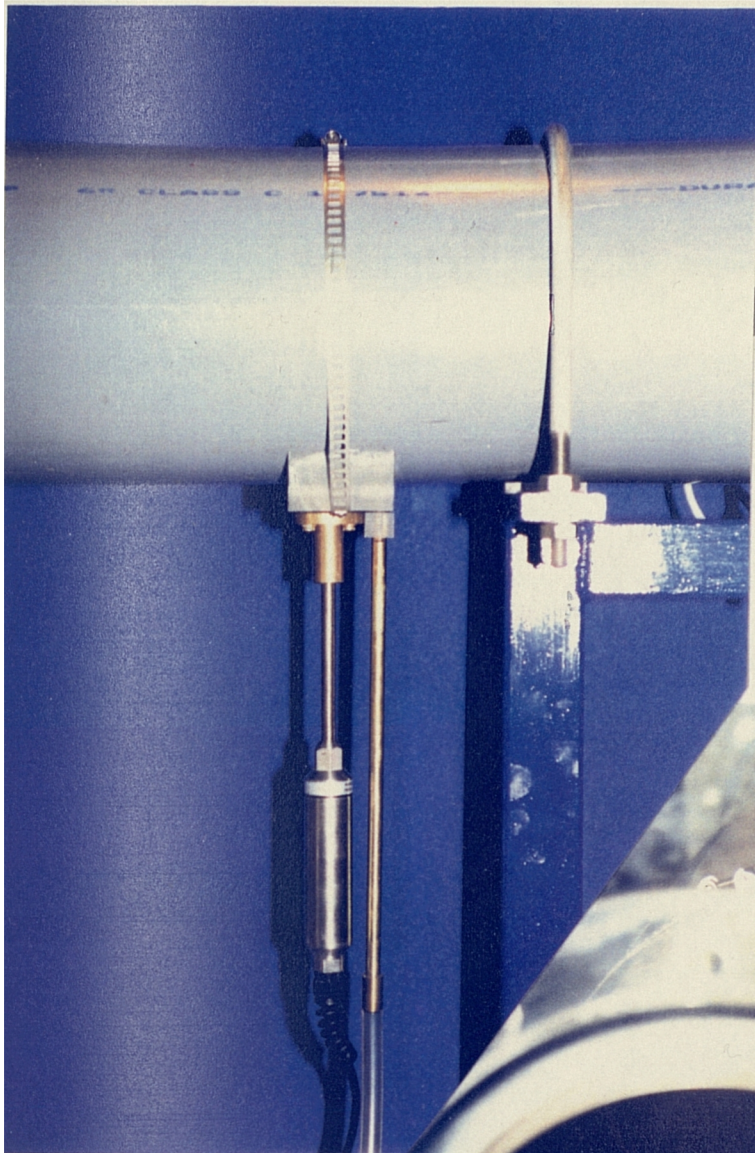


Plate 3.6
Nephelometer turbidity
probe located in the
invert of the outlet pipe

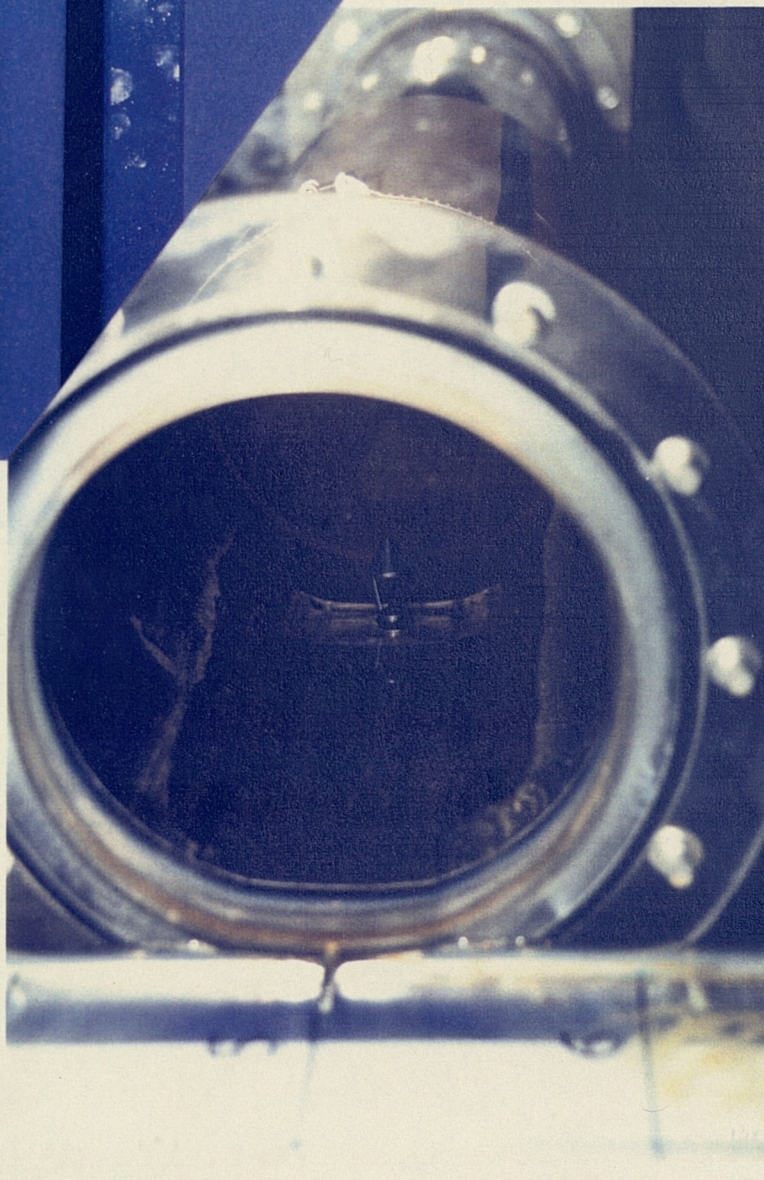


Plate 3.7 View inside
the inlet pipe, showing
the tip of the
nephelometer probe and
the deflector cap

Data from the probes was collected at a rate of 20 samples per second, and 10 second averages of the data were continuously logged throughout each test.

Observations of sediment deposition were made by eye, and also by photographs. In order to map the spatial distribution of sediments, a grid was drawn on the chamber bed. This consisted of 19 regularly spaced grid lines in the longitudinal direction, and 9 grid lines in the transverse direction. The grid spacing was therefore 100 mm longitudinally, and 97 mm across the chamber width. This grid system is illustrated in Figure 3.10, and also in Plate 3.8.

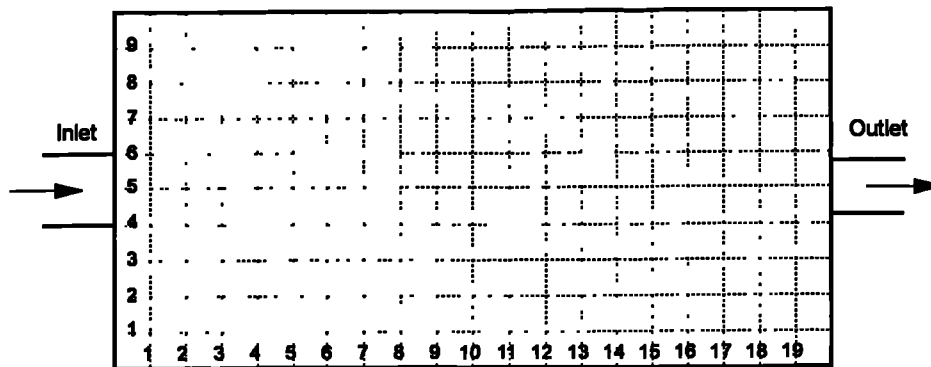


Figure 3.10 Grid system used for deposit mapping

As the depth of deposited sediment was always small (less than 2 mm) no attempt was made to record sediment depth, and distinctions were simply made on a subjective basis between areas of the chamber bed that were covered with sediment and those areas that were 'clean'.

3.4 Velocity Measurement

Figure 3.11 describes the notation that was used in all the laboratory velocity measurements. The longitudinal direction is referred to as the X direction and the velocity component in the X direction is referred to as the u velocity. Likewise, the vertical and transverse directions are named Y and Z, and the velocity components are v and w respectively.

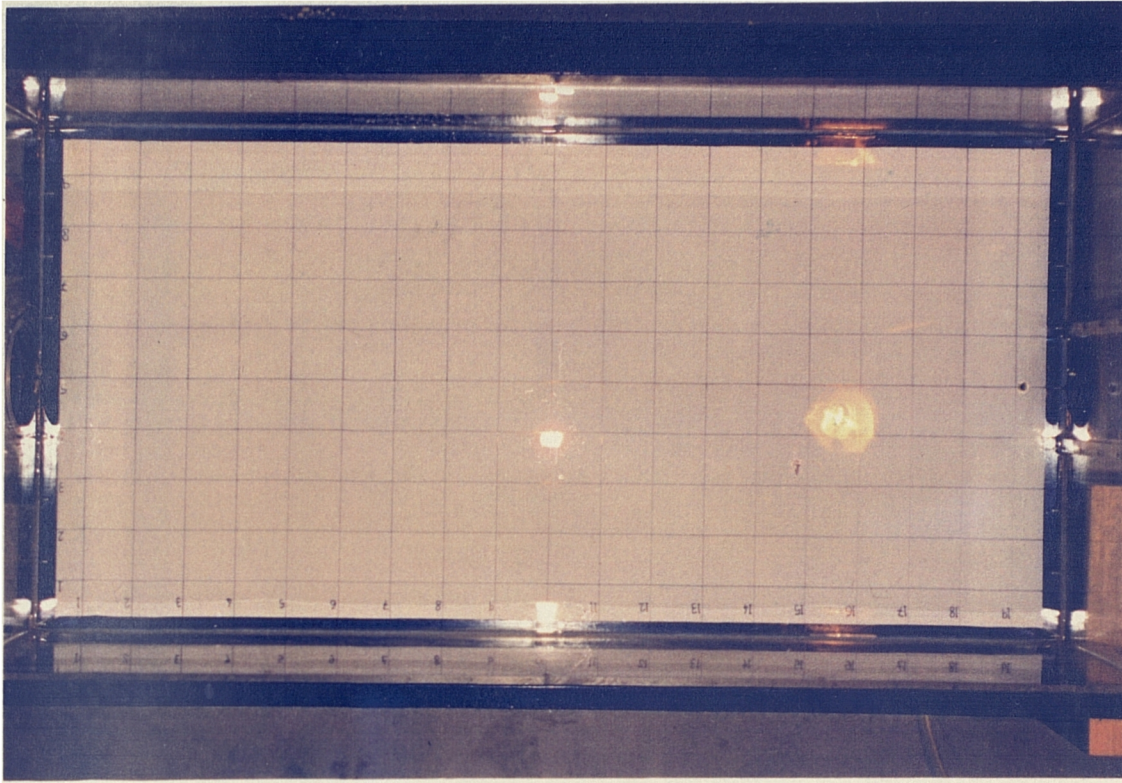


Plate 3.8 Grid used for sediment input tests - chamber inlet is on the left

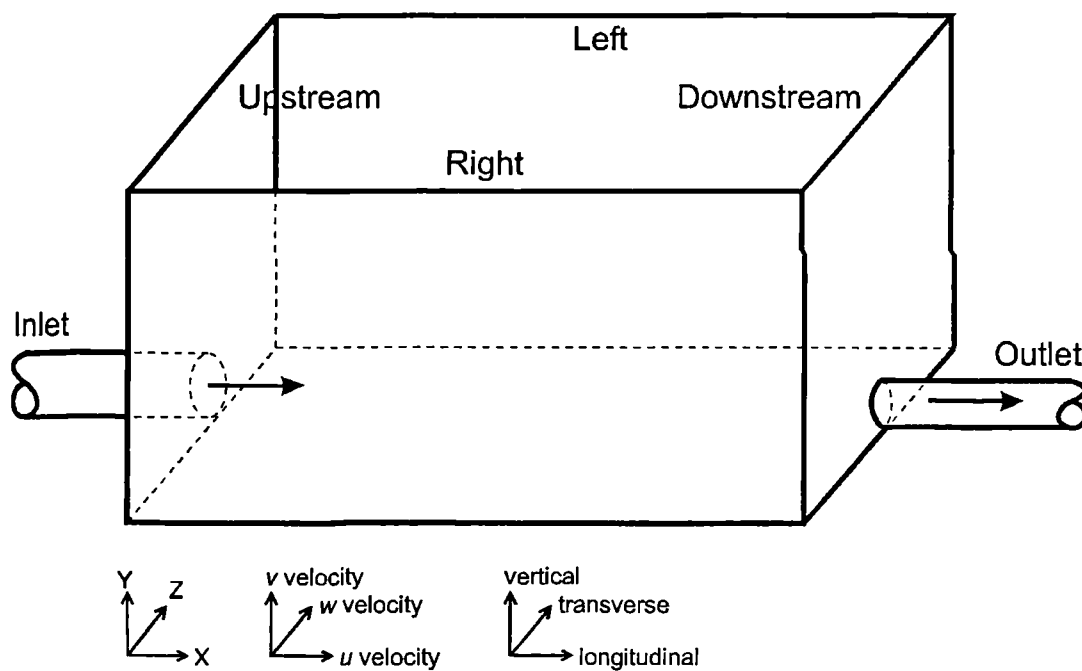


Figure 3.11 Definition sketch for the velocity measurements

The left and right hand sides of the chamber refer to the positions when looking from the inlet to the outlet, while upstream and downstream refer to the inlet and outlet ends respectively.

During the course of the project two types of velocity measurements were made in the model chamber. Initially a Nixon miniature propeller was used. This allowed the u and w velocity components to be estimated. A two-dimensional Laser Doppler Anemometry (LDA) system was used towards the end of the project - this was positioned to measure the u and v velocity components of the flow field.

3.4.1 Miniature Propeller

The velocity distribution in the chamber was measured using a Nixon miniature current propeller which had been pre-calibrated by the manufacturers to relate the frequency of propeller revolutions to the velocity of flow. A supporting frame was constructed that allowed the probe to be positioned at any vertical elevation over a grid of points in the horizontal plane. The probe was aligned in the direction of maximum flow velocity manually, using a small thread that was attached just above the propeller for reference (Plate 3.10). The supporting frame is shown in Figure 3.12 and Plate 3.9.

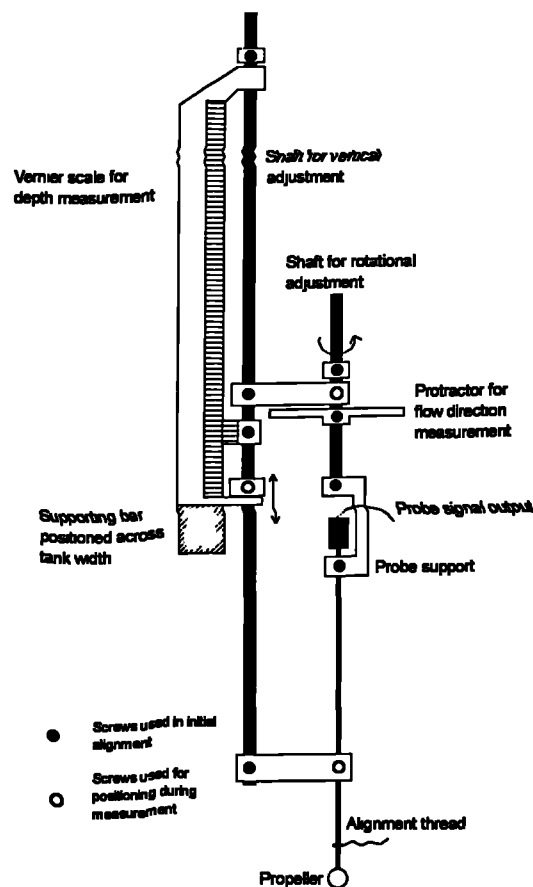


Figure 3.12 Current meter positioning structure

Plate 3.9 Nixon
miniature current
propeller and system
used for support and
alignment

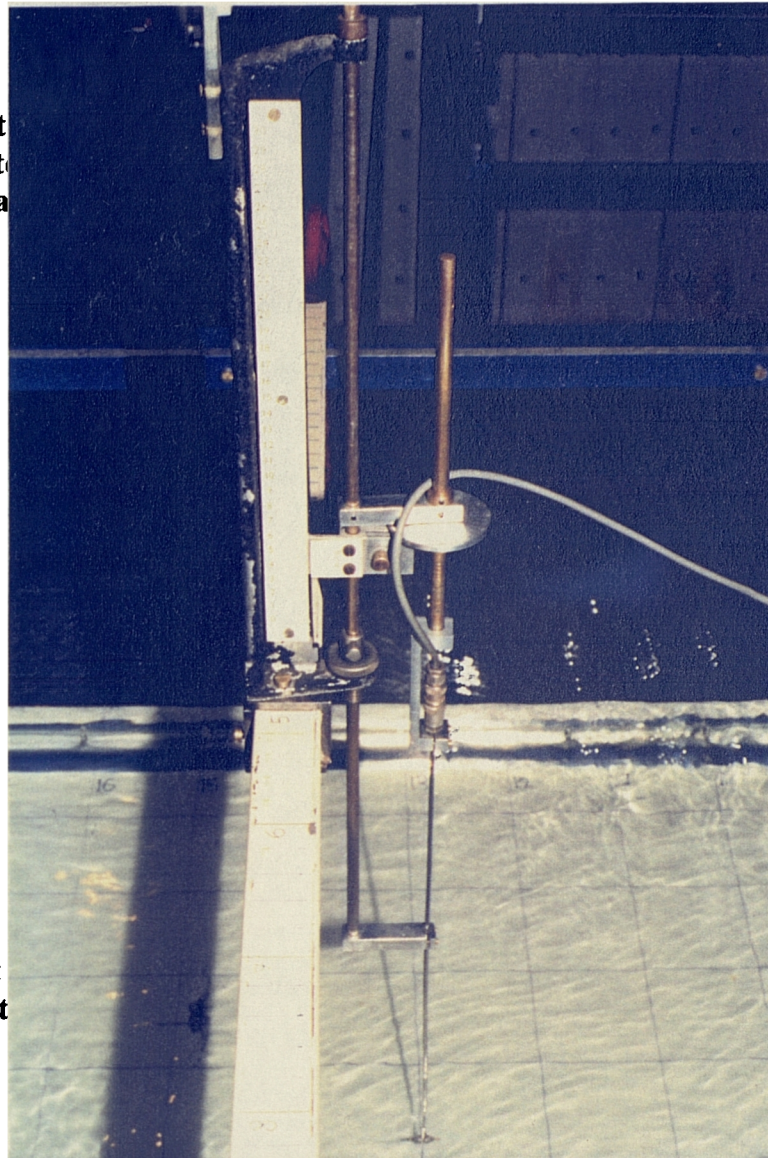
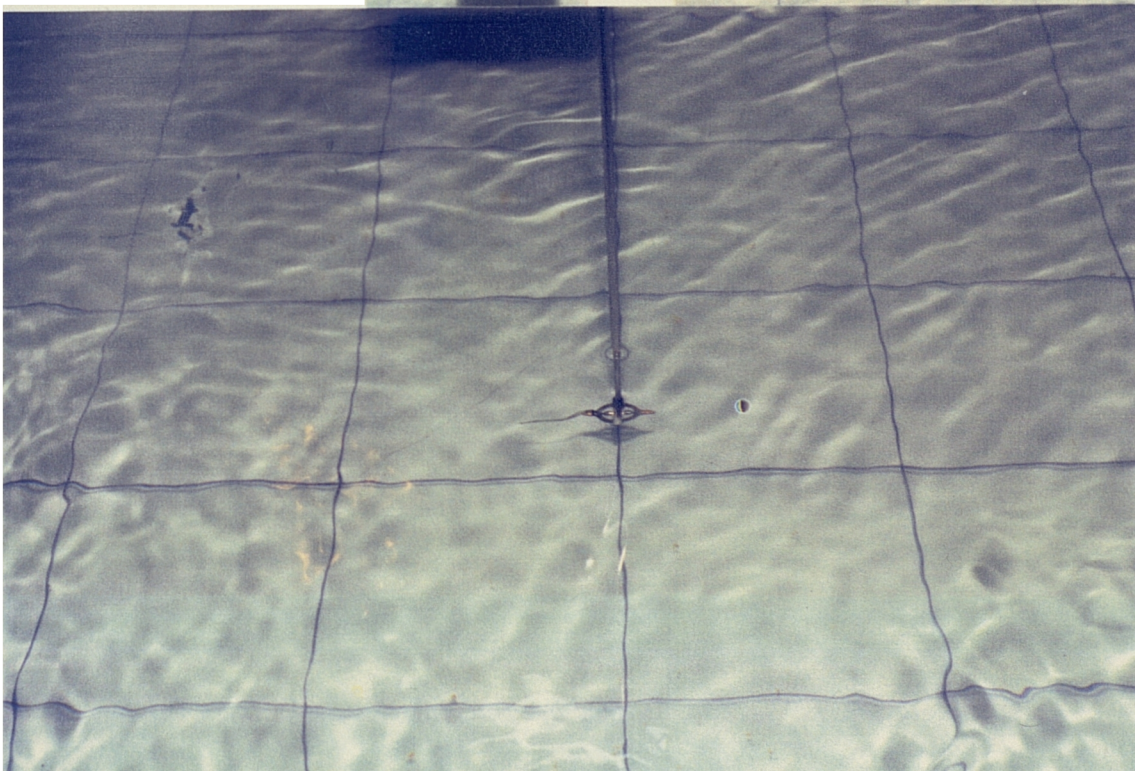


Plate 3.10 Nixon
miniature current
propeller with cotton
thread used for
alignment



Flows in the chamber were highly turbulent, and a continuous operating mode was thought most appropriate. At each measuring point the velocity was averaged over a period of at least 30 seconds, and at points of low velocity a minimum of 300 propeller revolutions were counted. The u (longitudinal) and w (transverse) components of velocity were derived trigonometrically from the recorded velocity and the corresponding probe alignment.

3.4.2 Laser Doppler Anemometry

The current propeller allowed the general characteristics of the flow field to be mapped easily. However, there were several disadvantages to its use, particularly in low speed, turbulent flows:

1. It is intrusive and the measuring volume is quite large;
2. It measures mean velocities and cannot assess turbulence;
3. It needs to be aligned manually with the flow parallel to the axis of rotation;
4. It requires calibration.

Towards the end of the project it was felt that a more precise method of velocity measurement was required. The capacity to measure turbulence, and to map the vertical velocity components, were considered essential. Laser Doppler Anemometry (LDA) systems have been used extensively in laboratory hydraulic model studies. For example, Lyn and Rodi (1990) used a two channel LDA system to monitor the mean flow and turbulence characteristics at the entrance of a model rectangular settling tank.

In an LDA system the flow velocity is calculated from the shift in frequency that occurs when a beam of laser light is scattered by particles in the flow. The details of LDA operation are not presented here, but may be found in a Dantec publication (Dantec, 1983). The main advantage of LDA over other methods of velocity measurement is that it is an optical technique and it therefore causes no physical disturbance to the flow. Further, there is no need for calibration. The main features of the LDA system used in this study are discussed below.

The LDA system consisted of a 50 mW Argon-ion laser operated with two component optics. In this case the LDA system was mounted horizontally at the side of the chamber, such that the orthogonal velocity components in the longitudinal and vertical directions were measured. Frequency shifting facilitated directional discrimination

for both components. This was essential for the laboratory chamber in which reverse flows and circulations were known to occur.

The measuring volume was smaller than that of the current propeller, having in this case a diameter of 0.39 mm and length 10.5 mm. This means that measurements with a high spatial resolution, and in particular measurements close to the solid boundaries such as the chamber bed could be made. When positioned horizontally at the side of the chamber, the measuring volume covered a vertical distance of less than 0.5 mm. This enabled accurate measurements of the vertical velocity gradients close to the bed to be made.

The system was operated in backscatter mode, in which the same optics were used both to transmit the laser beams and to receive the scattered light from which the velocity was determined. This mode of operation had the advantage that there were no potential problems with the location and alignment of the receiving optics. This was particularly useful in the case of the laboratory storage chamber where the width of the flow was large in comparison with the focal length of the lens. The focal length of the front lens was 600 mm, and this dictated the maximum penetration of the laser beam into the flow.

The LDA was mounted on a mechanical traverse which allowed the measuring volume to be positioned accurately in a three-dimensional co-ordinate system. The traverse was located alongside the left wall of the chamber and the extent of movement was such that the whole chamber length and depth, but only the left half of the chamber breadth could be accessed, as shown in Figure 3.13 and Plate 3.11.

The LDA measuring system requires that a certain number of light-scattering particles are present in the flow. These must be small enough to track the flow accurately, yet large enough to scatter sufficient light for the proper operation of the photodetector and the signal processor. The flow was therefore seeded with TIMIRON Supersilk MP-1005. The particles were composed of mica and titanium dioxide. 90% of the particles were below 15 μm in size, and the bulk density was approximately 25g/100ml.

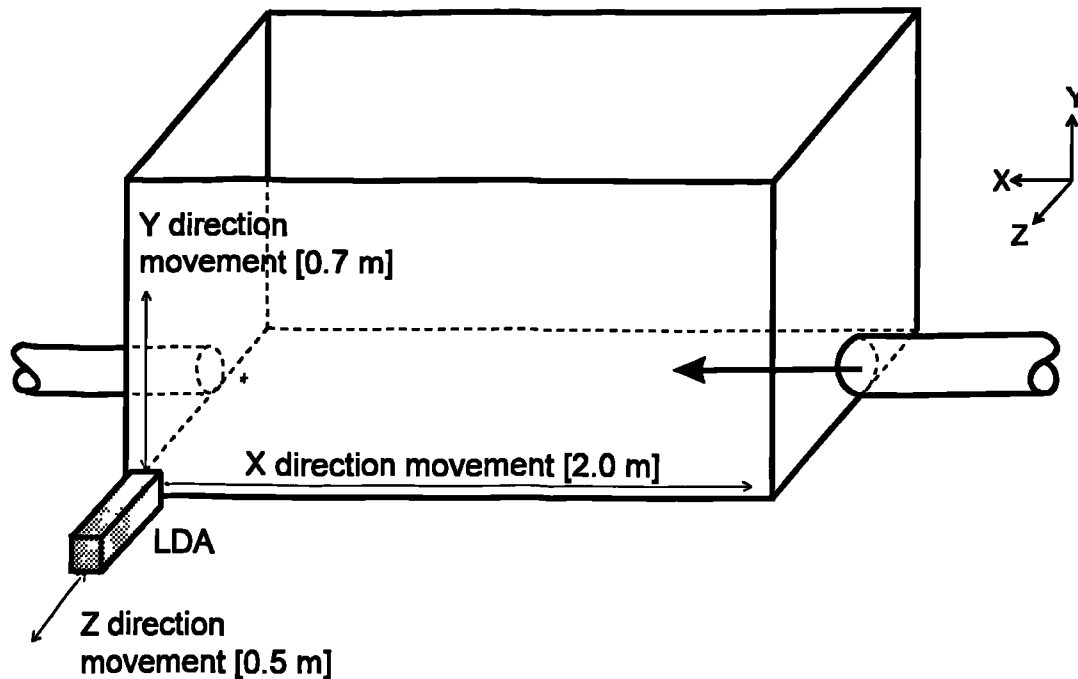


Figure 3.13 Laser traverse range

For safety reasons the top, back and sides of the chamber were encased in a wooden cover when the LDA system was operating. At the front of the chamber light resistant curtains were used. The 'blackout' also reduced possible interference from external light sources that could have affected the LDA.

In order to take velocity measurements very close to the bed, the traverse system allowed the LDA to be inclined at 10° to the horizontal. This is illustrated in Plate 3.12.

3.5 Conclusions

The experimental techniques and apparatus employed in this study have been described. The following two chapters provide details of the laboratory research which was undertaken. The initial phase of experimental research focused on the measurement of the sediment retention efficiency in laboratory scale storage chambers. This work is described in chapter 4. In the second phase of laboratory investigations, detailed measurements of the velocity distribution in the storage chambers were undertaken and these were related to the observations of sediment deposition. This work is described in chapter 5.

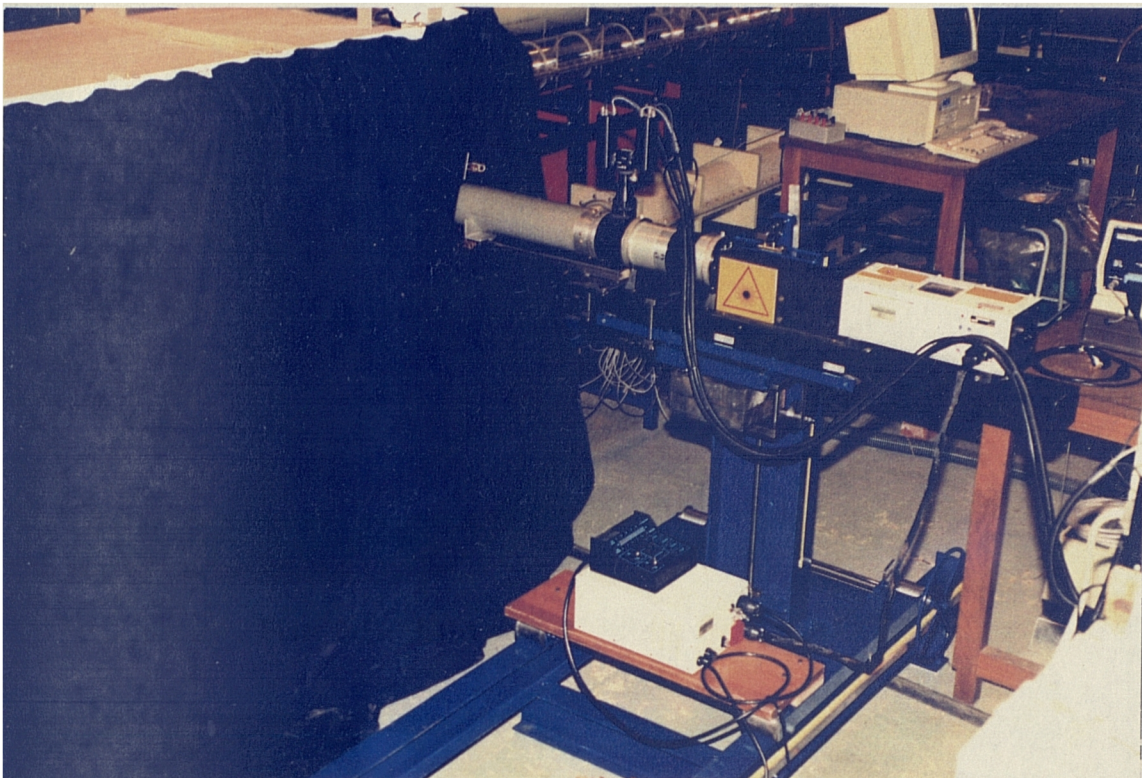


Plate 3.11 LDA system mounted on traverse

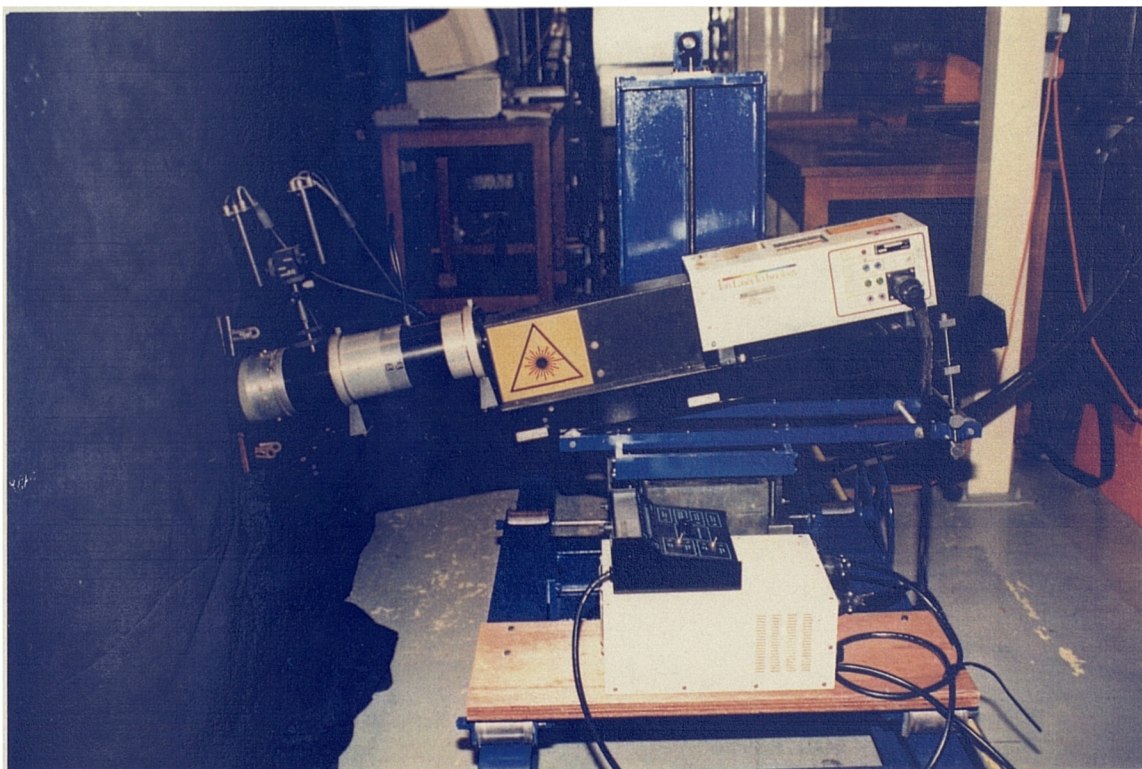


Plate 3.12 LDA system angled at 10° to the horizontal to facilitate near bed measurements

4. Storage Chamber Efficiency

4.1 Introduction

The sedimentation efficiency of a storage chamber is a measure of the proportion of incoming sediment load that settles on to the bed of the chamber. Some measure of a chamber's efficiency is desirable for two reasons: firstly, to enable the engineer to select the most appropriate design for a particular situation; and secondly, to improve the modelling capabilities of sewer flow quality models, specifically those which describe the performance of storage chambers and overflows. The extent of sediment deposition in storage chambers is one variable that is currently not well modelled (Crabtree *et al.*, 1994b).

Various authors have highlighted the importance of the chamber's internal geometry on its efficiency. Saul and Ellis (1992) suggested, for example, that efficiency was affected by the length to breadth ratio, the longitudinal gradient, the gradient of transverse benching, the width of the chamber and the diameter of the dry weather flow channel.

In this study, therefore, a laboratory system was devised which allowed the efficiency of a chamber to be measured. A comprehensive series of tests was planned that would allow the effect of each of these configuration variables to be assessed, both individually and in combination with each other. The laboratory efficiency tests are described in sections 4.2.1 to 4.2.3.

In the course of the experiments it was observed that the location of the sediments deposited to the bed of the chamber was closely related to the flow pattern that developed within the chamber. This observation, around which the remainder of the thesis is based, is introduced in section 4.2.4. In order to develop this theme, the laboratory efficiency test programme was curtailed. However, several suggestions for ways in which the experimental procedure might be improved for future test programmes are presented in section 4.2.5.

In section 4.3, selected sedimentation models are compared with the results of the efficiency tests carried out in the laboratory model chambers, and some conclusions are reached regarding the applicability of such models for storage chamber simulation.

4.1.1 Definition of Efficiency

In settling tank terminology the sedimentation efficiency, η , is defined as the proportion of the inflow sediment load that is settled. Hence, an efficient settling basin ($\eta = 1$) is one that settles all of the sediment that enters the chamber. The use of this term is a little confusing when applied to CSO and storage chamber design, where settlement of sediment onto the bed of the chamber presents problems in terms of the hydraulic performance and maintenance. It needs to be remembered that in such chambers $\eta = 0$ is desirable. The effectiveness of a chamber in achieving $\eta = 0$ is sometimes referred to as its self-cleansing performance. In this study all reference to efficiency implies the sedimentation efficiency and should not be confused with its inverse, the self-cleansing performance.

4.2 Laboratory Investigations of Efficiency

4.2.1 Laboratory Test Program

Initially, the basic chamber configuration described in section 3.2.1 was used for the efficiency tests. All the results presented in both this section and section 4.2.2 refer to the basic chamber configuration, which had a flat bottom and measured 2.0 m long by 0.97 m wide. Alterations to the chamber configuration are introduced for the first time in section 4.2.3.

As detailed in chapter 3, the model sediment used was 150 μm crushed olive stone, which was transferred to the model from a concentrated suspension. The inflow, and the rate of sediment introduction were computer controlled, and the concentration of sediment was measured at the inflow to and outflow from the model using nephelometer probes.

Tests were carried out in the basic chamber at four penstock settings, and at three different flow depths. All tests were carried out under steady flow conditions; the rate of inflow and outflow discharge were equal, and constant, throughout the test. Details of the penstock calibration can be found in section 3.2.4. The flowrate used

ranged from 4.28 l/s up to 17.55 l/s (Table 4.1) and tests were carried out with a constant inflow suspended sediment concentration of 250 mg/l.

Table 4.1 Flowrates used in the efficiency tests (l/s)

| Outlet penstock Gate Position | Flowrate (l/s) | | |
|----------------------------------|------------------------|------------------------|------------------------|
| | Flow depth = 200 mm | Flow depth = 300 mm | Flow depth = 400 mm |
| Open | 16.03 | - | - |
| 1/2 Open | 10.23 | 14.03 | 17.55 |
| 3/8 Open | 7.21 | 9.47 | 11.50 |
| 1/4 Open | 4.28 | 5.44 | 6.45 |

For each test clean water was discharged into the chamber for a 20 minute period prior to the input of any sediment. This was in order to establish steady flow conditions, in which inflow and outflow rates were equal, and to monitor the background turbidity of the water.

A constant concentration of sediment was then injected into the chamber over a 20 minute period ($t = 20$ to $t = 40$ mins.), and at $t = 40$ minutes both the sediment input and the inflow to the chamber were stopped. The monitoring of turbidity continued whilst the chamber drained until empty. This testing regime is illustrated schematically in Figure 4.1 and for each experiment 3 repeat tests were performed.

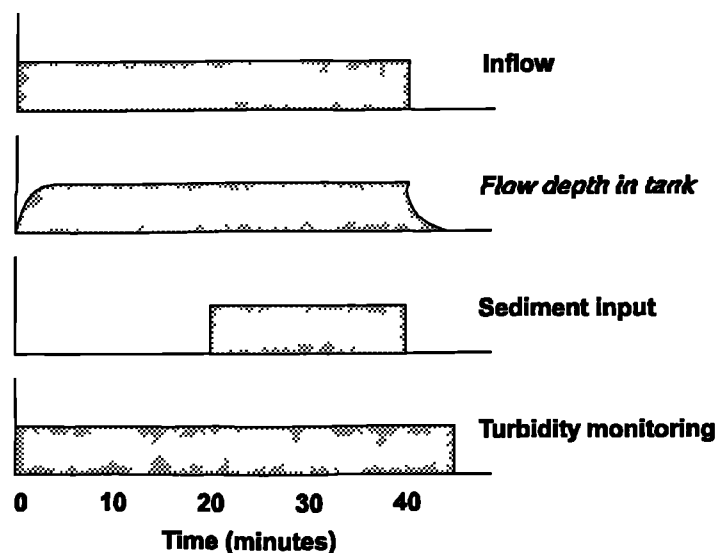


Figure 4.1 Efficiency test regime

Typical traces from both turbidity probes for a steady flow test with a constant rate of sediment input are illustrated in Figure 4.2.

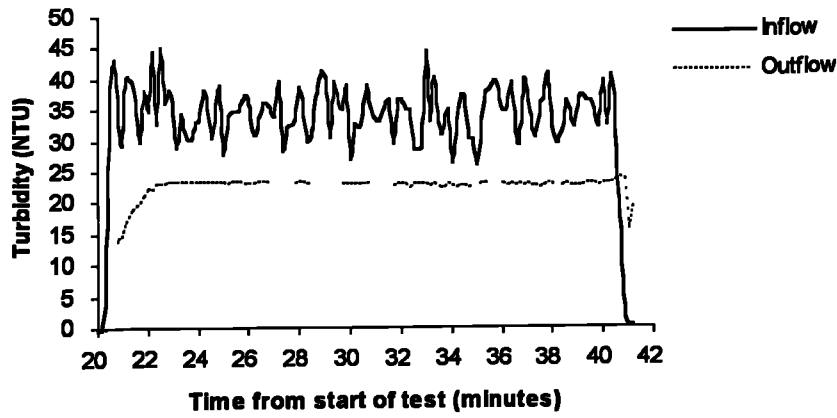


Figure 4.2 Turbidity at the inflow and outflow to the storage chamber

The continuously logged data from the turbidity probes was used to calculate the mean value of turbidity for each 10 second period over the duration of the tests. The raw data was sampled at a rate of approximately 20 measurements per second, so each 10 second mean concentration record was derived from approximately 200 samples. It can be seen that the ten second mean suspended sediment concentration at the inflow fluctuated about its mean value of 34.4 NTU (equivalent to approximately 250 mg/l). Further discussion relating to the accuracy and suitability of the measuring technique is presented in section 4.2.5.

The first part of the outflow trace was of exponential form. The outflow concentration at time t after the start of sediment input (C_t) was therefore generalised by an equation of the form:

$$C_t = C_{\max} \left(1 - e^{-\frac{t}{m}} \right) \quad (4.1)$$

where C_{\max} is the maximum outflow concentration and m is a response time coefficient.

Table 4.2 Values of the response time coefficient m

| | | | | | | | | | | |
|---|------|------|------|------|------|------|------|------|------|------|
| Flow depth (mm) | 200 | 200 | 200 | 200 | 300 | 300 | 300 | 400 | 400 | 400 |
| Penstock setting | Open | 1/2 | 3/8 | 1/4 | 1/2 | 3/8 | 1/4 | 1/2 | 3/8 | 1/4 |
| Cross-sectional mean velocity in chamber (mm/s) | 82 | 53 | 37 | 22 | 48 | 32 | 19 | 45 | 30 | 17 |
| Coefficient m | 0.53 | 0.49 | 0.66 | 0.89 | 0.84 | 0.79 | 1.38 | 0.65 | 0.81 | 1.30 |
| Time to reach transport equilibrium (minutes) | 2.44 | 2.26 | 3.04 | 4.10 | 3.87 | 3.64 | 6.36 | 2.99 | 3.73 | 5.99 |

As detailed in Table 4.2, the coefficient m ranged from 0.486 up to 1.382, with an inverse relationship between the value of m and the average cross-sectional velocity in the chamber. The time taken for the outflow concentration to attain a value equal to 99% of the maximum outflow concentration was calculated using Equation 4.1. These values are also presented in Table 4.2. It can be seen that the maximum period of time taken before a transport equilibrium existed in the chamber was 6.36 minutes. Thus, the sediment concentrations measured in the chamber after this point in time were considered appropriate for the calculation of the chamber's efficiency. For ease of analysis, the time $t = 30$ minutes (i.e. 10 minutes after the start of sediment input) was taken to be the start point for the efficiency calculations in all cases.

For both probes the background turbidity values recorded over the period $t = 10$ to $t = 20$ minutes were subtracted from all the measured data. Efficiency was calculated from the averaged inflow and outflow concentrations (C_{in} and C_{out}) between $t = 30$ and $t = 40$ minutes, using Equation 4.2:

$$\eta = \frac{C_{in} - C_{out}}{C_{in}} \quad (4.2)$$

The results of the efficiency tests for the basic chamber configuration are presented in the following section.

4.2.2 The Effect of Flow Variables on Chamber Efficiency

The results from the full programme of efficiency tests that were carried out on the basic chamber configuration are presented in Table 4.3.

Table 4.3 Efficiency results for the basic chamber configuration

| Outlet penstock gate position | Depth (m) | Flow (l/s) | Inlet velocity (m/s) | Outlet velocity (m/s) | X-section velocity (m/s) | Efficiency |
|-------------------------------|-----------|------------|----------------------|-----------------------|--------------------------|------------|
| Open | 0.2 | 16.03 | 0.565 | 0.91 | 0.0825 | 0.090 |
| 1/2 Open | 0.2 | 10.23 | 0.361 | 1.16 | 0.0526 | 0.182 |
| 1/2 Open | 0.3 | 14.03 | 0.495 | 1.59 | 0.0481 | 0.171 |
| 1/2 Open | 0.4 | 17.55 | 0.619 | 1.99 | 0.0451 | -0.009 |
| 3/8 Open | 0.2 | 7.21 | 0.254 | 1.19 | 0.0371 | 0.226 |
| 3/8 Open | 0.3 | 9.47 | 0.334 | 1.56 | 0.0325 | 0.146 |
| 3/8 Open | 0.4 | 11.50 | 0.406 | 1.90 | 0.0296 | 0.035 |
| 1/4 Open | 0.2 | 4.28 | 0.151 | 1.24 | 0.0220 | 0.646 |
| 1/4 Open | 0.3 | 5.44 | 0.192 | 1.57 | 0.0187 | 0.488 |
| 1/4 Open | 0.4 | 6.45 | 0.227 | 1.87 | 0.0166 | 0.215 |

Each efficiency value is the mean result from three repeat tests. Individual test results, including a plot of the continuous nephelometer probe output, are presented in Appendix C. Figure 4.3 shows plots of the efficiency against flow depth (4.3a), mean cross-sectional velocity (4.3b); mean inlet velocity (4.3c); and mean outlet velocity (4.3d).

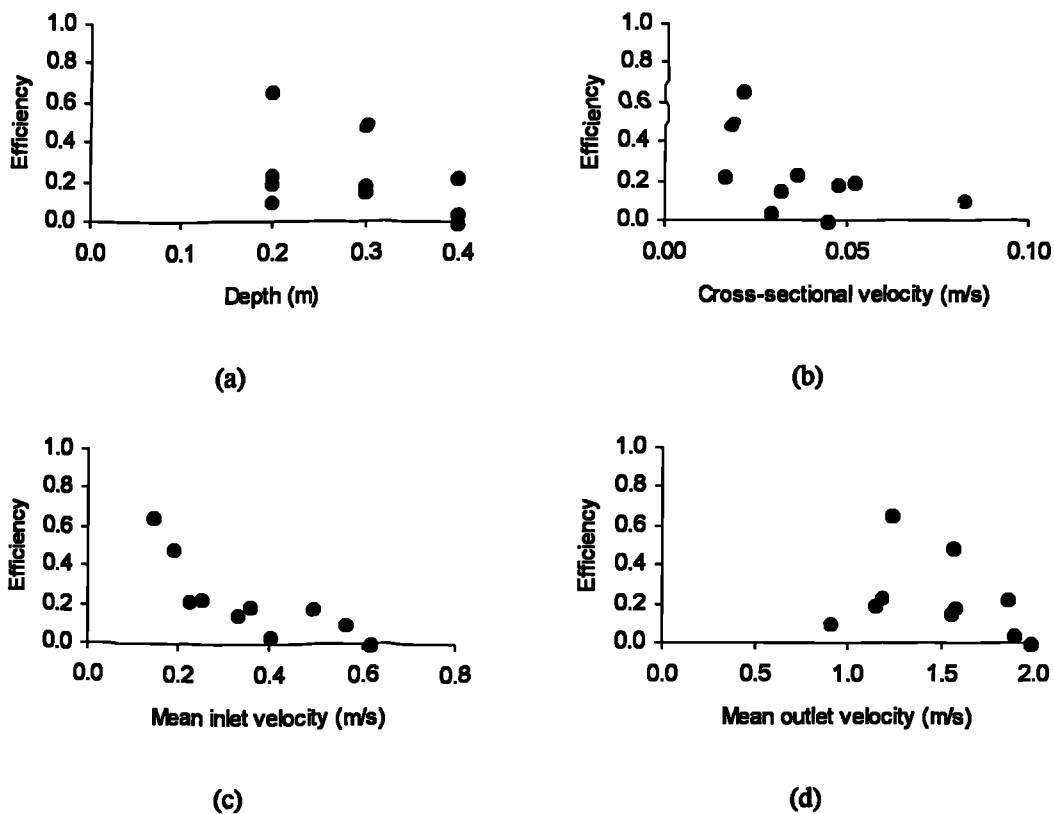


Figure 4.3 The effect of different flow variables on efficiency

It can be seen that the efficiency was essentially independent of both the flow depth and the mean outlet velocity. Some dependence on mean cross-sectional velocity could be identified, but efficiency showed a distinct inverse relationship with the mean inlet velocity (\bar{u}). This observation suggested that the performance of any chamber could be expressed in terms of the relationship between \bar{u} and η . The value of η tended towards unity once \bar{u} fell below 0.25 m/s as the flow conditions within the chamber at lower inlet velocities were more conducive to the settlement and deposition of sediments.

4.2.3 The Effect of Configuration Variables on Chamber Efficiency

A comprehensive series of tests was planned to allow the effect of changes in geometric and hydraulic parameters on the chamber efficiency to be empirically determined. The following parameters were identified for investigation: the length to breadth ratio; the benching gradient; the dry weather flow channel configuration; the longitudinal gradient and the level of inlet surcharge. Following the findings of the previous section, the intention was that each of the tested configurations would be compared with the others by means of its \bar{u}/η plot. This would be derived from a series of efficiency tests undertaken at different inflow rates.

An initial review was undertaken once the results of two geometric variations had been obtained. In the first of the two geometric variations the bed configuration was altered by the addition of benching. The benching had a transverse gradient of 1 in 4, and formed a V-shaped invert, as shown in Plate 4.1. No dry weather flow channel was incorporated into the chamber.

For the second variation, the benching was removed, and the width of the chamber was reduced to 0.8 m. This allowed the effect of a change in the length to breadth ratio from 2.06 to 2.5 to be investigated. In this case there was also a small change in the plan area, and a consequent reduction in the storage volume. Ellis (1992) argued that an increase in the length to breadth ratio and the introduction of transverse benching both acted to reduce chamber efficiency. The results of the efficiency tests on these two variations to the basic chamber configuration are presented in Table 4.4, and the results from all three chambers are compared in Figure 4.4.

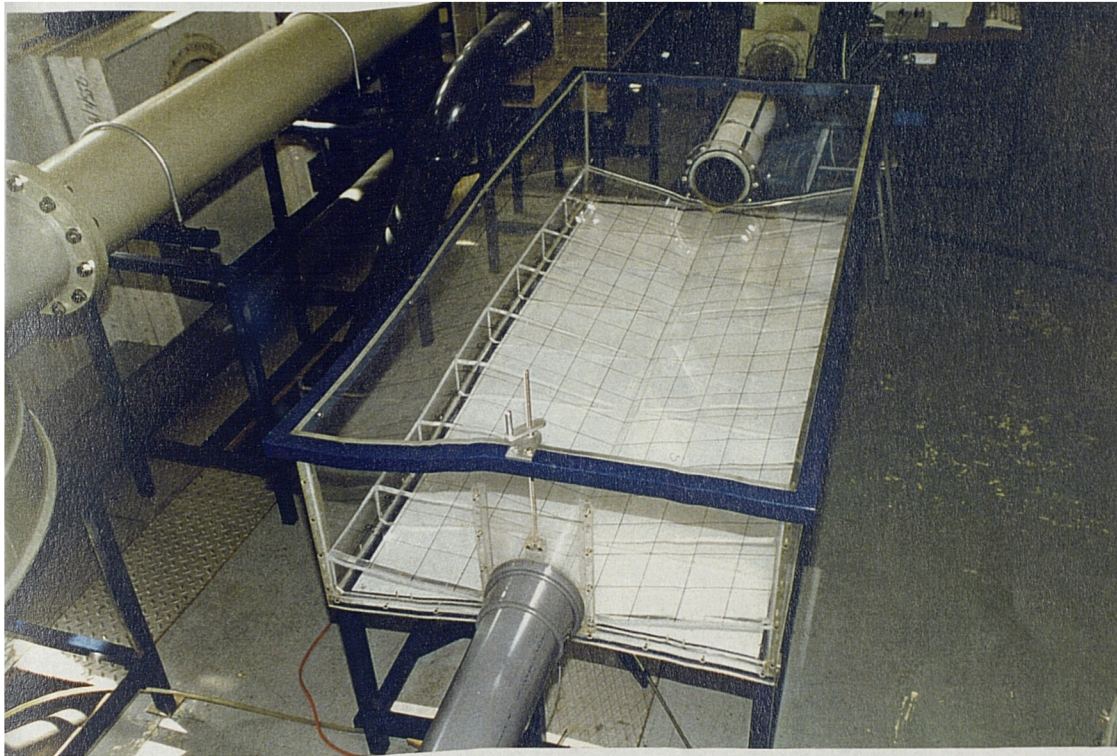


Plate 4.1 The laboratory storage chamber with benching at a gradient of 1 in 4, viewed from the outlet

Table 4.4 Efficiency results for two variations to the basic chamber configuration

| Chamber 2 Benching at 1 in 4 | | Chamber 3 Length to breadth ratio = 2.5:1 | |
|---|-------------------|--|-------------------|
| Mean inlet velocity (m/s) | Efficiency | Mean inlet velocity (m/s) | Efficiency |
| 0.151 | 0.705 | 0.176 | 0.507 |
| 0.192 | 0.409 | 0.212 | 0.599 |
| 0.227 | 0.362 | 0.247 | 0.493 |
| 0.254 | 0.322 | 0.282 | 0.435 |
| 0.334 | 0.198 | 0.317 | 0.327 |
| 0.361 | 0.197 | 0.388 | 0.019 |
| 0.406 | 0.188 | 0.459 | 0.089 |
| 0.495 | 0.149 | 0.564 | 0.026 |
| 0.565 | 0.114 | | |
| 0.619 | 0.134 | | |

In Figure 4.4 the \bar{u}/η plots of the three chambers are compared. This plot shows the mean efficiency results, which were derived from all the tests carried out for each different geometry and flow condition. The data for all three chambers followed a

similar pattern, with the efficiency falling rapidly in response to increases in the mean inlet velocity from $\eta = 0.6$ at $\bar{u} = 0.15$ m/s down to η below 0.25 for $\bar{u} = 0.35$ m/s. It appears that the effects of both the benching and the increased length to breadth ratio were to cause an increase in efficiency for $\bar{u} < 0.35$ m/s. The greatest difference between two configurations occurred at $\bar{u} = 0.23$ m/s; for this flow condition the efficiency of the chamber with the increased length to breadth ratio was more than double that of the basic chamber.

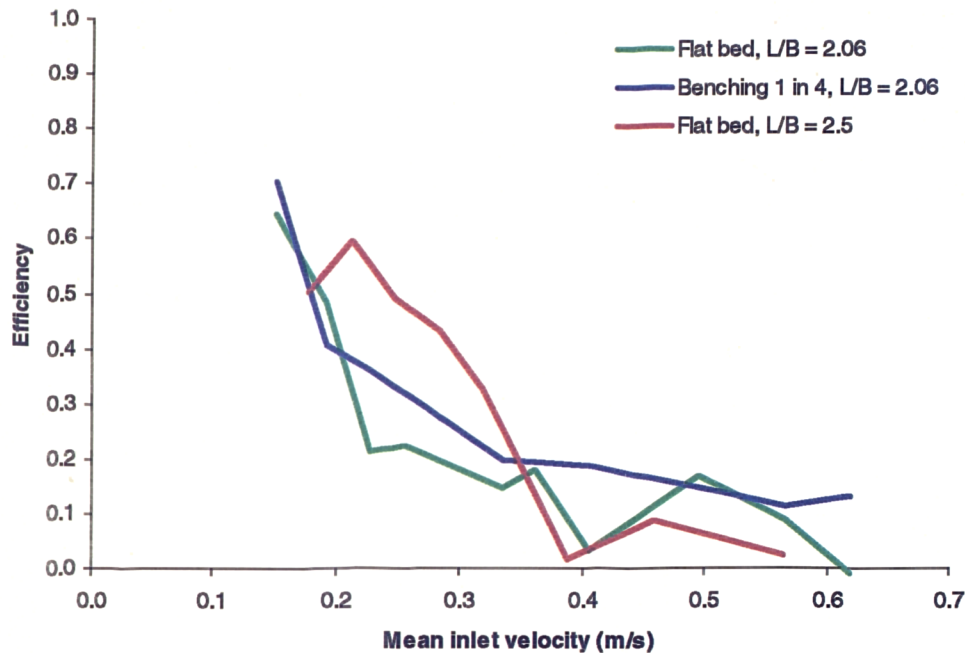


Figure 4.4 Mean efficiency plots for the storage chambers

Above $\bar{u} = 0.35$ m/s η remained approximately constant with any further increase in the inlet velocity. The chamber with benching, which experienced the lowest efficiency of the three configurations for low inflows, produced the highest efficiencies as the inlet velocity increased. Before reaching any firm conclusions, however, it is necessary to consider the validity of the data presented above.

In Figure 4.5 the individual test results are presented as hollow symbols, while the mean result for each flow condition is shown as a solid symbol with the same shape and colour. Significant scatter about the mean may be observed, and in some cases the within-sample variations are considerably larger than the variations between the mean values for different chambers. This observation is discussed further in section 4.2.5.

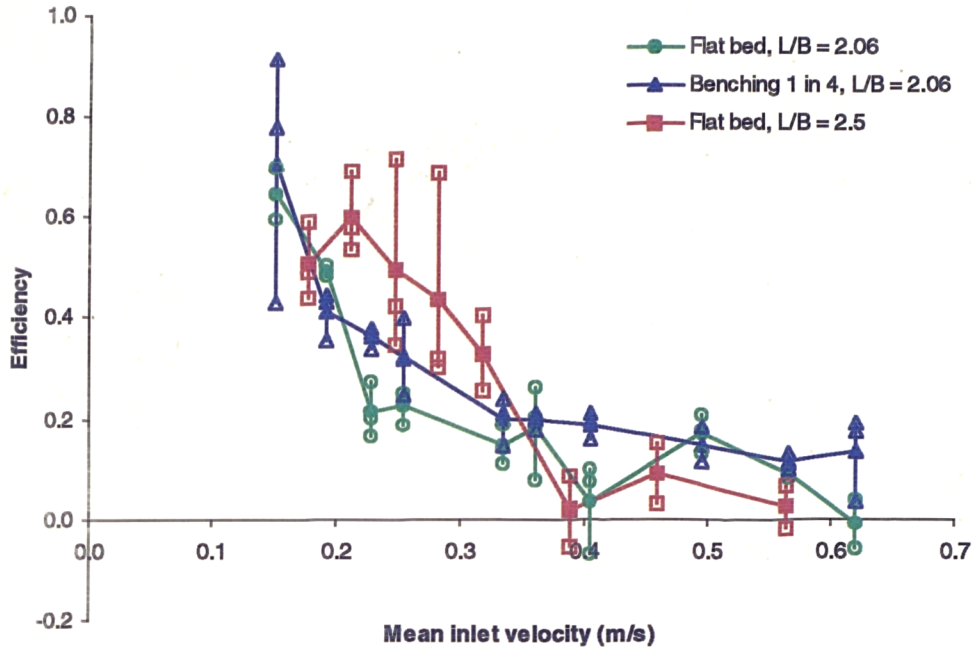


Figure 4.5 Individual efficiency plots for the storage chambers

4.2.4 The Distribution of Sediment

Some examples of the sketches of sediment deposition which were made following each of the efficiency tests are presented in Figure 4.6. The depth of sediment was not recorded, but, where present, the sediment formed a fine layer no more than 2 mm in depth. Assuming that the spatial extent of sediment coverage gives a reasonable indication of the efficiency, then it can be seen that as \bar{u} increased the efficiency decreased for all chamber configurations. It is equally apparent that for similar values of \bar{u} the differences in coverage between the three chambers were not significant. The observed patterns of sediment also, therefore, suggest that differences in efficiency between the three chambers were not pronounced. The assumption that efficiency and sediment coverage are correlated is discussed further in section 5.4.

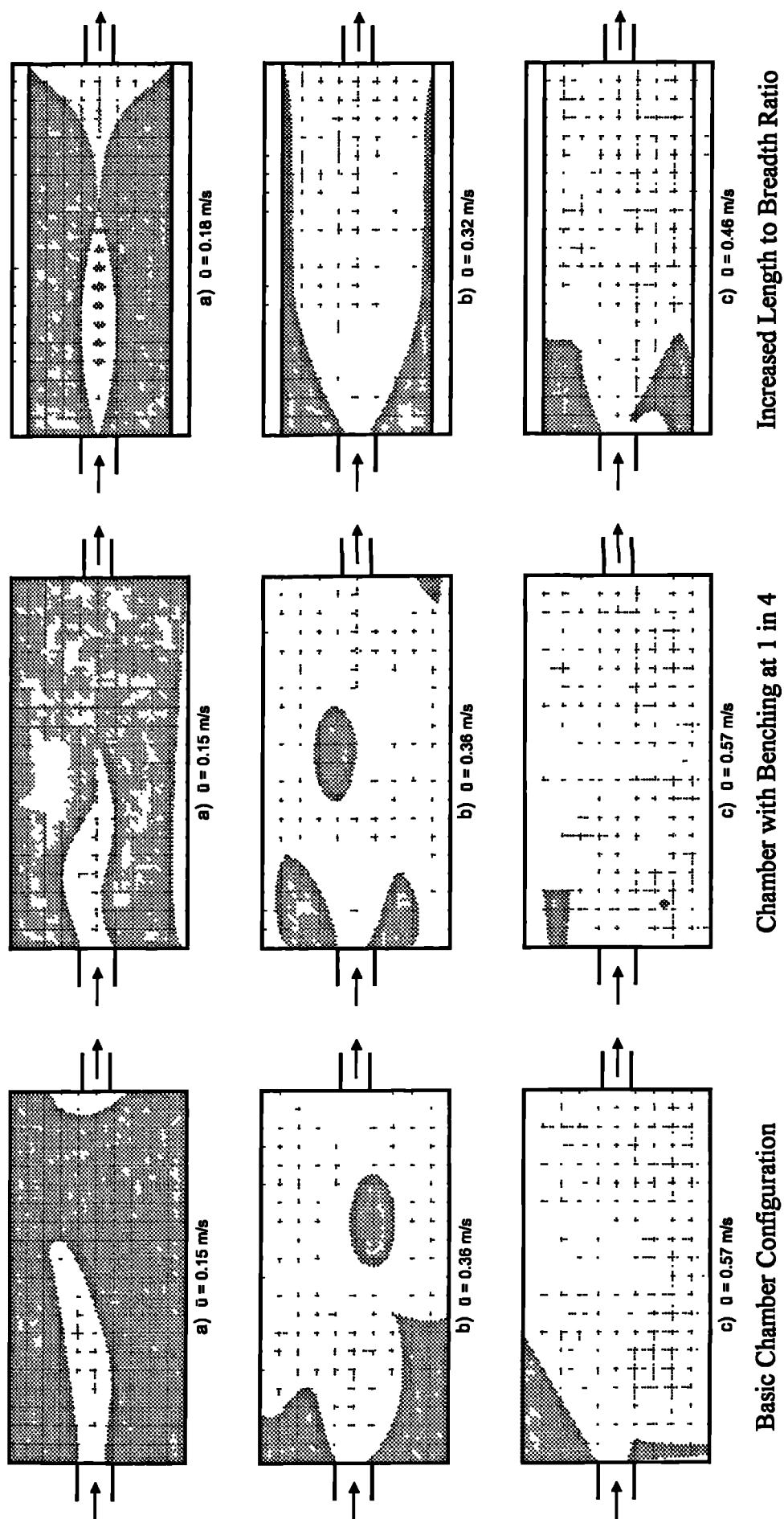


Figure 4.6 Sediment distribution on the chamber bed following efficiency tests

4.2.4.1 The effect of flow pattern on sediment distribution

The above discussion suggests that significant differences in chamber sedimentation efficiency did not occur as a result of alterations in geometric configuration. However, the location of the deposited sediments did vary between the three chambers, and furthermore, the location of the sediment deposits appeared to be a function of the flow field that developed in the chamber. Although detailed measurements of the flow patterns in the chambers were not undertaken at this stage (see Chapter 5), a general view of the velocity distribution was obtained by injecting Potassium Permanganate dye into the flow at the chamber inlet. It was clear that areas of the chamber bed associated with regions of high flow velocity did not experience any deposition, while in regions where the flow velocity was small deposition occurred.

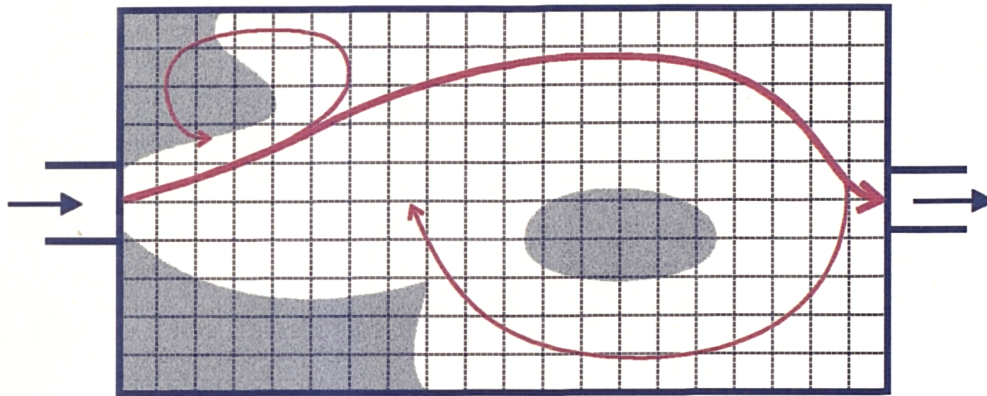


Figure 4.7 Sketch of sediment deposition and flow pattern for the basic chamber at a mean inlet velocity of 0.36 m/s

For example, the flow field in the basic chamber configuration, indicated in Figure 4.7, was characterised by a large clockwise flow circulation centred in the downstream half of the chamber, a small anticlockwise circulation in the upstream left hand corner of the chamber and a comparatively still zone in the upstream right hand corner. The flow velocity was low in the centre of each of the two circulations. The sediment deposition pattern for $\bar{u} = 0.36$ m/s clearly identifies three regions of sediment deposition associated with the areas of low flow velocity.

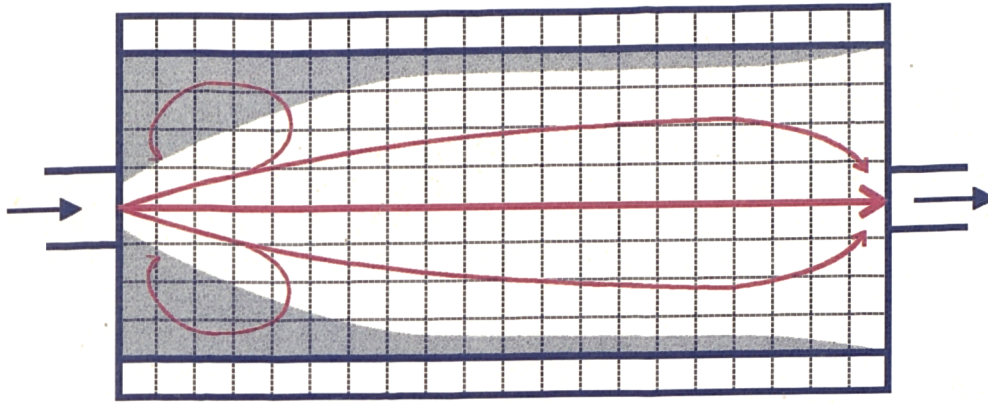


Figure 4.8 Sketch of sediment deposition and flow pattern for the chamber with increased length to breadth ratio at a mean inlet velocity of 0.32 m/s

Figure 4.8 shows that when the length to breadth ratio was reduced, a more symmetrical flow pattern was created. The highest flow velocities arose from the inlet jet as it passed straight through the chamber to the outlet. Areas of low flow velocity occurred closer to the two chamber walls, where sediment deposition was observed as a consequence.

The examples presented in Figures 4.7 and 4.8 suggested that the location of sediments deposited on the chamber bed was closely associated with the velocity distribution that developed within the chamber. Consequently, it was decided that the focus of the laboratory investigation should move from chamber efficiency measurements to an investigation into the interaction between the flow field and sediment deposition. This relationship is fully explored in the remainder of the thesis, starting at the beginning of chapter 5. In the final sections of chapter 4, however, the reporting of the efficiency tests is completed.

Although significant differences in efficiency could not be identified between the three chambers, the experimental data presented in Figure 4.5 showed considerable scatter between duplicate efficiency measurements. The following section therefore presents a number of ways in which the experimental procedure might be improved, both in terms of the laboratory set-up and the test regime.

4.2.5 Review of the Experimental Procedure

There may have been problems associated with the laboratory set-up and instrumentation used in the efficiency tests, and it is intended that the discussion presented here could form the basis for similar investigations undertaken in the future.

Figure 4.5 showed that repeat tests did not consistently reproduce the original test outcomes, and this observation implied that there may have been sources of error inherent in the experimental procedure. Three potential sources of error were identified, and these are discussed below.

4.2.5.1 Sediment Mixing in the Inlet

Substantial fluctuations in the inflow suspended sediment concentration, as, for example, shown in Figure 4.2, were observed in all tests. These indicated that the sediment was not as well mixed in the inlet flow as it ideally should have been. Although care had been taken in the experimental set-up (see chapter 3) to ensure that the sediments would be well mixed at the inflow to the chamber, the test results indicated that this had not been achieved. Considering the measures that had already been taken to ensure a fully mixed sediment input, it was felt that only fairly major alterations to the laboratory set-up would produce the necessary improvement in mixing. Two possible options may be suggested for future experiments: firstly, to introduce a mechanical mixing device downstream from the input point; or, secondly, to situate the input point upstream from a swan-neck, or similar physical discontinuity. Although an increase in the inlet pipe length would increase mixing, it is likely that such a measure would also increase the likelihood of sediment deposition upstream of the chamber inlet. Consequently this type of modification would appear to be inappropriate.

4.2.5.2 Nephelometer Probe Drift

On some occasions, systematic drift (upwards or downwards) in the readings from the probes was identified.

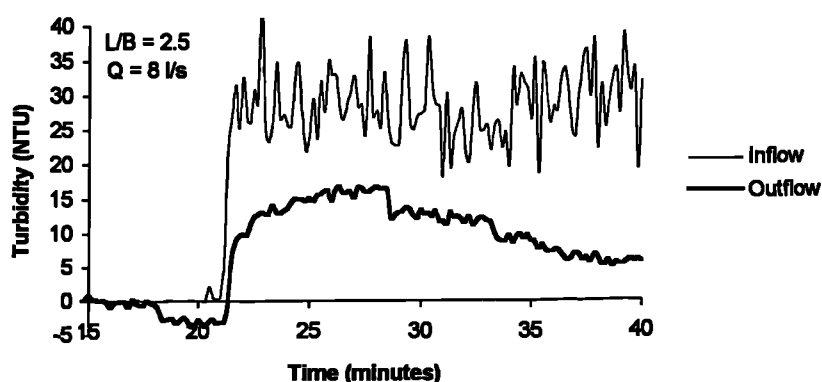


Figure 4.9 Example turbidity trace

In Figure 4.9, a downward drift can clearly be identified in both the period before sediment input began ($t = 15$ to $t = 20$ mins) and also in the sediment input phase of the experiment. In this case the problem was very clear, and the test results could simply have been excluded from the analysis. However, in other cases the decision as to whether drift had occurred or not was less clear. In Figure 4.10 it is questionable as to whether the outflow reading was affected by upward drift or not. The calculated efficiency in this case was -0.05, which is a meaningless result. No external reason for this drift could be found, and it was felt that the problem may have derived from an electronic fault in the probes themselves.

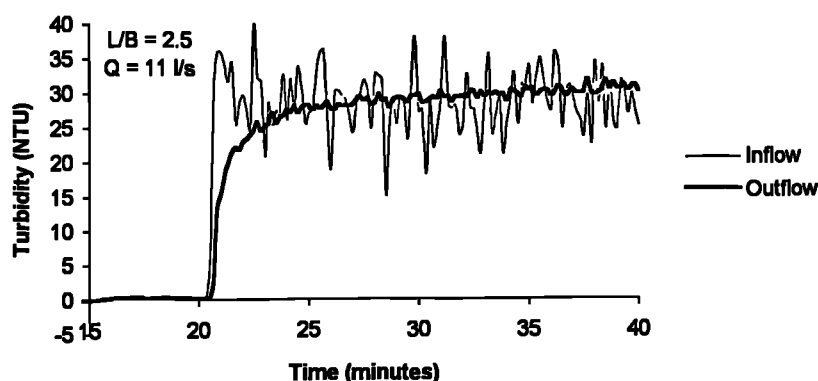


Figure 4.10 Example turbidity trace

Alternatives to the probes might be considered. Subsequent to the experimental phase of this research, Skipworth (in press) has achieved good measurements of sediment concentration in a laboratory pipe using both an on-line Malvern particle size analyser and by analysing manually extracted samples using a high sensitivity spectrophotometer. Another approach would be to dry and weigh the deposited sediment collected from the chamber bed (Ellis, 1992).

4.2.5.3 Probe Readings in the Outflow under Conditions of Low Discharge

At high flowrates a clear, steady, reading from the outflow probe was obtained. This is illustrated in Figures 4.2 and 4.10. At low flowrates, however, the outflow probe registered strong fluctuations, as shown, for example, in Figure 4.11. It can be seen that the fluctuations with the same magnitude occurred both with and without sediment input. This fluctuation could not therefore be attributed to poor sediment mixing. Instead, it is believed that it occurred as a result of reflections from the free surface which occurred in the outflow pipe when it was not surcharged. Repositioning

of the probe such that pipe full conditions could be guaranteed would have eliminated this problem.

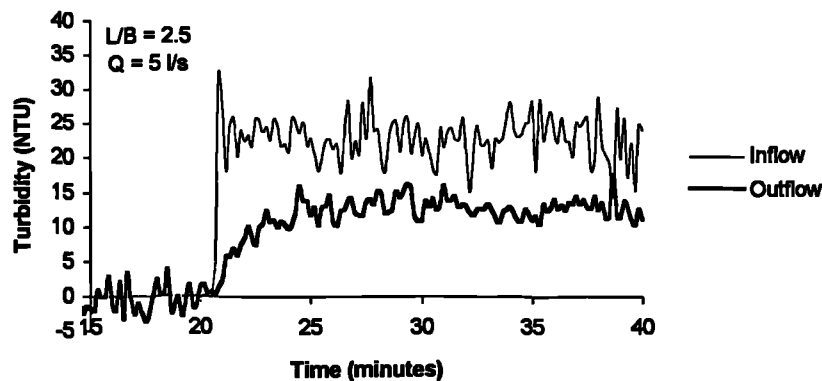


Figure 4.11 Example turbidity trace

4.2.5.4 Test Regime

The previous sections suggest that the experimental procedure may have lacked the sensitivity and accuracy to detect any differences in chamber efficiency that were present. However, the visual observations of the spatial extent of deposition in the three chambers presented in section 4.2.4 also suggested that any differences in the amount of deposition were probably minimal. The conclusions from this phase of research were therefore:

1. Efficiency varied as a function of the mean inlet velocity;
2. Significant differences in the efficiency of the three chambers tested could not be identified, although there was a suggestion that both benching and an increase in the length to breadth ratio caused an increase in efficiency for $\bar{u} < 0.35$ m/s.

These conclusions differ from those of, for example, Ellis (1992), who stated that both the benching and the length to breadth ratio were important determinants of a chamber's overall efficiency. The differences may originate in the test regime that was employed; Ellis used time-varying inflows, whilst the current test programme made use of a steady flow test regime.

Ellis (1992) suggested that a full scale storage chamber experienced three phases of operation, which may be termed 'filling', 'spilling' and 'emptying'. During the 'filling' stage he observed very turbulent - even violent - flow which resulted in the scour of

sediments from the chamber benching. He suggested that it was during this phase that the geometric configuration details were important in determining how effective the self-cleansing performance of the chamber was. As filling continued, the flow conditions became more tranquil, no further erosion occurred, and sediments began to settle out of suspension. These conditions were not greatly affected by the onset of spill, and hence this phase is referred to as 'spilling' operation. As the chamber drained, the 'emptying' stage, conditions remained still and resuspension of sediments was not observed. According to Ellis' observations, significant differences in performance between the three tested chambers would only have emerged if comparisons were made during the filling stage of operation. The addition of time-varying tests to the experimental programme should, therefore, be considered in any future test programme.

Lessard and Beck (1991) also classified chamber operation into different phases, and for an on-line chamber the stages equated to those identified by Ellis (1992). They chose to term the second stage 'dynamic sedimentation'.

The laboratory tests that have been described in this chapter were all carried out under steady flow conditions, and consequently only reflect chamber operation during the 'spilling' or 'dynamic sedimentation' phase of operation. Lessard and Beck (1991) suggested that the chamber behaviour during this phase was very similar to that of a primary clarifier or settling tank. Several models have been proposed in the literature to describe the settlement of sediment in settling tanks; these were presented in section 2.4.4. It is clearly desirable, therefore, to undertake a comparison between the experimental data and the existing models of sedimentation in settling tanks. Such a comparison is presented in section 4.3.

4.3 A Comparison of Theoretical and Modelled Efficiency

4.3.1 Introduction

In section 4.2.5.4 it was concluded that storage chamber efficiency, when evaluated under steady flow conditions, could be compared to the operation of a settling tank. It is therefore appropriate to compare the experimental data to a selection of the existing settling tank models. In section 2.4.4 a number of approaches to predicting storage chamber efficiency were described. These approaches could be classified into three broad groups, namely: hydraulic loading; empirical regression; and numerical simulation models.

A comparison was made between the efficiencies that were measured in the laboratory scale chamber and those predicted by selected models. At this stage the numerical simulation models were not considered, although it is this approach which will be developed in the remainder of the thesis. The following comparison considers only the hydraulic loading and empirical regression based models. Three hydraulic loading models were selected for comparison, namely: Camp (1946) (Equation 2.35); Equation 2.36; and EPA (1986) (Equation 2.37). In addition, the regression based models of Smith (1969), Escritt (1956), CIRIA (1973), and Garde *et al.* (1990), were also examined. The findings are summarised in Table 4.5.

4.3.2 Results of the Comparisons

The surface overflow rate model, described by Camp (1946) assumes laminar, uniform flow in which the rate of particle settlement is based on a settling velocity curve. The only additional data requirements are flow rate and the surface area of the chamber. The comparison between modelled efficiencies and those measured in the laboratory (Table 4.5) was excellent. The main disadvantage of this approach would appear to be that it does not allow for any variations that might arise from changes to the internal geometry, nor does it account for turbulence, or for any variations due to changes in the inflow suspended sediment concentration. A further disadvantage of this approach is its dependence upon accurate settling velocity data.

The surface overflow rate model (Equation 2.36) and the EPA (1986) method both use an average settling velocity, rather than the full settling velocity curve. Although this results in a reduction in computational effort, both methods appear to be highly sensitive to changes in the value of V_s . The surface overflow rate model was tested

using the d_{20} , d_{50} and d_{80} settling velocities of the model sediment, and substantial variations in the efficiency were noted. The measured data had higher efficiencies than the values predicted for the average sized particulate.

The EPA (1986) method showed a similar pattern, with the measured data falling close to the curve for the d_{80} modelled data. The inclusion of n , the turbulence term, produced an improvement over the surface overflow rate method which produced values of $\eta > 1$ once the settling velocity exceeded the surface overflow rate. In Table 4.5 the modelled data were calculated assuming a value of $n = 1$. However, variations in n between 1 and 100 resulted in practically no change to the efficiency. It is clear, however, that the effect of n would be greater for a higher $V_s/(Q/A)$ ratio.

The regression model of Smith (1969) performed poorly when the values of η_0 and c_e derived from full scale plants ($\eta_0 = 0.82$; $c_e = 0.0088$) were used. However, it was possible to find a good fit for the model by altering the coefficients to $\eta_0 = 1.417$, and $c_e = 0.00411$. As η_0 represents the fraction of particulate that would settle under quiescent conditions this value may be taken to equal 1, and in this case $c_e = 0.00303$. Equally, Escritt's model performed reasonably well once the values of coefficients c_1 and c_2 had been altered to 2.737 and 1.139 respectively, but gave efficiency values in a very narrow range, between 0.52 and 0.54, with the initial coefficients ($c_1 = 1.1$; $c_2 = 10$). The new coefficients were derived using a least squares regression technique. As both models employed two coefficients, the 'solver' facility in the Microsoft Excel spreadsheet software was employed to optimise the curve fit iteratively. The CIRIA model produced efficiencies over the full data range that were practically zero.

Although the methods of Escritt and CIRIA account for suspended sediment concentration, the laboratory data were for one concentration only, and the accuracy of the models with different concentrations cannot be quantified. Similarly, it was not possible to test the model of Tebbutt and Christoulas (1975) as this is essentially the same as Smith's method when variations in inflow suspended sediment concentration are neglected.

The methods of Escritt and CIRIA are both based on the retention time, rather than the surface overflow rate. However, it has been demonstrated theoretically (Hazen, 1904; Camp, 1946) that the removal of suspended matter depends upon surface area and not upon tank volume. In addition, the laboratory tests also demonstrated that the efficiency was dependent upon the flowrate (and hence the surface overflow rate) and could not be related to the flow depth (and hence the retention time). The laboratory

tests therefore confirmed the predictions of ideal settling theory, and it is not surprising that Escritt's model, which is dependent upon retention time, could not reproduce the observed efficiencies, even once the coefficients had been adjusted. A further problem associated with the use of detention period as a variable is the need to consider scale effects when comparing data to values derived experimentally in the laboratory chamber. It is believed that the failure of either the method of Escritt or CIRIA to adequately represent the measured data with the initial coefficients resulted from the need to scale the model in the time dimension, and this was not done.

The model of Garde *et al.* (1990) could not be tested as it involved the use of an empirically derived design chart which did not include settling velocity data comparable with that of the laboratory experiments. However, this is the only model presented that attempted to account for differences in geometry, in particular in the length to breadth ratio.

4.3.3 Discussion

The applicability of all the regression models was limited by their dependence upon coefficients and, in the case of the models reliant on detention time, by scale effects. It was possible to fit an equation of the type proposed by Smith (1969) to the experimental data, but it is not possible to say how the coefficients might be chosen for unknown chambers.

It may be concluded that, if the performance of a storage chamber comprises three phases of operation, as suggested by Ellis (1992) and Lessard and Beck (1991), then the dynamic sedimentation stage may be modelled accurately as a function of the surface overflow rate. The laboratory data suggested that Camp's method was the most accurate, but that the method proposed by the EPA was simpler to implement. It is reassuring to note that variants of this model have been implemented in both the urban drainage quality models MOUSE TRAP and MOSQUITO.

One further point that needs to be noted here is that, although the geometries tested did not exhibit differences in behaviour, situations certainly may be envisaged in which non-ideal settling chamber performance might occur, even during the 'dynamic sedimentation phase'. These will not be due to changes in the chamber bed configuration, however, but as a result of, for example, changes to the outflow (overflow) position that cause short-circuiting of the flow. Further discussion of this point is reserved for chapter 9. The parameter n in the EPA model might readily be used to represent such non-ideal behaviour.

Table 4.5 A comparison of measured and modelled efficiencies

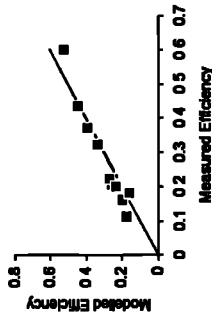
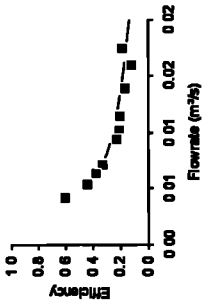
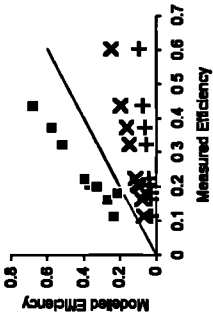
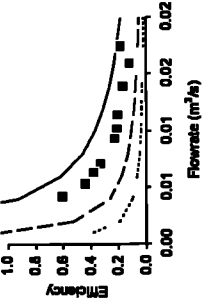
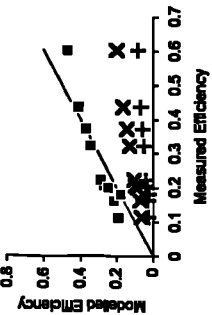
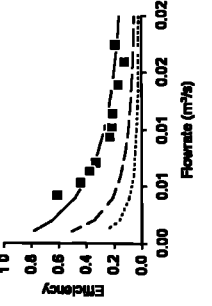
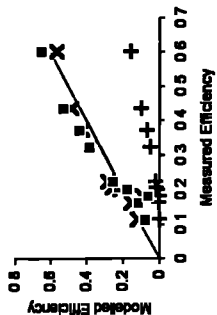
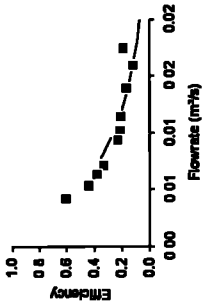
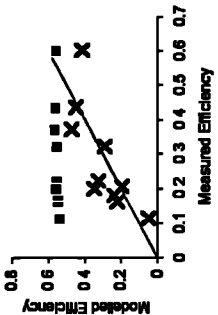
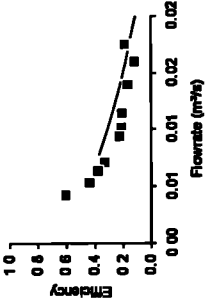
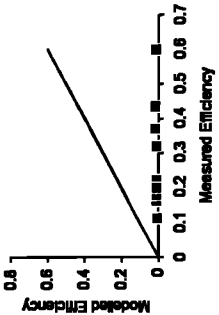
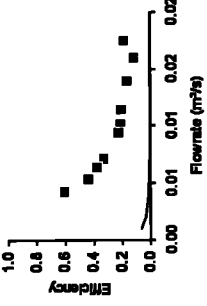
| Method | A comparison of measured and modelled efficiencies | The relationship between flowrate and efficiency |
|---|--|---|
| 1. Surface Overflow Rate Hazen (1904), Camp (1946) $\eta = (1 - X_c) + \int_0^{X_c} \frac{V_p}{V_c} dx$ |  <p>Modelled data</p> <p>Line of perfect agreement</p> |  <p>Modelled data</p> <p>Measured</p> |
| 2. Surface Overflow Rate $\eta = \frac{V_s}{Q/A}$ |  <p>Modelled data: d₈₀ Settling Velocity d₅₀ Settling Velocity d₂₀ Settling Velocity</p> <p>Line of perfect agreement</p> |  <p>Modelled data: d₈₀ Settling Velocity d₅₀ Settling Velocity d₂₀ Settling Velocity</p> <p>Measured</p> |
| 3. Surface Overflow Rate US EPA (1986) $\eta = 1 - \left(1 + \frac{1}{n} \frac{V_s}{Q/A}\right)^{-n}$ |  <p>Modelled data: d₈₀ Settling Velocity d₅₀ Settling Velocity d₂₀ Settling Velocity</p> <p>Line of perfect agreement</p> |  <p>Modelled data: d₈₀ Settling Velocity d₅₀ Settling Velocity d₂₀ Settling Velocity</p> <p>Measured</p> |

Table 4.5 continued

| Method | A comparison of measured and modelled efficiencies | The relationship between flowrate and efficiency |
|---|--|--|
| <p>4. Regression Smith (1969)</p> $\eta = \eta_0 e^{-c_e A}$ | <p>Modelled data: $\eta_0 = 1.0$, $c_e = 0.00303$ $\eta_0 = 1.42$, $c_e = 0.0041$ Smith's coefficients</p> <p>Line of perfect agreement</p>  | <p>Modelled data: $\eta_0 = 1.0$, $c_e = 0.00303$</p> <p>Measured</p>  |
| <p>5. Regression Escritt (1956)</p> $S_e = \frac{S_i}{c_1 t^{n_2} \log S_i}$ | <p>Modelled data: Escritt's coefficients $c_1 = 2.74$, $c_2 = 1.14$</p> <p>Line of perfect agreement</p>  | <p>Modelled data: $c_1 = 2.74$, $c_2 = 1.14$</p> <p>Measured</p>  |
| <p>6. Regression CIRIA (1973)</p> $\eta = (0.00043S_i + 0.51)(1 - e^{-0.7t_r})$ | <p>Modelled data: CIRIA's coefficients</p> <p>Line of perfect agreement</p>  | <p>Modelled data: CIRIA's coefficients</p> <p>Measured</p>  |

4.4 Conclusions

In this chapter, a laboratory system for the determination of storage chamber efficiency has been described. Efficiency tests were carried out on three chamber configurations, which allowed the effects of adding benching, and altering the length to breadth ratio to be examined. The tests demonstrated that chamber efficiency was a function of the mean inlet velocity.

The results of the efficiency tests did not reveal significant differences in performance between the three configurations. It is felt that this was due to lack of sensitivity in the experimental procedure and, more importantly, to the steady flow testing regime that was used. It was suggested that storage chamber operation might be divided into three phases, termed 'filling', 'dynamic sedimentation' and 'emptying'. It was concluded that the configuration variables tested would only have impacted on the chamber performance during the 'filling' phase. However, only the 'dynamic sedimentation' phase was tested. Lessard and Beck (1991) suggested that this phase was similar to the sedimentation that occurs in settling tanks, and the laboratory data was therefore compared to several settling tank models. Surface overflow rate based models gave good predictions of the chamber performance, and it was suggested that the EPA (1986) model could also be readily adapted to account for configuration changes, such as the overflow position, that might affect settling performance. This equation is already implemented in both MOUSE TRAP and MOSQUITO.

However, the most interesting conclusion to be reached from this phase of laboratory experiments was that sediment deposition was highly dependent upon flow characteristics within the chamber; it is this theme which will be developed in subsequent chapters of this thesis.

5. The Flow Field and Sediment Deposition

5.1 Introduction

The transport and deposition of sediment within a storage chamber are functions of the characteristics of the sediment, the characteristics of the bed surface, the properties of the fluid and the flow field close to the bed. Observations made during the experiments described in chapter 4 strongly suggested that sediment deposition was a function of the velocity distribution in the chamber. Ellis (1992) suggested that the local deposition of sediment on the bed of a laboratory model storage chamber could be related to the flow field by means of a critical bed shear stress below which deposition occurred. Section 5.2 describes the results of work that confirmed this hypothesis, and allowed an appropriate value for the critical bed shear stress for deposition to be identified. The experiments described in section 5.2 were carried out under steady flow conditions and in section 5.3 it is demonstrated that the concept of a critical bed shear stress for deposition was equally valid under time-varying inflow conditions. Section 5.4 demonstrates the way in which bed shear stress analysis may be applied in the estimation of chamber efficiency. The assumptions of the methodology are examined further in section 5.5.

5.2 Establishing the Critical Bed Shear Stress for Deposition

5.2.1 Introduction

In order to identify the critical bed shear stress for deposition, the velocity distribution in the chamber was established for one steady flow condition. This data was then used to estimate the shear stress distribution at the chamber bed. Reference was then made to sketches and photographs of sediment deposition which corresponded to the same flow condition, and the critical bed shear stress for deposition was identified.

5.2.2 The Velocity Distribution

The velocity distribution in the chamber was measured using a Nixon miniature current propeller for a steady flowrate of 15.9 l/s. The mean velocity in the inflow pipe was 0.561 m/s, with a corresponding Reynolds number of 1.066×10^5 . The depth of flow in the chamber was 0.196 m. For the chamber itself, it was assumed that the flow depth represented the characteristic length (Chow, 1959), and then the Reynolds number was found to be 4.654×10^4 . Hence the flow in the chamber could be described as fully turbulent.

The velocity was recorded in a series of cross sections, positioned at $X = 0.1, 0.2, 0.4, 0.8, 1.2, 1.6, 1.8$ and 1.9 m. Measurements at each cross section were made at intervals of 0.097 m in the transverse (Z) direction, and at depths $Y = 0.01, 0.02, 0.04, 0.08$ and 0.16 m. Measurements were therefore made at a total of 360 positions.

An example of the velocity distribution at a measurement depth of 0.08 m above the bed is illustrated in Figure 5.1. The main features of the flow field did not alter with depth. The flow was dominated by a clockwise circulation, with the inflow jet moving to the left wall of the chamber, then across the outlet, and returning towards the inlet in the right hand section of the chamber. A small anticlockwise circulation in the upstream left hand corner of the chamber was also identified, while the minimum velocities were observed in the centre of each circulation, and in the upstream right hand corner of the chamber. The maximum contrast between positive and negative u -velocities occurred in the profile at $X = 1.2$ m.

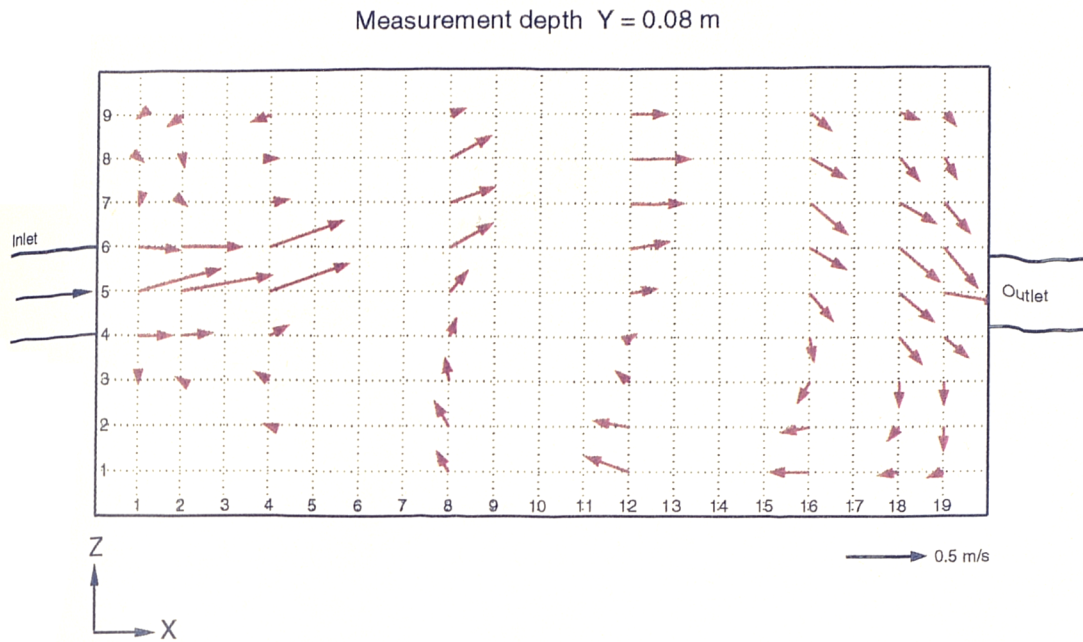


Figure 5.1 Steady flow velocity distribution at 0.08 m depth

It is interesting to note that, in the author's experience, most design engineers anticipate a symmetrical flow pattern for this type of chamber, yet circulatory flow patterns are typical in full scale chambers (Ellis, 1992). Furthermore, it was noted in the laboratory that the flow would settle into an anticlockwise circulation in approximately one out of every ten occasions. More detailed velocity measurements were taken at the chamber inlet and the velocity distribution was found to be asymmetric on entry to the chamber.

The occasional occurrence of reverse circulations may be explained in the following way. In a perfectly smooth and symmetrical model chamber a symmetrical flow pattern, in the form of a central jet and return currents along the two side walls, would arise. However, a flow pattern with two circulations is inherently less stable than one dominated by a single major circulation. This is because the velocity gradients in the flow are far steeper in the case of twin circulations. The random asymmetry that arises from turbulence in the flow appears to be sufficient to produce the single circulation. In most cases, Coriolis force caused the flow to develop a clockwise circulation (as the experiments were conducted in the Northern hemisphere). However, the influence of Coriolis force was not so strong that the clockwise circulation developed invariably. In some cases other forces dominated, for example physical disturbances to the laboratory model or the occurrence of particularly large turbulent fluctuation at a critical point in time for the circulation development, and an anticlockwise circulation arose instead. Flows in which an anti-clockwise circulation

was established were not used for velocity measurements. The nature of the flow circulation is discussed further, with respect to its numerical simulation, in chapter 6.

5.2.3 Sediment Transport and Deposition

Sediment deposition was investigated as follows. Once steady flow was established, 150 μm crushed olive stone sediment was input into the chamber for a 10 minute period. The sediment input was controlled such that the concentration at the chamber inlet was constant and approximately equal to 250 mg/l. After 10 minutes of sediment input a clear pattern of sediment deposition on the bed was observed, and this is illustrated in Plate 5.1. Except for the reduction to the period of sediment input, the experimental procedure was identical to that used for the efficiency tests, and was fully described in section 4.2.1.

The sediment deposition test was conducted independently of the velocity measurements, as several practical problems prohibited the use of the Nixon probe under conditions of sediment input. In particular, the probe quickly silted up with the sediment, and could not be accurately aligned with the flow direction when the water was cloudy as the alignment thread became invisible. Use of the LDA system (which is discussed in section 5.5) was also incompatible with sediment input, as the validated data rate was reduced to approximately one tenth when sediment concentrations of only 100 mg/l were introduced (Stovin, 1996). In addition, it would have required several tonnes of olive stone and several million litres of water passed to waste to have had sediment input throughout the programme of velocity measurements. The research was limited, therefore, in that the velocity distribution in the chamber was assumed to be unaffected by the presence of sediment in the flow. This appears to be a justifiable assumption, given:

1. the sediment concentration involved (250 mg/l) was substantially below the range of concentrations which are reported to have resulted in density currents (1000 mg/l (Larsen (1977); DeVantier and Larock (1987));
2. the sediment used was of low density and small particle size, and therefore unlikely to affect the mean flow field in the chamber.

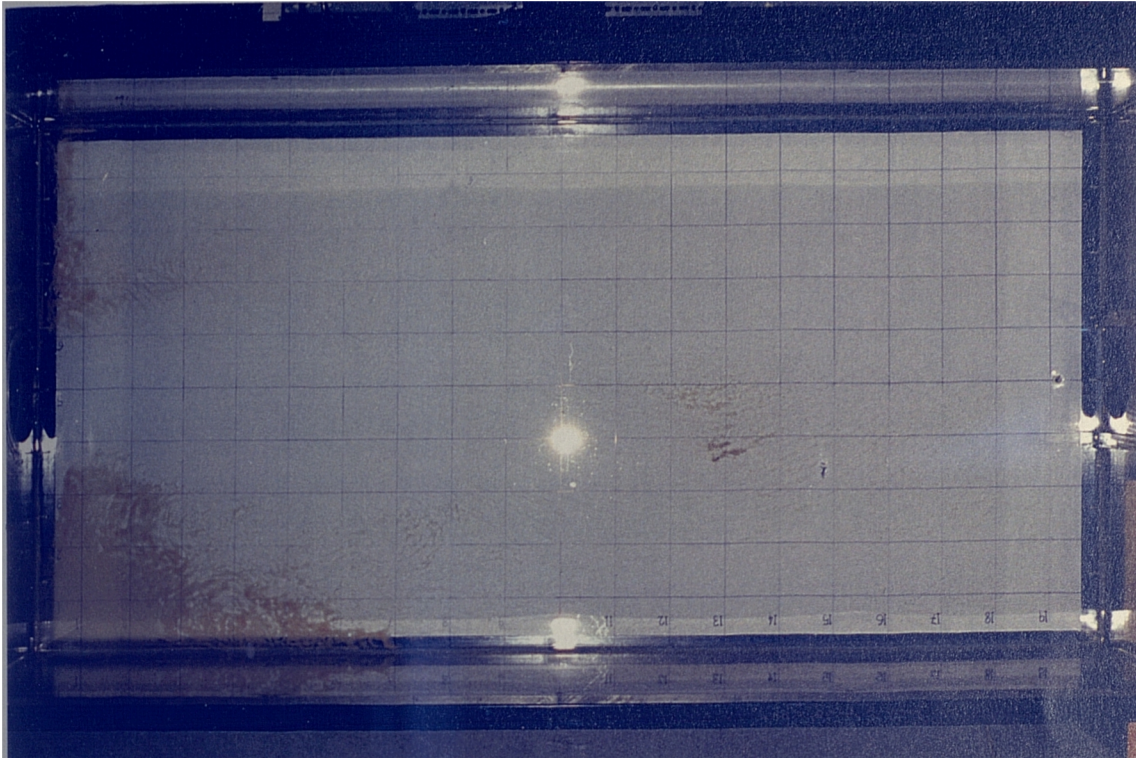


Plate 5.1 Sediment deposition under steady flow conditions

5.2.4 Bed Shear Stress Analysis

In section 2.4.3.3 it was shown that the velocity distribution in turbulent flows over a smooth surface is given by:

$$u = 2.5u_0 \ln \frac{9yu_0}{\nu} \quad (5.1)$$

in which u represents the velocity, u_0 represents the shear velocity, y represents the normal distance from the solid surface and ν represents the kinematic viscosity. The bed shear stress, τ_0 , may then be calculated from the bed shear velocity using:

$$\tau_0 = \rho u_0^2 \quad (5.2)$$

where ρ is the density of the liquid. Equations 5.1 and 5.2 were used to estimate the bed shear stress distribution in the laboratory chamber. The assumptions made in applying equations 5.1 and 5.2 to the laboratory data are discussed further in section 5.5.

At each grid location the resultant of the u - and w -velocity components measured at $Y = 0.01$ m in the vertical profile was used to calculate the value of τ_o . A contour plot of the distribution of τ_o for the steady flowrate of 15.9 l/s is presented in Figure 5.2.

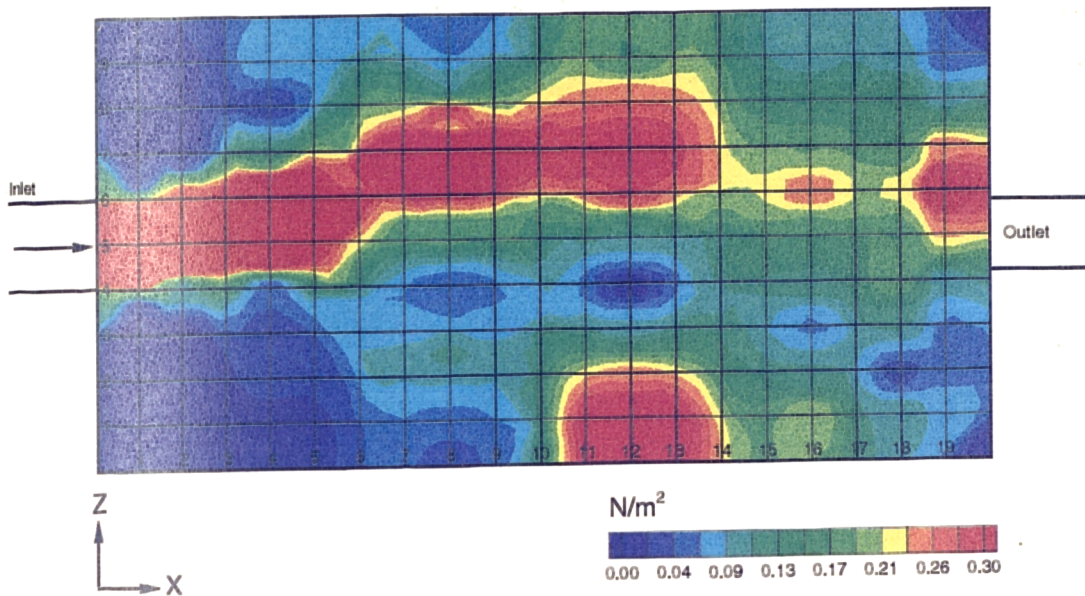


Figure 5.2 Bed shear stress distribution, steady flowrate = 15.9 l/s

It is clear that the zones of deposition apparent in Plate 5.1 correspond to zones of minimum bed shear stress in Figure 5.2. This indicates that the velocity distribution, and hence the bed shear stress, is the dominant control on depositional processes, and that the concept of a critical bed shear stress (τ_{cd}) below which deposition will occur is valid. By comparing the position of the boundary of the sediment free area in Plate 5.1 to the equivalent position in the contour plot of bed shear stress it was possible to identify the critical bed shear stress below which deposition occurred. For the 150 μ m crushed olive stone used in the tests τ_{cd} was found to lie between 0.03 and 0.04 N/m^2 .

Using a similar basis for bed shear stress evaluation, but with 75 μ m olive stone sediment and a rough concrete bed in the chamber, Ellis (1992) determined the critical bed shear as 0.16 - 0.20 N/m^2 . In dry weather flows in the combined sewer interceptor at Hildesheim the mean value of τ_{cd} was found to be 0.29 N/m^2 (Ristenpart and Uhl, 1993). These widely differing values clearly illustrate the influence of the properties of the bed and the sediment characteristics in determining the value of τ_{cd} . Although the concept of a critical bed shear stress for sediment deposition is generally applicable, the value of τ_{cd} suggested here is clearly only relevant to the specific laboratory circumstances in which it was derived.

5.3 Time-varying flow

5.3.1 The Velocity Distribution

In order to test the hypothesis that a critical bed shear stress for deposition existed under time-varying as well as steady flow conditions, measurements of the flow field were also made during a 20 minute time-varying inflow hydrograph, termed HYDRO1. The profile of this inflow hydrograph and the resultant profile of flow depth in the chamber are shown in Figure 5.3. The maximum depth of flow attained was 0.21 m. Once more, the Nixon miniature current probe was utilised for the velocity measurements.

Velocity measurements were made continuously at a total of 59 grid points in a horizontal plane. The length of time required to monitor each location made it impossible to consider investigating more than one depth. In addition, it was required that the probe should be submerged throughout the duration of the hydrograph, and hence a flow depth of 50 mm was arbitrarily selected for the velocity measurement during the time-varying flow test.

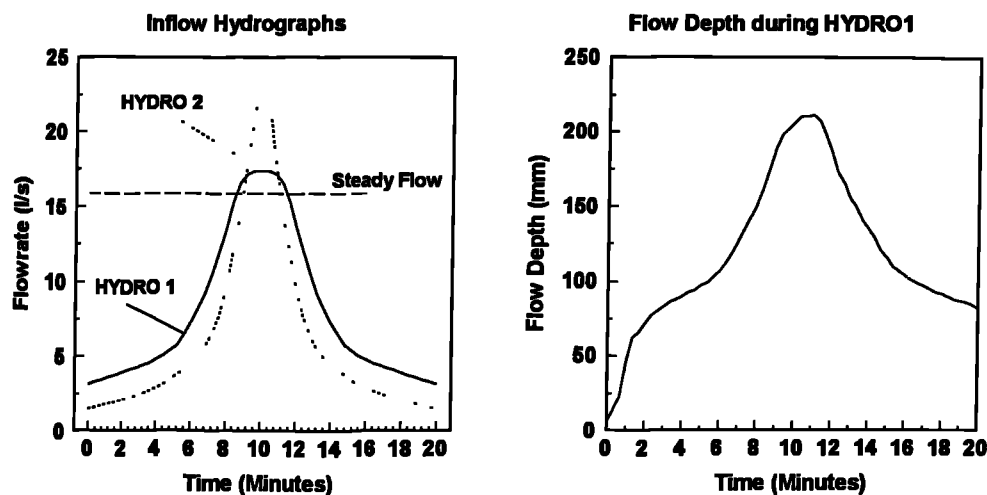


Figure 5.3 Time-varying inflow hydrographs

As each hydrograph was discharged through the model, the probe was continually re-aligned with the flow direction, and that direction was recorded. Velocity was averaged over a 10 second period. Following data collection, further smoothing of the data was carried out in order to reduce the influence of turbulent fluctuations, and the data for each 1 minute time interval was extracted for further analysis. In the final

analysis, the velocity value assigned to any given point in time was given by the velocity averaged over the 30 second period around that time.

Initially the flow direction followed the central axis of the chamber, but as the inflow exceeded outflow the inflow jet was deflected towards the left-hand wall. A clockwise circulation developed, and this occurred within one minute of the start of the hydrograph. A second, smaller, anti-clockwise circulation also developed which was centred on ($X = 0.15$ m, $Z = 0.8$ m), in the upstream left corner of the chamber. The flow pattern that developed at the peak of the hydrograph was very similar to that observed in the steady flow test, illustrated in Figure 5.1.

5.3.2 Sediment Transport and Deposition

A constant concentration of approximately 250 mg/l of 150 μ m crushed olive stone sediment was input into the chamber over the duration of the hydrograph, and photographs of the sediment distribution were taken at intervals of one minute. The constant concentration of sediment at the chamber inflow was maintained through the use of the HYDRO4 control software. This automatically regulated the speed of the peristaltic pump which was used to transfer the concentrated sediment suspension from the reservoir into the chamber inlet pipe. The total sediment load delivered was approximately equal to that input during the steady flow test.

Areas of the chamber that favoured sediment deposition were seen to alter in response to the changing flow pattern within the chamber. After two minutes (Plate 5.2) small quantities of sediment were observed to deposit at the centre of each of the zones of flow circulation, where flow velocities were least. The three main zones of deposition extended with time, until after four minutes (Plate 5.3) approximately one third of the chamber bed was covered with a thin layer of sediment. After four minutes the inflow discharge rose rapidly (Figure 5.3), and the sediment deposit began to reduce in extent. After six minutes (Plate 5.4) the boundary between the areas of bed that were clean and those where sediments remained were clearly defined, particularly in the case of the egg-shaped deposit associated with the main flow circulation. As the inflow discharge increased further, more erosion occurred. Plate 5.5 shows the reduced sediment deposit apparent after eight minutes. At the peak of the hydrograph the increased depth of flow coupled with the increased sediment concentration resulting from the resuspension of deposited sediments, made the chamber bed invisible. As the flow receded it was clear that conditions once more increasingly favoured deposition, and the area of bed covered with sediment progressively

increased until the end of the hydrograph. Plate 5.6 shows the extent of sediment coverage at the end of the hydrograph, while Plate 5.7 shows the final pattern of deposition observed once the chamber had drained.

A comparison of the results of the steady and time-varying flow tests showed that when sediments of similar concentration and load were introduced into the chamber during each test, the total quantity of sediment deposited was far greater in the time-varying test. This excess deposition was caused by the reduced flow velocities which occurred during the recession limb of the hydrograph.

Following both the steady flow and the hydrograph test, the chamber was immediately flushed with a second flow hydrograph, termed HYDRO2, which was free of sediment. In both cases the erosional effects of this second storm were very similar, and the final locations of the sediment deposits were the same, despite the dissimilar initial conditions. The flow velocities at the peak of the hydrograph were sufficient to ensure sediment resuspension over the entire bed area, and it was the flow field on the recession limb that determined the final location and extent of sediment deposition. Small amounts of sediment remained in both upstream corners of the chamber at the end of the hydrograph.

5.3.3 Bed Shear Stress Analysis

It should be noted that the measurement depth of 50 mm was selected to give representative information on the whole flow field, and not, at the time, with a view to conducting bed shear stress analysis. Ideally, the velocity measurements would have been made closer to the bed. A measurement depth of 10 mm, for example, would have given data more comparable with the steady flow analysis, and would also have reduced the importance of the assumptions made in the application of Equation 5.1, which are discussed further in section 5.5. Despite these limitations, the time-varying velocity data provided a valuable means by which the bed shear stress model of sediment deposition could be evaluated.

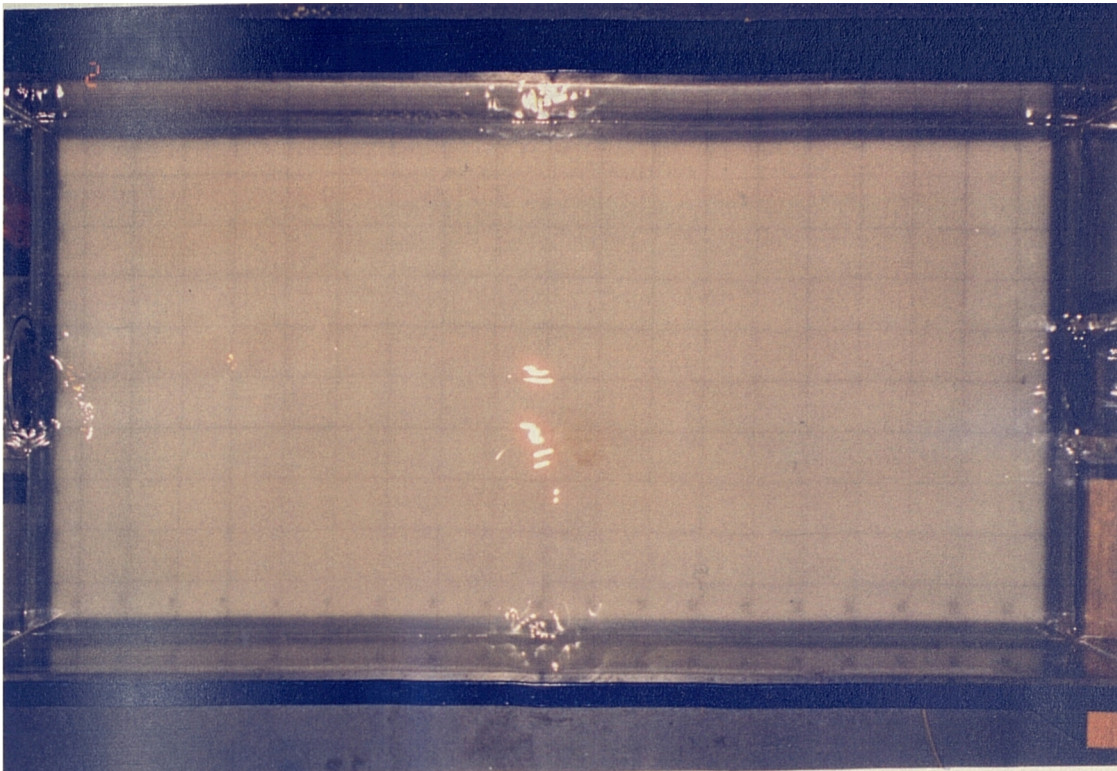


Plate 5.2 Sediment deposition after 2 minutes of the time-varying inflow hydrograph, HYDRO1

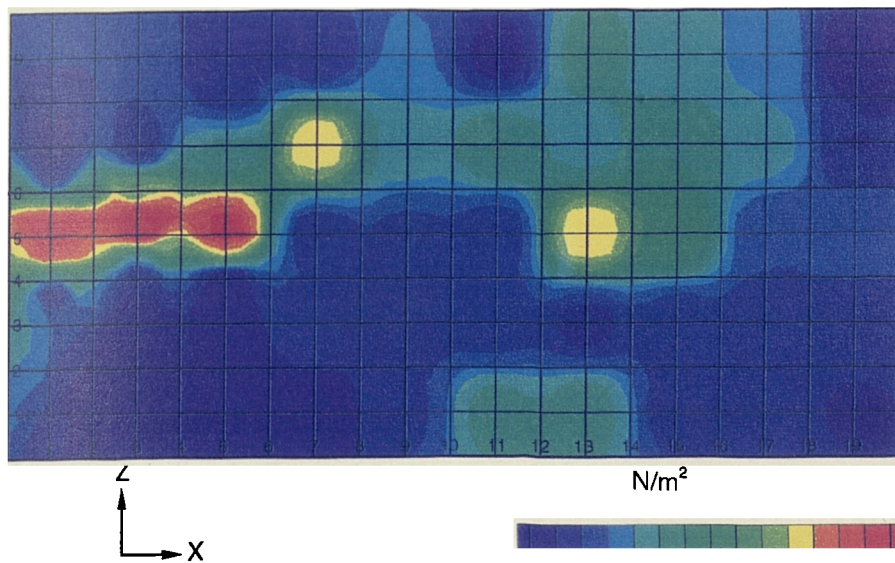


Figure 5.4 Calculated bed shear stress distribution after 2 minutes of the time-varying inflow hydrograph, HYDRO1

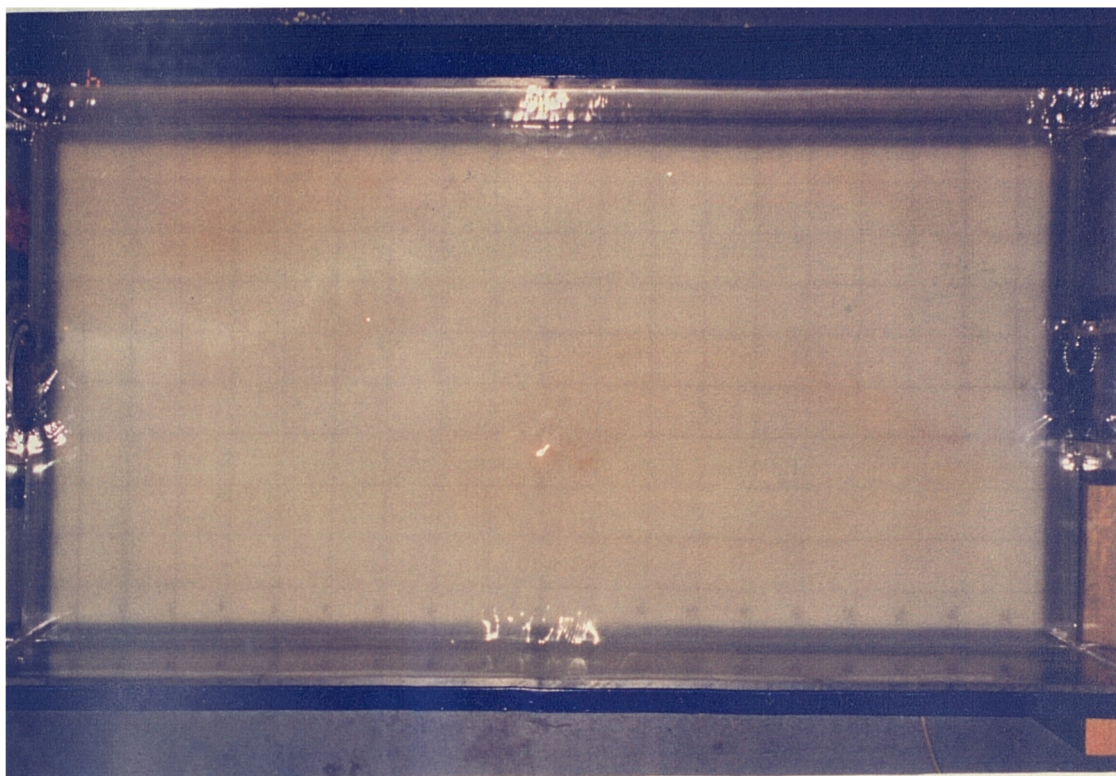


Plate 5.3 Sediment deposition after 4 minutes of the time-varying inflow hydrograph, HYDRO1

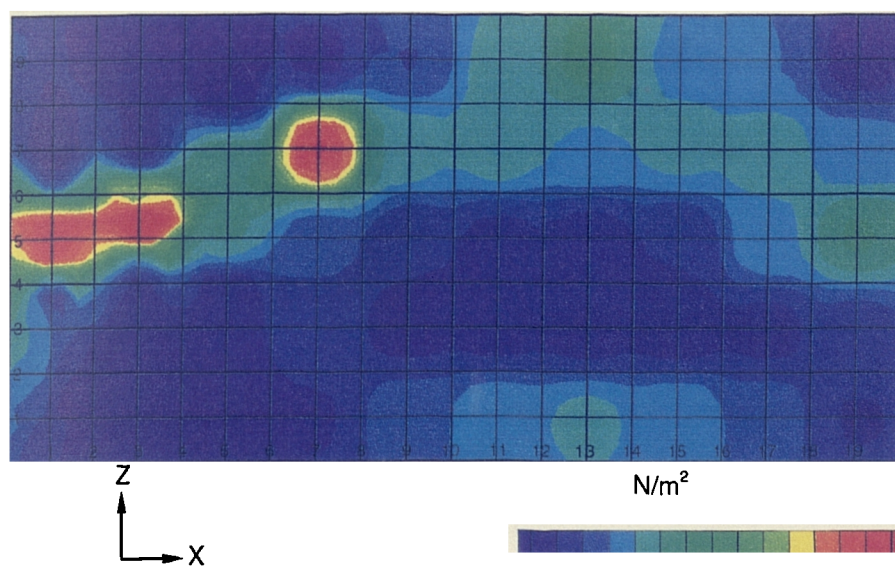


Figure 5.5 Calculated bed shear stress distribution after 4 minutes of the time-varying inflow hydrograph, HYDRO1

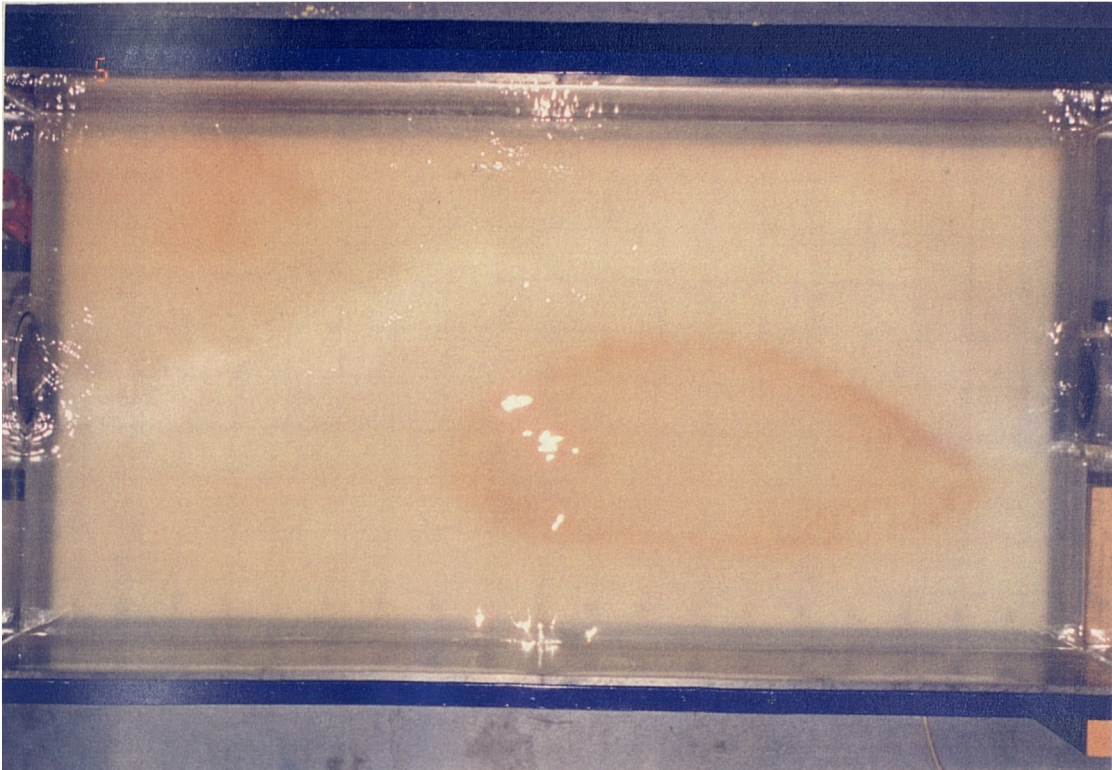


Plate 5.4 Sediment deposition after 6 minutes of the time-varying inflow hydrograph, HYDRO1

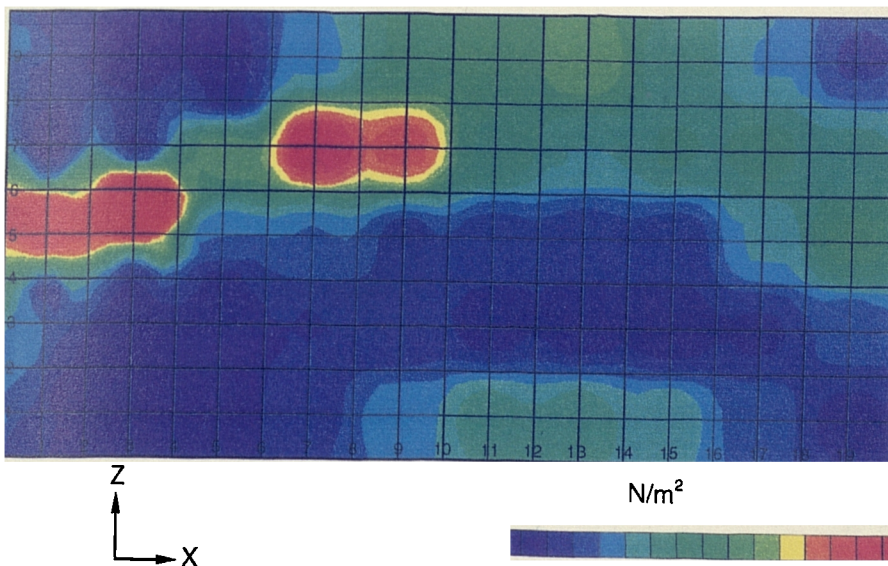


Figure 5.6 Calculated bed shear stress distribution after 6 minutes of the time-varying inflow hydrograph, HYDRO1

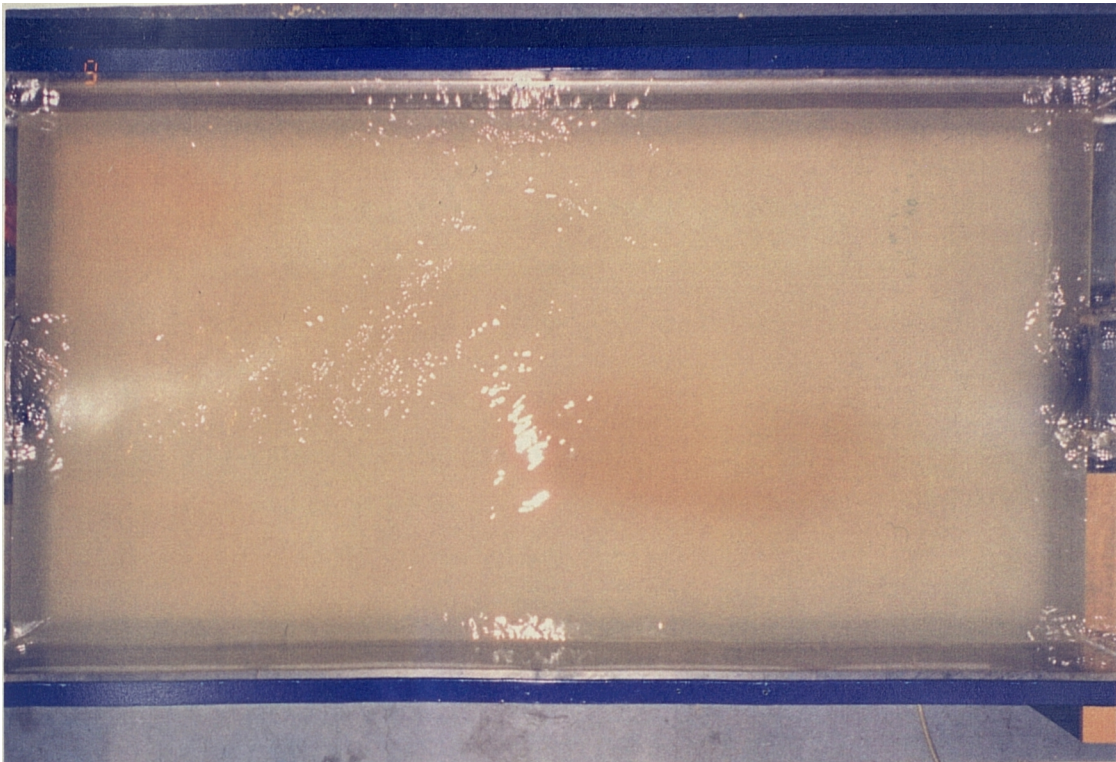


Plate 5.5 Sediment deposition after 8 minutes of the time-varying inflow hydrograph, HYDRO1

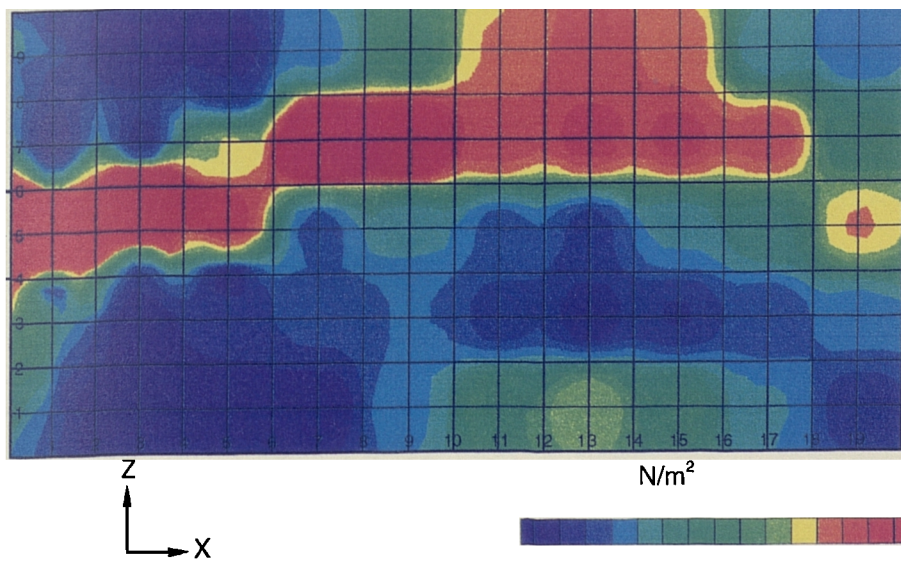


Figure 5.7 Calculated bed shear stress distribution after 8 minutes of the time-varying inflow hydrograph, HYDRO1

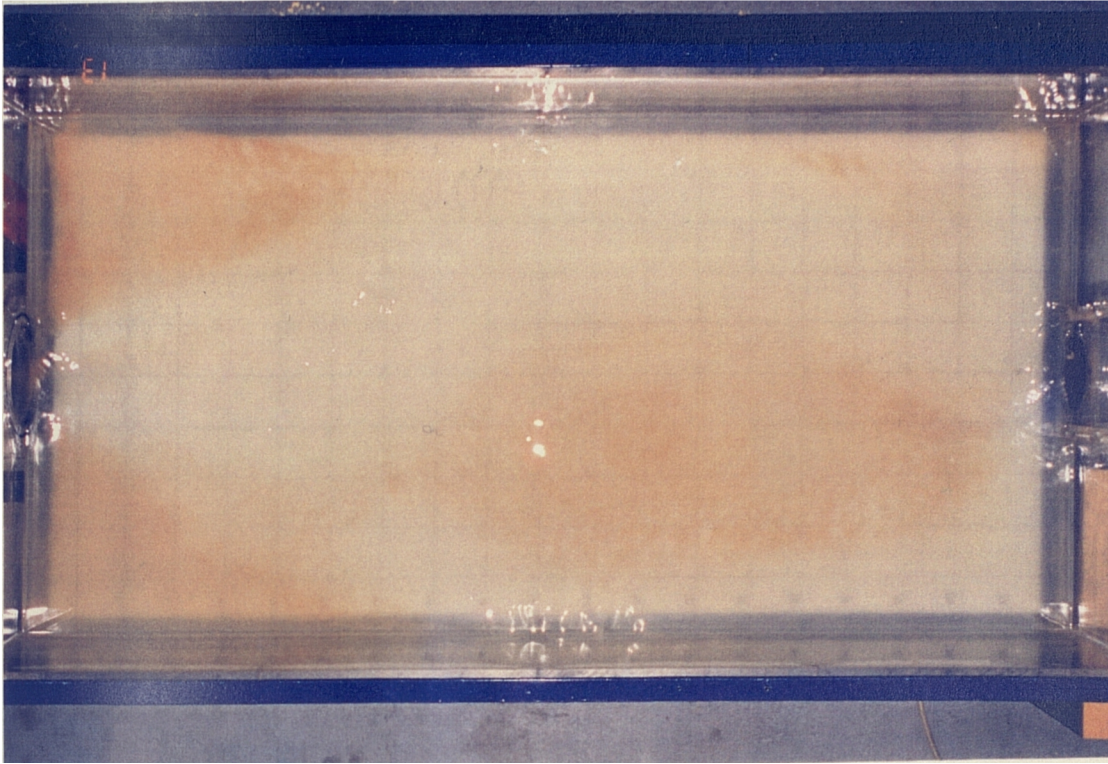


Plate 5.6 Sediment deposition after 20 minutes of the time-varying inflow hydrograph, HYDRO1

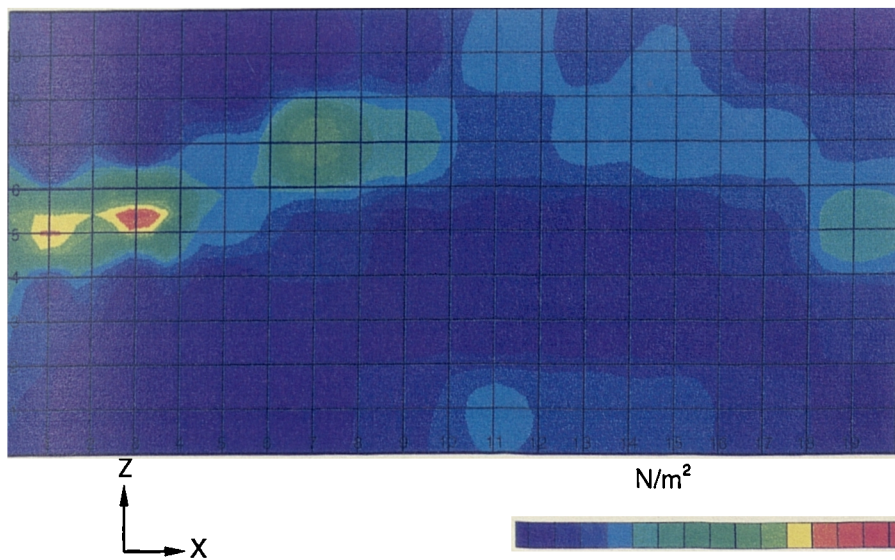


Figure 5.8 Calculated bed shear stress distribution after 20 minutes of the time-varying inflow hydrograph, HYDRO1

Using the measured velocity results from the time-varying flow tests, and equations 5.1 and 5.2, the approximate bed shear stress distribution was estimated for each one minute time interval over the duration of the hydrograph. The bed shear stress distributions corresponding to the sediment deposition shown in Plates 5.2 to 5.6 are shown in Figures 5.4 to 5.8. The 'blocky' appearance of the plots is simply a function of the interpolation routine that was used and the comparatively broad spacing of the data points. These results were compared with the observed zones of deposition. Two conclusions were made from the results: firstly, deposition occurred at a bed shear stress of less than 0.04 N/m^2 , which agreed with the findings of the steady flow tests; and secondly, that re-erosion of sediments occurred at a higher bed shear stress, $\tau_{ce} = 0.06 \text{ N/m}^2$. Once deposited, the sediments required a higher bed shear stress to initiate movement than that required to simply maintain the sediments in suspension. This phenomenon may be explained in terms of inter-particle forces and cohesion and has been well reported in the literature (CIRIA, 1994). In the full scale combined sewer at Hildesheim, Ristenpart and Uhl (1993) found a mean value of τ_{ce} of 0.70 N/m^2 , which was more than twice the value of τ_{cd} that they reported. They also demonstrated that τ_{ce} increased considerably following dry periods.

5.3.4 A Model of Sediment Deposition

These results were then used to develop a critical bed shear stress model for sediment deposition. A FORTRAN program was written that used the values of τ_{cd} and τ_{ce} to predict the presence, or not, of sediment on the bed for all monitored points, at any specified time during the discharge of HYDRO1. It was assumed that whilst the bed shear stress was less than 0.04 N/m^2 , deposition would occur. Once the velocity increased such that the bed shear stress exceeded 0.06 N/m^2 , then it was assumed that the bed would be free of sediment, but that as soon as the velocity decreased to produce a bed shear stress below 0.04 N/m^2 deposition would again occur.

The predicted pattern of sediment deposition, shown in Figure 5.9, compared well with that which was observed at the end of the test (Plate 5.7). It was concluded, therefore, that a sediment transport model based on critical bed shear values τ_{cd} and τ_{ce} is appropriate to describe sediment deposition within storage chambers in steady and time-varying flow conditions.

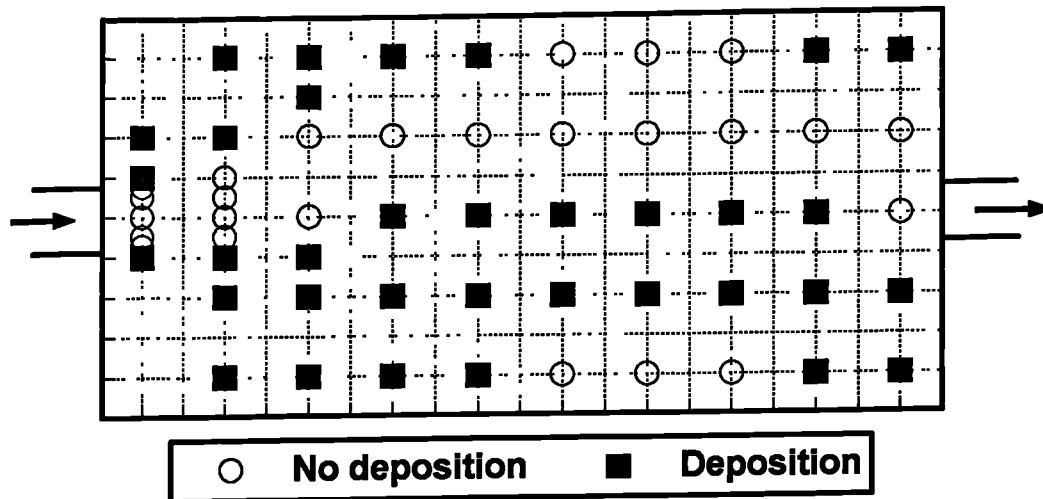


Figure 5.9 Predicted sediment deposition based on calculated shear stress

5.4 Efficiency Prediction from Bed Shear Stress Analysis

The preceding sections of this chapter have demonstrated that the pattern of sediment deposition could be predicted from the flow field by means of a critical bed shear stress (τ_{cd}), below which sediment deposition occurred. This technique did not, however, provide any indication of the amount of sediment deposited. It did not, therefore, allow any conclusions about the chamber's efficiency to be drawn. The observations regarding chamber efficiency that were presented in chapter 4 allow this problem to be examined further.

The proportion of the chamber bed where sediment deposition was observed to occur during the efficiency tests was termed the laboratory coverage parameter (C_1). C_1 was estimated from the sketches of the sediment deposition that were made following each test, examples of which were presented in Figure 4.5.

In Figure 5.10 efficiency is plotted against C_1 for the three chamber configurations that were tested. It is clear that all the chambers exhibited the same positive correlation between C_1 and η ; consequently data from all three configurations were combined in the analysis.

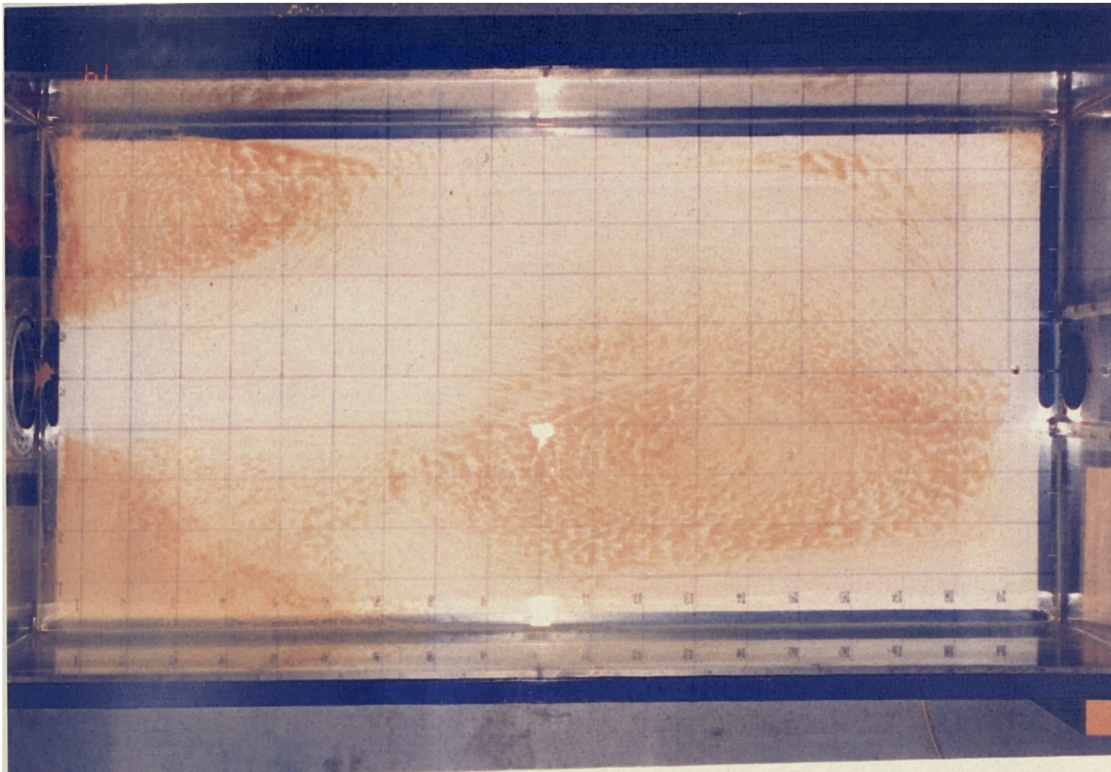


Plate 5.7 Sediment deposition following the time-varying inflow hydrograph, HYDRO1

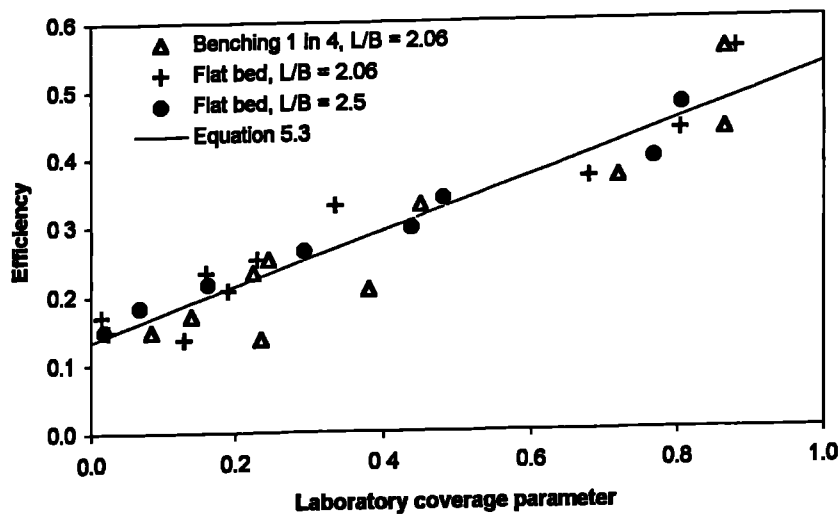


Figure 5.10 The relationship between bed sediment coverage and efficiency

Regression analysis of the data presented in Figure 5.10 suggested that η could be predicted from C_1 using:

$$\eta = 0.134 + 0.397C_1 \quad (5.3)$$

The observation that efficiency and the laboratory coverage parameter are related is significant. Having demonstrated in section 5.2 that the location of sediment deposits on the chamber bed was a function of bed shear stress distribution, it follows that, for any given flow situation, the value of C_1 will equate to the proportion of the bed for which $\tau_o < \tau_{cd}$. If this is denoted by C_{BSS} , it follows that C_{BSS} could be substituted into Equation 5.3 to allow efficiency to be predicted from the distribution of the bed shear stress.

It is reasonable to conclude therefore, that if both the location and the quantity of sediments that deposit are functions of the velocity distribution, then a numerical solution of the flow field could be used to predict the volume and distribution of deposited sediment in a prototype chamber. The following procedure for efficiency prediction is therefore proposed:

1. Build a numerical model of the chamber;
2. Obtain the flow field;
3. Obtain the bed shear stress distribution;
4. Using an appropriate critical bed shear stress value estimate the proportion of covered bed;
5. Predict efficiency from the coverage parameter using an equation of the form of Equation 5.3.

The procedure proposed here is developed in chapters 6, 7 and 8 of this thesis. However, some of the assumptions which have been made in the development of the approach are examined in the following section.

5.5 The Near-Bed Velocity Distribution

The analysis described in the previous section has proceeded on the assumption that the near-bed velocity distribution in the laboratory chamber could be approximated by the Prandtl-von Kármán universal velocity distribution law. However, this law should strictly only be applied to unidirectional boundary layer flows. Some authors have even questioned its applicability under those conditions. For example, Coles (1956) suggested that the log law only applied in the lowest 15% of the boundary layer. As a rough guide, it is often assumed that the boundary layer will be fully developed after a flow distance of twenty times the pipe diameter for pipe flows or twenty times the flow depth in open channel flow situations. It is also assumed that the boundary layer is equivalent to the flow depth in an open channel situation, and to half the pipe

diameter in pipe flow. The laboratory chamber, however, is characterised by a suddenly increased cross sectional area and circulatory three dimensional flow. Clearly, the conditions are quite different from fully developed unidirectional boundary layer flows, and there is a need to assess the validity of the universal velocity distribution law experimentally in this case. Near-bed velocity profiles were therefore assessed in the laboratory using Laser Doppler Anemometry (LDA). The LDA system was fully described in chapter 3. The laser beam was positioned at an angle of 10° to the horizontal in order that measurements could be made as close to the bed as possible.

For the flow condition described in section 5.2, near bed velocity data were collected for two slices. For the first slice, $Z=0.875$ m, measurements were made at 50 mm intervals along the chamber length and at six vertical positions: 1, 2, 4, 8, 16 and 32 mm. For the second slice, which was located on the central axis of the chamber at $Z=0.486$ m, the longitudinal spacing of measurements was the same, but the vertical spacing was reduced to give fourteen measurement points between 1 and 32 mm.

The criteria for data collection were that the data were validated on the u -velocity component only, and that measurements stopped after either 1000 validated samples or after three minutes had passed. Of the two velocity components measured using the LDA system, the u -velocity component was at least an order of magnitude greater than the vertical component. In some cases data could not be collected at all positions in the profile, as a result of blemishes on the chamber wall.

The profiles are shown in Figures 5.11 and 5.12, and it can be seen that in most cases they were logarithmic in form. In order to examine the data in greater detail, eight profiles were selected for further analysis and semi-logarithmic plots were produced. The selected profiles are indicated by vertical arrows in Figures 5.11 and 5.12. Profiles were selected on the basis that there should be four from each slice, that they should be approximately regularly spaced along the chamber length, that different types of flow conditions (i.e. inflow jet, still zone or recirculation) should be included, and that profiles with missing data should be rejected. From the $Z = 0.875$ m slice, profiles at $X = 0.20, 0.55, 1.15$ and 1.60 m were selected, while for the central slice the chosen positions were $X = 0.05, 0.40, 1.50$, and 1.80 m respectively. In Figure 5.13 the data from the central slice are plotted in the left-hand column, whilst the $Z = 0.875$ m slice data are shown in the right-hand column. Where the velocity scale is bracketed (Profiles for $Z = 0.875$ m, $X = 0.20$ and $X = 0.55$ m), this indicates that the flow direction was reversed.

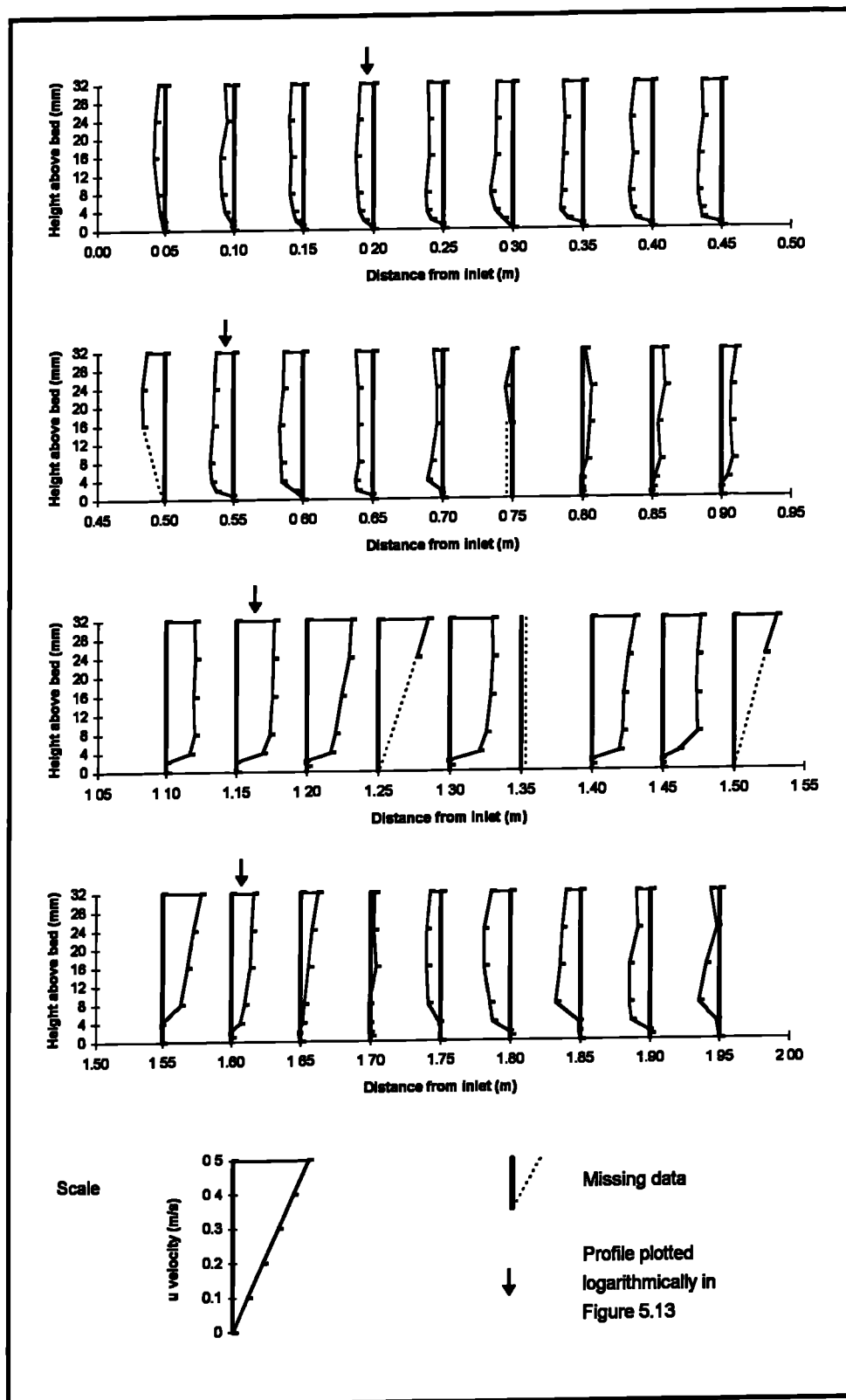


Figure 5.11 Near bed velocity profiles for the slice $Z = 0.875$ m

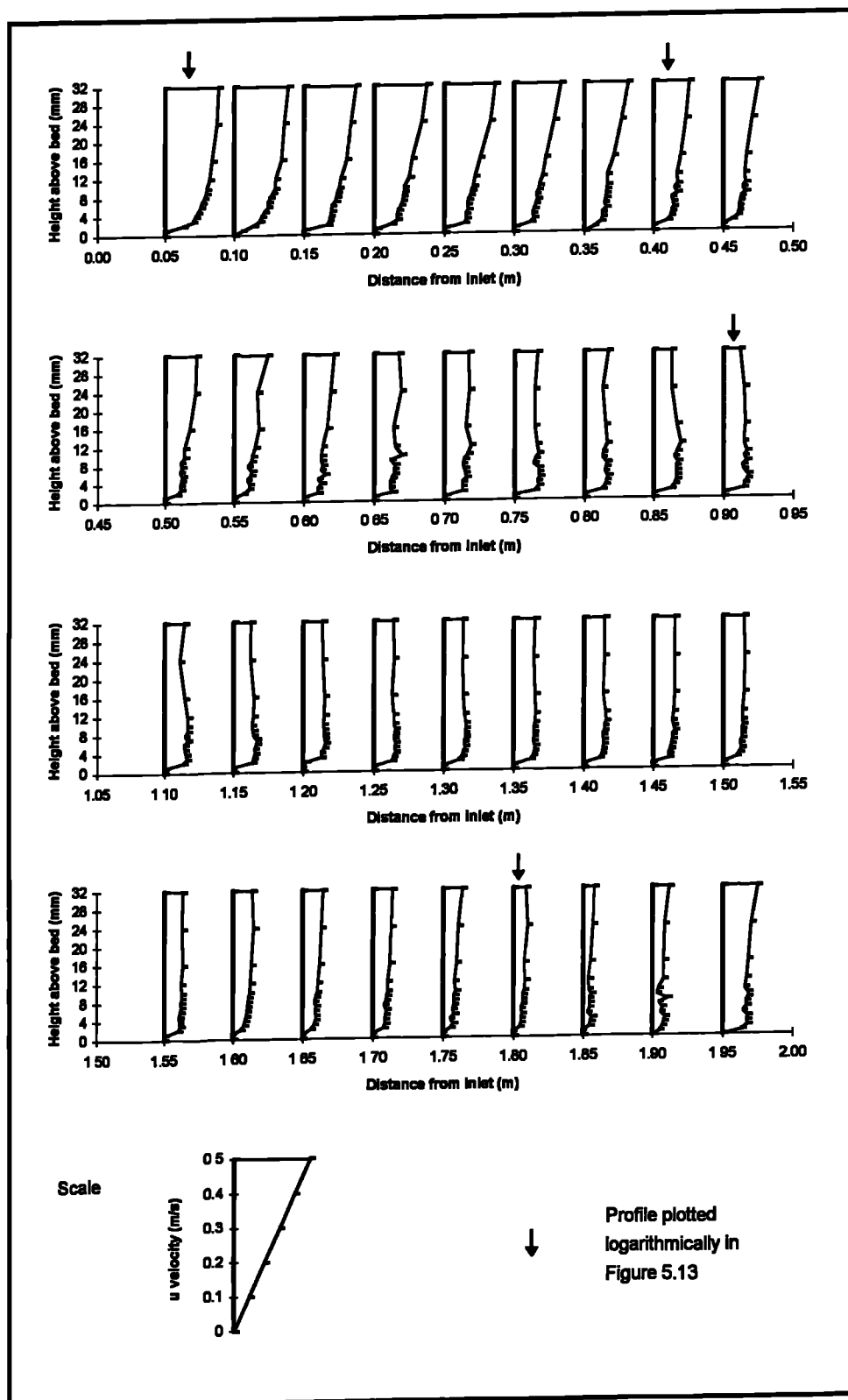


Figure 5.12 Near bed velocity profiles for the slice $Z = 0.486$ m

Figure 5.13 shows that in most of the selected locations the profiles were approximately logarithmic. The logarithmic distribution fitted the end of pipe profile ($Z = 0.486$, $X = 0.05$) particularly well. For the two profiles closest to the inlet for the slice at $Z = 0.875$ m, the velocity followed an approximately logarithmic distribution close to the bed ($Y \leq 10$ mm), but at greater depths the velocity decreased with increased distance above the bed. These two profiles were both in the upstream left hand section of the chamber, where a secondary anti-clockwise circulation in the flow pattern has previously been identified. This suggests that the assumption of a logarithmic velocity distribution was not valid throughout the entire flow depth in some regions of the chamber, and in particular in those regions associated with reverse flows and circulations. In the analysis described in this chapter, however, it was only necessary to assume that the velocity distribution in the lowest 10 mm of the flow followed a logarithmic law, as it was the velocity measured at 10 mm above the chamber bed which was input into the bed shear stress estimations.

As the velocity distributions presented in Figure 5.13 represented the u -velocity component only, the observed deviations from the logarithmic velocity distribution may simply indicate that the horizontal velocity vector rotated about its vertical axis through the flow depth. They may also indicate that the flow pattern was unsteady. These observations highlight a need for further research into near-bed velocity distributions under quasi-steady three dimensional flow conditions.

For the purpose of bed shear stress estimation in the current research, however, it was concluded that it was acceptable to assume that the vertical velocity distribution was logarithmic, given that the velocity measurements had been made sufficiently close to the chamber bed in regions where the flow patterns were complex.

It was also assumed that the depth of sediment could be neglected; the distance of the measured velocity above the bed, y , was invariably taken as 0.01 m. This assumption is justified by the fact that the sediment depth never exceeded 1 mm, and at the same time, the accuracy of the probe position above the bed was no better than ± 1 mm. Furthermore, the velocity measurement derived from a Nixon propeller meter actually represents the mean velocity over a measurement depth of 15 mm.

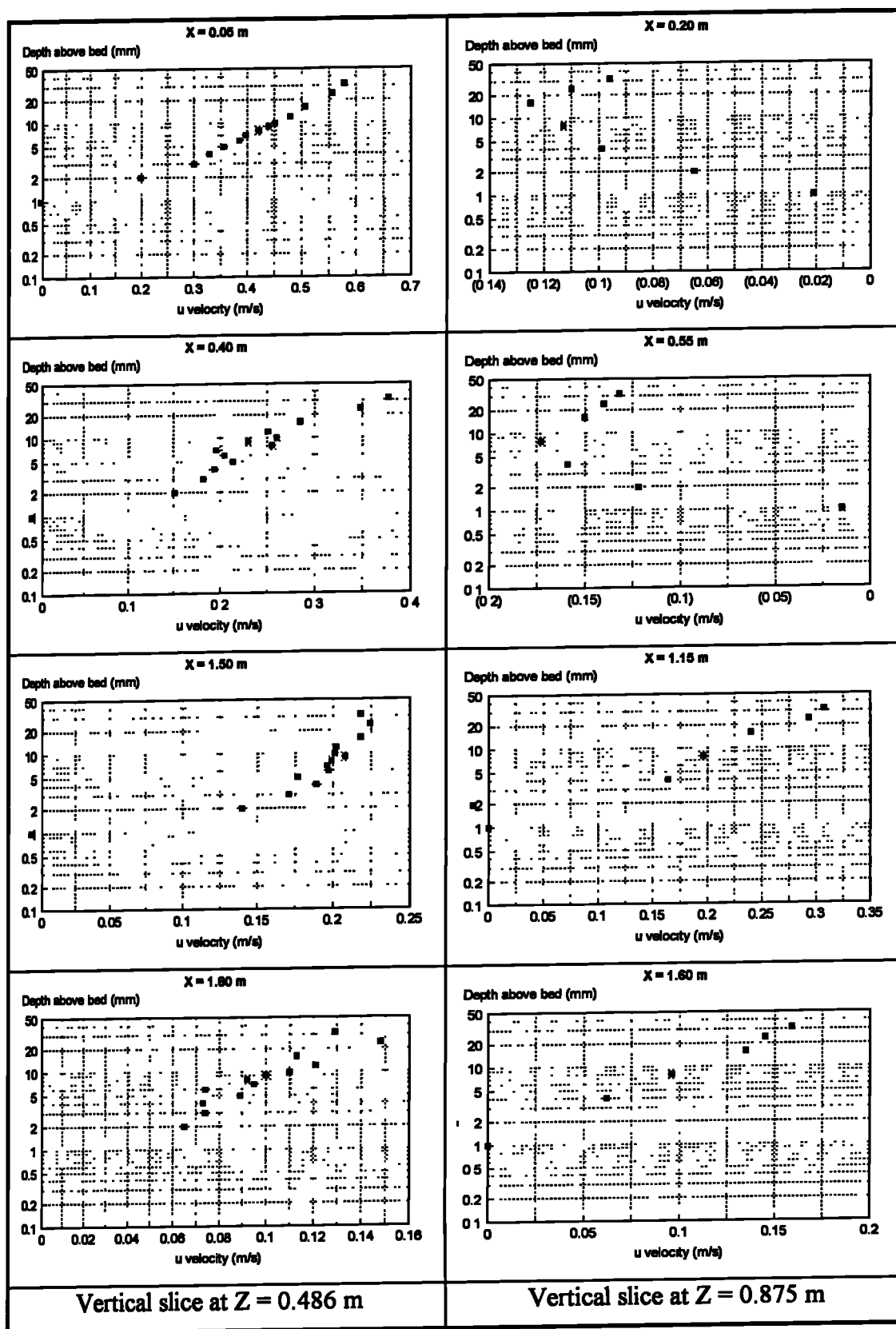


Figure 5.13 Near bed velocity profiles

5.6 Conclusions

The velocity distribution in the storage chamber was the primary control on sedimentation. The distribution of deposited sediment could be predicted from knowledge of the velocity distribution in the chamber and the values of the critical bed shear stresses, τ_{cd} and τ_{ce} , alone. It may be argued therefore that the velocity distributions computed mathematically may be used to predict sediment deposition in prototype storage chamber designs.

The magnitude of the critical bed shear stress for the re-erosion of deposited sediment was greater than the critical bed shear stress for sediment deposition. For the laboratory sediments τ_{ce} was 0.06 N/m² and τ_{cd} was 0.03 - 0.04 N/m². The value of τ_{cd} was found to be the same in steady and time-varying flow conditions. Other authors have identified very different values for τ_{cd} , and it is stressed that these two values of critical bed shear stress depend on properties of the sediment, and of the bed.

Detailed laboratory measurements have confirmed that the velocity distribution in the near bed region was approximately logarithmic, and that the assumptions made in the estimation of bed shear stress were acceptable.

6. Flow Simulations

6.1 Introduction

In chapter 5 it was demonstrated that an accurate description of the flow field within a storage chamber was sufficient to allow one to predict both the distribution and the quantity of sediment that would deposit. The controlling mechanism was found to be a critical bed shear stress (τ_{cd}), above which sediments would not deposit and below which sedimentation would occur. For the olive stone sediment in the laboratory experiments the value of τ_{cd} was found to be 0.04 N/m^2 . Following on from this it was proposed that computational fluid dynamics (CFD), in the form of the FLUENT software, could be used to predict the flow field in a storage chamber, and thereby predict any areas of bed likely to be subject to erosion and deposition, and also the efficiency of the chamber. General purpose CFD packages that are now in existence have the capabilities to simulate complex, three-dimensional, turbulent, multi-phase flows, involving, for example, chemical reaction, heat transfer, free surface phenomena and unsteady flows. Particle tracking facilities also give additional scope for transport modelling.

Some recent examples of hydraulic engineering problems that have been addressed using general purpose CFD software include that presented by Wilkinson and Waldie (1994) who used the FLUENT CFD software to model an oil/water separator. They used a two dimensional model and employed stochastic particle tracking to predict oil droplet trajectories, whereas Saul and Svejksky (1994) demonstrated that the FLUENT software could be applied to predict the gross solids separation efficiency in the three dimensional complex flow patterns that exist in a hydrodynamic separator. Similarly, Xu and Sparks (1994) showed how a three dimensional CFD simulation could be used to study an annular chlorine contact tank, examining the effects on flow patterns and residence times of the inlet and outlet arrangements.

This chapter marks a transition point in the research between laboratory investigations and numerical modelling. The principles of CFD were outlined in chapter 2, but an

outline of the FLUENT software, which has been employed in this research, is presented in section 6.2. It should be noted at this stage that the intention was not to develop new CFD software, but simply to examine the possibility of applying a commercially available CFD package to the particular problem of sedimentation in storage chambers. Section 6.3 outlines the way in which the laboratory steady flow velocity distribution described in chapter 5 was simulated and in section 6.4 qualitative and quantitative assessments of simulation accuracy are presented. The laboratory flow field was also mapped for a second model chamber, in which the depth of flow was increased to 0.7 m, thereby surcharging the inlet. Simulation of this flow condition provided validation data for the simulation procedures described in section 6.3.

It was concluded that accurate simulations of the velocity distributions measured in the laboratory could be obtained using the FLUENT CFD software. In chapter 7 the simulated flow patterns are used to develop methodologies for the prediction of storage chamber efficiency.

6.2 The FLUENT CFD software

At Sheffield University, the CFD package FLUENT is available, and details of the software are given below.

FLUENT is a general purpose computational fluid dynamics program for modelling fluid flow, heat transfer, and chemical reaction. In FLUENT, the conservation equations for mass, momentum, energy, and chemical species are solved using a control volume based, finite difference method. The software is capable of addressing a broad range of fluid flow problems and has comprehensive set-up options for the problem definition and the numerical solution. Full details of the theoretical basis for FLUENT and the use of the model can be found in the User Manual (Fluent, 1993). The options that were seen to be relevant to the simulation of storage chambers are outlined below.

The first stage in any CFD simulation is the definition of the model geometry and the computational grid. With the FLUENT software this may be achieved in one of two ways. Models that require only a simplified rectilinear representation may be defined within the FLUENT program itself. It is more usual, however, to use the FLUENT pre-processor, PreBFC, to define the geometry and a structured grid for the model. The Boundary Fitted Co-ordinates (BFC) geometry definition consists of a hierarchy of elements: *points*, defined in terms of Cartesian co-ordinates; *curves*, created from defining points and represented as composite Bezier cubics; and *surfaces*, created from

defining curves and represented as composite Bezier surfaces. Any irregular, complex geometry, in two- or three-dimensions, may be created on this basis. The regularly structured (I, J, K) grid matrix is then mapped onto the geometry and the internal cells are generated by interpolation. FLUENT makes a distinction between the *computational* grid and the *physical* grid. The computational grid consists of strictly rectangular shaped cells in which the calculations are performed, whereas the physical grid represents the distorted computational grid which fits into the physical boundaries of the model.

Once the geometry and grid have been established, the physical models, fluid properties, and boundary conditions that describe the problem are then defined by the user in the FLUENT program itself. The use of turbulence models in CFD was discussed in chapter 2. Current versions of the FLUENT software offer the user three turbulence models: the k- ϵ model; the Renormalization-Group (RNG) k- ϵ model; and the Reynolds Stress Model (RSM), although the RNG k- ϵ model was not available at the time that the research described in this chapter was undertaken. By default, the standard k- ϵ model is used.

FLUENT uses the properties of the flow adjacent to the wall/fluid boundary to predict the shear stress on the fluid at the wall. In laminar flow this calculation simply depends on the velocity gradient at the walls while in turbulent flow a log-law is applied at the wall. Wall roughness parameters and frictionless walls can be defined, but the default values are for a smooth wall.

FLUENT allows the movement of discrete spherical particles to be modelled within the simulated flow field. The process of computing the trajectories of these discrete particles is referred to as *particle tracking*. The use of particle tracking simulations in FLUENT is discussed fully in chapter 7.

6.3 The Simulations

Initially, the steady flow set-up described in chapter 5, for which a comprehensive set of velocity data had been collected, was simulated using FLUENT, and a set of comparisons between the measured and simulated flow fields was undertaken. The simulation of this chamber is referred to as SIM1.

All details of the FLUENT set-up are given in Appendix A, where an unedited print out of the FLUENT LP (Line Print) file is presented. The LP file is output from FLUENT in

ASCII format, and contains a record of all the inputs to the model set-up. The important details of the set-up are however summarised below. The storage chamber was defined using a 3 dimensional Boundary Fitted Co-ordinates (BFC) system, and the grid size was 82 x 12 x 32 cells (length x height x breadth). Figure 6.1 illustrates the way in which selected cell volumes in the computational domain were mapped onto their real locations in the model geometry.

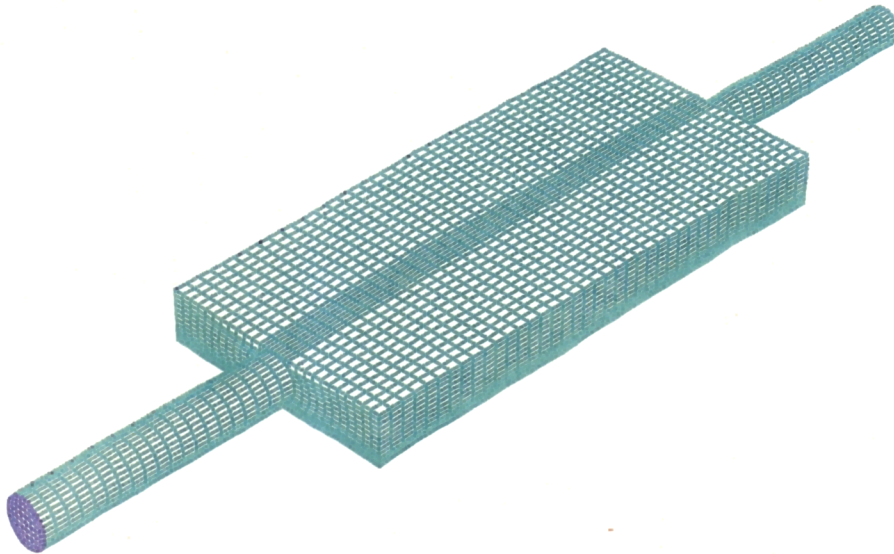


Figure 6.1 FLUENT simulation geometry

The choice of the grid size is important for the overall accuracy of the simulation. As a general rule, a finer grid mesh will produce a more accurate simulation. On the other hand, larger problems take longer to run. The largest problem size is dictated by computer memory, and the installation at the University of Sheffield at the time of the research was limited to problems with fewer than 75,000 nodes. It was essential to ensure that the grid size was appropriate for the size of flow features that were of interest. In this case, the laboratory research identified two circulations in the flow field, the smaller of which was located in the upstream left hand corner of the chamber. It can be seen from Figure 6.1 that this region was mapped with approximately 10 cells longitudinally, 10 cells transversely and 10 cells vertically, which was considered to be sufficient to allow this recirculation to be simulated accurately.

The concept of mapping the chamber geometry onto the computational grid may be more easily understood with reference to the inlet. The inlet geometry, shown in Figure 6.2, consists of a round hole (the inlet) positioned in a rectangular wall. FLUENT uses a finite difference numerical discretisation technique. This means that the

physical domain of the problem must be divided into calculation volumes which are topologically cubic. In the case of the inlet example illustrated here only two dimensions are visible. Therefore, the computational space is divided up into topological squares, which are fitted (i.e. mapped) onto the geometric boundaries of the problem. Figure 6.2 clearly shows that although each division of the mapped surface is a four sided element, the elements fit into the defined geometry exactly. Computational problems can arise if the cell mappings are too distorted, but FLUENT carries out error checking before commencing any calculations, and the grid mapping shown below created no problems. In this example the grid mapping has also been adjusted to give a higher density of computational cells close to the bed of the chamber.

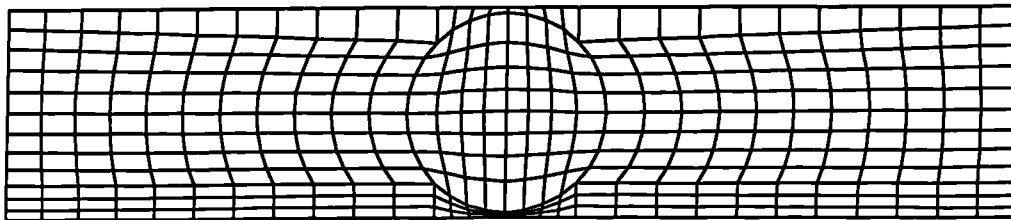


Figure 6.2 Computational grid mapping at the chamber inlet

The inlet cells themselves are coloured blue in Figure 6.1. For all the inlet cells the u velocity was set to the mean inlet velocity used in the laboratory, i.e. 0.561 m/s. The inlet was defined as a 1 m length of pipe. This was so that the constant inlet velocity boundary condition would have developed into a parabolic velocity distribution, characteristic of pipe flows, at the chamber entrance. Similarly the outlet was also defined by a 1 m length of pipe, ensuring that the outlet geometry for the chamber was modelled correctly.

Theoretically, CFD may be used to calculate the position of the free water surface in a simulation of this type. This would be achieved by considering the simulation domain to contain two phases, air and water. The densities of the two phases would allow their relative positions to be determined. In Version 4.2 of FLUENT this type of computation was not possible when the BFC geometry definition was used. This was not a major problem, given that the position of the free water surface was actually known from the laboratory experiments. The free water surface was instead represented by a wall, but links to all velocity components were cut. This meant that the wall had no frictional influence on the flow pattern below.

It was noted in chapter 5 that the Reynolds number of the flow in the laboratory storage chamber indicated that the flow was fully turbulent. It was therefore necessary to implement a turbulence model in the simulation. With respect to the choice of turbulence model (i.e. the k- ϵ model, the RNG k- ϵ model or the RSM), the simulation was carried out using the default k- ϵ turbulence model. It is recognised that the choice of turbulence model may, in some types of flow situation, be critical in determining whether an accurate representation of the mean flow field will result. The reasons for the choice of turbulence model are therefore presented below:

1. The k- ϵ model has been used or recommended by the authors of a number of different numerical models of settling tanks (for example, Stamou *et al.*, 1989);
2. The k- ϵ model is widely used, and available in practically all commercial CFD software packages. One of the objectives of this research was to assess whether CFD in general might be applied by engineers to the design of storage chambers, and it was considered important to use generally available options and avoid software specific implementations wherever possible;
3. The RSM is computationally more intensive and less stable than the k- ϵ model (Fluent, 1993);
4. The RNG k- ϵ model was not implemented in the software when the research described in this chapter was undertaken.

In initial experiments, the converged solution to the simulation described above was totally symmetrical, with a central jet directed from the inlet to the outlet, and a pair of return currents along the two side walls, as shown in Figure 6.3.

This simulation result differed, therefore, from the asymmetric circulation observed in the laboratory experiments. The laboratory investigations had suggested that, in repeat tests, the direction of the flow circulation was not entirely predictable, in that an anticlockwise rather than a clockwise circulation could, on occasion, develop. In section 5.2.1 it was suggested that any small disturbance would cause this twin circulation to transform itself into a single dominant circulation, but that the direction of that circulation would be a function of Coriolis and other forces. In order to test the stability of the solution, a disturbance was introduced into the flow. The disturbance was in the form of a PATCH of w velocity = 1 m/s (i.e., a transverse velocity from the right to the left of the chamber) in all cells in the six rows immediately downstream from the inlet.

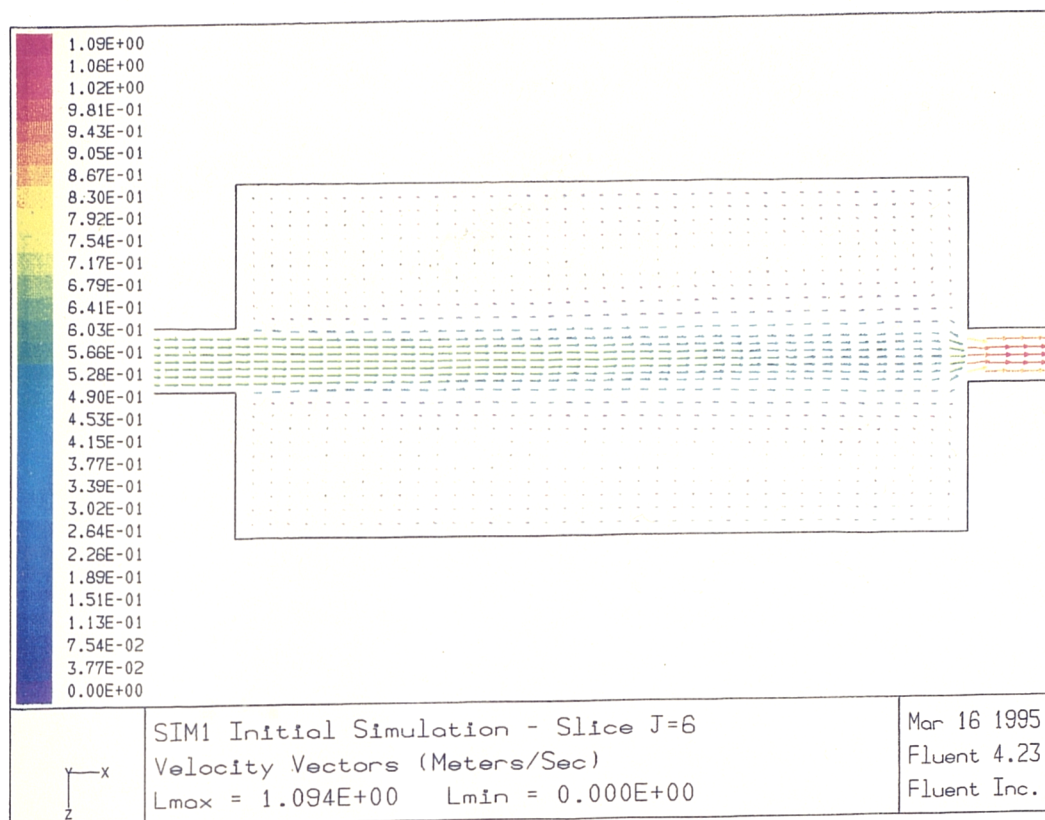


Figure 6.3 Initial simulation results for SIM1

A 'PATCH' is not like a boundary condition. It is a temporary imposition on a flow field, but its influence remains as the simulation proceeds. It is just the same as placing a diverter in the path of the inlet jet in the laboratory model, causing the circulation to change from clockwise to anticlockwise. Once the diverter was withdrawn the flow pattern would continue to circulate in an anticlockwise direction, and it would be stable. Even though the inlet boundary condition (the flow velocity) remained the same, the final flow pattern would be different.

Following the introduction of a PATCH of w -velocity the simulation was once more allowed to attain a converged solution. In this case the resulting flow field very closely resembled that which had been observed in the laboratory. Figure 6.4 and 6.5 illustrate the improved simulation results, and these should be compared to Figure 5.1 which showed the laboratory data.

The exact velocity and location of the PATCH were not thought to be critical, although later experiments suggested that they should be chosen carefully. Comprehensive tests to establish guidelines for the velocity and location of the PATCH were not undertaken, and this is therefore identified as a topic requiring further research.

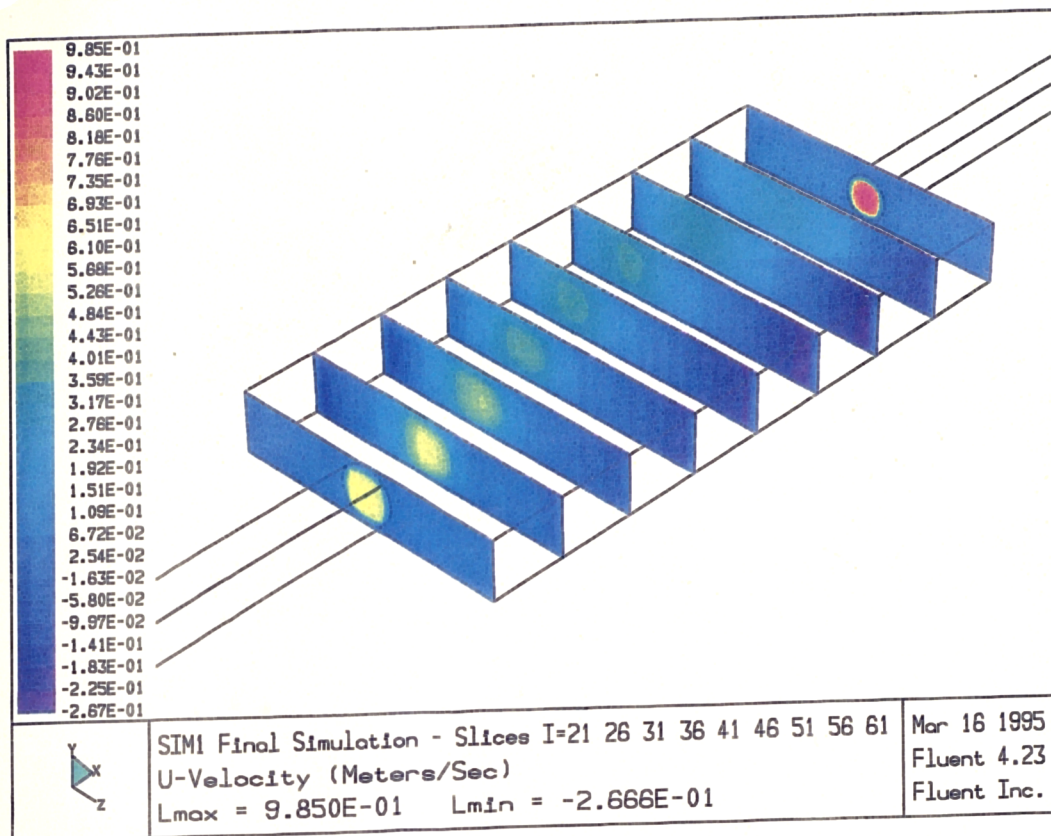


Figure 6.4 u -velocity contours for SIM1

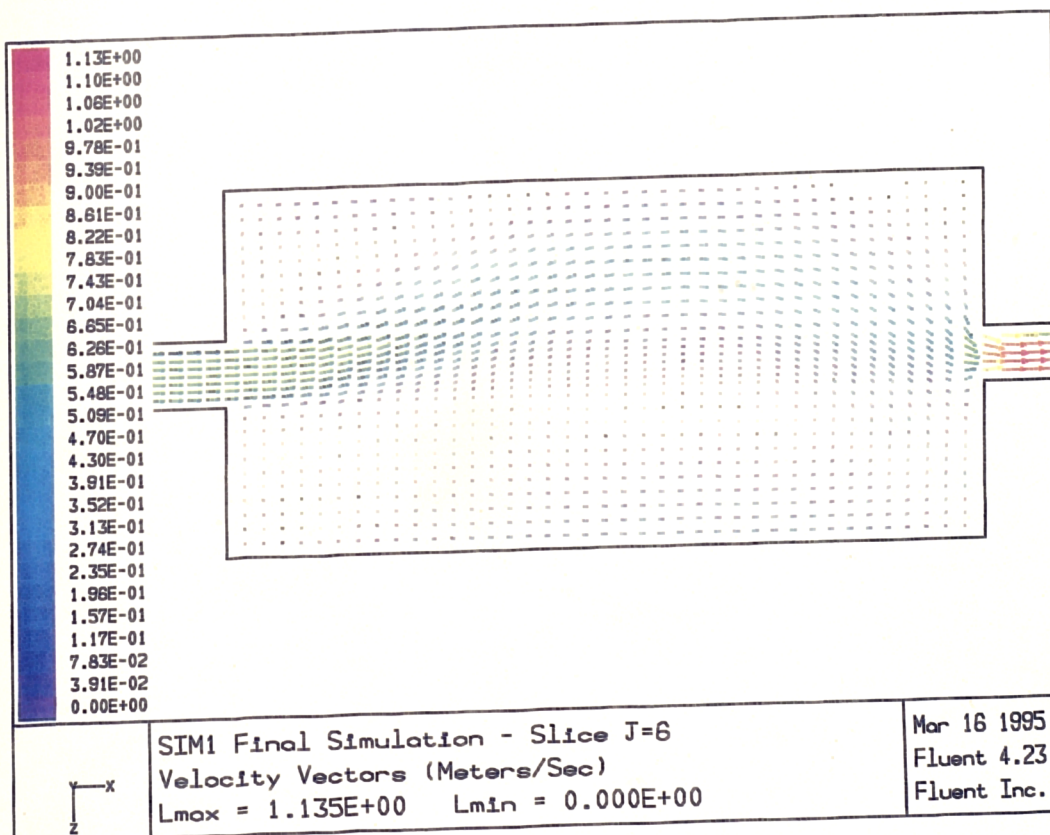


Figure 6.5 Mid-depth velocity vectors for SIM1

However, this experience suggested that flow disturbances comparable in scale to that detailed above should probably be introduced into any flow field simulation in order to identify the flow conditions that would result under the imperfect conditions that occur in reality. Further evidence for this conclusion was obtained when a chamber with a length to breadth ratio of ~ 8.1 was simulated. Flow field data for a similarly dimensioned laboratory chamber had been obtained by Ellis (1992). The first solution suggested a symmetrical flow pattern, whilst the laboratory data showed an asymmetric flow field close to the inlet. Disturbance of the simulation in the manner described above accurately reproduced this phenomenon.

6.4 Assessment of Simulation Accuracy

6.4.1 Introduction

In the previous section it was demonstrated that a good representation of an observed laboratory flow field could be obtained using the FLUENT CFD software. In this section the accuracy of the simulations, from a quantitative and a qualitative viewpoint, have been examined. Velocity measurements for one further laboratory configuration were undertaken, and a simulation of this flow was obtained. Accuracy was assessed qualitatively using vector plots and directional error contours to examine the main features of the flow field. Quantitative comparisons were then made for individual velocity components, using all measured data points.

6.4.2 A Qualitative Assessment of Simulation Accuracy

The second laboratory chamber configuration differed from the first in that the flow depth was increased to 0.7 m. The inlet velocity was once again 0.561 m/s, and the increased flow depth was attained by closing down the outlet penstock gate. The flow depth of 0.7 m corresponds to an inlet surcharge level of $3.68 D_{\text{inlet}}$. This configuration is referred to as SIM2, and the simulation was undertaken in exactly the same way as SIM1. Figures 6.6 and 6.7 illustrate the simulated flow field.

As for SIM1, measurements of the u and w velocity components were made using the Nixon current propeller at the following grid intersections: $X = 0.1, 0.2, 0.4, 0.8, 1.2, 1.6, 1.8$ and 1.9 ; $Y = 0.02, 0.04, 0.08, 0.16, 0.32, 0.48$ and 0.60 m; and at 0.0972 m intervals in the transverse (Z) direction.

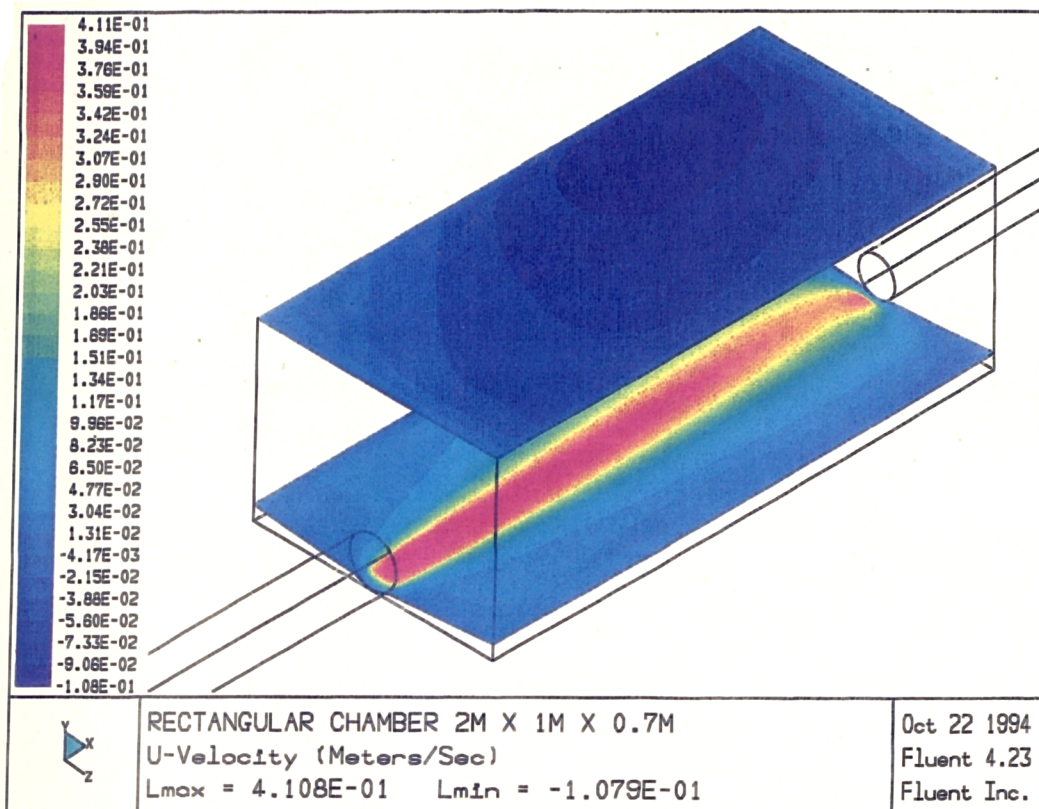


Figure 6.6 u -velocity contours for SIM2

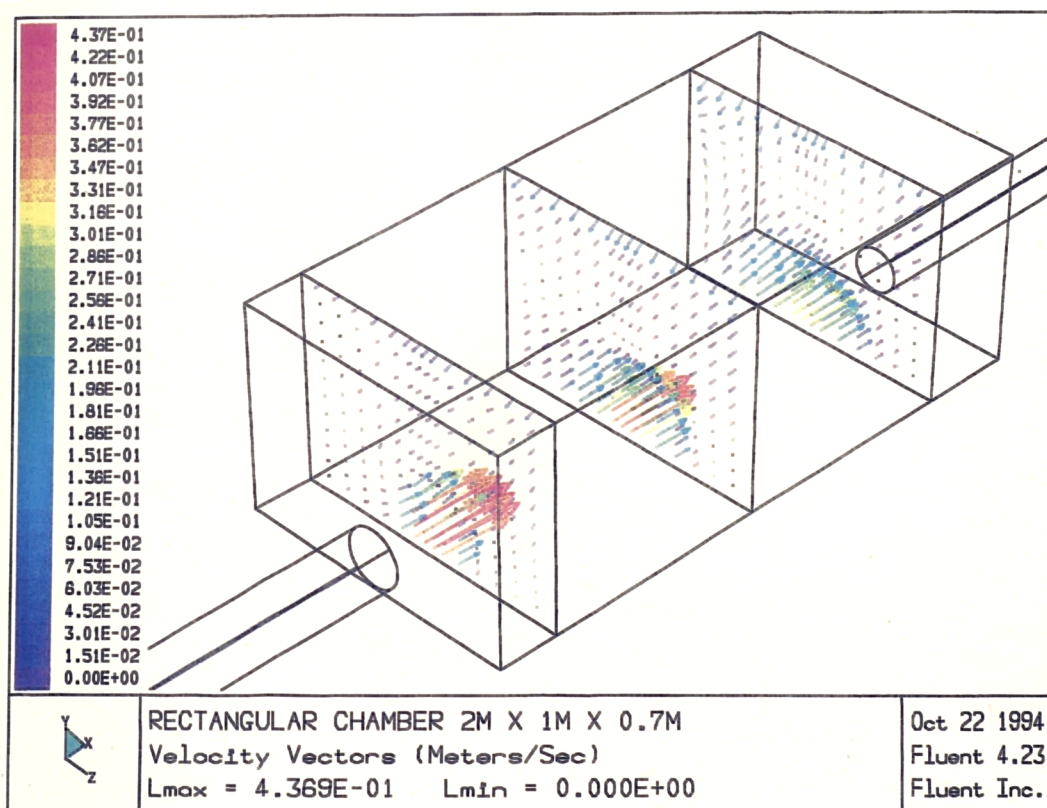


Figure 6.7 Velocity vectors for SIM2

Additional measurements were also made with the LDA system, for both SIM1 and SIM2. The LDA system, described in chapter 3, facilitated measurement of the v velocity components. For both validations two slices were selected for detailed measurements - $Z = 0.486$ and $Z = 0.875$ m. These two slice positions represent the fifth and ninth grid intersections in the Z direction. Measurements were made at longitudinal intervals of 0.05 m, and at vertical intervals of 0.03 m for SIM1 and 0.05 m for SIM2. Measurements were not possible in the regions $X = 0.95 - 1.05$ or $Y = 0.50 - 0.55$ due to obstruction from the chamber support structure.

Table 6.1 Flow measurement locations

| | Method | Components measured | SIM1 | SIM2 |
|-------------------|-------------------------|---------------------|--|--|
| Horizontal slices | Nixon current propeller | u and w | $Y = 0.01$ $Y = 0.02$ $Y = 0.04$ $Y = 0.08$ $Y = 0.16$ | $Y = 0.02$ $Y = 0.04$ $Y = 0.08$ $Y = 0.16$ $Y = 0.32$ $Y = 0.48$ $Y = 0.60$ |
| Vertical slices | LDA | u and v | $Z = 0.486$ $Z = 0.875$ | $Z = 0.486$ $Z = 0.875$ |

The slices where measurements were made are summarised in Table 6.1. For each of these slices a vector plot has been produced, showing both the measured and the simulated velocities. Example comparisons, for the horizontal slice $Y = 0.08$ m and the vertical slice $Z = 0.875$ m are presented in Figure 6.8 and 6.9 respectively. Comparisons for all the slices listed in Table 6.1 are presented in Appendix B.

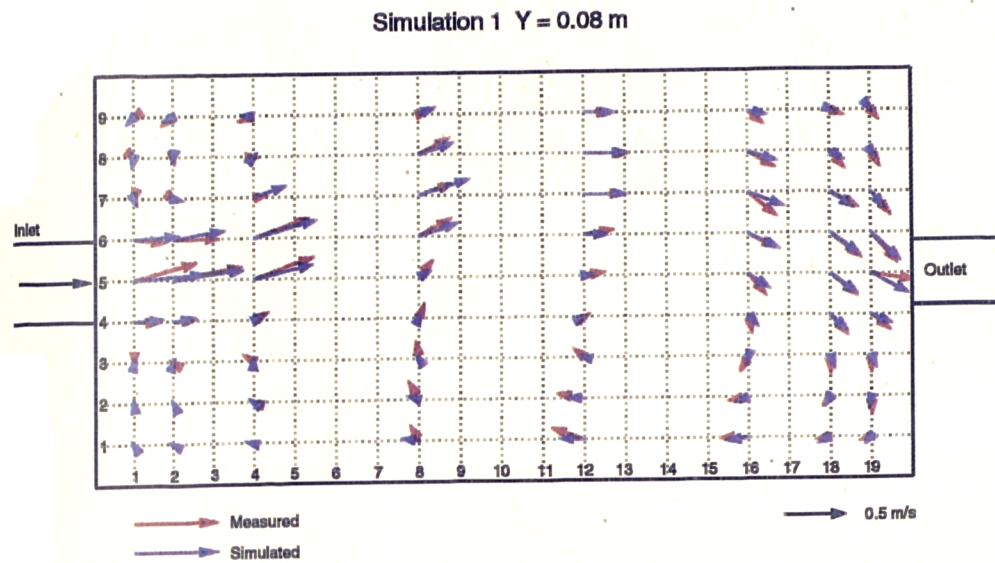


Figure 6.8 An example comparison between measured and simulated velocity (Simulation 1, horizontal slice $Y = 0.08 \text{ m}$)

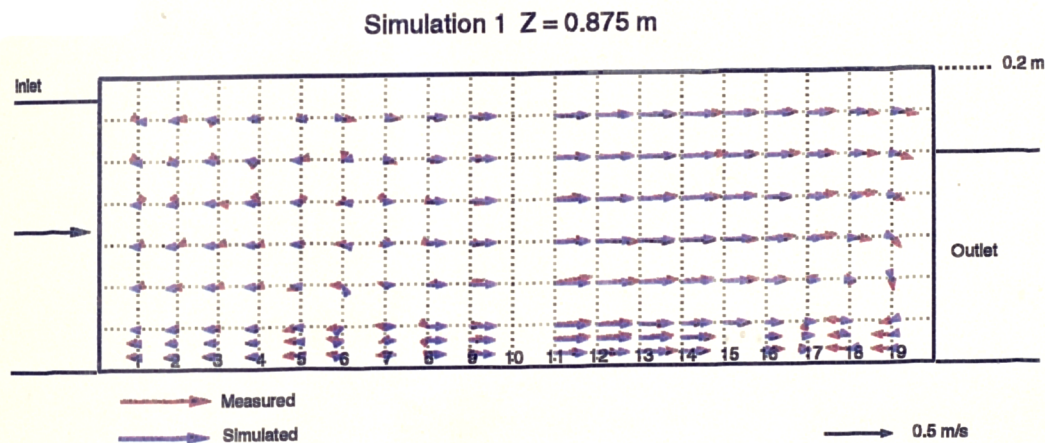


Figure 6.9 An example comparison between measured and simulated velocity (Simulation 1, vertical slice $Z = 0.875 \text{ m}$)

The specific grid intersections where the simulation data were reported did not necessarily coincide with the positions where the laboratory measurements were taken. For this reason, in order to enable comparisons between the two to be undertaken, the simulated velocity data were interpolated onto the measured data matrix using the TecPlot software.

For the horizontal slices the vector plots show the resultant of the u and w velocity components, while for the vertical slices the resultant of the u and v velocity

components were displayed. The vector plots allow comparisons between the measured and the simulated flow fields to be made very easily.

Appendix B also includes contour plots of the directional error associated with each slice through the flow field. The directional error contour plot for the data presented in Figure 6.8 is reproduced in Figure 6.10 as a sample illustration. The plots show the angular deviation between 0° and a maximum of 180° . They do not indicate whether the deviation is clockwise or anticlockwise, although this may readily be evaluated from the accompanying vector plots.

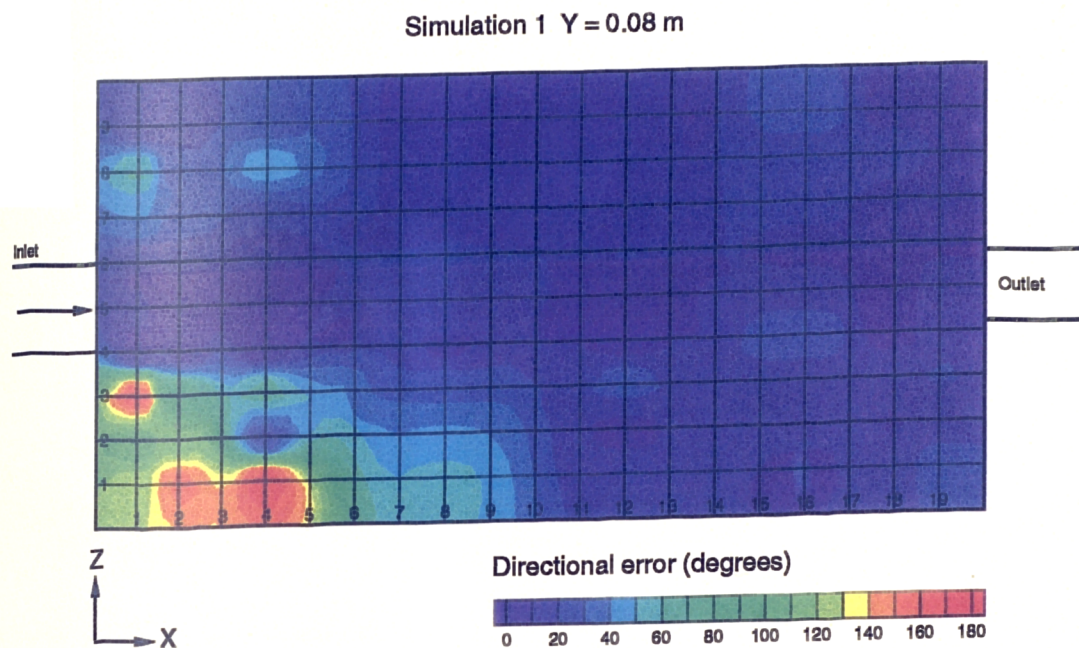


Figure 6.10 An example of the directional error contour plots presented in Appendix B

The vector plots were then employed to produce a single three-dimensional flow diagram for each of the two validation cases, Figures 6.11 and 6.12 respectively. These plots were designed to show more clearly the locations where discrepancies between the measured and simulated flow fields occurred.

Figure 6.11 shows that the large scale features of the measured flow field were reproduced by the simulation in the case of SIM1. The measured flow field was described in chapter 5. The flow was dominated by a clockwise circulation which occupied most of the chamber plan area. In the left hand corner at the upstream end of the chamber a secondary anticlockwise circulation was identified, while velocities in the upstream right hand corner were very low indeed. The flow was essentially two dimensional, with little difference throughout the depth. The main difference between

the simulated flow and that which was measured in the laboratory was the shape and extent of the return current associated with the main circulation. In the case of the simulation, the current did not curve back to join the inflow jet as quickly and remained close to the right hand wall much further towards the upstream end of the chamber. It was also noted that the simulated inflow jet crossed to the left wall within a shorter distance of the inlet, and consequently that the secondary circulation in the upstream left hand corner extended less far downstream.

Figure 6.12 shows that the flow field in SIM2 was far more complex than in SIM1, and that the vertical flow component was more significant. The measured flow field was essentially symmetrical about the longitudinal chamber axis ($Z=0.486$), but divided into two vertical flow layers. In the lower flow layer, the inflow jet followed a straight path to the outlet along the centre of the chamber. At the downstream end twin return currents developed, where the flow moved a small distance upstream along the two side walls. Some of the inflow jet was also deflected upwards at the downstream end of the chamber. This produced an upper layer to the flow field in which the velocities were moderate, and where the flow direction was principally from the downstream to the upstream end of the chamber. The dominant features of the flow field were accurately reproduced in the simulated flow pattern, although the return currents associated with the side walls close to the bed at the downstream end of the chamber were less vigorous. In both the measured data and the simulation results it was observed that the mid-depth (slice $Y = 0.32$) flow velocities were comparatively small. In the case of the simulated flow field an anticlockwise circulation could be identified at this depth; this had not been detected in the laboratory.

Both the comparisons suggested that the FLUENT simulations reproduced the main features of the measured flow fields. Particularly reassuring was the observation that the simulation produced the asymmetric circulatory pattern observed in SIM1, and also the more symmetrical pattern that arose in SIM2, using the same simulation conditions and the same PATCH procedure. It appeared that the simulations were least able to replicate the measured data in situations where low velocity circulations and reverse flows were present. The next section provides a quantitative evaluation of the simulation performance.

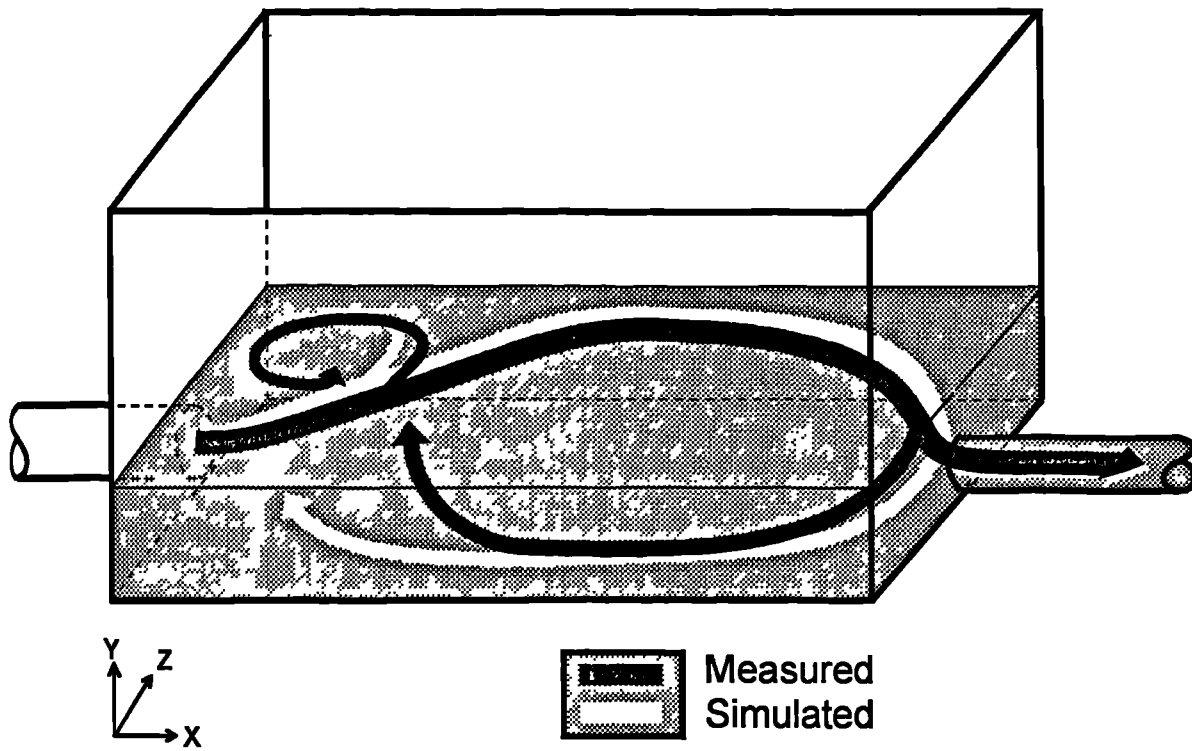


Figure 6.11 Flow comparison for SIM1

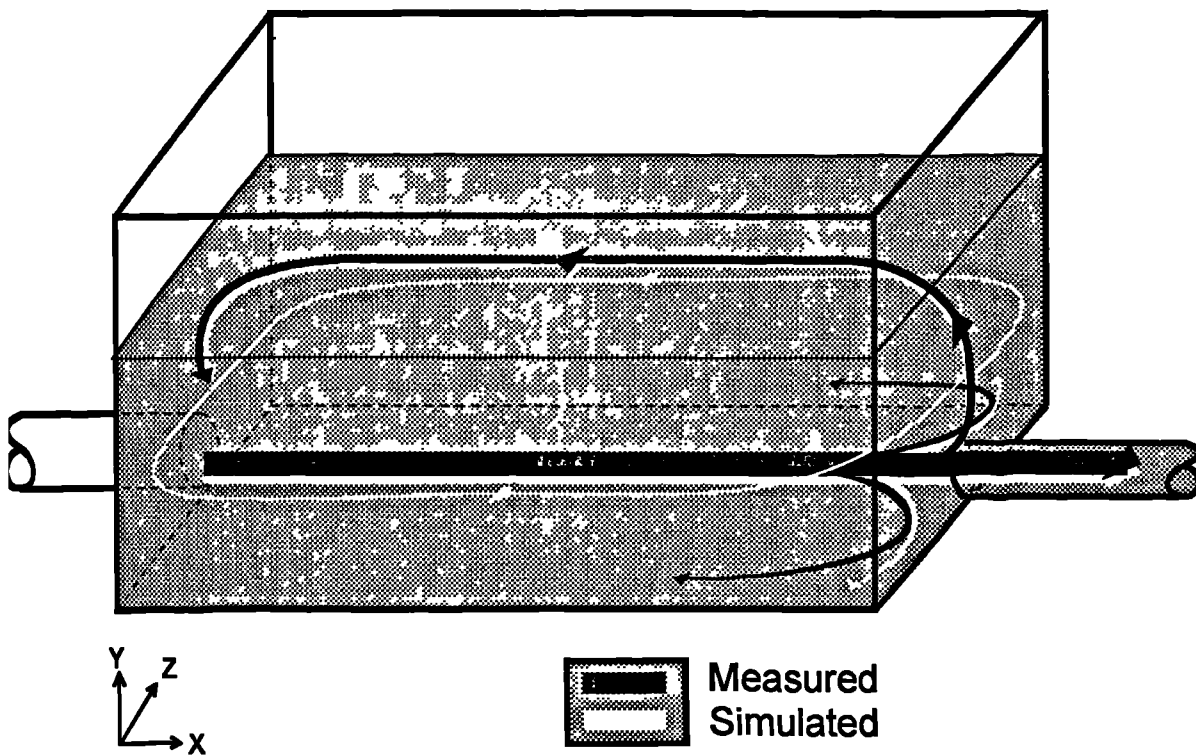


Figure 6.12 Flow comparison for SIM2

6.4.3 A Quantitative Assessment of Simulation Accuracy

The above discussion has pointed to areas where the simulated flow field differed notably from the measured data. However, in addition to this qualitative assessment of the simulation accuracy, a method of quantifying the error was sought.

If the simulated u -velocity at a point is denoted by u_{sim} , and the measured u -velocity is expressed as u_m , then the following estimates of the error of the simulation at that point (ε_e) might be considered:

1. $\varepsilon_e = \frac{u_{sim}}{u_m}$, i.e., the ratio of simulated to observed velocity;
2. $\varepsilon_e = u_{sim} - u_m$, i.e., the difference between the simulated and the observed velocity;
3. $\varepsilon_e = \frac{u_{sim} - u_m}{u_m}$, i.e., the difference between the simulated and the observed velocity expressed as a proportion of the observed value;
4. $\varepsilon_e = \frac{u_{sim} - u_m}{\bar{u}}$, i.e., the difference between the simulated and the observed velocity expressed as a proportion of the mean inlet velocity.

Option 1 was rejected because high values of ε_e could arise from very small errors, if the flow velocity itself was small, whereas comparatively large errors in regions of high velocity appeared far less significant. Option 2 gave more meaningful results in this respect, but the results were not dimensionless, being expressed in m/s. Two approaches to converting the error into a dimensionless parameter were investigated. In the first, option 3, the difference was expressed as a proportion of the observed value. The main disadvantage of this approach is as with option 1; errors can appear to be extremely large in areas where the measured velocity component was small. The final technique that was selected is option 4. In this case the error is expressed as a proportion of the mean inlet velocity and the error is non-dimensional. The errors for the v - and w -velocity components were expressed in the same way, i.e., for the v -

component, $\varepsilon_e = \frac{v_{sim} - v_m}{\bar{u}}$.

In Table 6.2 and Table 6.3 the calculated errors for each of the three velocity components are summarised for SIM1 and SIM2 respectively. Each data point with a given Y position was grouped with all the data from the same depth for the analysis.

Thus the results are presented for the 'slices' $Y = 0.01$, $Y = 0.02$, etc. Summary data for all points measured are also presented. ϵ_{mean} is the mean of the errors calculated over all the points in the slice under consideration. If the errors are randomly distributed then the value of ϵ_{mean} will be zero. However, if there is a systematic error of overprediction or underprediction then ϵ_{mean} will be positive or negative. Similarly, ϵ_{max} and ϵ_{min} are the maximum and minimum values of ϵ_r . For example, if the value of ϵ_r is 0.2 then the simulated velocity overpredicted the measured value by an amount equivalent to 20% of the mean inlet velocity, whilst a value of $\epsilon_r = -0.1$, means an underprediction equivalent to 10% of the mean inlet velocity. The statistic $\epsilon_{10\%}$ means the percentage of data points for which the value of ϵ_r is within $\pm 10\%$ of the mean inlet velocity.

Table 6.2 Error statistics for SIM1

| | ϵ_{mean} | ϵ_{max} | ϵ_{min} | $\epsilon_{10\%}$ |
|--------------------------------|--------------------------|-------------------------|-------------------------|-------------------|
| <u>u velocity</u> | | | | |
| $Y = 0.01$ | 0.057 | 0.397 | -0.293 | 48.61 |
| $Y = 0.02$ | 0.056 | 0.389 | -0.199 | 52.78 |
| $Y = 0.04$ | 0.038 | 0.264 | -0.212 | 69.44 |
| $Y = 0.08$ | 0.024 | 0.274 | -0.145 | 73.61 |
| $Y = 0.16$ | 0.022 | 0.301 | -0.186 | 69.44 |
| $Z = 0.875$ | 0.003 | 0.369 | -0.219 | 55.63 |
| $Z = 0.486$ | -0.083 | 0.233 | -0.305 | 54.72 |
| Overall | -0.003 | 0.397 | -0.305 | 58.41 |
| <u>w velocity</u> | | | | |
| $Y = 0.01$ | 0.043 | 0.227 | -0.229 | 65.28 |
| $Y = 0.02$ | 0.023 | 0.185 | -0.216 | 63.89 |
| $Y = 0.04$ | 0.011 | 0.180 | -0.239 | 72.22 |
| $Y = 0.08$ | 0.006 | 0.147 | -0.223 | 70.83 |
| $Y = 0.16$ | 0.009 | 0.158 | -0.192 | 77.78 |
| Overall | 0.018 | 0.227 | -0.239 | 70.00 |
| <u>v velocity</u> | | | | |
| $Z = 0.875$ | 0.009 | 0.146 | -0.112 | 97.89 |
| $Z = 0.486$ | -0.010 | 0.092 | -0.118 | 99.06 |
| Overall | 0.001 | 0.146 | -0.118 | 98.39 |

Table 6.2 shows that SIM1 was a reasonably good representation of the observed data. Although there does not appear to have been any systematic error in the overall predictions, an overprediction in the u and w velocities close to the chamber bed can be identified. On average the near bed velocity was overpredicted by 6%, whilst in the worst case the overprediction was equivalent to 40% of the mean inlet velocity. However, over 58% of the u -velocity predictions were within a value equivalent to

10% of \bar{u} of the observed data. The v and w velocity predictions compared more favourably to the observed data, although this is not surprising given that the actual velocities involved were considerably smaller.

The comparisons for SIM2 were generally more favourable in terms of the proportion of errors below the 10% of mean inlet velocity threshold. The reason for this is that the flow velocities in the second simulation were generally much smaller than in the first due to the increased depth of flow. When expressed as a proportion of the mean inlet velocity these values obviously have a smaller impact. However, the most extreme errors exceeded 50% in some cases. Once again, a small overprediction in the near bed u -velocity component was identified.

Table 6.3 Error statistics for SIM2

| | ϵ_{mean} | ϵ_{max} | ϵ_{min} | $\epsilon_{10\%}$ |
|--------------------------------|--------------------------|-------------------------|-------------------------|-------------------|
| <u>u velocity</u> | | | | |
| Y = 0.02 | 0.057 | 0.305 | -0.208 | 60.61 |
| Y = 0.04 | 0.034 | 0.376 | -0.572 | 59.60 |
| Y = 0.08 | 0.023 | 0.342 | -0.324 | 61.62 |
| Y = 0.16 | -0.025 | 0.335 | -0.413 | 59.60 |
| Y = 0.32 | -0.023 | 0.160 | -0.260 | 70.71 |
| Y = 0.48 | -0.045 | 0.106 | -0.390 | 69.70 |
| Y = 0.64 | 0.058 | 0.279 | -0.067 | 69.70 |
| Z = 0.486 | -0.083 | 0.483 | -0.423 | 52.22 |
| Z = 0.875 | 0.047 | 0.276 | -0.125 | 80.00 |
| Overall | -0.003 | 0.483 | -0.572 | 65.68 |
| <u>w velocity</u> | | | | |
| Y = 0.02 | -0.007 | 0.090 | -0.107 | 97.98 |
| Y = 0.04 | -0.008 | 0.089 | -0.125 | 97.98 |
| Y = 0.08 | -0.008 | 0.088 | -0.115 | 97.98 |
| Y = 0.16 | -0.014 | 0.067 | -0.194 | 100.00 |
| Y = 0.32 | -0.012 | 0.043 | -0.059 | 100.00 |
| Y = 0.48 | 0.002 | 0.043 | -0.045 | 100.00 |
| Y = 0.64 | 0.026 | 0.144 | -0.083 | 95.96 |
| Overall | -0.003 | 0.144 | -0.125 | 98.56 |
| <u>v velocity</u> | | | | |
| Z = 0.486 | -0.015 | 0.574 | -0.091 | 99.17 |
| Z = 0.875 | 0.010 | 0.145 | -0.086 | 99.75 |
| Overall | -0.002 | 0.574 | -0.091 | 99.47 |

6.5 Discussion

From the above discussion it is clear that the simulations undertaken with the FLUENT CFD software produced good models of the observed flow fields. Large scale flow circulations, both horizontal and vertical, were successfully simulated. In some regions, notably those where low velocity return currents arose, the simulations could have been improved upon. The observed discrepancies between the simulation and the measured laboratory data were, however, considered to be sufficiently minor to conclude that the research should proceed to the sediment transport modelling phase. This aspect of the research is described in the following chapter.

However, it is appropriate, at this stage, to consider a number of issues relating to the accuracy of the simulations which have emerged as a result of experience gained following the completion of this phase of the research. It is now apparent that the choice of turbulence model, the simulation of the free surface, and the simplification of the outlet geometry might have provided sources of error. These factors are expanded upon below.

In both SIM1 and SIM2, the default k- ϵ turbulence model was employed. The reasons for this choice were presented in section 6.3. However, one deficiency of the k- ϵ model is that it includes an isotropic description of the turbulent viscosity. It is therefore not well suited to the prediction of highly non-isotropic turbulence such as that which arises in swirling flows. Although the observed patterns in the storage chamber did not exhibit truly swirling flow, the complex flows did include zones of recirculation and zones of low velocity. This suggests that other turbulence models, including the RSM and the RNG k- ϵ turbulence model which are implemented in the current version of FLUENT, might enable more accurate flow simulations to be obtained in the future.

In both SIM1 and SIM2 the free water surface was modelled using a friction free wall. This is because the simulation of a full free surface involves the modelling of a two phase flow which could not be used in conjunction with a Boundary Fitted Co-ordinate geometry definition in version 4.2 of the software. In this case, any error in the definition of the position of that friction free wall would distort the pressure distribution in the flow, and consequently the simulated velocity distribution would be affected. Later versions of FLUENT (v. 4.3) do allow full implementation of free surface flows with BFC geometries, and might also provide improvements to the models presented here.

Finally, in both SIM1 and SIM2 the outlet was modelled as the 0.15 m diameter outlet pipe. However, in the case of SIM2, the laboratory set-up actually used the outlet penstock closed down to a little over 1/4 open (see chapter 3 for a description of the penstock operation). Initially it was decided that this simplification should be made in order to minimise the modelling complexity. The outlet grid was not rectilinear, but fitted to the circular geometry in the same way as the inlet grid illustrated in Figure 6.2. It was not possible simply to alter the cell type from LIVE to WALL in the upper three quarters of the outlet to represent the penstock, as the division between cells was neither perfectly horizontal, nor did any cell boundary coincide exactly with the position of the lower penstock edge. By retaining the SIM1 outlet definition it was possible to produce the simulation geometry and grid for SIM2 simply by translating the position of the upper surface and increasing the number of vertical grid divisions.

It was anticipated that this simplification would only impact on the flow field in a minor, localised way. In the laboratory velocity measurements (see for example page B-10 in Appendix B) it was noted that the outlet only appeared to affect the flow field in a small zone which extended no more than 200 mm upstream from the outlet. Furthermore it was felt that the use of an imposed free surface in the case of the simulation would also tend to dampen out the effect of any errors in the way in which the outlet was represented. In a complex three-dimensional flow field of this type it is virtually impossible to quantify the anticipated errors theoretically. For this reason, an additional simulation was carried out at a later stage, and this confirmed that when the correct outlet geometry was used the effects on the flow field extended no more than 100 mm upstream from the outlet.

6.6 Conclusions

It was demonstrated that the CFD software FLUENT could be successfully employed to predict the velocity distribution for two laboratory flow situations. The simulation procedure that was adopted has been described in detail. Default settings were used wherever possible, illustrating that CFD software may be used without extensive user experience, as an engineering design tool. Where the accuracy of the simulation was poor, some suggestions for improvements that could be made to the simulation procedure have been presented.

However, the focus of this study is the development of a methodology for sediment deposition prediction, and further optimisation of the fluid flow simulation was not warranted. The CFD simulation resulted in a good representation of the observed flow field, and subsequent attention was focused on how such a simulation might be applied to the modelling of sedimentation in storage chambers. This next phase of the research is described in chapter 7.

7. Efficiency Prediction Using Fluent

7.1 Introduction

In the previous chapter it was demonstrated that the CFD software FLUENT could be used to accurately simulate the flow field that had been measured in a laboratory storage chamber. In this chapter the possibilities of using the simulation data to predict the sedimentation efficiency of the chamber are discussed. Efficiency was defined in chapter 4 as the proportion of the inflow sediment load that is settled to the chamber bed. In order to measure efficiency in the laboratory, olive stone sediment was continuously injected into the laboratory model and continuous measurements of the sediment concentration in the inflow to and outflow from the chamber were made. It was suggested that the performance of a chamber could be expressed in terms of the relationship between the mean inlet velocity (\bar{u}) and the chamber efficiency (η). The relationship characteristically took the form of a curve that approached an efficiency of 1 for low mean inlet velocities and fell towards zero as the mean inlet velocity increased. For brevity, this relationship is referred to as the \bar{u}/η curve.

In this chapter two different approaches to the problem of efficiency prediction using CFD are presented. In the first case, described in section 7.2, FLUENT was used to model the flow field in the chamber, and the bed shear stress distribution predicted by FLUENT was used to determine the distribution of sediment on the chamber bed. An entirely different approach is described in section 7.3, where the particle tracking facility in FLUENT was used. A distinction is made between the \bar{u}/η curves estimated using bed shear stress analysis and the particle tracking technique. These are referred to as the \bar{u}/η_{BSS} curve and the \bar{u}/η_{PT} curve respectively.

All tests used the basic laboratory chamber simulation (SIM1) outlined in the previous chapter. In order to establish the \bar{u}/η curve, five further simulations were carried out, in which mean inlet velocities of 0.05, 0.1, 0.2, 0.4, and 0.8 m/s were used. These conditions were selected to reproduce the range of test conditions used in the

laboratory. The simulations were in all other respects identical to that which has already been described.

7.2 Efficiency Prediction Based on the Bed Shear Stress Distribution

7.2.1 Introduction

In chapter 5 it was demonstrated in a laboratory chamber that:

1. The pattern of sediment deposition could be predicted from the flow field by means of a critical bed shear stress (τ_{cd}) below which sediment deposition occurred. This statement was shown to be valid under both steady and time-varying flow conditions;
2. The proportion of the chamber bed covered with sediment following a laboratory efficiency test (C_l) could be employed to predict the observed efficiencies over a broad range of mean inlet velocities.

$$\eta = 0.134 + 0.397C_l \quad (7.1)$$

It follows from these two observations that the proportion of the bed where the shear stress is lower than τ_{cd} , termed the predicted coverage (C_{BSS}), should equate to C_l , and consequently that C_{BSS} could be substituted for C_l in Equation 7.1 to enable the chamber efficiency to be predicted directly from the results of the bed shear stress analysis:

$$\eta_{BSS} = 0.134 + 0.397C_{BSS} \quad (7.2)$$

The following procedure for efficiency prediction was therefore hypothesised:

1. Build a CFD model of the chamber;
2. Obtain the flow field;
3. Obtain the bed shear stress distribution;
4. Using an appropriate critical bed shear stress value estimate the proportion of covered bed (C_{BSS});
5. Predict efficiency from C_{BSS} via Equation 7.2.

The way in which this procedure was implemented is outlined in the following section.

7.2.2 Efficiency Prediction

In turbulent flows FLUENT applies the log law of the wall (Equation 5.1) to predict the shear stress on the fluid at the wall. Thus, the method of estimating bed shear stress using FLUENT is the same as that applied to the laboratory velocity measurements. The calculations are based on the velocity components at the node nearest to the wall. For each of the five flow simulations, the three components of the wall shear stress acting on the chamber bed were output directly from FLUENT by means of a LINE-PRINT (LP) file.

The bed shear stress (τ_0) acting on each cell was calculated as the magnitude of the resultant of the X- Y- and Z-direction wall shear stress components. τ_0 was then compared to τ_{cd} , the critical bed shear stress for deposition, and if $\tau_0 < \tau_{cd}$, then deposition was assumed for that particular cell. The value of τ_{cd} was taken as 0.04 N/m^2 , as determined in the laboratory. It can be seen from Figure 7.1 that the simulated bed shear stress distribution was very similar to the distribution which was derived from the laboratory velocity measurements. The latter distribution was first shown in Figure 5.4, and is reproduced here again as Figure 7.2. The main difference between the two plots relates to the simulation error in the positioning of the return current close to the right-hand wall (see chapter 6).

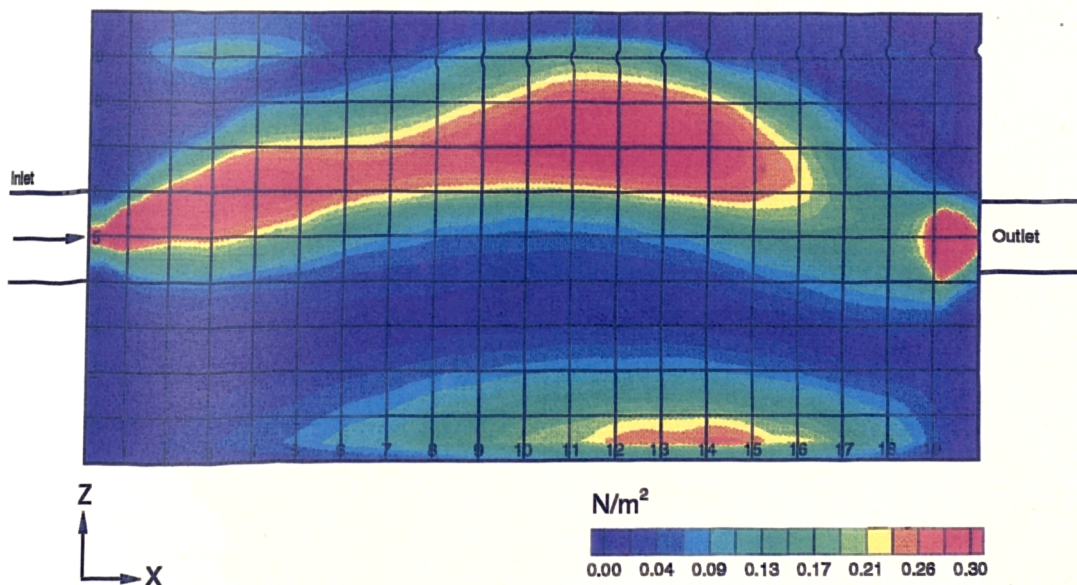


Figure 7.1 Simulated bed shear stress distribution

In order to calculate C_{BSS} , the exact position of each cell was determined from the UNIVERSAL file output, and this was used to determine the area of bed that each cell

represented. C_{BSS} was defined as the proportion of bed where the bed shear stress fell below τ_{cd} .

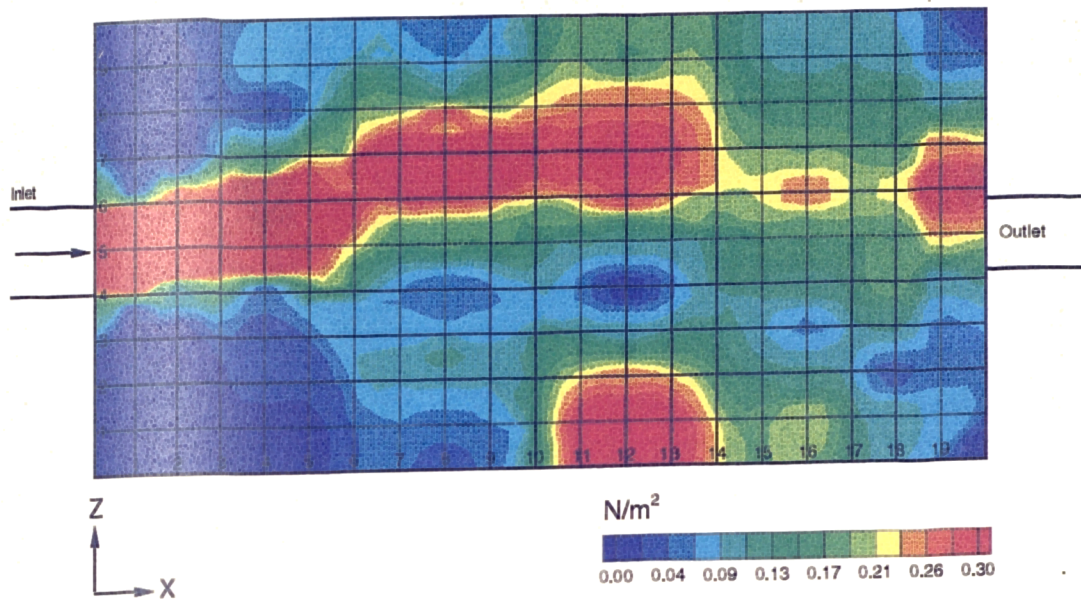


Figure 7.2 Bed shear stress distribution calculated from laboratory measurements

A comparison was made between the values of C_{BSS} predicted from the simulations and the values of C_I , which had been determined in the laboratory. Figure 7.3 shows that, for the mean inlet velocities of 0.4 m/s or greater, the values of C_{BSS} were higher than the values of C_I .

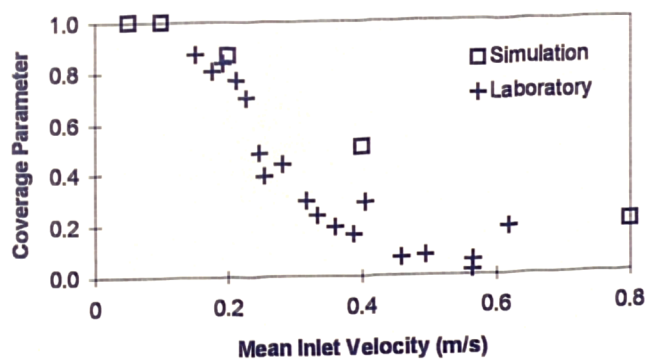


Figure 7.3 Simulated and measured values for the coverage parameter

There are a number of factors which may have contributed to the observed differences, including the discrepancies between the measured and simulated flow fields which

were discussed in chapter 6. Any errors in the flow simulation would inevitably have produced errors in the predicted distribution of bed shear stress.

There were also several potential sources of error in the laboratory measurements. The laboratory determinations of τ_{cd} and C_l were both based on the subjective interpretation of laboratory sketches and photographs, whilst the problems experienced with the laboratory estimation of efficiency have been fully discussed in chapter 4.

It was concluded, however, that the predicted values of C_{BSS} were sufficiently similar to the measured C_l data to support the general approach presented here. For these reasons a new calibration was carried out, which related the values of C_{BSS} to the laboratory efficiency data directly. The equation was:

$$\eta = 0.0779e^{2.05C_{BSS}} \quad (7.3)$$

The results of the application of this regression are shown in Figure 7.4. The regression was carried out using the data for inlet velocities of 0.1 m/s or greater. This was because C_{BSS} actually reached its maximum possible value of 1 at that velocity (i.e. the bed shear stress nowhere exceeded 0.04 N/m² and complete coverage of the bed with sediment was inferred). It may be seen that when C_{BSS} is unity, η is 0.6 (from equation 7.3), and that values of η greater than 0.6 cannot be predicted using this approach. When the efficiency is 0.6 the chamber bed will be completely covered with sediment, but 40% of the incoming sediment load will still exit from the chamber. For lower value of the mean inlet velocity, less sediment will exit and the sediment layer on the chamber bed will be thicker. The efficiency may exceed 0.6, but the coverage will still be 100%. As the bed shear stress method does not account for the depth of deposited sediment, it can only be said that when the coverage is 100%, the efficiency is at least 0.6. It should be noted, however, that the range of application identified here ($0 \leq \eta \leq 0.6$) is a function of the critical bed shear stress for deposition identified in the laboratory. For other bed roughness values or sediment types it is probable that a different range of application would be identified.

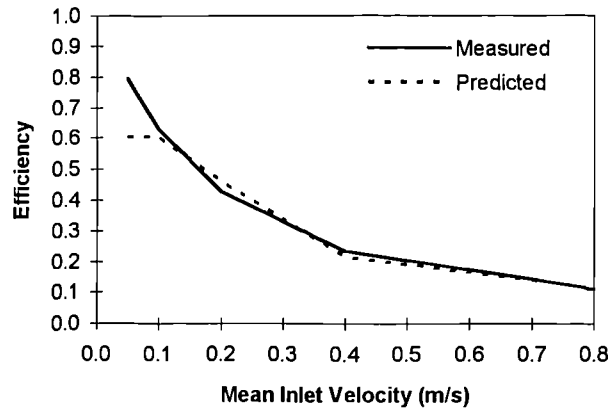


Figure 7.4 Efficiency curve derived from simulated C_{BSS} data

The effect of altering the value of τ_{cd} is illustrated in Figure 7.5. As one would expect, the lower values of τ_{cd} produced smaller values for C_{BSS} at a given inlet velocity. However, the shape of the efficiency curve was in all cases similar. It should be noted that the value of $\tau_{cd} = 0.01 \text{ N/m}^2$ was sufficiently low to eliminate the plateau of coverage values at low inlet velocities. However, the critical bed shear stress for deposition found in the laboratory experiments was 0.04 N/m^2 , and this value should therefore be used in the further analysis.

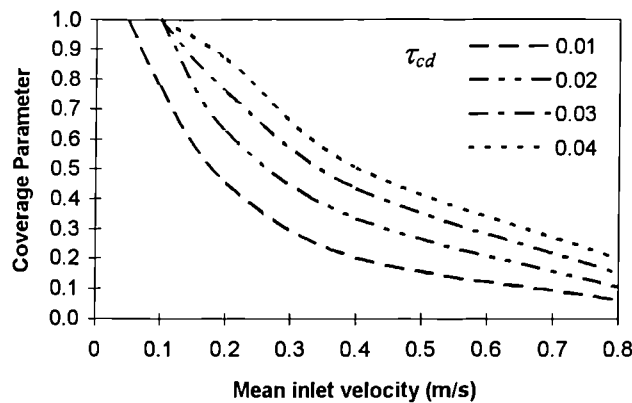


Figure 7.5 Values of the coverage parameter for different values of τ_{cd}

7.2.3 Summary

A method for predicting chamber efficiency from the FLUENT bed shear stress data has been presented. The method is summarised below:

1. Build a CFD model of the chamber;
2. Obtain the flow field;
3. Obtain the bed shear stress distribution;
4. Using an appropriate critical bed shear stress value (in this case 0.04 N/m^2), estimate the predicted coverage (C_{BSS});
5. Predict efficiency from C_{BSS} via Equation 7.3.

It was noted that the range of application for the method was restricted to $0 \leq \eta \leq 0.6$. This resulted from the fact that the predicted coverage was unity for any value of η greater than 0.6.

In chapter 8 this approach is implemented, along with the particle tracking technique discussed below, in the prediction of comparative chamber efficiencies for ten storage chamber configurations.

7.3 Particle Tracking with FLUENT

7.3.1 Introduction

In addition to solving transport equations for one fluid phase, FLUENT allows the computation of the trajectories of spherical particles dispersed within it. An investigation was therefore carried out to assess the potential of the particle tracking routine to estimate storage chamber efficiency.

Particle tracking presents a potentially attractive option for efficiency prediction as it is independent of the empirically derived critical bed shear stress values and the coverage/efficiency relationship. It requires only flow field simulation data and the particle properties.

The various options offered by FLUENT for particle tracking which appear to be of relevance to this application are described in more detail in section 7.3.2 below. The mathematical approach used in the particle tracking routine is not described here, but may be found in the FLUENT user manual (Fluent, 1993).

In section 7.3.3 each of the set-up options for particle tracking is addressed in turn, and the procedure by which the particle tracking was optimised to best replicate the laboratory \bar{u}/η curve is described.

In addition to efficiency prediction, a preliminary investigation was carried out to assess whether the particle tracking simulations might also be used to indicate the distribution of sediment on the chamber bed. This research is described in section 7.3.4.

7.3.2 Particle Tracking Options

The particle tracking routine requires the physical properties of the particles, the input location of the particles and the way the particles respond to boundaries to be defined. It is also necessary to select a number of options which relate to the way in which the simulation is carried out. Appendix A includes a complete list of all the available particle tracking set-up options; those which appeared to be relevant to this particular application are discussed in detail below.

7.3.2.1 Injection location and particle size

Particle injections may be defined individually or as a group. The main advantage of the grouped particle input facility is that it enables particles for which either the size or position varies over a range of values to be simulated. It is possible, for example, to input a group of physically identical particles using a horizontal line across the centre of a pipe to define a range of injection locations. Only the first and last positions need to be specified, and all other values are determined via linear interpolation. Alternatively, it is possible to input particles at a single location, for which the particle size is varied. Although it is actually possible to vary size and position simultaneously, FLUENT advises the user in general to supply a range for only one of the initial conditions in a given group. Otherwise it is possible that simultaneous inputs of a spatial distribution and a size distribution place all the small particles at the beginning of the range and the large particles at the end of the range.

One technique for setting a range of particles is simply to define the upper and lower limits of the group, and use the linear interpolation provided by FLUENT to select an appropriate value for each particle in the range. However the mass fractions in a particle distribution do not vary linearly, and the Rosin-Rammler particle size distribution is provided as an alternative. The distribution was derived to describe coal dust, and was found to be appropriate for crushed and ground materials generally (Rosin and Rammler, 1933). It should, therefore, provide a suitable description of the particle size distribution of the crushed olive stone used in this research. The Rosin-Rammler distribution function is based on the assumption that an exponential

relationship exists between the particle diameter d , and the mass fraction of particles with diameter greater than d , M_d :

$$M_d = \exp\left(-\left(\frac{d}{\bar{d}}\right)^{n_{sp}}\right) \quad (7.4)$$

FLUENT refers to \bar{d} as the mean diameter and to n_{sp} as the spread parameter. The Rosin-Rammler distribution fitted to the 150 μm crushed olive stone (see Figure 7.6) yields values of 59 μm and 1.65 for \bar{d} and n_{sp} respectively.

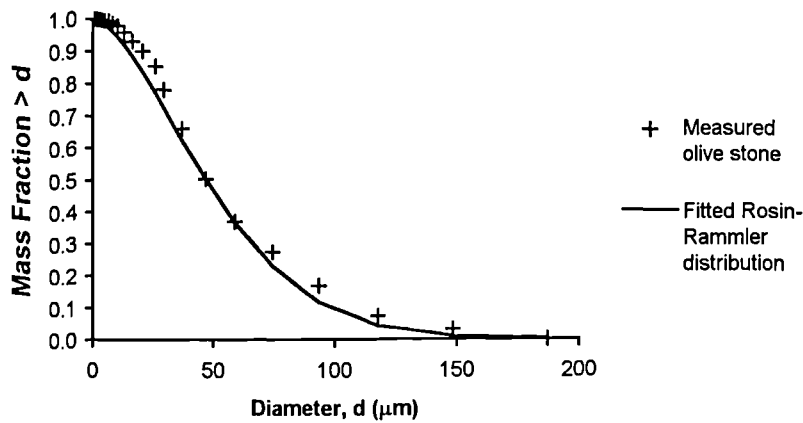


Figure 7.6 Rosin-Rammler distribution for 150 μm crushed olive stone

In addition to the particle size and distribution, the particle density must also be defined. It is not possible to define a range of densities, only a constant value for all particles.

The use of particle groups, in which the injection location or particle size were varied across the group, is discussed in section 7.3.3.

7.3.2.2 Particle boundary conditions

Particle boundary conditions are required to specify the way in which a particle that comes into contact with the boundary will be treated. The boundary condition, or trajectory fate, can be defined separately for each cell type (e.g. inlet, wall or outlet). The available conditions are:

1. *Reflect* – rebounds the particle off the boundary in question;
2. *Trap* – terminates the trajectory calculations and records the fate of the particle as *trapped*;

3. *Escape* – reports the particle as having escaped when it encounters the boundary in question, and trajectory calculations are terminated;
4. *Saltation* – in order to prevent ‘trickling’ of a particle along a wall, places the particle in the flow a small distance from the wall as though it was leaping back into the flow.

7.3.2.3 *Stochastic particle tracking in turbulent flows*

In turbulent flows the movement of a particle will be affected by the random fluctuations in the flow field. A particle injected in one position will therefore follow a different path to that of an identical particle injected at the same location at a different instant in time. When uncoupled particle tracking is undertaken (see section 7.3.2.5), the flow field is represented by the mean flow, and the user may choose either to compute the particle trajectory based on the mean velocity field, ignoring the effects of turbulence on the particle trajectories, or to include turbulent velocity fluctuations in the particle force balance. Because random numbers are used in the simulation of the turbulent velocity fluctuations, this process is termed *stochastic* particle tracking. The turbulent fluctuations are random, but based on the computed local turbulence intensity. Stochastic particle tracking is equivalent to a Lagrangian random walk model. This type of model has been implemented in a number of sedimentation simulations (for example, Bayazit (1972) and Hoyal *et al.* (1995)).

7.3.2.4 *Solution Parameters*

The user may control a wide array of solution parameters (FLUENT, 1994) and the complete list is presented in Appendix A. These control the behaviour of the particle in the flow and at boundaries, the way in which the tracking is reported, and the calculation process. Those parameters that were considered relevant for the application presented in this thesis are:

1. The maximum number of steps [default 5000];
2. Step length factor [default 20];
3. Maximum number of wall reflections allowed per cell [default 25].

7.3.2.4.1 *Maximum number of steps*

The maximum number of steps defines the maximum number of time steps used to compute a single particle trajectory. When the maximum number of steps is exceeded, FLUENT abandons the trajectory calculation for the current particle injection and reports the trajectory fate as *aborted*. The limit on the number of integration time

steps eliminates the possibility of a particle being caught in a recirculating region of the continuous flow field and being tracked infinitely.

7.3.2.4.2 Step length factor

The step length factor controls the integration time step. The accuracy of the dispersed phase trajectory prediction depends on the time step chosen for the integration of the equation of motion for the particle. The time step is computed by FLUENT based on a characteristic time that is related to an estimate of the time required for the particle to traverse the current continuous phase control volume. If this estimated time is defined as Δt^* , the time step Δt used in the model is defined by Equation 7.5 where λ is the step length factor:

$$\Delta t = \frac{\Delta t^*}{\lambda} \quad (7.5)$$

7.3.2.4.3 Number of wall reflections

When the maximum number of wall reflections allowed per cell has been exceeded, FLUENT will *abort* the particle trajectory calculations, and report the injection as *aborted*. Clearly this function may be likened to the concept of a critical bed shear stress for deposition. If the near bed velocities are insufficient to maintain the particle in suspension then deposition (i.e. an *aborted* particle trajectory calculation) will be assumed.

The effect of each of these parameters on the particle tracking results is discussed in section 7.3.3.

7.3.2.5 Coupled or uncoupled calculations

The trajectory and mass transfer calculations are based on the force balance on the particle using the local fluid phase conditions as the particle moves through the flow. FLUENT may be used to predict the particle movement based on a fixed flow field (termed an uncoupled approach), or to include the effect of the particle on the flow (termed a coupled approach). In the coupled approach, the fluid flow pattern is affected by the particle (and vice versa), and alternate calculations of the fluid phase and the particle track may be made until a converged coupled solution is achieved.

7.3.2.6 Limitations

The particle tracking formulation used by FLUENT contains the assumption that the particle concentration is sufficiently dilute that particle-particle interactions and the effects of the particle volume fraction on the fluid phase are negligible. In practice these issues imply that the dispersed phase must be present at a fairly low volume fraction, perhaps less than 10-12%. The particle calculations performed by FLUENT also have limitations when the particles of interest are of sub-micron size. FLUENT's particle tracking routine assumes that an individual particle can be traced throughout its entire trajectory in the current flow field. This procedure must be used with care when the flow field is time-dependent.

7.3.3 Optimisation of Efficiency Prediction using Particle Tracking

7.3.3.1 Introduction

In order to determine the most appropriate set-up options for efficiency prediction, a large number of particle tracking experiments were carried out. The set-up options which were included in the optimisation process related to the particle physical properties, the injection location, the boundary conditions and the solution parameters identified in section 7.3.2.4. The most important considerations were that the selected set-up would produce results that could be interpreted physically, and that they represented a valid basis for the comparison of chambers with differing geometries. It was also desirable that the method should be optimised to produce an efficiency curve that reproduced the laboratory data.

As with the bed shear stress analysis, flow simulations for five different inlet velocities enabled the \bar{u}/η_{PT} curve to be graphed. All particles were introduced at $X = 0.02$ m, that is in the extruded inlet pipe 0.98 m upstream of the chamber inlet. Chamber efficiency was calculated from the proportion of injected particles that did not *escape* through the outlet. It was assumed that the flow field was not influenced by the particles, and therefore only uncoupled calculations were performed. This assumption, which was also discussed in chapter 5, is justified by the low density and concentration of the olive stone sediment used in the laboratory tests. The mean diameter of the olive stone sediment was 47 μm and the flow field was not time dependent. It may be concluded therefore that none of the limitations outlined in section 7.3.2.6 were applicable in this case.

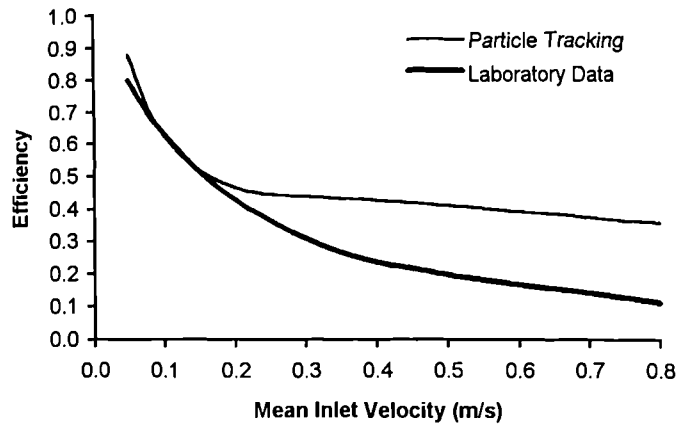


Figure 7.7 Particle tracking efficiency curve compared with the laboratory data

Figure 7.7 shows the optimised particle tracking efficiency curve, compared with the efficiency curve derived from the laboratory experiments. It can be seen from Figure 7.7 that the predicted curve was a good fit for the lowest values of \bar{u} (below 0.2 m/s), but that the efficiency was overpredicted towards the top end of the velocity range. For the mean inlet velocity of 0.8 m/s the predicted efficiency was 0.354, while the measured value was only 0.113. The discrepancies between the predicted and measured efficiencies are discussed in section 7.3.3.5. The set-up options which were used in the production of this curve are presented in Table 7.1.

Table 7.1 Particle tracking configurations

| | |
|------------------------------|--------------------------------|
| Particle size | 4.7E-05 m |
| Inlet distribution | 68 fully distributed particles |
| Particle density | 2,500 kg/m ³ |
| No. of simulations | 50 |
| Wall boundary condition | Reflect |
| Step length factor | 20 |
| Max. no. of wall reflections | 25 |
| Max. no. of time steps | 99,999 |

In order to assess the effect of each of the particle tracking set-up options on the efficiency predictions, a full programme of sensitivity tests should have been undertaken. This would have enabled the effects of all options, both individually and

in combination, to have been assessed, and would also have enabled the identification of the configuration which best replicated the laboratory data. However, the number of tests which would have been required to carry out a rigorous sensitivity analysis made such an approach impractical in this case. For example, to assess only three variations on each of the eight set-up options for five flow simulations would have required $5 \times 3^8 (= 32805)$ efficiency predictions to be made.

Instead, the particle tracking set-up options were examined on an individual basis, and adjusted until a reasonable fit (see Figure 7.7) of the laboratory data had been obtained. Several decisions were reached only once the comparative testing of different chamber geometries, the subject of chapter 8, was underway.

In order to illustrate the effects of the various set-up options, each is now considered in turn; their influence on the efficiency is discussed and justification for the selection that was finally made is presented. In each of the following comparisons all the set-up options except for the one under consideration take their final, optimised values, as itemised in Table 7.1. Section 7.3.3.2 addresses the physical properties of the particles, section 7.3.3.3 describes the selection of boundary conditions, while solution parameters are discussed in section 7.3.3.4.

7.3.3.2 *Physical properties*

7.3.3.2.1 *Density*

The density of the model olive stone sediment was found to be $1,500 \text{ kg/m}^3$ (see chapter 3). The particle density affects the speed with which an individual particle falls towards the chamber bed. One would expect, therefore, that the use of a higher particle density would result in higher efficiency values. Figure 7.8 shows that this was indeed the case. However, it is interesting to note that the differences became less significant as the values of the mean inlet velocity increased, and that in all cases a minimum efficiency value of around 0.4 was approached once the mean inlet velocity exceeded 0.4 m/s. At the lower velocities, the curve which most closely matched the laboratory data was for a density of $2,500 \text{ kg/m}^3$, and this artificially high particle density was selected for the simulations.

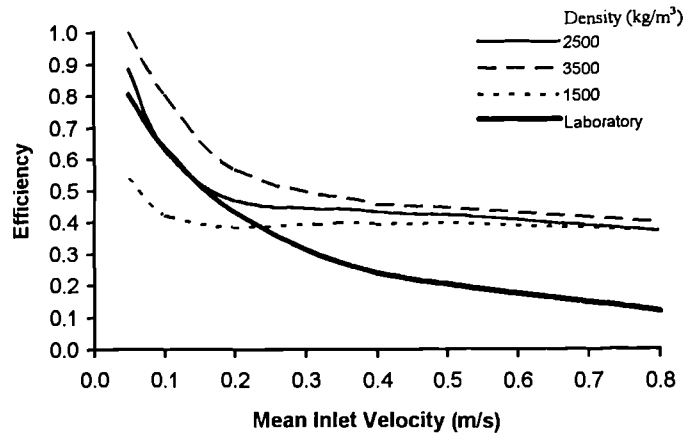


Figure 7.8 The effect of density changes

7.3.3.2.2 Particle size and injection location

As has already been discussed in section 7.3.2.1 above, it is not advisable to vary both particle size and input location simultaneously. The following tests illustrate why a single diameter, spatially distributed particle input was finally selected. These tests were undertaken for just one mean inlet velocity, 0.4 m/s. The initial density was given as 2,500 kg/m³, and the initial particle velocities were matched with the inlet flow velocity, 0.4 m/s. Stochastic particle tracking as well as mean flow field tracking were performed.

Two preliminary tests were carried out. Each test consisted of a number of runs. In each run a group of 100 particles was defined for the particle tracking. In Test 1 the particle diameter was kept constant for each run whilst the injection location was varied across the group. On the other hand, in Test 2, locations were kept constant and the Rosin-Rammler particle size distribution was used to produce a variation in particle size across the 100 injections of the group. Table 7.2 summarises the test runs that were carried out.

Test 1 – Single particle diameter, distributed injection location

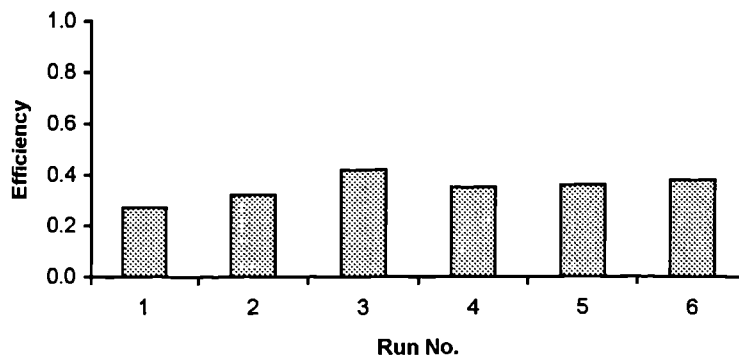
In the first test the injection locations were grouped to fall either on a central horizontal line across the inlet width (runs 1-3), or on a vertical line down the centre of the inlet (runs 4-6). For each condition three particle diameters were tested, namely 28 (runs 1 and 4), 47 (runs 2 and 5) and 88 µm (runs 3 and 6). These values represent the d_{20} , d_{50} and d_{80} values respectively, for the 150 µm olive stone. The test results are shown graphically in Figure 7.9.

Table 7.2 Particle distribution/input location test details

| Test | Run | X (m) | Y (m) | Z (m) | Diameter (μm) | Efficiency |
|------|-----|----------|-------------|-------------|-------------------------------|------------|
| 1 | 1 | 0.02 | 0.100 | 0.423-0.549 | 28 | 0.27 |
| | 2 | 0.02 | 0.100 | 0.423-0.549 | 47 | 0.32 |
| | 3 | 0.02 | 0.100 | 0.423-0.549 | 88 | 0.42 |
| | 4 | 0.02 | 0.037-0.163 | 0.486 | 28 | 0.35 |
| | 5 | 0.02 | 0.037-0.163 | 0.486 | 47 | 0.36 |
| | 6 | 0.02 | 0.037-0.163 | 0.486 | 88 | 0.38 |
| 2 | 1 | 0.02 | 0.037 | 0.486 | R-R | 0.58 |
| | 2 | 0.02 | 0.068 | 0.486 | R-R | 0.44 |
| | 3 | 0.02 | 0.100 | 0.486 | R-R | 0.34 |
| | 4 | 0.02 | 0.132 | 0.486 | R-R | 0.25 |
| | 5 | 0.02 | 0.163 | 0.486 | R-R | 0.29 |
| | 6 | 0.02 | 0.100 | 0.423 | R-R | 0.27 |
| | 7 | 0.02 | 0.100 | 0.454 | R-R | 0.26 |
| | 8 | 0.02 | 0.100 | 0.517 | R-R | 0.47 |
| | 9 | 0.02 | 0.100 | 0.549 | R-R | 0.62 |

All runs that used the mean flow field tracking resulted in an efficiency of 0, i.e., all particles escaped through the outlet. These results are not included in figure 7.9. For the stochastic tracking, it was clear that the particle diameter had some impact on the efficiency result. As one would expect, the larger particles produced higher efficiencies. There appeared to be greater variability between runs 1-3 (the horizontal distribution) than between runs 4-6 and the difference between the lowest and highest efficiency was 15%.

| Diameter (μm) | 28 | 47 | 88 | 28 | 47 | 88 |
|----------------------------|-------|-------|-------|-------|-------|-------|
| Y (m) | 0.100 | 0.100 | 0.100 | Range | Range | Range |
| Z (m) | Range | Range | Range | 0.486 | 0.486 | 0.486 |

**Figure 7.9 Single diameter distributed input test (Test 1)**

Test 2 – Single injection locations, Rosin-Rammler particle size distribution

In the second test the Rosin-Rammler particle size distribution was used and injections were made at discrete positions. Once more, the efficiency for all mean flow tracks was zero. For the stochastic particle tracking large variations occurred (see Figure 7.10), suggesting that the tracking calculations were highly sensitive to injection position. The lowest efficiency was recorded for those particles injected to the left and top of the inlet pipe. Higher efficiencies were obtained for the particle injected towards the right edge. In this case the difference between the maximum and minimum predicted efficiency was 37%, more than twice the deviations experienced in Test 1.

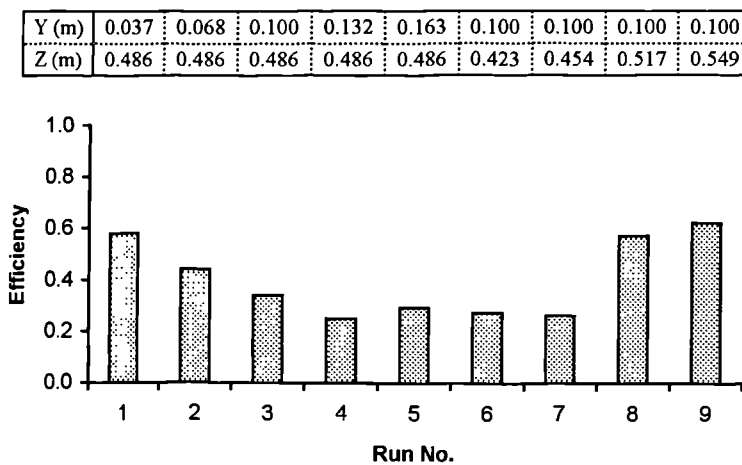


Figure 7.10 Discrete injections with the Rosin-Rammler size distribution (Test 2)

Conclusions

Test 2 demonstrated that the particle tracking routine was very sensitive to input location, and particularly to the vertical position. Observations of the actual tracks revealed that particles injected centrally frequently remained within the jet and passed through the outlet. On the other hand, those injected at either side were most likely to be diverted from the jet and into one of the recirculating flows. Similarly, those injected close to the invert showed a greater tendency to settle on the bed. The results of Test 1 suggested that efficiency was far less sensitive to the choice of particle size. Because of the striking effects observed when particle location was altered, a fully distributed, single diameter particle injection at the inlet was selected. Particles were spaced at intervals of 0.02 m in the vertical and horizontal directions, which gave a

total of 68 particles. The positions of the 68 particles are displayed in Figure 7.11, relative to the inner surface of the inlet pipe.

It should be noted that in a full-scale storage chamber the sediment particles may not be homogeneously distributed at the inlet; it has been hypothesised that a density gradient may exist, with increased sediment concentrations towards the pipe invert. The representation used in the particle tracking injection locations does, however, accurately model the fully mixed conditions at the inlet to the laboratory chamber.

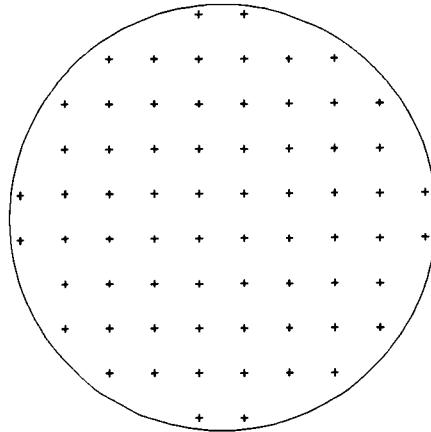


Figure 7.11 Inlet particle injection distribution

7.3.3.3 The number of simulations

As described above, particles were tracked using a stochastic representation of the turbulence in the flow. Because the tracking was stochastic, a number of repeat tests was necessary to ensure that the estimated efficiency was representative of the result that would be obtained for an infinite number of simulations, that is, for the population mean. To establish the exact number of tests that were required to obtain a result that was statistically significant, a total of 100 repeat tests were carried out. The particle group injection was in the form described above. The 100 tests were taken to represent a finite population, and the population statistics are presented in Table 7.3.

Table 7.3 Population statistics for the experimental data

| Population statistic | | Value |
|----------------------|------------|--------|
| Size | n_p | 100 |
| Mean | μ_p | 0.438 |
| Standard deviation | σ_p | 0.0574 |

It was assumed that a maximum deviation of $\pm 2.5\%$ from the population mean at a confidence level of 99% would be acceptable. If \bar{x} is the sample mean, then the 99% confidence limits for the true mean of the population are defined by $\bar{x} \pm (2.58 \sigma_p / \sqrt{n_s})$ where n_s is the sample size. The value of n_s which results in confidence limits of ± 0.025 is approximately 35, and as this value represented the minimum acceptable sample size, it was decided that 50 samples should be used. With 50 samples, the 99% confidence limits for the population mean are $\bar{x} \pm 0.021$.

7.3.3.4 Boundary conditions

In section 7.3.2.2 it was indicated that a particle reaching a boundary of the model may be treated in one of four ways: reflect; trap; escape or saltate. This section provides details of the conditions which were selected for the model outlet, free surface, walls and bed.

In order to distinguish particles that left the chamber through the outlet and those that remained within it, the boundary condition for the outlet cells was uniquely set to *escape*. Equally, as particles would never settle out at the upper free surface, this boundary condition was invariably set to *saltate*. However, three possible boundary conditions for the chamber bed and side walls were considered in detail. These were:

1. *Trap* condition for chamber bed with *reflect* condition at the side walls;
2. *Reflect* condition at the bed and walls;
3. *Saltate* condition at bed and walls.

The \bar{u}/η_{PT} curves for these three options are presented in Figure 7.12. It should be noted that these options do not form a closed set, and the possible merits and drawbacks of some further options are discussed at the end of this section.

7.3.3.4.1 Trap / Reflect combination

In this case the chamber bed was defined with a particle *trap* boundary condition. This meant that a particle only had to touch the bed once for tracking to cease. The boundary condition at the walls was set to *reflect*, as it would be unrealistic to simulate sedimentation to the chamber walls. Particles that neither escaped nor were *trapped* were reported as *aborted* when the maximum number of wall reflections had been exceeded. These *abort* conditions are discussed fully in the following section. Efficiency was defined as the proportion of *trapped* and *aborted* particles, i.e. all those not exiting from the chamber.

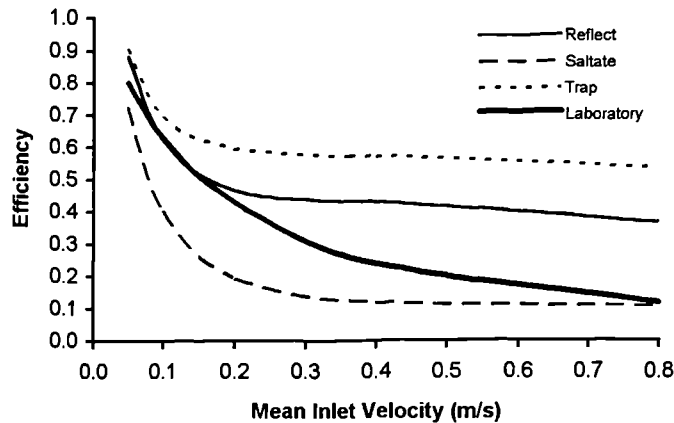


Figure 7.12 The effect of boundary conditions

Initial investigations showed that very few particles escaped from the chamber, even at high inlet velocities, and that efficiency predictions were too high. Particles were observed to settle in locations where the chamber bed had been observed to be clean in the laboratory tests.

The problem with this approach is that in reality particles may bounce from the chamber bed once or a series of times. They may also be resuspended from the bed by turbulent fluctuations in the flow after they have deposited. This boundary condition was therefore judged to be too rigid.

7.3.3.4.2 *Reflect condition*

In this case both wall and bed cells were defined with the *reflect* boundary condition. Physically, particles either quickly passed to the outlet, where they were reported as *escaped*, or they remained circulating within the chamber until either the maximum number of time steps or the maximum number of wall reflections was exceeded. In the regions of low bed velocities, the particles would also be *aborted* if the maximum number of wall reflections was exceeded. The maximum number of time steps was set to the highest possible value, 99,999, in order to ensure that particles that might escape after one or two circulations had a chance to do so. It is reasonable to assume that the *aborted* particles represent those that would settle out to the bed of the chamber in reality. Hence, efficiency was defined as the proportion of *aborted* particles.

One drawback with this approach was found to be the requirement for long simulation times. This was due to the high value selected for the maximum number of time steps.

A further drawback to this approach was the use of the maximum number of wall reflections allowed per cell as an *abort* criterion. The default value of 25 came into effect differently depending on the local velocity and the physical dimensions of the cell wall. Because the body fitted co-ordinate system was used to define the problem geometry, cell sizes were not regular. Clearly, where the cell wall section was large and the local bed velocity was low, a high number of wall reflections were possible. It was felt that it might be inappropriate to use a criteria that was dependent to some extent on the problem definition.

To further test the appropriateness of the *reflect* boundary condition, it was also applied to an additional chamber configuration. The chamber was longer and thinner than SIM1, with length 9.72 m and breadth 0.2 m, and the flow field was not characterised by recirculation zones. Instead the flow could be compared to flow in a narrow channel. This is the geometry referred to as 'VLNG' in chapter 8. At inlet velocities of less than 0.2 m/s, the efficiency was very high. The chamber is so long that at low velocities a very high proportion of the particles settled to the bed before they reached the outlet. For simulations at a higher mean inlet velocity, however, the high cross sectional velocity produced scouring at the bed that prevented settling out from occurring. These predictions are physically meaningful, and thereby suggest that the *reflect* boundary condition is probably appropriate for the prediction of sediment deposition in storage chambers.

7.3.3.4.3 *Saltate condition*

This condition differs very little from condition no. 2, but in this case both wall and bed cells were defined with the *saltate* boundary condition. The advantage of this condition over *reflect* is that repeated wall reflections do not occur to the same extent and it can be assumed that the tracking is independent from the problem geometry.

The efficiency curve produced using this boundary condition resembled laboratory data more closely than any other, particularly at the higher mean inlet velocities.

As with the *reflect* condition, it was noted that the saltation condition also produced extremely long calculations when the maximum number of time steps was set to 99,999.

However, a far greater problem was identified in the results of the particle tracking for the long, thin chamber geometry (VLNG). Virtually no particles remained in this chamber, even at the lowest inlet velocity. The *saltate* condition was ensuring that the particles were bounced along from one cell to the next, reaching the outlet before the

maximum number of time steps had been exceeded. In the real physical situation particles would gradually settle to the bed in this type of flow condition. *Saltation* does not allow for this process to be accounted for, simulating only the particles that remain in the chamber because they are trapped in a recirculating flow.

In conclusion, it may be restated that both the *trap* and *saltate* conditions failed to represent the depositional processes of real sediments. With the *trap* condition any particle that touched the bed once was deposited, while at the other extreme, the saltation condition allowed no particles whatsoever to settle out. The *reflect* condition produced reasonable results, which appeared to represent the real physical processes that occur. Questions may be raised concerning the maximum number of wall reflections condition, in that the results could be affected by the way in which the computational grid was mapped on to the chamber geometry. However, it was concluded that this problem could be addressed by using care in the problem geometry set-up to ensure that differences between the cell sizes on the bed were minimised.

One further boundary condition was considered. This involved the use of two different boundary conditions at the chamber bed, depending on the bed shear stress analysis. The cells with bed shear stress values greater than the critical value were set to *reflect*, while those with lower bed shear stress values were set to *trap*. The effort required to set up this boundary condition was considerable, as the bed shear stress results had to be individually examined and the cell types defined manually. It would, however, have been relatively simple to automate the set-up procedure had the methodology been selected for use. The results of simulations performed using this boundary condition are presented in Figure 7.13.

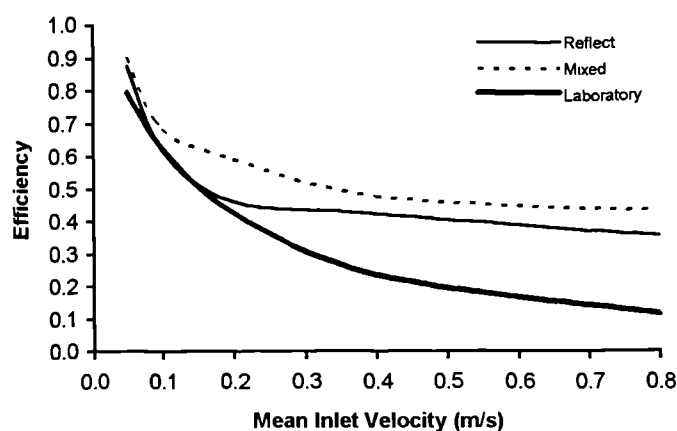


Figure 7.13 The effect of a mixed boundary condition at the bed

It can be seen that the mixed boundary conditions produced a small increase in deposition across the entire inlet velocity range, and that this technique did not reproduce the laboratory data quite as closely as the *reflect* condition did. The similarity in shape of the *mixed* results and the laboratory data, does however suggest that a functional relationship between the two might exist, and there is clearly scope for additional work to be carried out with respect to this approach.

The use of the *reflect* boundary condition for the whole of the bed had the advantage that the particle tracking results were entirely independent of the bed shear stress analysis, and for these reasons the *reflect* condition for the bed and walls was selected.

7.3.3.5 Solution Parameters

The third group of configuration parameters for consideration are the solution parameters: the number of time steps; the step length factor and the number of wall reflections.

7.3.3.5.1 Maximum number of steps

It can be seen (Figure 7.14) that the default value of 5,000 time steps was too small for any particles to reach the outlet whatsoever, and for this reason the number selected was increased by an order of magnitude. In the case of the laboratory chamber, no differences between the efficiencies predicted with 50,000 or 99,999 time steps could be identified. However, experiments with a long thin chamber suggested that some particles were failing to reach the outlet because of this limit, and the maximum available value (99,999) was therefore selected.

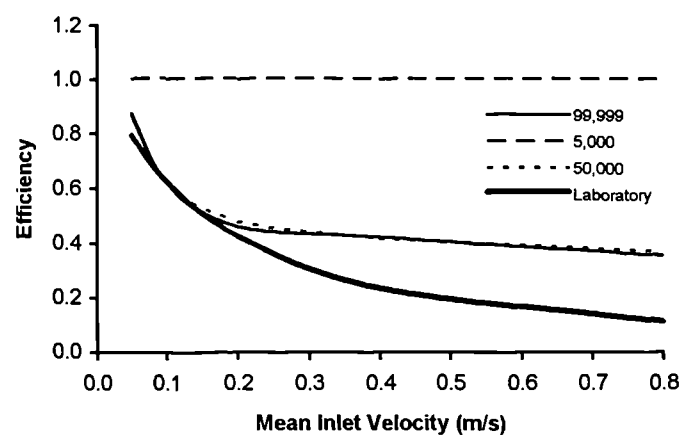


Figure 7.14 The effect of the number of time steps

7.3.3.5.2 Step length factor

Figure 7.15 shows that neither halving nor doubling the step length factor had any significant effect on the resulting efficiency prediction. There therefore seemed no justification for using a step length factor different from the default value of 20.

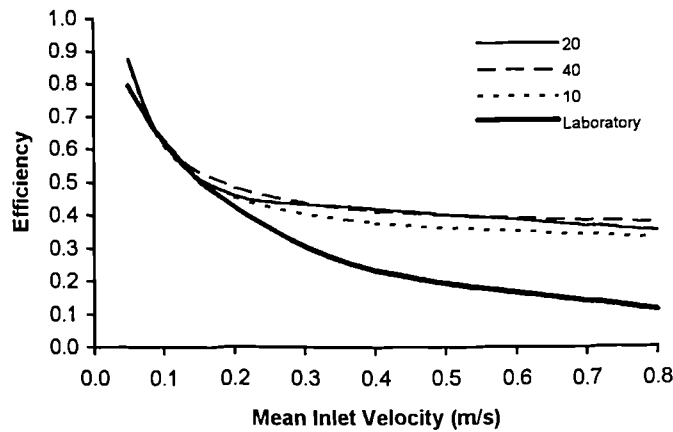


Figure 7.15 The effect of the step length factor

7.3.3.5.3 Number of wall reflections

The selection of the number of wall reflections was found to be a very important parameter, with apparently small differences having significant effects on the efficiency prediction (Figure 7.16). With 10 reflections almost three-quarters of the particles settled out, even at the highest velocities, whereas with 40 reflections the efficiency was much lower. The value of 25 gave the predictions that were closest to the laboratory data for the lowest inlet velocities, and the simulation times were noticeably shorter than when a value of 40 was used. In addition, the default value for the number of wall reflections was 25, and as an attempt was being made to use default values wherever possible, this value was selected.

The results presented in Figure 7.16 suggest that it may be appropriate to vary the maximum number of wall reflections as a function of the mean inlet velocity. There does not, however, appear to be a simple physical reason why this should be the case, and further work is required to justify this proposal.

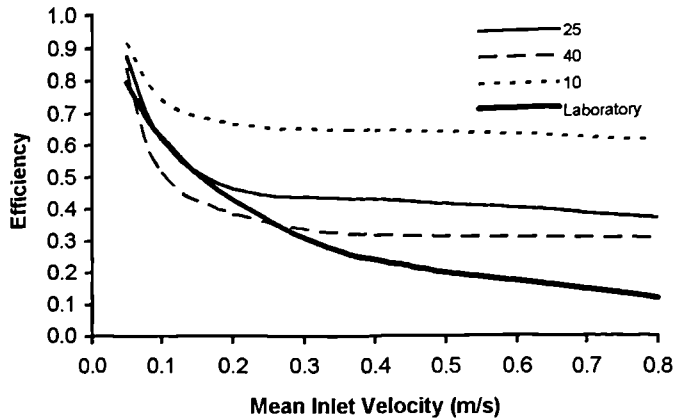


Figure 7.16 The effect of the maximum number of wall reflections

7.3.4 Discussion

The previous sections have presented justifications for each of the values selected for the particle tracking set-up options. In combination, the chosen values resulted in a \bar{u} / η curve which matched the laboratory data reasonably well. It was noted that at higher flowrates the particle tracking analysis tended to overpredict the efficiency, and it was acknowledged that, had a full programme of sensitivity analysis been undertaken, then improvements to the efficiency predictions may have been obtained.

It is also possible, however, that the lower values of efficiency observed in the laboratory reflected the fact that erosion, as well as deposition, was occurring in the laboratory chamber. It may, therefore, be appropriate to direct further research into the development of an erosion function for the particle tracking approach.

7.3.5 Particle Tracking and Sediment Deposit Location

One of the major drawbacks of the particle tracking technique, as discussed in the previous sections, is its inability to predict the distribution of deposited sediments on the chamber bed. The results of each particle tracking simulation were normally presented in terms of the total number of *aborted* and *escaped* particles, and these totals were used to estimate efficiency. It was assumed that all *aborted* particles represented those which deposited on the chamber bed, but further examination of the data, to determine the exact positions associated with the deposited particles, was not undertaken. This section of the thesis presents a preliminary investigation which was

undertaken in order to ascertain the feasibility of using the particle tracking routine to predict the location of sediment deposition.

The case file for the simulated laboratory chamber with $\bar{u} = 0.4$ m/s was used, and the STEP-BY STEP TRACKING REPORT in the SECOND PHASE SOLUTION PARAMETERS option list was activated. This meant that, for each particle tracked, every individual movement was reported, and that included the final destination of the particle. The results file that was generated with this reporting option was huge (0.02 Mb per particle), and the number of tracked particles had to be limited to 544 (eight repeats of the 68 particle input simulation). Analysis of the output data file was carried out using specially written FORTRAN code, and, of the 544 particles, 197 were reported as *aborted*; $\eta = 0.36$. Approximately 10% of the *aborted* particles actually ceased movement in positions other than the chamber bed, either on the side walls or on the surfaces of the inlet and outlet pipes. The position of the remaining 176 particles were found, and the total number of particles depositing on each cell of the chamber bed were obtained. A contour plot of the data is presented in Figure 7.17. It should be noted that the distribution illustrated in Figure 7.17 was derived from a total of only 176 particles; for this reason the distribution appears patchy, and the plot does not represent a statistically significant outcome. The number of particles depositing on each cell of the chamber bed ranged from zero to three, and these two values represent the zones where the probability of deposition was deemed to be minimum and maximum respectively. This example clearly shows that it is possible to obtain the spatial distribution of deposited particles from the FLUENT particle tracking simulations, although the procedure cannot currently be described as practical due to problems associated with handling and storing the large amounts of data generated by the STEP-BY-STEP TRACKING REPORT. It may be suggested that the implementation of a FINAL DESTINATION REPORT option in FLUENT would overcome this current limitation.

Furthermore, if Figure 7.17 is compared with the observed pattern of sediment deposition (Plate 5.1), it may be seen that the predicted distribution resembles the observed pattern reasonably well. With the limited number of particles considered in the construction of Figure 7.17, a better correlation cannot be expected. However, it is promising to note that the large area of deposition, which was observed to occur in the upstream right hand corner of the laboratory chamber, was clearly predicted in the analysis of the particle tracking data.

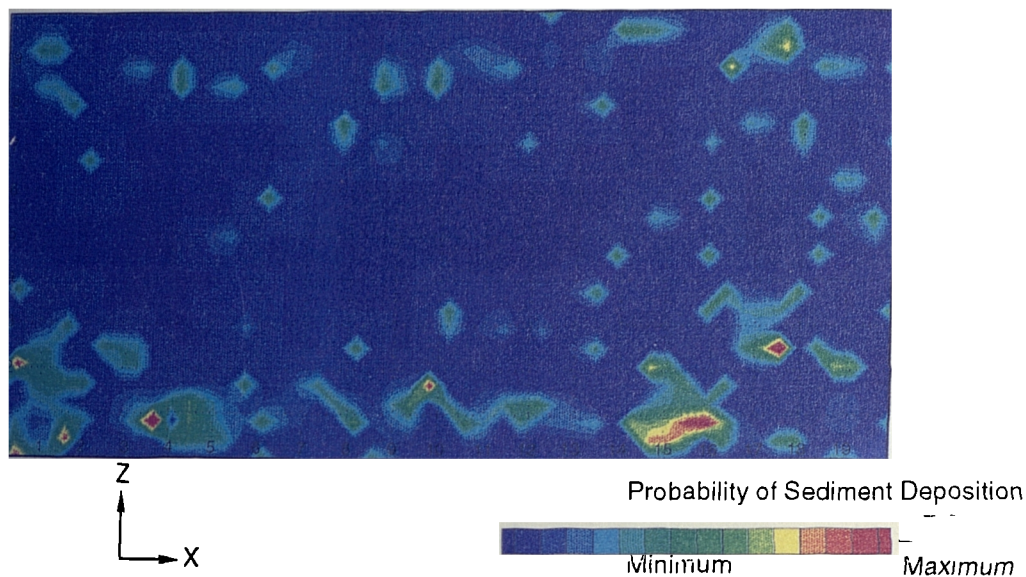


Figure 7.17 Spatial distribution of sediments from particle tracking

This example shows that the particle tracking technique has the *potential to provide* information concerning not only the sedimentation efficiency of a chamber, but also the likely spatial distribution of the deposited material.

7.4 Conclusions

7.4.1 A Comparison of Techniques

Both bed shear stress analysis and particle tracking methodologies have advantages and disadvantages, which are outlined in Table 7.4.

The two sediment deposition models each describe only a subset of the processes that affect deposition in the chamber. The bed shear stress methodology is based upon an evaluation of the proportion of the chamber bed where deposition will occur, but it does not take any account of the potential availability or build-up of sediment. On the other hand, the particle tracking technique does account for the processes that transport sediment particles to different locations within the chamber. However, the basis for deposition in the bed shear stress model may be justified theoretically and has been validated in the laboratory; the criteria for deposition in the particle tracking model have been derived on a trial-and-error basis that has a far less sound empirical and theoretical basis. The discussions of the previous section clearly indicate that there is considerable potential to explore the particle tracking technique further.

Table 7.4 Comparison of the bed shear stress and particle tracking techniques for efficiency prediction

| Critical bed shear stress | Particle Tracking |
|--|--|
| Unaffected by sediment availability. | Dependent upon sediment availability. |
| Dependent on an empirically derived value for τ_{cd} . | Independent of τ_{cd} . |
| Not able to detect differences in efficiency between chambers where the bed shear stress is everywhere $< \tau_{cd}$. | |
| Requires solution of flow field only. | Simulations additional to flow field solution required - often more than twice as much computational time. |
| Efficiency predicted indirectly via a calibration relationship. | Wide variety of set-up options. Optimisation procedure required. |
| Uses average flow conditions at the bed only. | Effects of entire flow field and turbulent fluctuations accounted for. |

The efficiency estimates produced for the control chamber using the two models both differed from the efficiency characteristics that were measured in the laboratory. Acknowledging that neither technique provides a complete model of the sedimentation process, it is suggested that each technique may be used independently to provide comparative performance data.

The general applicability of the bed shear stress method depends on establishing appropriate values for the critical bed shear stress in full-scale chambers, whilst many of the particle tracking options could require adjustment before the technique can be applied to a full scale situation. These observations suggest that a programme of field work would complement this research, and allow its results to be extrapolated to full-scale applications.

7.4.2 Summary Points

The relationship between the mean inlet velocity (\bar{u}) and the chamber efficiency (η) takes the form of a curve that characteristically approaches 1 for low mean inlet

velocities and zero as the mean inlet velocity is increased. For brevity, this relationship is referred to as the \bar{u}/η curve.

The chamber efficiency may be predicted from the FLUENT simulation using the bed shear stress distribution. The proportion of the bed where bed shear stresses fall below the critical value is used to estimate the efficiency by means of a known calibration relationship. When the efficiency is predicted in this way, it is referred to as the bed shear stress efficiency estimate, and termed η_{BSS} .

Efficiency may also be predicted from the proportion of *aborted* particles in a particle tracking simulation. When the efficiency is predicted in this way, it is referred to as the particle tracking efficiency estimate, and this is abbreviated to η_{PT} . This approach results in an overprediction of efficiency at high inlet velocities. The particle tracking routine may also be used to predict the positions on the chamber bed where deposition is likely to occur.

It is important to note that the two different techniques yield different efficiency predictions. This results from the fact that neither of them is a complete description of the sedimentation process. The use of both techniques, separately and combined, gives greater insight into the likely performance of a chamber. In the following chapter a comparative assessment of chamber efficiency, based on CFD, is described for ten different storage chamber configurations.

8. Efficiency Prediction for Different Chambers

8.1 Introduction

A principal aim of this research project was to be able to predict the effects of geometric configuration on the efficiency of a storage chamber. Laboratory studies suggested that efficiency could be predicted from the flow field, and in the preceding chapter two methodologies have been outlined which facilitate the prediction of chamber efficiency by means of a numerical simulation of the flow field.

In this chapter, these two techniques are applied to 10 different chamber configurations, and the comparative effects of geometry on efficiency are quantitatively described. The basis for the selection of the 10 chambers which were tested is outlined in section 8.2.

For each chamber a simulation record was produced. The record contained geometric information, flow patterns and particle tracking results in visual form, as well as the \bar{u}/η_{PT} and \bar{u}/η_{BSS} curves. The simulation records are presented in section 8.3.

The results are discussed in section 8.4, and regression equations that describe efficiency as a function of the inlet velocity and the geometric configuration are presented in section 8.5.

The results are discussed in section 8.6, and the findings are related to the results of work that has previously been reported on the performance of full-scale chambers. The conclusions of the comparative efficiency prediction research are presented in section 8.7.

8.2 Configuration Selection

The efficiency of a storage chamber is a function of the flow conditions, the characteristics of the sediments and the chamber's internal geometry. For a

rectangular on-line chamber, the following four geometric parameters are thought to be most relevant to the self-cleansing operation (Roebuck, 1989; Balmforth, 1990; Saul and Ellis, 1992):

1. The length to breadth ratio;
2. The gradient of transverse benching, if any;
3. The number, shape and gradient of dry weather flow channel(s), if any;
4. The longitudinal gradient.

There are other geometric factors that might affect efficiency, and these include the type of roof support or the chamber inlet geometry. However, the first four have received the greatest attention in the literature, and hence the programme of comparative performance assessment was restricted to these elements.

In addition to these geometric parameters, the level of inlet surcharge, which is a hydraulic parameter, was also considered to be important.

FLUENT numerical flow field simulations were therefore used to investigate each of these parameters. In order to facilitate a comparative assessment of the effect that different geometrical and hydraulic parameters have on chamber efficiency, nine further chambers, based on the basic laboratory chamber geometry, were simulated. The values of the relevant set-up parameters are given in Table 8.1.

Table 8.1 Configurations details of the simulated chambers

| Chamber | Length (m) | Breadth (m) | Depth (m) | Gradient of Transverse Benching | Longitudinal Gradient | DWF Diameter (m) | Length / Breadth | Level of Inlet surcharge |
|---------|---------------|----------------|--------------|---------------------------------------|--------------------------|------------------------|---------------------|--------------------------------|
| TANK | 2.00 | 0.97 | 0.20 | None | None | None | 2.06 | 1.05 |
| VLNG | 9.72 | 0.20 | 0.20 | None | None | None | 48.60 | 1.05 |
| LONG | 4.00 | 0.49 | 0.20 | None | None | None | 8.23 | 1.05 |
| STUB | 1.00 | 1.94 | 0.20 | None | None | None | 0.51 | 1.05 |
| BEN1 | 2.00 | 0.97 | 0.20 | 1 in 4 | None | None | 2.06 | 1.05 |
| BEN2 | 2.00 | 0.97 | 0.20 | 1 in 4 | None | 0.06 | 2.06 | 1.05 |
| LGD1 | 2.00 | 0.97 | 0.20 | None | 1 in 50 | None | 2.06 | 1.05 |
| LGD2 | 2.00 | 0.97 | 0.20 | None | 1 in 200 | None | 2.06 | 1.05 |
| SUR1 | 2.00 | 0.97 | 0.45 | None | None | None | 2.06 | 2.37 |
| SUR2 | 2.00 | 0.97 | 0.70 | None | None | None | 2.06 | 3.68 |

Each chamber was given a unique four letter identifier, with the control geometry (i.e. that tested in the laboratory) being referred to as 'TANK'. The names given to the other nine geometries are shown in the first column of Table 8.1 above.

For each geometry, five hydraulic simulations were performed in order to establish the \bar{u}/η curves. Mean inlet velocities of 0.05, 0.1, 0.2, 0.4 and 0.8 m/s were simulated. Thus fifty simulations were undertaken in total.

In all the simulations the chamber plan area remained constant. In classical sedimentation theory sediment deposition is a function of chamber plan area and mean inlet velocity alone (see section 2.3.4.2) and, consequently, no difference in the efficiency of the ten chambers for a given inlet flow condition would be predicted.

8.3 Description of the Simulation Record

A 'simulation record' has been produced for each of the tested geometric variations, and these are presented in Figures 8.2 to 8.11. The unique four letter identifier for each chamber geometry appears in the top right hand corner of the Figure, and each record comprises four sections: geometry, velocity distribution, particle tracking and efficiency. Details of the information presented in each of the four sections is presented below.

8.3.1 Geometry

A black and white line drawing of the geometry is shown, along with a listing of the chamber length, breadth and flow depth. Details of the benching, dry weather flow (DWF) channel and the longitudinal gradient are also presented.

8.3.2 Velocity distribution

Although five simulations were completed for each geometric variation, the velocity distribution for the mean inlet velocity of 0.4 m/s is illustrated in all cases. However, the flow patterns were not generally affected by changes in the mean inlet velocity for a given chamber geometry. One or more slices were selected in order to show the dominant features of the flow field. The velocity vectors are colour coded according to their magnitude, with red indicating high velocity (0.5 m/s), green moderate velocity (0.25 m/s) and blue indicating a velocity close to zero.

8.3.3 Particle tracking

The particle tracks that are illustrated represent a small sample of the simulations that were actually undertaken. It should be stressed at this point that the tracks shown in the simulation record are illustrative only; the efficiency was actually calculated from the results of 3600 particle tracking simulations. However, the tracks give a clear impression of the range of paths and destinations that occurred. The particle properties and the simulation procedure followed the guidelines set out in chapter 7, but for the purpose of this illustration the number of introduced particles was reduced from 68 to 5. The distribution of the particles in the inlet cross-section is shown in Figure 8.1.

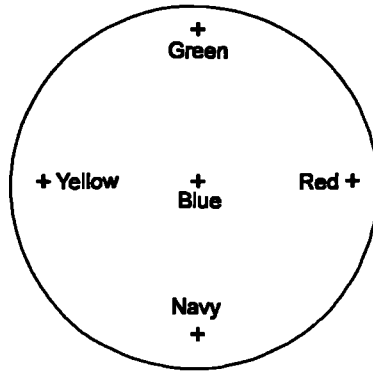


Figure 8.1 Particle distribution in the inlet, looking downstream

8.3.4 Efficiency

The results of the efficiency predictions are presented in the final section of the simulation record. The \bar{u}/η_{BSS} and \bar{u}/η_{PT} curves for the particular chamber in question (solid lines) are shown alongside the \bar{u}/η_{BSS} and \bar{u}/η_{PT} curves of TANK (dashed lines) for comparison.

In section 7.2 it was shown that efficiency predictions greater than 0.6 could not be identified with the bed shear stress analysis technique. This upper limit was reached in several configurations, and in these instances the \bar{u}/η_{BSS} plots do not show efficiency data for the lowest values of mean inlet velocity.

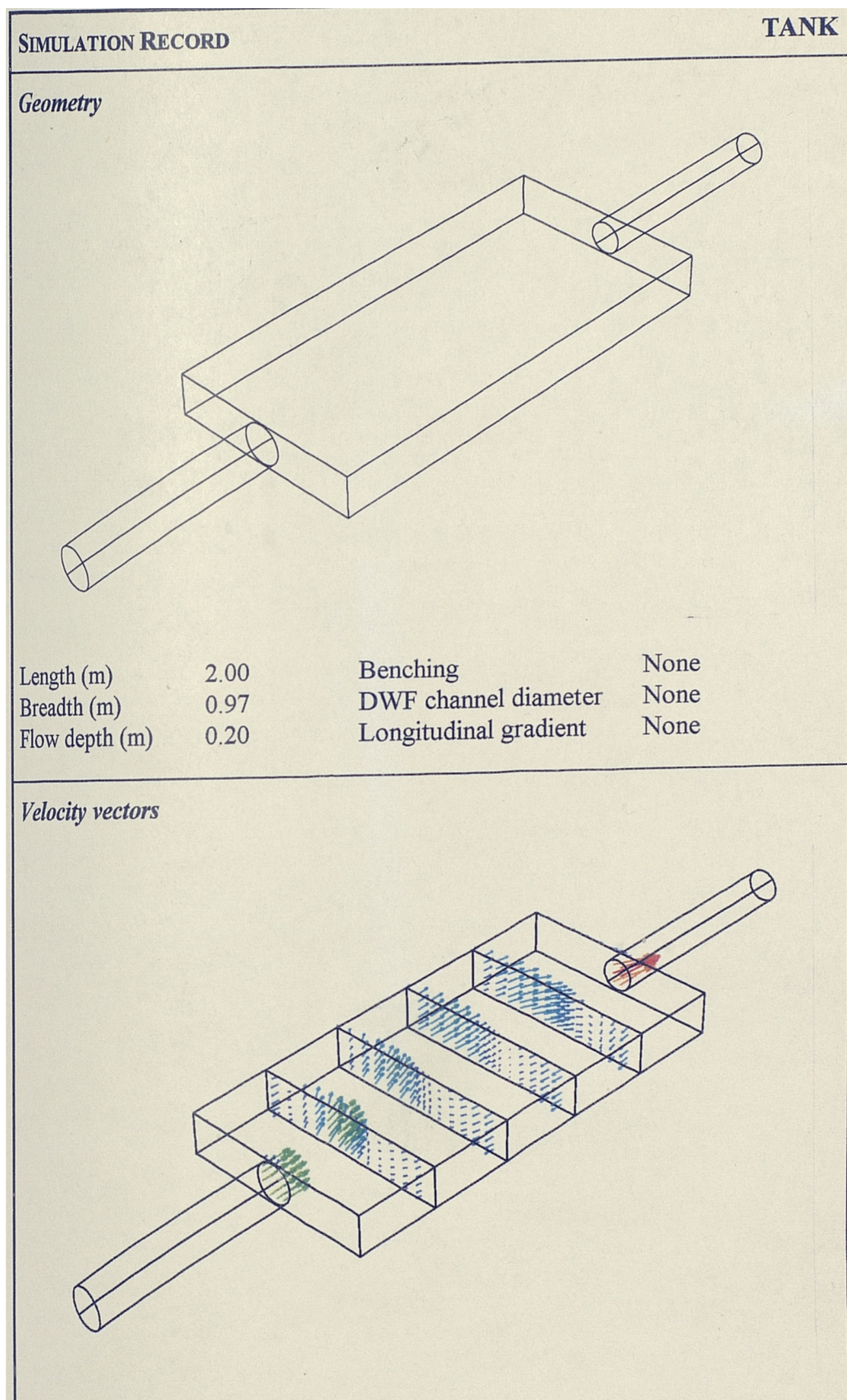
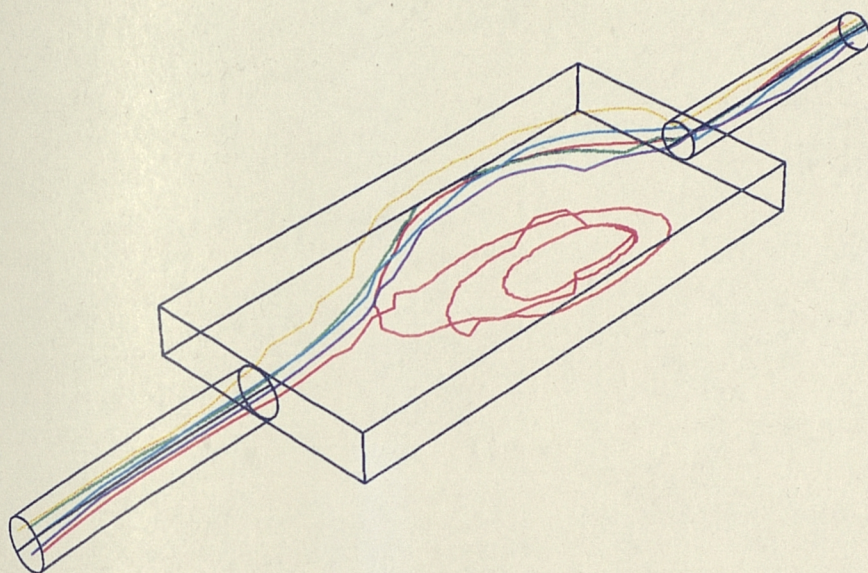
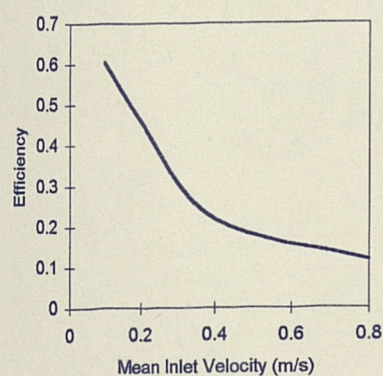


Figure 8.2 a) Simulation record for TANK: Geometry and velocity vectors

Particle tracking*Efficiency*

| Method | Inlet velocity (m/s) | | | | |
|-------------------|----------------------|-------|-------|-------|-------|
| | 0.05 | 0.1 | 0.2 | 0.4 | 0.8 |
| Bed shear stress | 0.605 | 0.605 | 0.461 | 0.219 | 0.117 |
| Particle tracking | 0.872 | 0.622 | 0.464 | 0.424 | 0.354 |

Bed Shear Stress



Particle Tracking

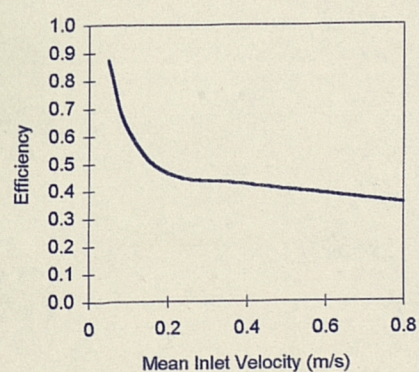


Figure 8.2 b) Simulation record for TANK: Particle tracking and efficiency

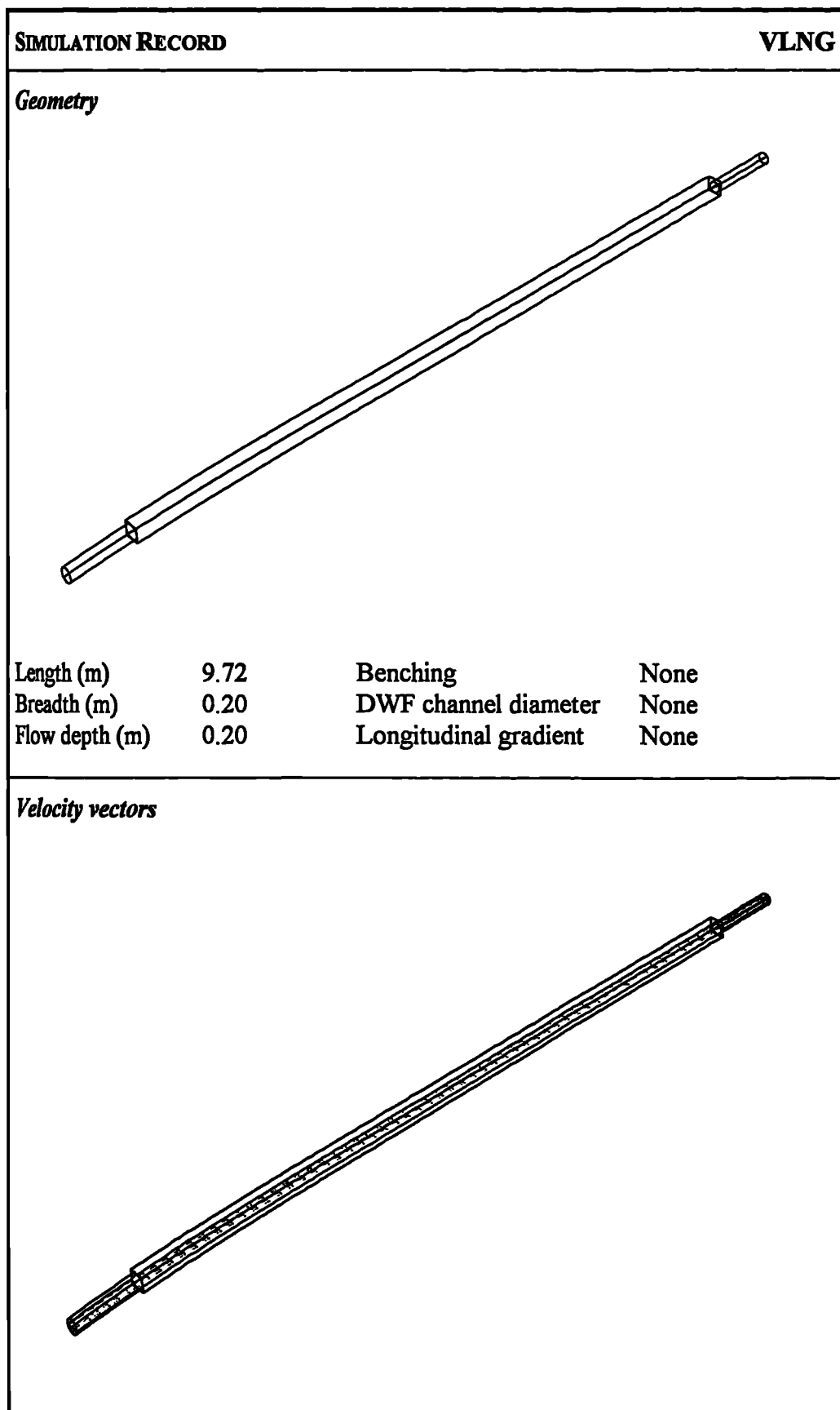
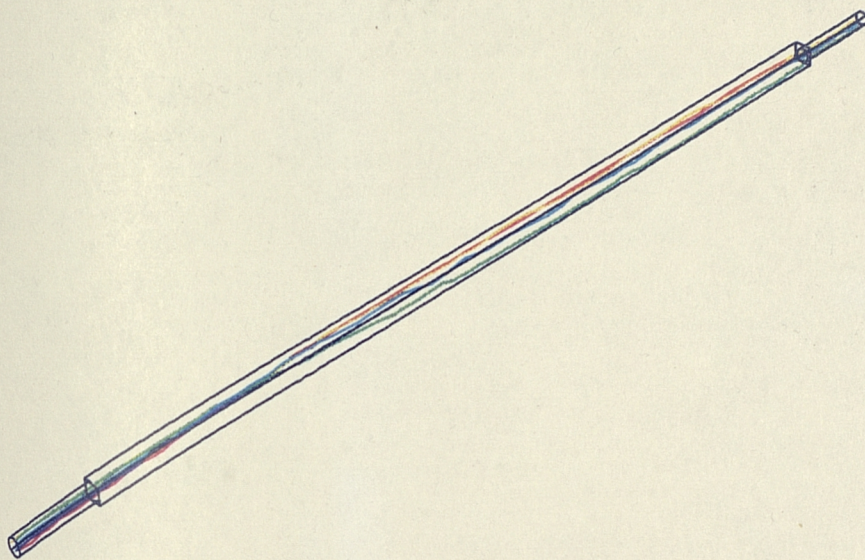
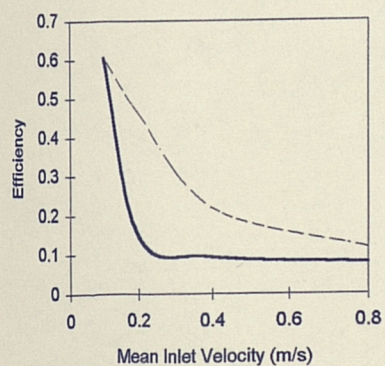


Figure 8.3 a) Simulation record for VLNG: Geometry and velocity vectors

Particle tracking*Efficiency*

| Method | Inlet velocity (m/s) | | | | |
|-------------------|----------------------|-------|-------|-------|-------|
| | 0.05 | 0.1 | 0.2 | 0.4 | 0.8 |
| Bed shear stress | 0.605 | 0.605 | 0.146 | 0.094 | 0.080 |
| Particle tracking | 1.000 | 0.930 | 0.394 | 0.155 | 0.098 |

Bed Shear Stress



Particle Tracking

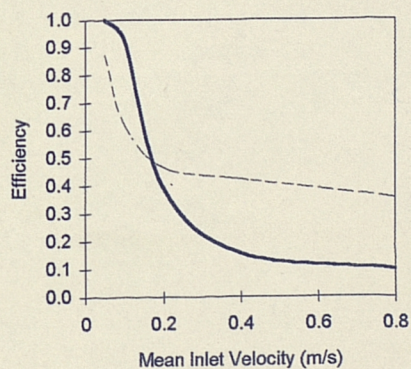


Figure 8.3 b) Simulation record for VLNG: Particle tracking and efficiency

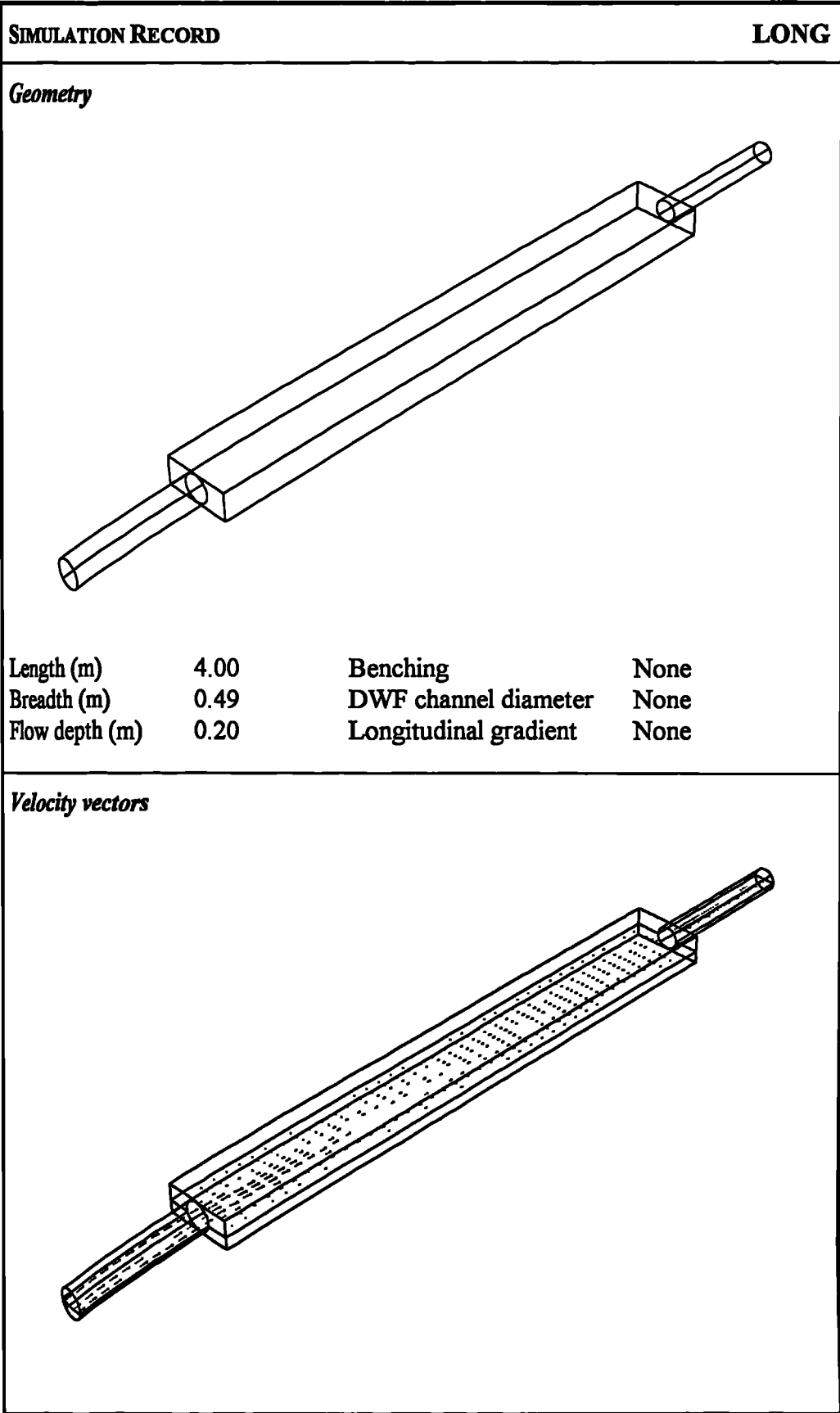
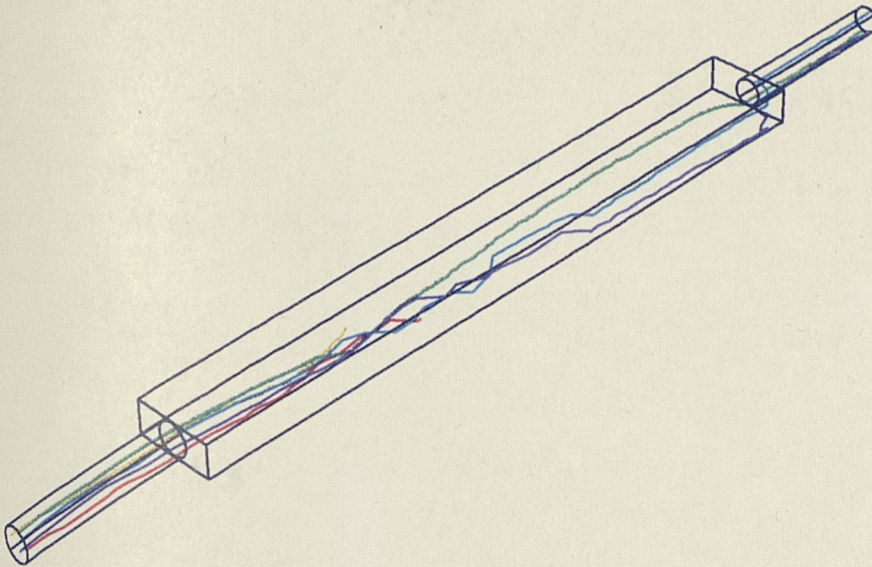
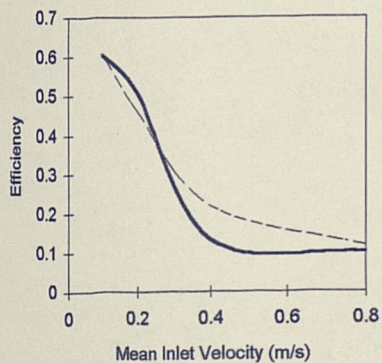


Figure 8.4 a) Simulation record for LONG: Geometry and velocity vectors

Particle tracking*Efficiency*

| Method | Inlet velocity (m/s) | | | | |
|-------------------|----------------------|-------|-------|-------|-------|
| | 0.05 | 0.1 | 0.2 | 0.4 | 0.8 |
| Bed shear stress | 0.605 | 0.605 | 0.508 | 0.134 | 0.101 |
| Particle tracking | 0.992 | 0.892 | 0.694 | 0.574 | 0.514 |

Bed Shear Stress



Particle Tracking

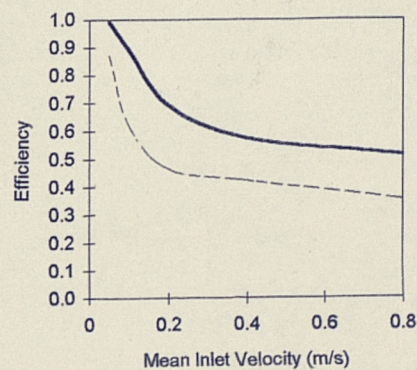
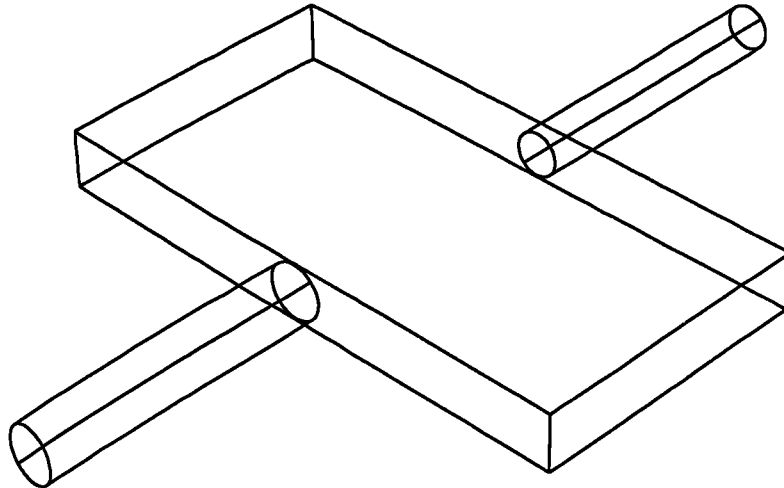
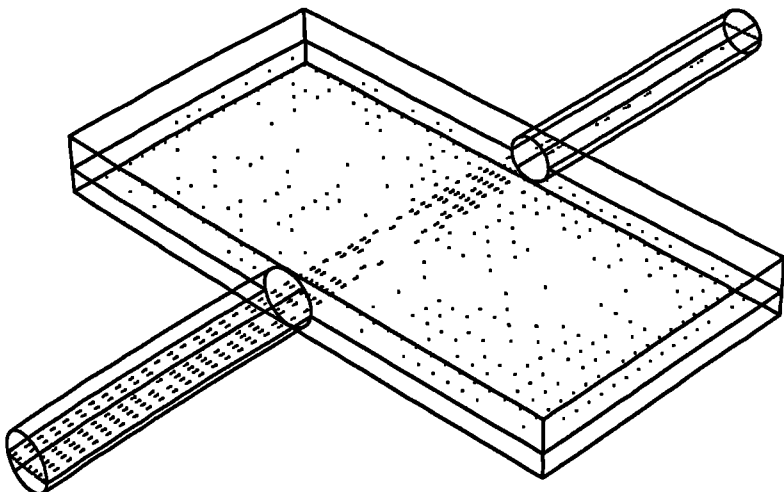
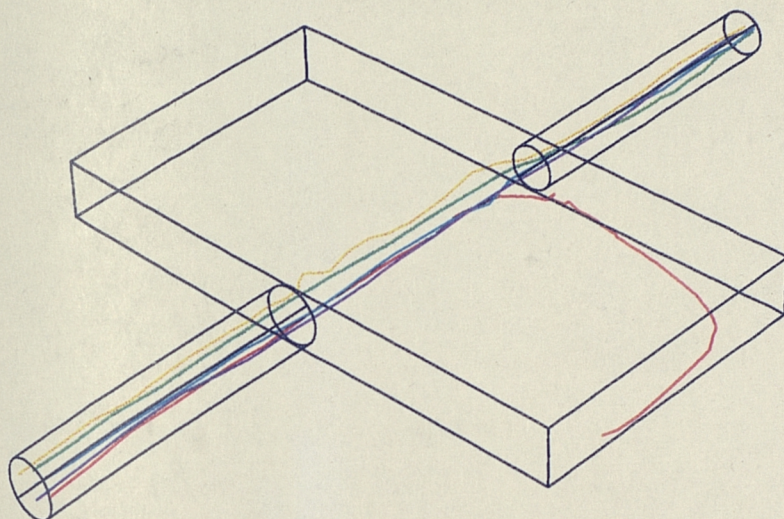


Figure 8.4 b) Simulation record for LONG: Particle tracking and efficiency

SIMULATION RECORD**STUB****Geometry**

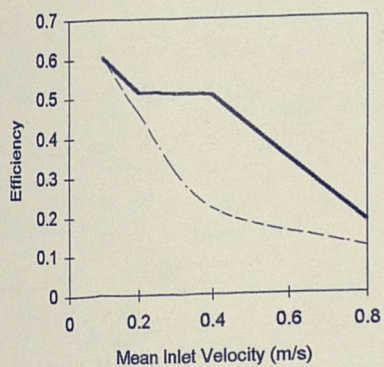
| | | | |
|----------------|------|-----------------------|------|
| Length (m) | 1.00 | Benching | None |
| Breadth (m) | 1.94 | DWF channel diameter | None |
| Flow depth (m) | 0.20 | Longitudinal gradient | None |

Velocity vectors**Figure 8.5 a) Simulation record for STUB: Geometry and velocity vectors**

Particle tracking*Efficiency*

| Method | Inlet velocity (m/s) | | | | |
|-------------------|----------------------|-------|-------|-------|-------|
| | 0.05 | 0.1 | 0.2 | 0.4 | 0.8 |
| Bed shear stress | 0.605 | 0.605 | 0.514 | 0.505 | 0.183 |
| Particle tracking | 0.376 | 0.176 | 0.140 | 0.115 | 0.116 |

Bed Shear Stress



Particle Tracking

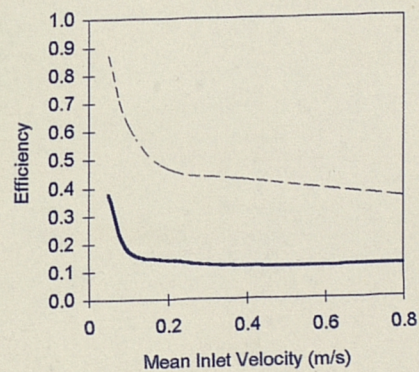


Figure 8.5 b) Simulation record for STUB: Particle tracking and efficiency

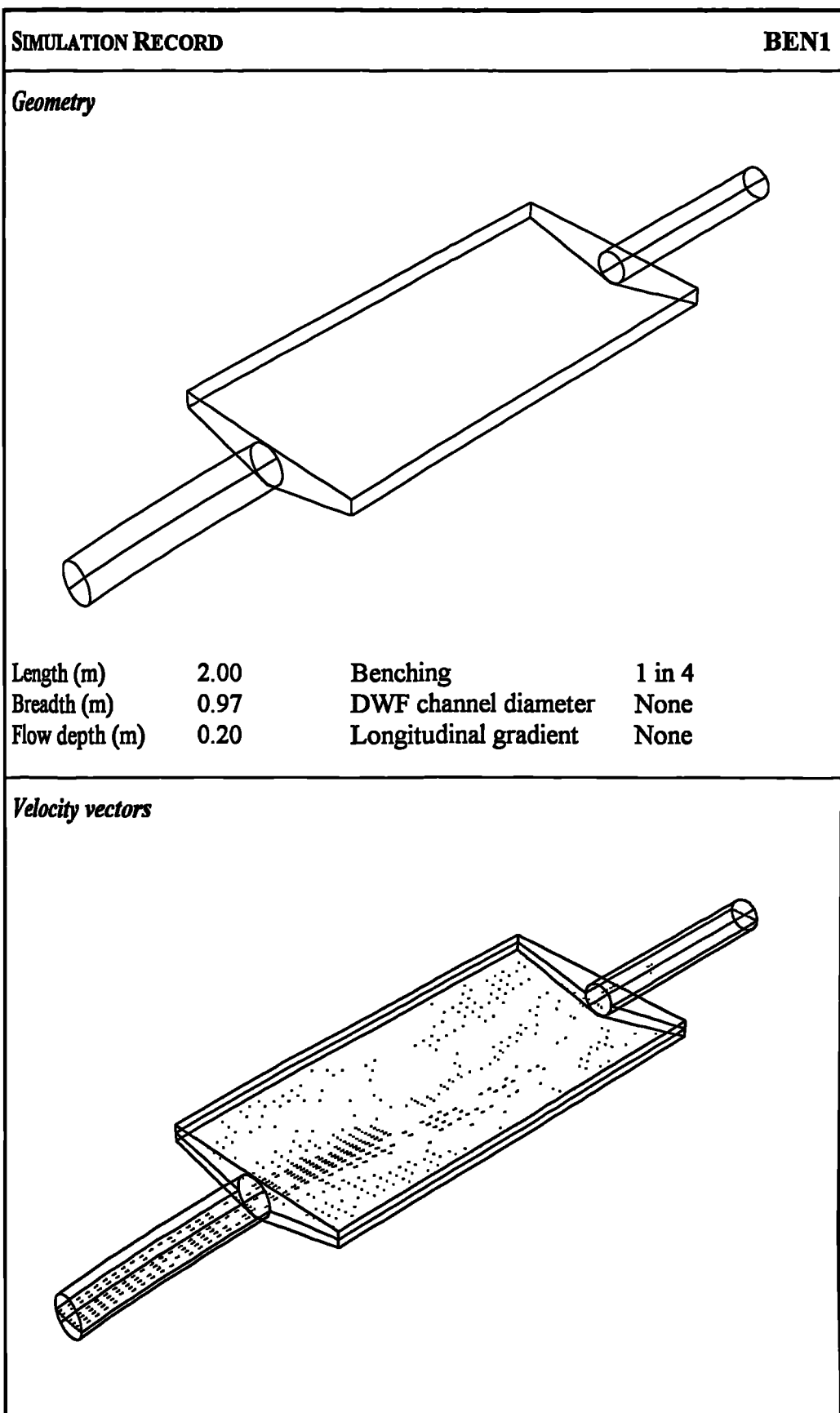
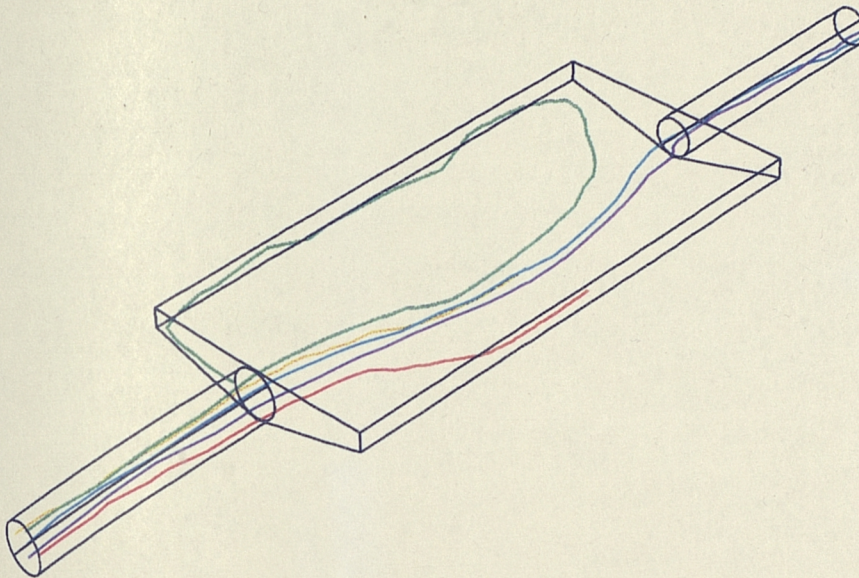
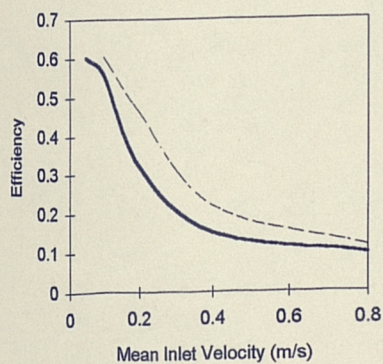


Figure 8.6 a) Simulation record for BEN1: Geometry and velocity vectors

Particle tracking*Efficiency*

| Method | Inlet velocity (m/s) | | | | |
|-------------------|----------------------|-------|-------|-------|-------|
| | 0.05 | 0.1 | 0.2 | 0.4 | 0.8 |
| Bed shear stress | 0.601 | 0.560 | 0.320 | 0.152 | 0.098 |
| Particle tracking | 0.906 | 0.664 | 0.504 | 0.409 | 0.362 |

Bed Shear Stress



Particle Tracking

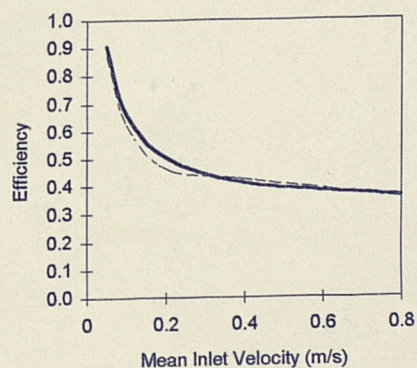
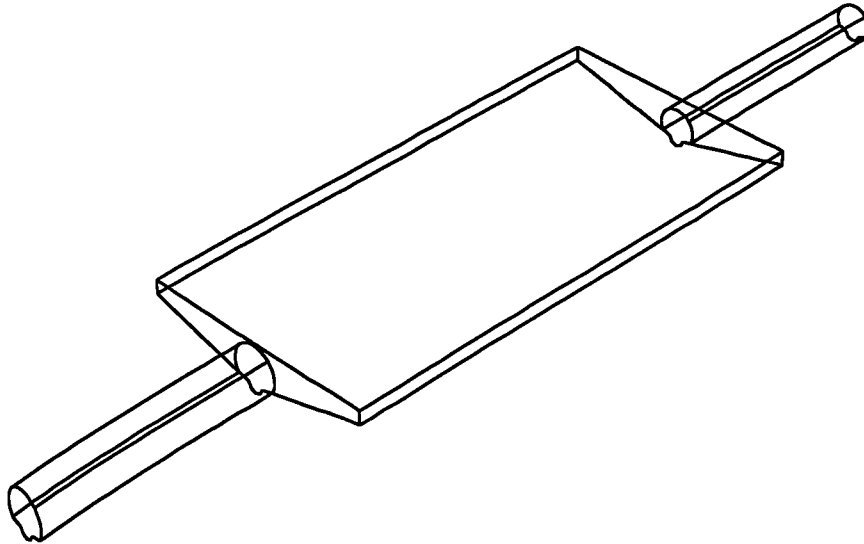
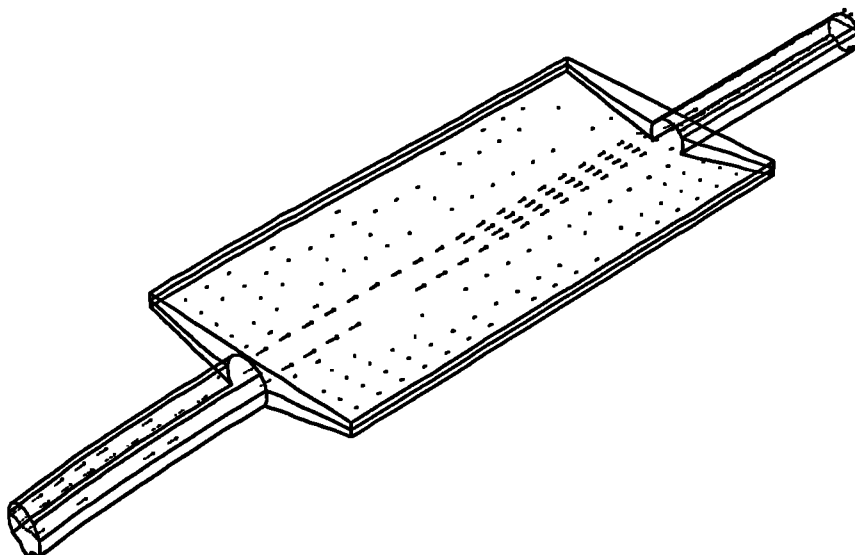
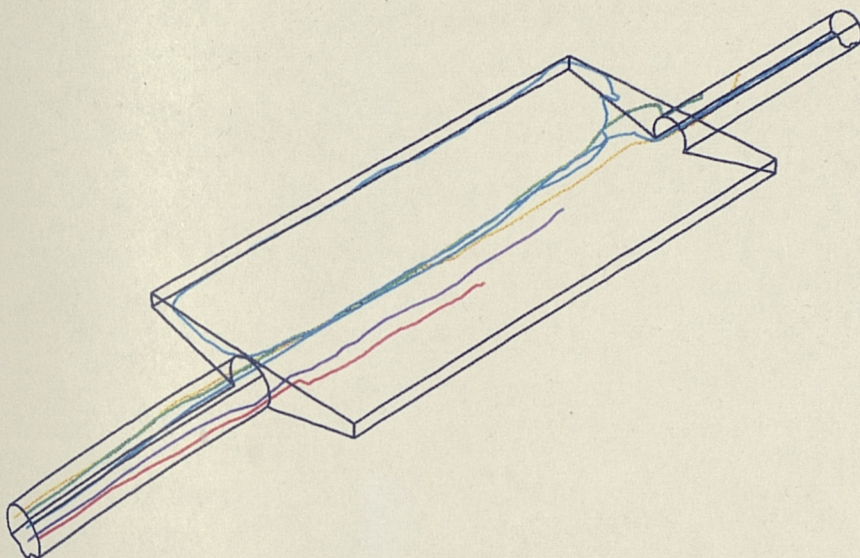


Figure 8.6 b) Simulation record for BEN1: Particle tracking and efficiency

SIMULATION RECORD**BEN2****Geometry**

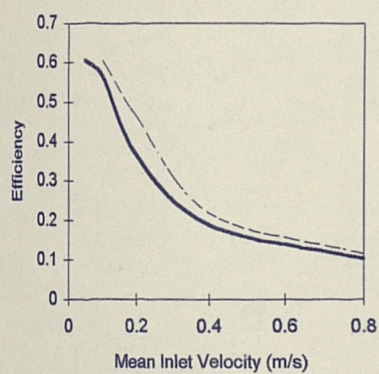
| | | | |
|----------------|-------|-----------------------|--------|
| Length (m) | 2.00 | Benching | 1 in 4 |
| Breadth (m) | 0.972 | DWF channel diameter | 0.06 m |
| Flow depth (m) | 0.2 | Longitudinal gradient | None |

Velocity vectors**Figure 8.7 a) Simulation record for BEN2: Geometry and velocity vectors**

Particle tracking*Efficiency*

| Method | Inlet velocity (m/s) | | | | |
|-------------------|----------------------|-------|-------|-------|-------|
| | 0.05 | 0.1 | 0.2 | 0.4 | 0.8 |
| Bed shear stress | 0.605 | 0.565 | 0.364 | 0.188 | 0.104 |
| Particle tracking | 0.426 | 0.331 | 0.326 | 0.341 | 0.319 |

Bed Shear Stress



Particle Tracking

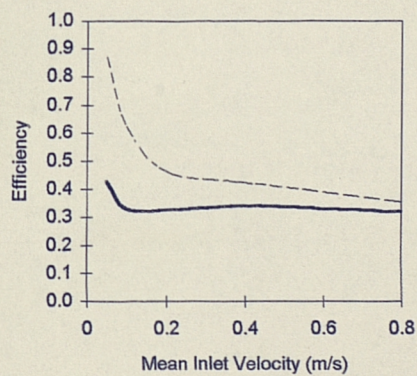


Figure 8.7 b) Simulation record for BEN2: Particle tracking and efficiency

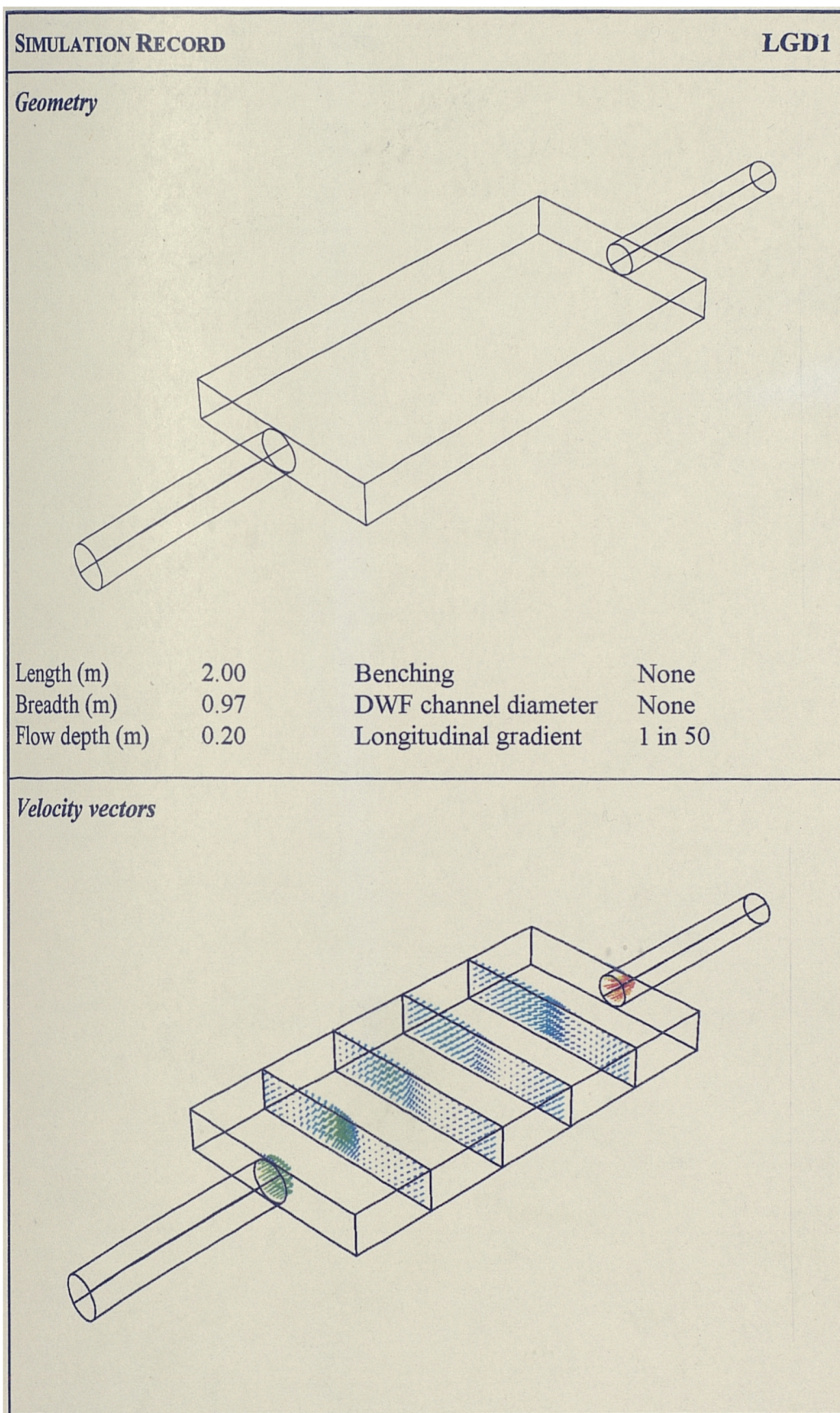
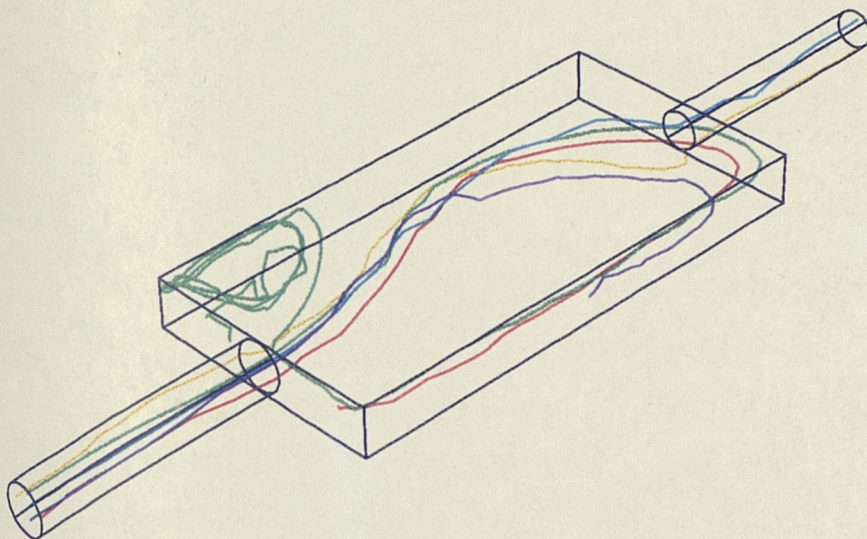
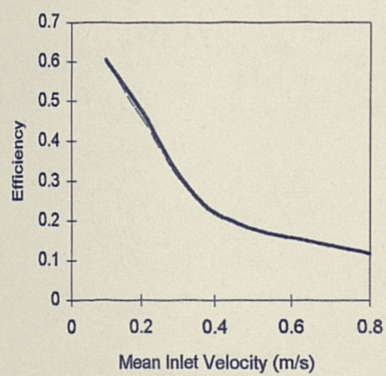


Figure 8.8 a) Simulation record for LGD1: Geometry and velocity vectors

Particle tracking*Efficiency*

| Method | Inlet velocity (m/s) | | | | |
|-------------------|----------------------|-------|-------|-------|-------|
| | 0.05 | 0.1 | 0.2 | 0.4 | 0.8 |
| Bed shear stress | 0.605 | 0.605 | 0.479 | 0.221 | 0.116 |
| Particle tracking | 0.872 | 0.647 | 0.414 | 0.338 | 0.304 |

Bed Shear Stress



Particle Tracking

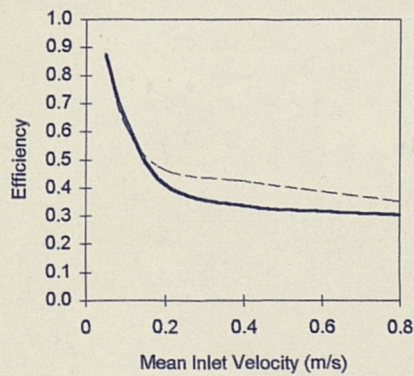
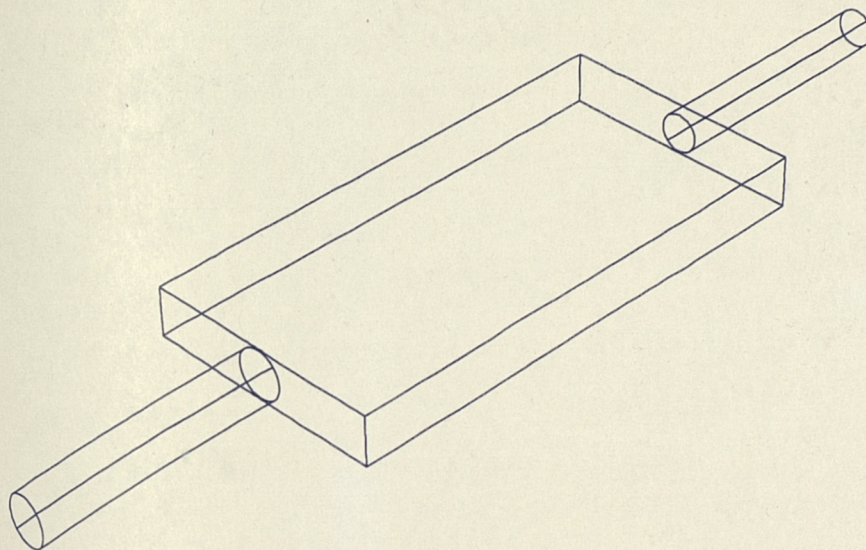


Figure 8.8 b) Simulation record for LGD1: Particle tracking and efficiency

SIMULATION RECORD

LGD2

Geometry

| | | | |
|----------------|------|-----------------------|----------|
| Length (m) | 2.00 | Benching | None |
| Breadth (m) | 0.97 | DWF channel diameter | None |
| Flow depth (m) | 0.20 | Longitudinal gradient | 1 in 200 |

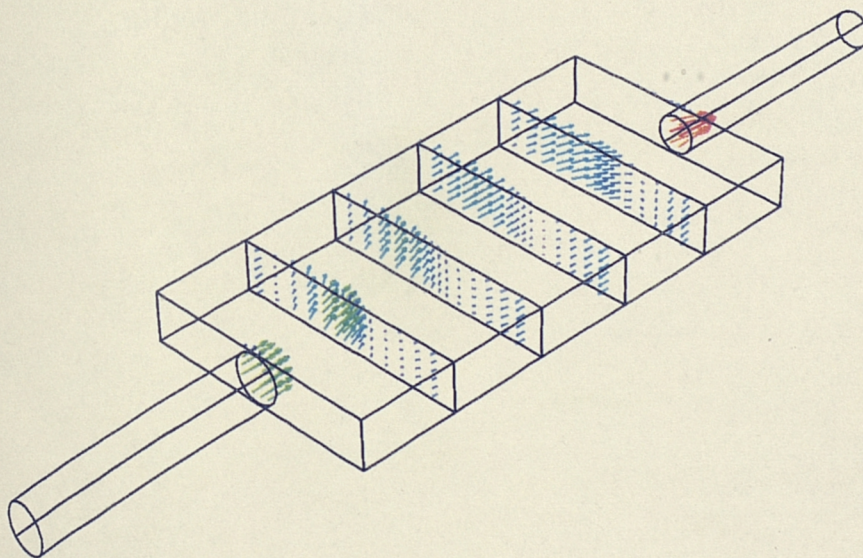
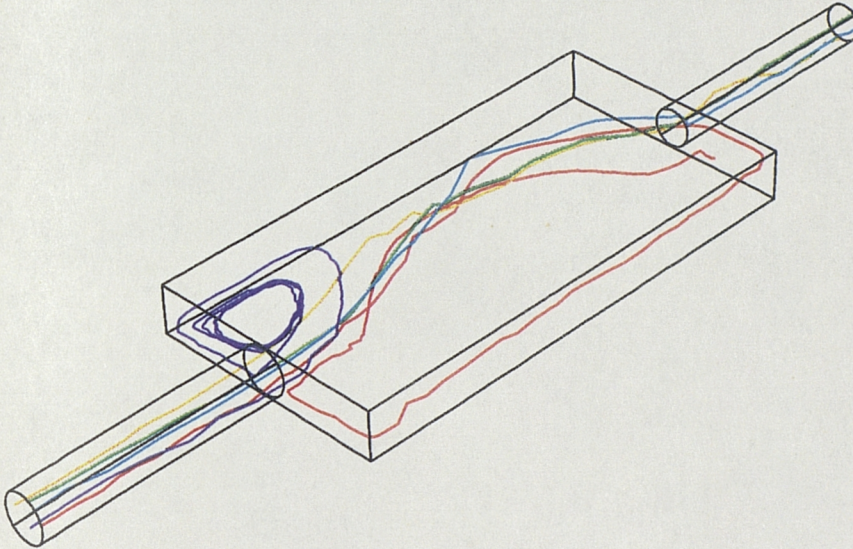
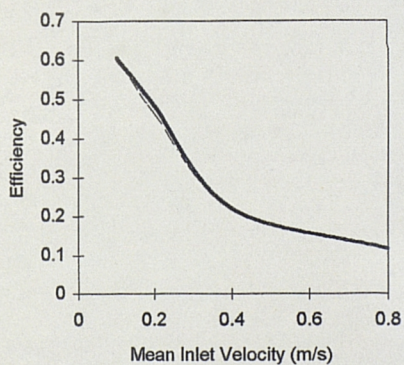
Velocity vectors

Figure 8.9 a) Simulation record for LGD2: Geometry and velocity vectors

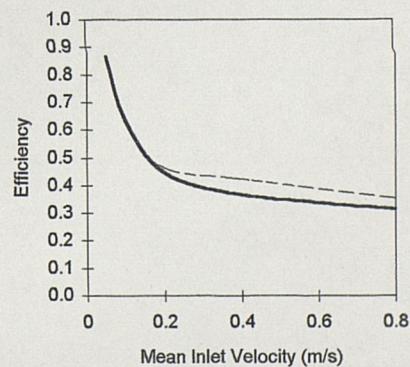
Particle tracking*Efficiency*

| Method | Inlet velocity (m/s) | | | | |
|-------------------|----------------------|-------|-------|-------|-------|
| | 0.05 | 0.1 | 0.2 | 0.4 | 0.8 |
| Bed shear stress | 0.605 | 0.605 | 0.482 | 0.220 | 0.116 |
| Particle tracking | 0.867 | 0.638 | 0.447 | 0.367 | 0.313 |

Bed Shear Stress



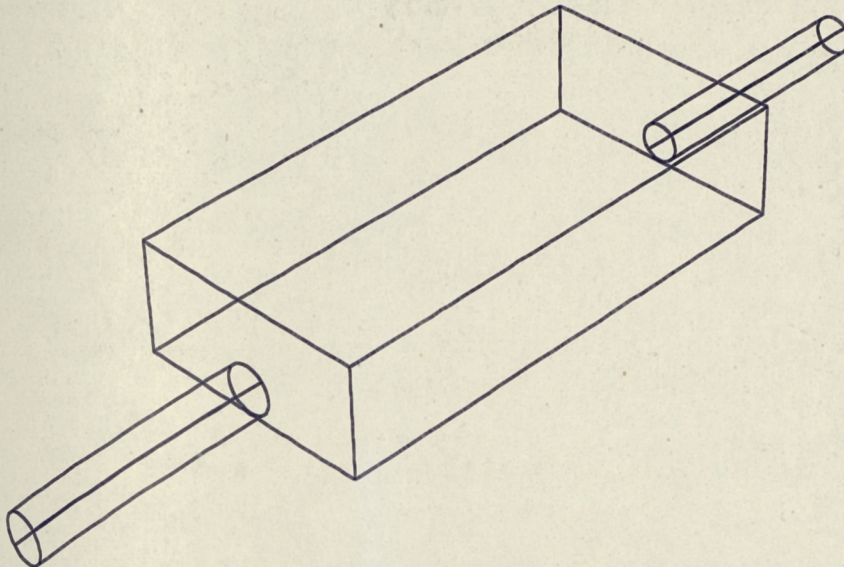
Particle Tracking

**Figure 8.9 b) Simulation record for LGD2: Particle tracking and efficiency**

SIMULATION RECORD

SUR1

Geometry



| | | | |
|----------------|------|-----------------------|------|
| Length (m) | 2.00 | Benching | None |
| Breadth (m) | 0.97 | DWF channel diameter | None |
| Flow depth (m) | 0.45 | Longitudinal gradient | None |

Velocity vectors

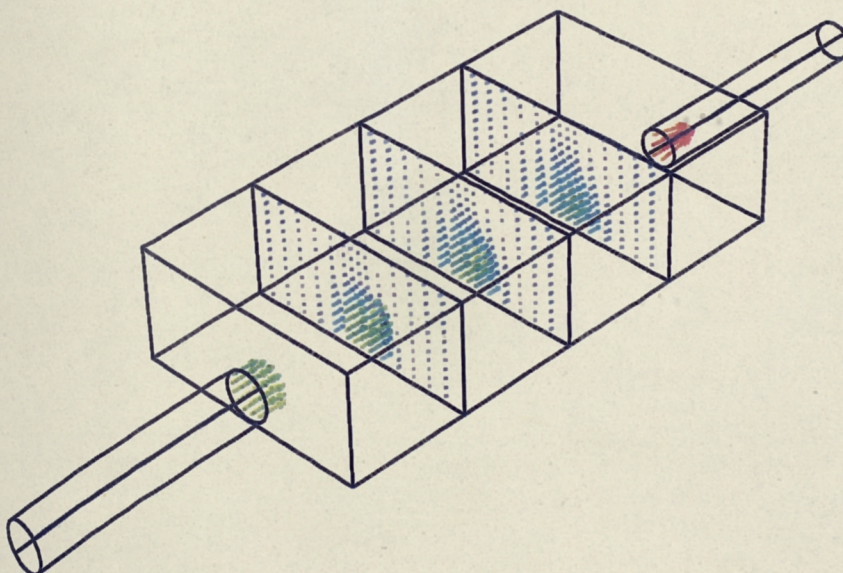
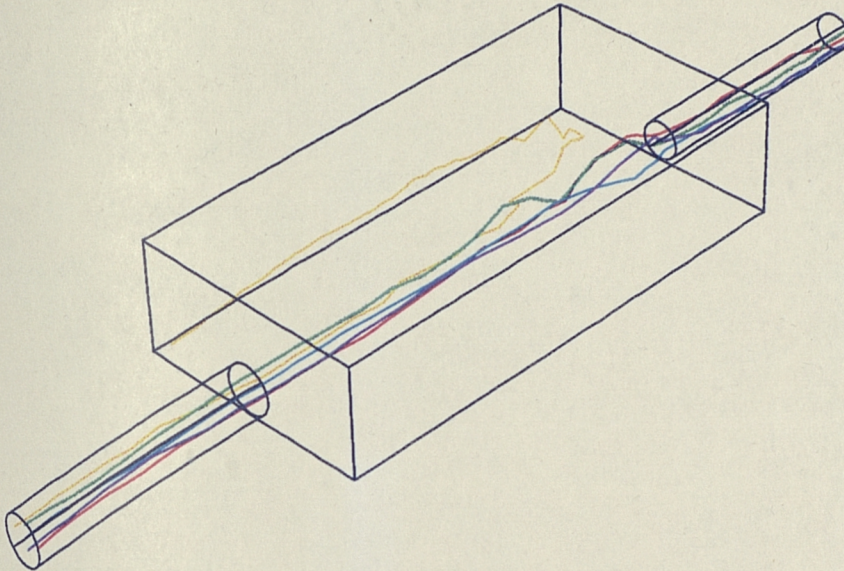
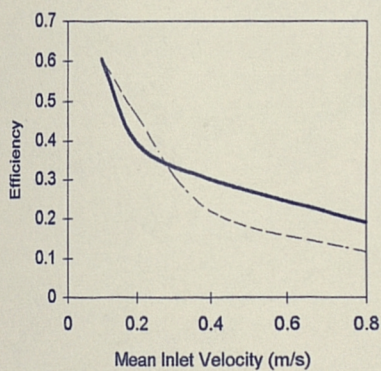


Figure 8.10 a) Simulation record for SUR1: Geometry and velocity vectors

Particle tracking*Efficiency*

| Method | Inlet velocity (m/s) | | | | |
|-------------------|----------------------|-------|-------|-------|-------|
| | 0.05 | 0.1 | 0.2 | 0.4 | 0.8 |
| Bed shear stress | 0.605 | 0.605 | 0.393 | 0.300 | 0.190 |
| Particle tracking | 0.569 | 0.395 | 0.362 | 0.343 | 0.335 |

Bed Shear Stress



Particle Tracking

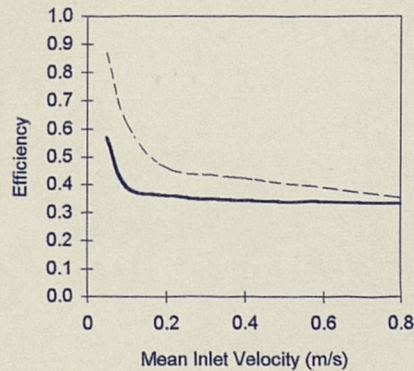


Figure 8.10 b) Simulation record for SUR1: Particle tracking and efficiency

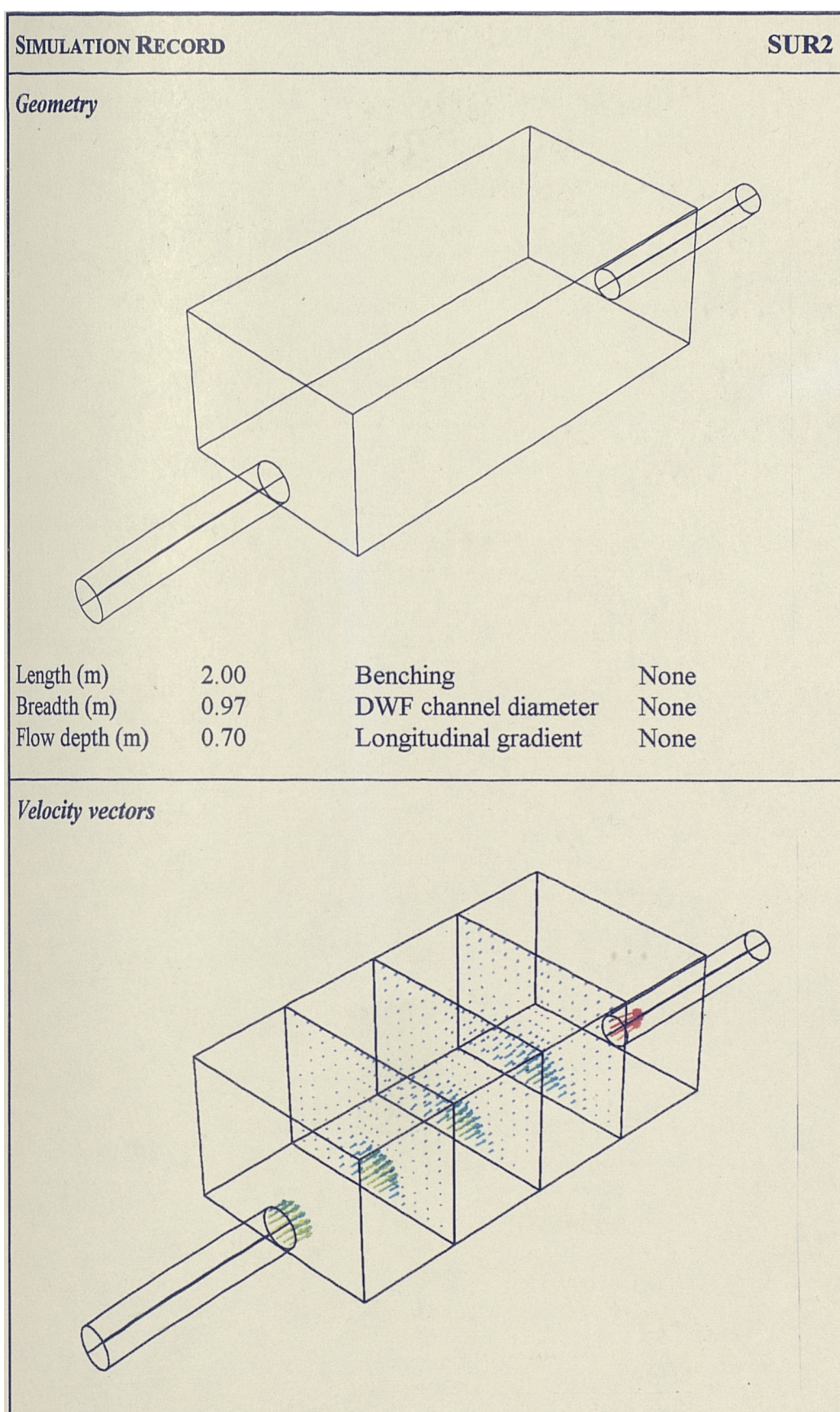
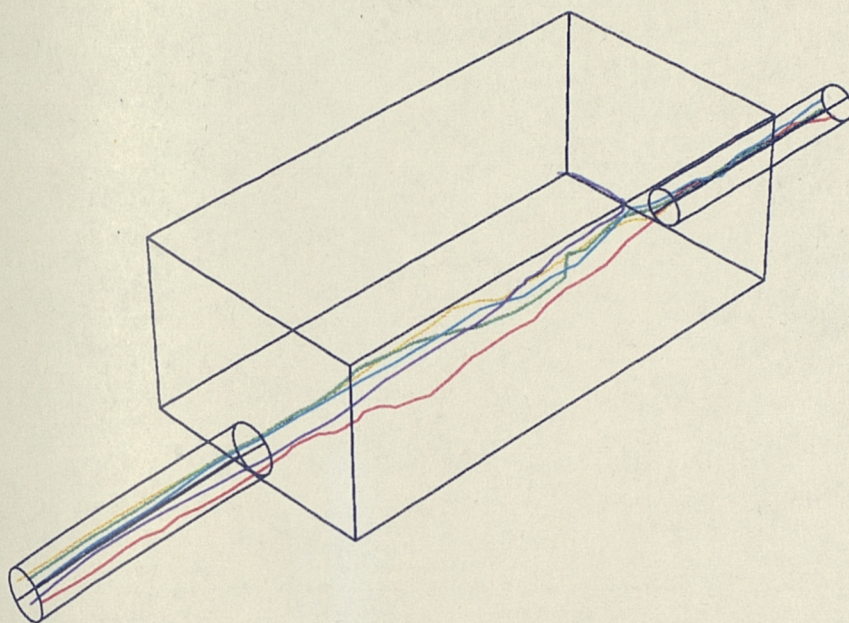
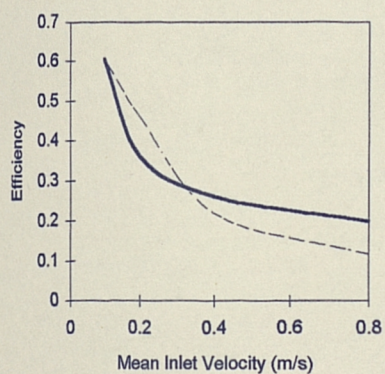


Figure 8.11 a) Simulation record for SUR2: Geometry and velocity vectors

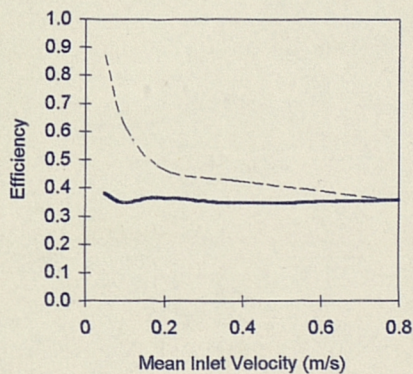
Particle tracking*Efficiency*

| Method | Inlet velocity (m/s) | | | | |
|-------------------|----------------------|-------|-------|-------|-------|
| | 0.05 | 0.1 | 0.2 | 0.4 | 0.8 |
| Bed shear stress | 0.605 | 0.605 | 0.361 | 0.260 | 0.199 |
| Particle tracking | 0.382 | 0.350 | 0.366 | 0.346 | 0.358 |

Bed Shear Stress



Particle Tracking

**Figure 8.11 b) Simulation record for SUR2: Particle tracking and efficiency**

8.4 Analysis

8.4.1 Bed Shear Stress

Figure 8.12 shows the \bar{u}/η_{BSS} curves for the ten chambers. It can be seen that there are significant differences between the \bar{u}/η_{BSS} curves for the ten chambers, and that the differences are not constant throughout the range of mean inlet velocities examined. Indeed, there are instances of one chamber having a higher efficiency than another under some flow conditions but not under others. For example, the chamber LONG has a higher efficiency than TANK for inlet velocities below 0.2 m/s, but then its efficiency drops substantially below that of TANK in the middle velocity range. The reverse is true for the relationship between SUR1 or SUR2 and TANK.

The effects of the four different geometric parameters on the predicted efficiency are now examined in some detail.

8.4.1.1 Length to Breadth Ratio

The most dramatic effects occurred when the length to breadth ratio was altered. The short, broad chamber (STUB) had the highest efficiency values, while, for a given mean inlet velocity, the chamber efficiency decreased for an increase in the length to breadth ratio. For the mean inlet velocity of 0.4 m/s, the shortest chamber had an efficiency of 0.51, whilst the longest chamber had an efficiency of 0.09.

This effect arises because the cross-sectional area of the chamber decreases as the length to breadth ratio is increased. The average cross-sectional velocity through the chamber consequently increases, and hence the stresses at the bed also increase. The data confirm the observations of Ellis (1992), for example, that the length to breadth ratio should be as high as possible if sedimentation is to be minimised.

8.4.1.2 Longitudinal Gradient

Altering the longitudinal gradient of the chamber in the range zero to 1 in 50 had practically no effect at all on the chamber efficiency.

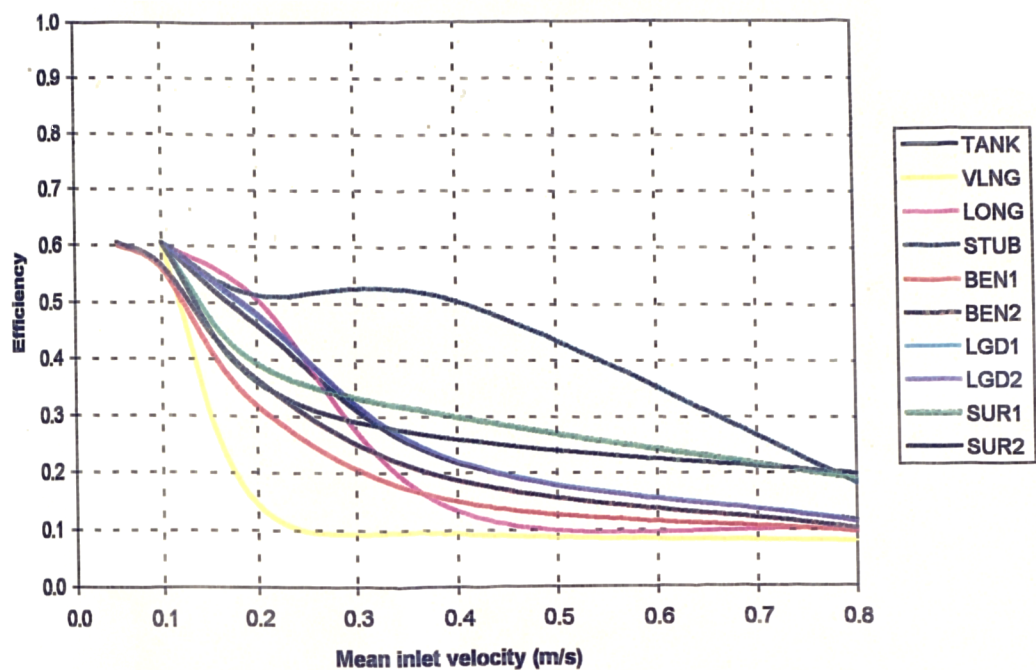


Figure 8.12 Efficiency comparison based on bed shear stress analysis

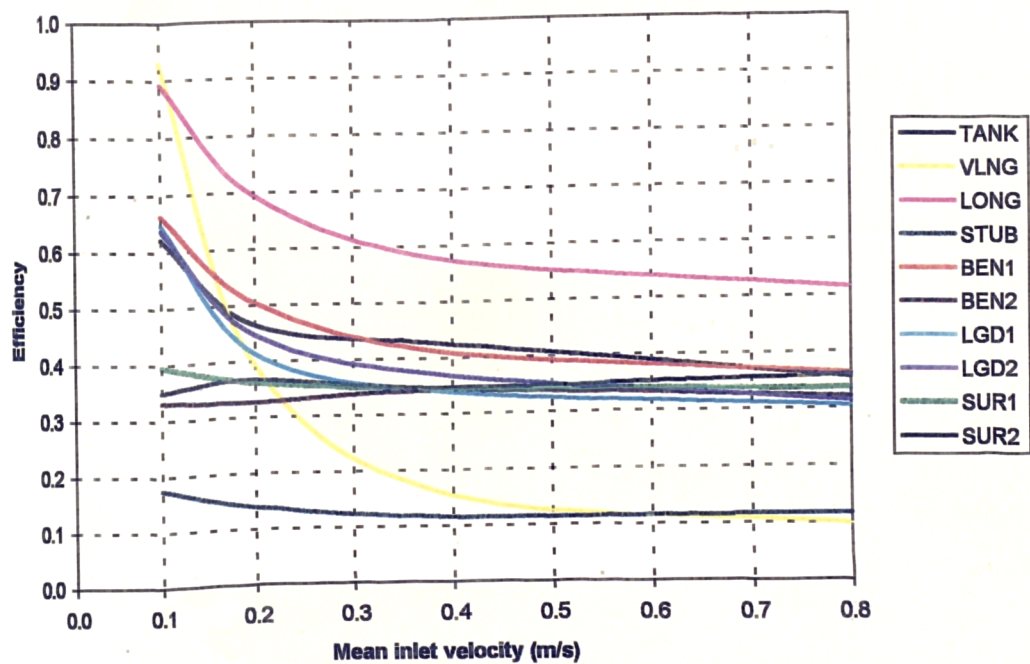


Figure 8.13 Efficiency comparison based on particle tracking

8.4.1.3 Inlet Surge

For the chambers in which the depth was increased to produce surcharged conditions at the inlet, SUR1 and SUR2, the efficiency was less at low mean inlet velocities (< 0.3 m/s), but higher than the control chamber for the higher mean inlet velocities. However, the differences in efficiency at two different levels of surcharge were quite small.

The flow patterns in both surcharged conditions were very different to those observed in the control chamber. Instead of the asymmetric circulation, the inflow jet passed straight through the chamber with small return currents alongside both the side walls. The main return current occurred at the free surface, and at this depth all the velocity vectors were orientated towards the inlet. The chamber named SUR2 is identical to SM2, which was described in chapter 6 with reference to the validation of the FLUENT flow simulation. Clearly, a transition between asymmetric and symmetric flow patterns occurs somewhere between the depths corresponding to 1.05 and 2.37 times the inlet diameter. Further work to identify the hydraulic conditions at which this transition occurred was not undertaken.

8.4.1.4 Benching and DWF

The effect of adding benching at a gradient of 1 in 4 was to reduce the efficiency over the entire range of mean inlet velocities. Two hydraulic reasons account for this effect. The cross-sectional area of flow was reduced by the benching, and so the average cross-sectional velocity and the bed shear stress was increased. Equally, the slope of the benching created a component of vertical bed shear stress in addition to the longitudinal and lateral stress components.

The addition of a DWF channel in BEN2 did not further reduce the efficiency relative to BEN1. Instead, the efficiency was increased over the whole range of mean inlet velocities, falling between that of TANK and BEN1. Shear stresses in the DWF channel appeared to be quite low, and deposition was predicted in its vicinity.

8.4.2 Particle Tracking

8.4.2.1 Length to Breadth Ratio

As with the bed shear stress model, the particle tracking results showed that changes to the length to breadth ratio of the chamber had the greatest impact on the efficiency

results, and these are shown in Figure 8.13. However, the effects were not the same as those identified using the bed shear stress analysis.

For the three chambers, STUB, TANK and LONG, the effect of the length to breadth ratio on efficiency was the exact reverse of the trends identified by the bed shear stress technique; in this case, the efficiency for the longer chambers was higher. At a mean inlet velocity of 0.4 m/s, the efficiency for STUB, TANK and LONG were 0.12, 0.42, and 0.57 respectively. These differences may be explained by making reference to the flow pattern in each chamber.

For STUB the flow pattern consisted of a central jet, with symmetrical return currents down either side of the chamber. Most particles remained within the main jet as they travelled from the inlet to the outlet, and only a small number passed into the recirculation zones where they were trapped. This is a particularly interesting observation as it has significant implications for chamber design. With a chamber designed in this way the side sections would fill with flow at the start of the storm, and the sediment contained within this flow volume would deposit. Subsequent flows would, however, be passed through to treatment, with no further significant deposition occurring in the side sections.

In the TANK simulation the flow pattern was asymmetric, with two clear recirculation zones. In this case, some particles passed straight through, whilst others entered the recirculation zones where they became trapped.

In the case of LONG, the flow pattern was asymmetric, but return currents were not significant. However, the particles had further to travel to the outlet, and therefore a greater chance of exceeding the maximum number of wall reflections and depositing on the chamber bed.

Because the length of the fourth chamber, VLNG, was even greater, one might have expected even higher efficiencies. Instead, the efficiency values were similar to those predicted using the bed shear stress technique. In both cases, the efficiency fell steeply from above 0.95 to below 0.2 between the mean inlet velocities of 0.1 and 0.3 m/s. At higher velocities the values fell marginally further. Here, the small cross-sectional area of the chamber ensured that flow velocities close to the bed were too high for the maximum number of wall reflections allowed in the particle tracking simulations to be exceeded very often.

8.4.2.2 Longitudinal Gradient

A tendency for efficiency to decrease as the longitudinal gradient increased was identified. A gradient of 1 in 50, LGD1, produced a 20% reduction in efficiency at a mean inlet velocity of 0.4 m/s. This observation correlates well with previous field and laboratory observations (Saul and Ellis, 1992).

8.4.2.3 Inlet Surge

Both chambers in which the inlet was deeply surcharged (SUR1 and SUR2) showed a reduction in efficiency throughout the range of mean inlet velocities tested, and the differences were most marked at the lowest velocities. An efficiency of below 0.4 was achieved in SUR2 at the mean inlet velocity of 0.05 m/s. The particle tracks were similar to those observed in STUB, in that they largely passed through the main jet flow, and did not enter into the return current which was present in the upper region of the flow field.

8.4.2.4 Benching and DWF

The introduction of benching at a gradient of 1 in 4 (BEN1) had only a marginal impact on the particle tracking results; the efficiency was approximately 5% higher for the mean inlet velocity of 0.2 m/s. It is thought that this may have arisen from the fact that the benching caused a reduction in the settling depth, thereby increasing the likelihood of particles depositing on the bed surface.

8.5 Regression Analysis

Further analysis was undertaken in an attempt to generalise the efficiency curves into two single functional relationships: one for the bed shear stress simulation results; and a second one for the particle tracking simulation results. This involved the application of regression analysis.

At the outset it should be noted that the simulation data are not entirely suitable for this type of analysis. The main problem is that the number of configurations assessed (10) was small compared with the large number of parameters that were varied, and that, in most cases, the effects of each parameter were only evaluated in isolation. It should not be assumed that the effect of the interaction of different geometric components will necessarily be the same as the regression analysis of the individual component impacts might indicate. Independent simulation assessments would be

required to establish the performance of a chamber design which combined several of the geometric components.

Regression relationships do, however, provide a useful representation of the measured data, with which interpolation between measured values may be undertaken. They also allow the parameters which are most critical, in terms of their impact on the result, to be identified. The analysis presented below should, therefore, be considered in the light of the limitations which have been highlighted.

The factors which control chamber efficiency may be classified into four groups: geometric; hydraulic; sediment properties and the properties of the fluid.

The geometric variables which have been considered are length (L), breadth (B), the longitudinal slope (S_l), the transverse slope (benching gradient) (S_b), the diameter of the chamber inlet (D) and the diameter of the dry weather flow channel (D_{DWF}). The hydraulic factors considered to be important are the inflow discharge (Q_{in}), the continuation flow discharge (Q_{cont}) and the depth of flow (H), whilst the properties of the sediment may be described by its diameter (d) and its settling velocity (ω). The properties of the fluid are its density (ρ), viscosity (μ), surface tension (σ) and acceleration due to gravity (g). Thus the full functional relationship for storage chamber efficiency may be represented by:

$$\eta = f(L, B, S_l, S_b, D, D_{DWF}, Q_{in}, Q_{cont}, H, d, \omega, \rho, \mu, \sigma, g) \quad (8.1)$$

However, the experimental work described in this thesis involved steady flow tests in which the values of Q_{in} and Q_{cont} were always equal. These two terms may therefore be replaced by a single discharge term, Q : The functional relationship, equation 8.1, becomes:

$$\eta = f(L, B, S_l, S_b, D, D_{DWF}, Q, H, d, \omega, \rho, \mu, \sigma, g) \quad (8.2)$$

Furthermore, it was demonstrated in chapter 4 that the mean inlet velocity was a particularly important variable in the determination of a chamber's separation efficiency. As the mean inlet velocity was, in all cases, directly proportional to Q , it is appropriate to represent the discharge term Q by the mean inlet velocity, \bar{u} :

$$\eta = f(L, B, S_l, S_b, D, D_{DWF}, \bar{u}, H, d, \omega, \rho, \mu, \sigma, g) \quad (8.3)$$

In order to reduce all parameters to dimensionless terms, and in line with the recommendations made by Whittington (1963), three parameters were selected to

represent the three fundamental dimensions mass, length and time. These were ρ , D and ω respectively. Equation 8.3 reduces to 11 dimensionless groups.

$$\eta = f\left(\frac{L}{D}, \frac{B}{D}, S_i, S_b, \frac{D_{DWF}}{D}, \frac{\bar{u}}{\omega}, \frac{H}{D}, \frac{d}{D}, \frac{\mu}{\rho D \omega}, \frac{\sigma}{\rho D \omega^2}, \frac{gD}{\omega^2}\right) \quad (8.4)$$

Note that the terms S_i and S_b are dimensionless. Of the 11 groups included in equation 8.4, the last four were constant in all the simulations. It is therefore appropriate, for the regression analysis, to reduce equation 8.4 to contain only the first seven dimensionless groups:

$$\eta = f\left(\frac{L}{D}, \frac{B}{D}, \frac{H}{D}, S_b, S_i, \frac{D_{DWF}}{D}, \frac{\bar{u}}{\omega}\right) \quad (8.5)$$

Multiple regression analysis was applied to the efficiency predictions derived using the flow simulations and bed shear stress analysis to determine a single functional relationship. It was shown in section 7.2.2 that the range of efficiency values that could be predicted using the technique of bed shear stress analysis was restricted to $0 < \eta < 0.6$. All tests that resulted in values of η at the upper limit of this range were excluded from the regression analysis. The regression equation, for which the value of R^2 was 0.91, was found to be:

$$\eta_{BSS} = 10^{-24.9} \left(\frac{L}{D}\right)^{15.02} \left(\frac{B}{D}\right)^{15.58} \left(\frac{H}{D}\right)^{0.11} (S_b)^{-0.032} (S_i)^{-0.0044} \left(\frac{D_{DWF}}{D}\right)^{0.014} \left(\frac{\bar{u}}{\omega}\right)^{-0.77} \quad (8.6)$$

Equivalent analysis was applied to the efficiency predictions based on particle tracking analysis, and the regression equation was found to be:

$$\eta_{PT} = 10^{135.9} \left(\frac{L}{D}\right)^{-77.80} \left(\frac{B}{D}\right)^{-79.44} \left(\frac{H}{D}\right)^{-0.3} (S_b)^{0.0034} (S_i)^{-0.0073} \left(\frac{D_{DWF}}{D}\right)^{-0.035} \left(\frac{\bar{u}}{\omega}\right)^{-0.26} \quad (8.7)$$

In this case the value of R^2 was 0.90. The chamber VLNG was excluded from the analysis presented in Equation 8.7 above, because, as explained in section 8.4.2, the efficiency data did not fit with the other length to breadth variations in a straightforward manner. Regression analysis undertaken with the complete data set resulted in a very poor R^2 value (0.59).

It can be seen that in both equations 8.6 and 8.7 above, the first two terms dominate the retention efficiency prediction, with each term being raised to an almost identical large power. In an attempt to assess the importance of the chamber length and

breadth, these first two terms were combined. The first term was multiplied by the inverse of the second to give L/B , the length to breadth ratio, and the regressional analysis was repeated.

$$\eta = f\left(\frac{L}{B}, \frac{H}{D}, S_b, S_l, \frac{D_{DWF}}{D}, \frac{\bar{u}}{\omega}\right) \quad (8.8)$$

The results of the analysis are presented in equations 8.9 and 8.10 below. The values of R^2 were 0.91 and 0.84 respectively.

$$\eta_{BSS} = 33.04 \left(\frac{L}{B}\right)^{-0.266} \left(\frac{H}{D}\right)^{0.0825} (S_b)^{-0.0348} (S_l)^{-0.0081} \left(\frac{D_{DWF}}{D}\right)^{0.0139} \left(\frac{\bar{u}}{\omega}\right)^{-0.773} \quad (8.9)$$

$$\eta_{PT} = 1.469 \left(\frac{L}{B}\right)^{0.528} \left(\frac{H}{D}\right)^{-0.0578} (S_b)^{0.0244} (S_l)^{0.0209} \left(\frac{D_{DWF}}{D}\right)^{-0.0347} \left(\frac{\bar{u}}{\omega}\right)^{-0.261} \quad (8.10)$$

Equations 8.9 and 8.10 above are considerably more meaningful. In both cases, it is clear that the mean inlet velocity and the length to breadth ratio are the dominant controls on the efficiency. It is interesting to note, however, that although both equations reveal an inverse dependence of efficiency on the mean inlet velocity, the effect of the change in length to breadth ratio appears to have opposite effects in equations 8.9 and 8.10. In the case of bed shear stress the efficiency reduces in response to an increase in the length to breadth ratio; for the particle tracking data an increased efficiency results. This effect has already been noted in the qualitative data analysis presented in section 8.4.

The range of application for equations 8.9 and 8.10 is given in Table 8.2. Note that the ranges presented in Table 8.2 reflect the fact that there is an upper limit of 0.6 on the efficiency that may be predicted from the bed shear stress analysis, and that the efficiency data from the chamber VLNG were excluded from the analysis of the particle tracking results.

Table 8.2 Application ranges for efficiency equations

| Parameter | Bed Shear Stress Equation 8.4 | Particle Tracking Equation 8.5 |
|-------------|----------------------------------|-----------------------------------|
| η | 0 - 0.6 | 0 - 1 |
| \bar{u}/w | 92 - 1468 | 92 - 1468 |
| L/B | 0.51 - 48.6 | 0.51 - 8.23 |
| S_l | 0 - 0.02 | 0 - 0.02 |
| S_b | 0 - 0.25 | 0 - 0.25 |
| D_{DWF}/D | 0 - 0.316 | 0 - 0.316 |
| H/D | 1.05 - 3.68 | 1.05 - 3.68 |

8.6 Discussion

In the description of the efficiency curves above it has emerged that, in some cases, the predictions made with the bed shear stress analysis differed significantly from those made with the particle tracking results. The most notable example of this is that a negative correlation between the length to breadth ratio and efficiency was obtained with the bed shear stress analysis, whilst a positive correlation was identified in the particle tracking results.

The advantages and disadvantages of using each method have already been discussed in chapter 7, where one of the advantages of particle tracking was considered to be its ability to take sediment supply into account. In the case of the chamber STUB, for example, the results indicated a very high efficiency using the bed shear stress method, and a very low efficiency with the particle tracking technique. The bed shear stress method showed that if the sediments were spread equally throughout the chamber then a high proportion would deposit in the regions of the return currents by the chamber side walls. The particle tracking analysis, on the other hand, showed that very few particles would in fact be supplied to those 'dead' areas, and so the amount of deposition would be small.

The two methods do not therefore represent alternative means of calculating chamber efficiency, but instead should be treated as complementary, partial descriptions of the processes affecting sedimentation. In chapter 7 it was shown that it is possible to use a bed shear stress deposition criteria in conjunction with particle tracking simulations. It was also indicated that the results of particle tracking simulations could be used to

indicate the location of deposited sediments in addition to the overall efficiency. There is clearly considerable scope to develop an approach to deposition analysis which is based on a combination of the two approaches which have been employed separately in this chapter.

However, it is clear that in all the chambers studied both methods did produce results that were physically meaningful in terms of the processes affecting sediment transport and deposition. Both methods would independently provide useful information when different chamber designs are being considered.

Changes to the length to breadth ratio had marked effects on the chamber performance. However, the effects of the other geometric alterations were surprisingly small when compared with reported field observations (Saul and Ellis, 1992). In chapter 4 it was suggested that the variations in the laboratory efficiency measurements between differently configured chambers were small because a steady flow testing regime had been employed. The same explanation is offered for the failure of the simulations to produce any marked effects. For example, the inclusion of benching may have little effect when the chamber is full and overflowing, but produce notable differences in performance at the filling and emptying stages of the storm. Significant erosion of deposited sediments occurs as a chamber fills and the DWF channel is first overtopped. DWF channels are included in chambers to contain the flow and maximise the flow velocity during dry weather but their influence is minimal once the chamber is full. Similarly, the washing down of benching surfaces towards the DWF channel at the end of the storm may greatly improve the chambers overall efficiency. The effects of a change in longitudinal gradient are also most likely to be apparent as the chamber drains.

8.7 Conclusions

The bed shear stress analysis and the particle tracking technique both enabled comparative statements about the effects of geometry on chamber efficiency to be made. Regression equations were found that enabled efficiency to be predicted from the mean inlet velocity and the chamber's geometric configuration. In both cases the equations appeared to be physically meaningful, and good correlation coefficients were obtained. It was recognised, however, that they were limited by the failure to address interaction effects and the need to exclude certain data sets from the analysis. For both techniques, the regression analysis indicated that the mean inlet velocity and the length to breadth ratio were the most significant determinants of chamber efficiency.

The importance of testing for a full range of mean inlet velocities has been illustrated. It cannot simply be said that any particular geometric feature improves efficiency as a rule. A number of the geometric parameters under consideration resulted in both comparative increases and decreases in efficiency depending on the flow condition at which the comparison was made.

In almost all cases, the effects of altering the different geometric parameters did not manifest themselves in the same way with the two methods, but provided meaningful information about the processes that affect sedimentation in the chamber. It was suggested therefore that the two techniques should be viewed as complementary sources of information, and that further research would be required to evaluate new approaches in which the two methods might be combined.

Of all the geometric parameters that were tested, altering the length to breadth ratio had the greatest impact on efficiency prediction, whatever the method of prediction. However, it was also suggested that some of the geometric parameters would have revealed greater impacts under time-varying flow conditions.

There is considerable scope for further work to examine ways in which the approaches of bed shear stress analysis and particle tracking may be combined with time-varying inflow hydrographs to better estimate the true impact of all configuration variables.

9. Conclusions, Discussion and Suggestions for Further Work

9.1 Introduction

In the first section of this chapter, the main conclusions to the thesis are presented. These are grouped into conclusions that relate to the laboratory phase of research, the analysis and finally the numerical simulation. Section 9.3 is a discussion, in which some concepts relating to the overall aims of the project are discussed. Finally, in section 9.4, some suggestions for further work are presented.

9.2 Conclusions

Laboratory phase:

1. A laboratory system which allowed sediment to be input continuously into a model storage chamber was devised. The system also included the use of internally positioned nephelometer probes for continuous turbidity measurement. These allowed the sediment concentrations at the inflow and outflow to the chamber to be estimated. The sediment used in the laboratory tests was 150 μm crushed olive stone.
2. Efficiency (η) was defined as the proportion of the incoming sediment load that settled to the chamber bed. A self-cleansing chamber was defined as one which did not experience any long-term build-up of deposited sediments. By definition, therefore, the efficiency of a completely self-cleansing chamber is zero. Efficiency measurements were carried out in three different chamber geometries and under a range of hydraulic conditions. The main findings were that:

- Of the hydraulic parameters considered, the efficiency was found to be highly dependent on the mean inlet velocity (\bar{u}). The efficiency of any individual chamber could be expressed in terms of a plot of η against \bar{u} .
 - The three chambers tested did not exhibit significant deviations from each other in terms of their \bar{u}/η plots. This observation is discussed in section 9.3.1 below.
 - The sedimentation behaviour observed in the laboratory chambers corresponded to ideal settling theory, and suggested that the model used in the sewer quality model MOUSE TRAP was an appropriate representation of the settling phenomenon. Although ideal settling theory is implemented in MOSQUITO, it is only used to model overflow performance. It is therefore recommended that the same model is extended to enable sedimentation in storage chambers to be evaluated.
3. During the efficiency tests it became apparent that the distribution of sediments on the chamber bed corresponded to the flow patterns in the chamber; the areas where deposition occurred were the positions of low flow velocity in the chamber. This observation led to a change of emphasis in the laboratory research, as detailed velocity measurements were made to clarify this point.
4. Velocity measurements were made under two flow conditions, using both a Nixon miniature current propeller and a laser doppler anemometry system to ensure measurements of all three velocity components were made. These measurements were used in the estimation of bed shear stress, and in the validation of the CFD flow simulations. Additional measurements were made close to the bed in order to confirm the validity of the approach adopted for the estimation of bed shear stress.

Analytical phase:

1. The velocity data were used to predict the bed shear stress, using the assumption of a logarithmic velocity distribution in the near-bed boundary layer. The shear velocity (u_0) was estimated from the measured velocity (u) at a distance (y) from the bed, using:

$$u = 2.5u_0 \ln \frac{9yu_0}{\nu} \quad (9.1)$$

in which ν is the kinematic viscosity.

The bed shear stress, τ_0 , was then calculated from the bed shear velocity using:

$$\tau_0 = \rho u_0^2 \quad (9.2)$$

2. The bed shear stress distribution was compared with the observed pattern of sediment deposition. It was found that the two patterns coincided, and a critical bed shear stress, below which sediment deposition occurred, was identified. For the crushed olive stone sediment on the perspex chamber bed, the value of τ_{cd} was found to be 0.04 N/m².
3. It was shown that, in addition to enabling the sediment distribution to be predicted under steady flow conditions, the bed shear stress model also allowed transient sediment deposition and erosion under time-varying inflow conditions to be estimated.
4. A regression relationship that related the distribution of deposited sediment to the chamber efficiency was identified. As the bed shear stress enabled the distribution of sediment to be predicted, it followed that chamber efficiency could also be estimated through analysis of the bed shear stress.

Numerical simulation

1. Following on from the results of the laboratory tests, it was hypothesised that computational fluid dynamics (CFD) could be used to predict the flow field, and thereby the bed shear stress and the efficiency.
2. It was demonstrated that accurate predictions of measured flow fields could be obtained using the FLUENT CFD software. Two cases were presented, in which three-dimensional flow simulations were compared with laboratory results.
3. Prediction of efficiency, based on bed shear stress analysis of the simulated flow data, was shown to be feasible, and a calibration relationship between the simulation results and the laboratory observations was derived. The efficiency, η , was given by:

$$\eta = 0.779e^{2.05C_{BSS}} \quad (9.3)$$

where C_{BSS} is the proportion of the chamber bed for which the bed shear stress obtained from the simulated flow field fell below the value of τ_{cd} , 0.04 N/m².

4. A second method for efficiency prediction was also investigated. This involved the use of the particle tracking facility in FLUENT. The particle tracking routine allows one to predict the trajectory of particles based on the local flow field. In turbulent flows this is a stochastic process; it therefore allows a statistical estimate of the final destinations of a large number of input particles to be made. Simulation parameters affecting the particle tracking routine were optimised to replicate the laboratory efficiency results. It was also demonstrated that particle tracking could be used to predict the exact position where a particle, or ultimately a large number of particles, deposited.
5. Finally, the two techniques for efficiency prediction (bed shear stress and particle tracking) were implemented to examine the differences in efficiency arising from a number of geometric and hydraulic configurations. The parameters investigated were the length to breadth ratio (L/B) the benching gradient (S_b), the longitudinal gradient (S_l), the dry weather flow channel (D_{DWF}) and also the level of surcharge (H/D). Both techniques suggested that the length to breadth ratio was the most important geometric parameter, although different conclusions were reached depending on the predictive technique employed. However, the mean inlet velocity (\bar{u}) was found to have a significant impact in both cases. Regression relationships (Equations 8.9 and 8.10) relating efficiency to geometric configuration and the flow velocity were presented. These equations are reproduced below:

$$\eta_{BSS} = 33.04 \left(\frac{L}{B} \right)^{-0.266} \left(\frac{H}{D} \right)^{0.0825} (S_b)^{0.0348} (S_l)^{-0.0081} \left(\frac{D_{DWF}}{D} \right)^{0.0139} \left(\frac{\bar{u}}{\omega} \right)^{-0.773} \quad (9.4)$$

$$\eta_{PT} = 1.469 \left(\frac{L}{B} \right)^{0.528} \left(\frac{H}{D} \right)^{-0.0578} (S_b)^{0.0244} (S_l)^{0.0209} \left(\frac{D_{DWF}}{D} \right)^{-0.0347} \left(\frac{\bar{u}}{\omega} \right)^{-0.261} \quad (9.5)$$

9.3 Discussion

There are two points that appear to warrant further discussion at this point. The first is the question of why both the laboratory experiments and, to some extent, the numerical simulation results did not identify significant differences in chamber efficiency due to alterations to the geometric configuration. The second question relates to the concept of designing storage chambers for self-cleansing operation.

9.3.1 Efficiency Results

In chapter 4 it was shown that model chambers with three different internal geometries exhibited comparable efficiency characteristics. This result apparently contradicts the observations that led Saul and Ellis (1992) to suggest that a number of design parameters did affect the chamber performance. Two parameters that they mentioned in particular were the length to breadth ratio and the gradient of the transverse benching. These are the parameters which were examined in the laboratory tests.

In chapter 4 it was suggested that the instrumentation used in the experiments might have lacked the sensitivity to detect small changes in performance that occurred. It is acknowledged at this stage that a number of experimental improvements were identified. However, there was other evidence that strongly suggested that the measured data were a fair representation of the true situation. In particular, sketches of the deposited sediment made following each test showed little difference between the three chambers under comparable flow conditions.

It seems most likely that this result was due to the steady flow test regime that was used, and also to the restricted geometrical range that was examined. These points are expanded upon in section 9.4.

9.3.2 Design for Self-Cleansing Operation

It was stated at the outset of this thesis that one of the aims was to produce guidelines for the design of chambers for self-cleansing operation. In the light of observations made during the progress of the research, it appears that this objective ought now to be reviewed. There are two important factors that make this objective problematic:

1. The research has shown that, above all else, the chamber efficiency is a function of the inflow rate. If the inflow is high the surface overflow rate is high and little deposition occurs. Conversely, where the inflow rate is reduced, the flow is more tranquil, the surface overflow rate is reduced and deposition is encouraged. The tested chambers were effectively capable of operating at an efficiency of anywhere between zero and unity, in response to different inflow conditions. One has to anticipate, therefore, that during its normal operation, with transient flow conditions, any storage chamber will operate both as an efficient settling tank and as an effective self-cleansing chamber.

2. The second problem arises when a storage chamber is combined with a combined sewer overflow in a single structure. If the storage chamber is to be self-cleansing then there are conflicting design objectives. CSOs are required to be designed to optimise sediment separation such that clean water is spilled at the overflow weir. This is best achieved by encouraging sedimentation in the CSO storage chamber. Increasing pressure from the National Rivers Authority, and equivalent regulatory bodies overseas, appears to be placing the focus on CSO performance, and the compromise between CSO separation performance and storage chamber self-cleansing performance is clearly unsatisfactory.

These two observations suggest that the design of storage chambers for self-cleansing operation perhaps should not be pursued further. Instead chambers should be designed for optimum CSO separation and with planned maintenance programmes. Research effort should be directed towards the optimisation of cleaning schedules the use of automatic cleaning systems, and improved separation efficiencies at overflow weirs. Due consideration needs also to be given to more radical strategies, including the removal of sediments at source.

9.4 Suggestions for Further Work

In chapter 4 a number of suggestions were made concerning possible adaptations that could be made to the laboratory system to improve its usefulness in the assessment of efficiency in model studies. Similarly, the discussion at the close of chapter 5 highlighted a number of interesting research topics in the field of turbulence, and the measurement of bed shear stresses. However, it is the author's opinion that the most interesting course for future research to follow would be in developing the use of CFD - and in particular particle tracking - for engineering problems that involve sediment deposition. A number of specific goals are outlined below.

1. It was shown in chapter 6 that good simulations of measured velocity distributions could be obtained, but it was felt that the results could be optimised through more informed use of turbulence models, improved free surface simulation and better representation of the outlet geometry.
2. The work was restricted to steady flow simulations, and yet the importance of transient flows in storage chamber performance have been highlighted. It is clearly desirable to explore the possibilities of undertaking time-varying simulations. The version of the FLUENT software released in 1996 does allow this to be done, even

with complex boundary-fitted geometries. The laboratory velocity data collected during the time-varying inflow hydrograph (chapter 5) represent a database against which such simulations could be verified.

3. All the geometries examined were essentially boxes with an inlet and an outlet at opposite ends, and there is a need to consider some of the more complex geometries found in reality. In particular there is a need to assess:

- The effect of a second outlet in the form of an overflow weir, and particularly the effect of the relative positions of the two outlets. It may be useful to bias this work towards identifying configurations that provide good separation at the overflow weir, rather than good self-cleansing performance;
- The effect of inlet or outlet positions offset from the centre line of the chamber and tanks that are not rectangular in plan;
- Chambers with more than one compartment - in order to assess the best combinations in terms of performance and maintenance requirements.

4. The particle tracking routine has been shown to model deposition reasonably well; there is no reason in theory why it could not also be used to model erosion. In addition the routine needs to be developed such that the final destinations of particles can be extracted more readily from the software. It may be appropriate to develop a new particle tracking routine independently from FLUENT, using FLUENT simply to produce the flow simulations. This would allow complex boundary functions for erosion and deposition to be developed with considerably more freedom than is currently available.

Finally, there is a need for the research to be underpinned by a comprehensive programme of field investigations. There does not appear to be in the UK at the moment any form of storage chamber database, and it is extremely difficult to ascertain the real effects that geometric parameters have on chamber performance. At this stage it is felt that relatively basic information collected from a large number of chambers would be of perhaps more use than detailed monitoring of individual structures. It is suggested that this should include geometry and operational details such as the number of times filled or number of spill events, maintenance carried out and any reported problems. Only with this type of feedback from the Water Industry can the CFD research be developed with confidence.

REFERENCES

- Abbott, M.B. and Basco, D.R., 1989, *Computational fluid dynamics - An introduction for engineers*, Longman Scientific and Technical.
- Ackers, P., Harrison, A.J.M. and Brewer, A.J., 1968, The hydraulic design of storm sewage overflows incorporating storage, *J. Inst. Mun. Eng.*, Vol. 95, 31-37.
- Ackers, P. and White, W.R., 1973, Sediment transport: New approach and analysis, *J. Hyd. Div., ASCE*, Vol. 99, No. HY11, 2041-2060.
- Ackers, P., 1984, Sediment transport in sewers and the design implications, *Proc. Int. Conf. on the Planning, Construction, Maintenance and Operation of Sewerage Systems*, 12-14 September, Reading, England, BHRA, 215-230.
- Alarie, R.L., McBean, E.A. and Farquhar, G.J., 1980, Simulation modeling of primary clarifier, *J. Env. Eng. Div., ASCE*, Vol. 106, No. EE2, 293-309.
- Arthur, S., in press, *Near bed solids transport in combined sewers*, PhD thesis, Wastewater Technology Centre, University of Abertay Dundee.
- Ashley, R.M. and Crabtree, R.W., 1992, Sediment origins, deposition and build-up in combined sewer systems, *Wat. Sci. Tech.*, Vol. 25, No. 8, 1-12.
- Ashley, R.M., Wotherspoon, D.J.J., Coghlan, B.P. and McGregor, I., 1992, The erosion and movement of sediments and associated pollutants in combined sewers, *Wat. Sci. Tech.*, Vol. 25, No. 8, 101-114.
- Ashley, R.M. (editor), 1995, *Proceedings of the International Conference on Sewer Solids — Characteristics, Movement, Effects and Control*, 5-8 September 1995, University of Abertay Dundee.
- ATV, 1991, *Richtlinien für die Bemessung und Gestaltung von Regenentlastungsanlagen in Mischwasserkanälen*, ATV Arbeitsblatt A128. [Cited in Pecher, 1992].
- Balmforth, D.J., 1990, The pollution aspects of storm-sewage overflows, *J. IWEM*, Vol. 4, No. 3, 219-226.
- Bayazit, M., 1972, Random walk model for motion of a solid particle in turbulent open-channel flow, *J. Hydraulic Research*, No. 1, 1-14.
- Bertrand-Krajewski, J.L., Briat, P. and Scrivener, O., 1993, Sewer sediment production and transport modelling: a literature review, *J. Hyd. Res.*, Vol. 31, No. 4, 435-460.

- Brownbill, V.R., 1992, *Tank sediment quality at Littleborough*, Internal report, School of Geography, University of Manchester.
- BSI (British Standards Institution), 1990, *British standard methods of test for soils for civil engineering purposes*, BS 1377.
- Camp, T.R., 1946, Sedimentation and the design of settling tanks, *Trans. ASCE*, Vol. 111, 895-936.
- Cant, J.A., 1991, *Detention tank design and maintenance (incorporating a design guide)*, WRc report no. UM1233.
- CEC (Council of the European Communities), 1991, *Directive concerning urban waste water treatment*, (91/271/EEC), Official Journal L135, 30 May 1991.
- Celik, I., Rodi, W. and Stamou, A.I., 1985, Prediction of hydrodynamic characteristics of rectangular settling tanks, *Proc. Int. Symp. on refined Flow Modelling and Turbulence Measurements*, Iowa. [Cited in Stamou *et al.*, 1989].
- Chadwick, A. and Morfett, J., 1993, *Hydraulics in Civil and Environmental Engineering*, Second Edition, E & FN Spon.
- Chebbi, G. and Bachoc, A., 1992, Characterization of suspended solids in urban wet weather discharges, *Wat. Sci. Tech.*, Vol. 25, No. 8, 171-180.
- Chow, V.T., 1959, *Open channel hydraulics*, McGraw-Hill.
- CIRIA (Construction Industry Research and Information Association), 1973, *Cost effective sewage treatment - the creation of an optimising model*, Report 46, 2, CIRIA, London, 13.
- CIRIA (Construction Industry Research and Information Association), 1987, *Sediment movement in combined sewerage and storm water drainage systems - Phase 1*, Report PR1.
- CIRIA (Construction Industry Research and Information Association), 1994, *Design of sewers to control sediment problems*, Funders Report/CP/27, London.
- Clifforde, I.T., Saul, A.J. and Tyson, J., 1986, Urban pollution of rivers - the UK water industry research programme, *Int. Conf. on Water quality modelling in the inland natural environment*, Bournemouth, 10-13 June, 485-491.
- Closet, J.F. and Svensson, G., 1993, *Conclusions regarding the modeling of pollutant removal into stormwater tank*, Mousetrap development report, DHI.
- Coleman, N.L., 1981, Velocity profiles with suspended sediment, *J. Hyd. Res.*, 19, No. 3, 211-229.

- Coles, D., 1956, The law of the wake in the turbulent boundary layer, *J. Fluid Mechanics*, 1, 191-226.
- Crabtree, R.W., 1987, Urban river pollution in the UK: the WRc river basin management programme, (*contributing chapter for 'Geomorphology and public policy, ed J. Hooke*), WRc Swindon.
- Crabtree, R.W., 1988, *A classification of combined sewer sediment types and characteristics*, WRc Report No. ER 324E.
- Crabtree, R.W., Forster, C.F., Nalluri, C. and Williams, D.J.A., 1989, *Recommendations for further research into combined sewer sediment deposits*, FWR Report No. FR0040, FWR, Marlow.
- Crabtree, R.W., Ashley, R.M. and Saul, A.J., 1991, *Review of research into sediments in sewers and ancillary structures*, FWR Report No. FR0205, FWR, Marlow.
- Crabtree, R., Garsdal, H., Gent, R., Mark, O. and Dörge, J., 1994a, Mousetrap - a deterministic sewer flow quality model, *Wat. Sci. Tech.*, Vol. 30, No. 1, 107-115.
- Crabtree R.W., Becker, M., Bryan, D., Gent, R.J. and Threlfall, J.L., 1994b, *Review of UPM modelling tools*, FWR Report No. FR0442, FWR, Marlow.
- DHI (Danish Hydraulic Institute), 1994, *MouseTrap user manual*, Version 1.00.
- Dantec, 1983, *Laser Doppler Anemometry*, Publ. No. 3205, Dantec, Denmark.
- Davis, P.S. and Parkinson, A.D., 1990, Littleborough combined sewer overflow - a new approach to planning and design, *Proc. Fifth Int. Conf. on Urban Storm Drainage*, Osaka, Japan, 23-27 July, 1359-1364.
- Davis, P.S. and Crabtree, R.W., 1991, *Evaluation of interim water quality planning procedures: The Littleborough case study*, FWR Report No. FR0204, FWR, Marlow.
- Delo, E.A., 1988, *Estuarine Muds Manual*, Hydraulics Research Report SR 164, Wallingford.
- DeVantier, B.A. and Larock, B.E., 1987, Modeling sediment-induced density currents in sedimentation basins, *J. Hyd. Eng.*, Vol. 113, No. 1, 80-94
- Dobbins, W.E., 1944, Effect of turbulence on sedimentation, *Trans. ASCE*, Vol. 109, 629-656.
- Einstein, H.A., 1942, Formulas for the transportation of bed load, *Trans. ASCE*, Vol. 107, 561-577.

- Einstein, H.A. and Chien, N., 1955, *Effects of heavy sediment concentration near the bed on velocity and sediment distribution*, Univ. of Cal., Berkeley and US Army Corps of Engr., Missouri River Div., Rep. No. 8. [Cited in Coleman, 1981].
- Ellis, D.R., 1992, *The design of storm drainage storage tanks for self cleansing operation*, PhD thesis, University of Manchester.
- EPA (United States Environmental Protection Agency), 1986, *Methodology for analysis of detention basins for control of urban runoff quality*, EPA 440/5-87-001.
- Escritt, L.B., 1956, *Sewerage and sewage disposal*, Contractor's record, London, 282. [Cited in Tebbutt and Christoulas, 1975].
- Fluent, 1993, *FLUENT user's guide*, Version 4.2, Fluent inc.
- FWR (Foundation for Water Research), 1994, *Urban pollution management (UPM) manual*, FR/CL 0002, Marlow
- Garde, R.J., Ranga Raju, K.G. and Sujudi, A.W.R., 1990, Design of settling basins, *J. Hyd. Res.*, Vol. 28, No. 1, 81-91.
- Geiger, W.F., 1986, Variation of combined runoff quality and resulting pollutant retention strategies, *Urban storm water quality and effects upon receiving waters*, TNO Committee on Hydrological Research, Proceedings and Information No. 36, Int. Conf., Wageningen, The Netherlands, 71-91.
- Gent, R.J., Crabtree, R.W. and Eperson, M., 1994, *Improved MOSQUITO application procedures*, Foundation for Water Research, Report No. FR 0443.
- Gupta, K and Saul, A.J., 1994, Storage tank design for the retention of pollutants, *Proc. HYDROTOP '94*, April 12-15, Marseilles, France.
- Halliwell, A.R. and Saul, A.J., 1980, The use of hydraulic models to examine the performance of storm sewage overflows, *Proc. Instn. Civ. Engrs*, Part 2, 69, June, 245-259.
- Hazen, A., 1904, On sedimentation, *Trans. ASCE*, Vol. LIII, 45-71.
- Hedley, G. and King, M.V., 1971, Suggested correlation between storm sewage characteristics and storm overflow performance, *Proc. ICE*, Vol. 48, 399-411.
- Hedley, G. and Lockley, J.C., 1978, Use of retention tanks on sewerage systems: A five year assessment, *Water Poll. Control*, 178-187.
- Hjulström, F., 1935, Studies of the morphological activity of rivers as illustrated by the river Fyris, *Bulletin of the Geological Institute, University of Uppsala*, 25,

- 221-527. [Cited in K. Richards, 1982, *Rivers - form and process in alluvial channels*, Methuen].
- Hoyal, D.C.J.D., Depinto, J.V., Atkinson, J.F. and Taylor, S.W., 1995, The effect of turbulence on sediment deposition, *J. Hydraulics Research*, Vol. 33, No. 3, 349-360.
- Imam, E, McCorquodale, J.A. and Bewtra, J.K., 1983, Numerical modeling of sedimentation tanks, *J. Hyd. Eng.*, Vol. 109, No. 12, 1740-1754.
- Knott, G.E. and Taylor, A.J., 1985, *The use of detention tanks for flow attenuation - a review of current practice*, WRc Report No. 171E, WRc Engineering, Swindon.
- Krauth, Kh., 1973, Entlassung der Gewässer durch Behandlung des Regenwassers in Regenüberlaufbecken, *Wasserwirtschaft*, H2, 42. [Cited in Ellis, 1992].
- Laplace, D, Bachoc, A., Sanchez, Y. and Dartus, D, 1992, Trunk sewer clogging development - description and solutions, *Wat. Sci. Tech.*, Vol. 25, No. 8, 91-100.
- Larsen, P., 1977, *On the hydraulics of rectangular settling basins - experimental and theoretical studies*, Report No. 1001, Dept. Wat. res. Eng., Lund Inst. Technol., Lund, Sweden.
- Launder, B.E. and Spalding, D.B., 1974, *Lectures in mathematical models of turbulence*, Academic Press, New York.
- Lessard, P. and Beck, M.B., 1991, Dynamic simulation of storm tanks, *Water Research*, Vol. 25, No. 4, 375-391.
- Lyn, D.A. and Rodi, W., 1990, Turbulence measurements in model settling tank, *J. Hyd. Eng.*, Vol. 116, No. 1, 3-21.
- May, R.W.P., Brown, P.M., Hare, G.R. and Jones, K.D., 1989, *Self cleansing conditions for sewers carrying sediment*, Hydraulics Research Report No. 221, Wallingford.
- McCorquodale, J.A., Moursi, A.M. and El-Sabakhy, 1988, Experimental study of flow in settling tanks, *J. Env. Eng. Div., ASCE*, Vol. 114, No. 5, 1160-1174.
- Michelbach, S. and Wöhrle, C., 1992, Settleable solids in a combined sewer system - measurement, quantity, characteristics, *Wat. Sci. Tech.*, Vol. 25, No. 8, 181-188.
- MHLG, 1970, *Ministry of Housing and Local Government Technical Committee on storm overflows and the disposal of storm sewage, Final Report*, HMSO, London.

- Morris, G., 1992, Consent standards for storm sewage overflow, *Combined Sewer Overflow - Practice and Performance*, Hydro Research and Development Seminar, Hull, 6 October 1992.
- Morris, G., 1993, The new standards - what it means in practice, *Combined Sewer Overflows - Complying with the new NRA standards*, Hydro Research and Development Seminar, Leeds, June 1993.
- Moys, G. D., 1987, *Modelling of stormwater quality including tanks and overflows (MOSQUITO) design specifications*, Report No. SR 127, Hydraulics Research Limited.
- Nicholson, J. and O'Connor, B.A., 1986, Cohesive sediment transport model, *J. Hyd. Eng., ASCE*, Vol. 112, No. 7, 621-640.
- Nicoll, E.H. and McGillivray, R., 1978, Report of the working party on storm sewage (Scotland) A review, *Water Poll. Control*, 157-172.
- North West Water, 1983, Improving rivers, estuaries and coastal waters in the North West, A consultation paper, North West Water, Warrington. [Cited in Crabtree, 1987].
- National Rivers Authority (NRA), 1993, *Guidelines for AMP2, Periodic Review*, Version 2.
- Osborne, M.P. and Shamash, M.J., 1993, *Wallingford procedure: water quality supplement*, Wallingford Software Ltd.
- Ostendorf, D.W., 1986, Hydraulics of rectangular clarifiers, *J. Env. Eng., ASCE*, Vol. 112, No. 5, 939-952.
- Parchure, T.M. and Mehta, A.J., 1985, Erosion of soft cohesive sediment deposits, *J. Hyd. Eng., ASCE*, Vol. 111, No. 10, 1308-1326.
- Pecher, R., 1992, Stormwater treatment in combined systems in Germany, *Wat. Sci. Tech.*, Vol. 26, No. 7-8, 1841-1849.
- Pratt, C.J., 1995, A review of source control of urban stormwater runoff, *J.CIWEM*, 9, April, 132-139.
- Ristenpart, E. and Uhl, M., 1993, Dynamic behaviour of sewer sediment, *Proc. Sixth Int. Conf. on Urban Storm Drainage*, Niagara Falls, Canada, 12-17 September, 748-753.
- Roebuck, I.H., 1989, Practical considerations of the design of detention tanks, *Municipal Engineer*, Vol. 6, 231-239.

- Rosin, P. and Rammler, E., 1933, The laws governing the fineness of powdered coal, *Journal of the Institute of Fuel*, Vol. 7, 29-36.
- Saul, A.J. and Ellis, D.R., 1992, Sediment deposition in storage tanks, *Wat. Sci. Tech.* Vol. 25, No. 8, 189-198.
- Saul, A.J. and Svejksky, K., 1994, Computational modelling of a Vortex CSO structure, *Wat. Sci. Tech.*, Vol. 30, No. 1, 97-106.
- Schamber, D.R. and Larock, B.E., 1981, Numerical analysis of flow in sedimentation basins, *J. Hyd. Div, ASCE*, Vol. 107, No HY5, 575-591.
- Scottish Development Department (SDD), 1977, *Storm Sewage: separation and disposal - report of the working party on storm drainage*, HMSO, Edinburgh.
- Scottish Development Department (SDD), 1980, *Settling velocities of particulate matter in sewage*, HMSO, Edinburgh.
- Sharman B.J., 1994, The use of detention storage to reduce overflow spill, *Proc 2nd Int. Conf. on Hydraulic Modelling*, Stratford-upon-Avon, 14-16 June, 253-262.
- Sharpe and Kirkbride, 1959, Storm-water overflows: the operation and design of a stilling pond, *Proc. ICE*, Vol. 13, 445-466.
- Shaw, C.T., 1992, *Using computational fluid dynamics*, Prentice Hall International (UK) Ltd.
- Shiba, S. and Inoue, Y., 1975, Dynamic response of settling basins, *J. Env. Eng. Div., ASCE*, Vol. 101, No. EE5, 741-757.
- Shields, A., 1936, Anwendung der Aehnlichkeitsmechanik und der turbulenzforschung auf die geschiebebewegung, *Mitteilung der Preussischen versuchsanstalt fuer Wasserbau und Schiffbau*, Heft 26, Berlin. [Cited in Coleman, 1981].
- Skipworth, P.J., in press, *The erosion and transport of cohesive-like sediment beds in sewers*, PhD thesis, The University of Sheffield.
- Smith, R., 1969, Preliminary design of wastewater treatment systems, *J. Sanit. Engng. Div., ASCE*, Vol. 95, SA1, 117.
- Söderlund, G. and Lehtinen, H., 1972, Comparison of discharges from urban storm-water run-off, mixed storm overflow and treated sewage. *Proc. 6th Int. Conf. Adv. Wat. Pollut. Res.*, Ed. S.H. Jenkins, Pergamon Press, Oxford.
- Stamou, A.I., Adams, E.W. and Rodi, W., 1989, Numerical modeling of flow and settling in primary rectangular clarifiers, *J. Hyd. Res.*, Vol. 27, No. 5, 665-682.

- Stotz, G. and Krauth, Kh., 1986, Detention basins and their capabilities for the retention of pollutants, *1st Wageningen Conf. on Urban Stormwater Quality and Effects upon Receiving Waters*, CHO-TNO, October.
- Stovin, V.R., 1996, *The use of LDA with sediment laden flows*, Internal report, Department of Civil and Structural Engineering, The University of Sheffield.
- Takamatsu, T., Naito, M., Shiba, S. and Ueda, Y., 1974, Effects of deposit resuspension on settling basin, *J. Env. Eng. Div., ASCE*, Vol. 100, No. EE4, 883-903.
- Tebbutt, T.H.Y. and Chrisoulas, D.G., 1975, Performance relationships for primary sedimentation, *Water Research*, Vol. 9, 347-356.
- Thornton, R.C. and Saul, A.J., 1986, Some quality characteristics of combined sewer flows, *J. Inst. Public Health Engineers*, Vol. 14, No. 3, 35-39.
- Torfs, H, 1995, *Erosion of mud/sand mixtures*, PhD thesis, Katholieke Universiteit Leuven, Belgium.
- Vanoni, V.A., 1946, Transportation of suspended sediment by water, *Trans. ASCE*, Vol. III, 67-133. [Cited in Coleman, 1981].
- Verbanck, M.A. (editor), 1992a, Origin, occurrence and behaviour of sediments in sewer systems, Proceedings of the First International Workshop on Sewer Sediments, Brussels 4-6 September 1991, *Wat. Sci. Tech.*, Vol. 25, No. 8.
- Verbanck, M.A., 1992b, Field investigations on sediment occurrence and behaviour in Brussels combined sewers, *Wat. Sci. Tech.*, Vol. 25, No. 8, 71-82.
- Von-Kármán, T., 1930, *Mechanische Aehnlichkeit und Turnulenz, Nachrichten von der Gesellschaft der Wissenschaften zu Goettingen, Fachgruppe I (Mathematik)*, Num. 5, 58-76. [Cited in Coleman, 1981].
- Whittington, R.B., 1963, A simple dimensional method for hydraulic problems, *J. Hyd. Div., ASCE*, Vol. 89, No. HY5, 1-27.
- Wilkinson, D and Waldie, B., 1994, Experimental and numerical modelling of gravity separators, *Proc 2nd Int. Conf. on Hydraulic Modelling*, Stratford-upon-Avon, 14-16 June, 107-130.
- Williams, D.J.A., Williams, P.R. and Crabtree, R.W., 1989, *Preliminary investigations into rheological properties of sewer sediment deposits and development of a synthetic sewer sediment material for laboratory studies*, FWR Report No. FR0016, FWR, Marlow.
- WRc/WAA, 1994, *Sewerage rehabilitation manual*, Third Edition, WRc Marlow.

- Xu, Y. and Sparks, T., 1994, A numerical simulation of the hydraulics of an annular chlorine tank, *Proc 2nd Int. Conf. on Hydraulic Modelling*, Stratford-upon-Avon, 14-16 June, 93-105.
- Yang, T.C., 1973, Incipient motion and sediment transport, *J. Hyd. Div., ASCE*, Vol. 99, No. HY10, 1679-1704.

APPENDIX A -
The Fluent Line-Print File

This file was output directly from the FLUENT software. The file details all the parameters that were relevant to the numerical simulation of the laboratory storage chamber and the particle tracking experiments. The numerical simulation of the flow field is described fully in chapter 6, while the details of the particle tracking are presented in chapter 7.

The file has been annotated with the numbers ① to ⑩. These numbers indicate parts of the LP file that were important to the configuration of the storage chamber simulation. For any section without an annotation it should be assumed that these settings were the default for this version of the software, and that they were not altered during any stage of the research.

- ① This section describes the chamber geometry. The term ‘boundary fitted co-ordinates’ refers to the fact that the geometry was set up using the pre-processor software, PreBFC. It may be seen that the problem was defined as 82 cells long, 14 cells high and 32 cells wide. The exact location of each node point is not given in the LP file, but may be seen in Figure 6.1.

In the LP file, the cell types are presented for each longitudinal slice ($K = 1$ to $K = 32$). Here, however, the file has been edited in order to avoid printing slices of the same type more than once. For example, the left wall ($K = 1$) and the right wall ($K = 32$) have exactly the same cell type definition. They are shown under the heading CELL TYPES: $K=1$ and 32. In each cell type listing one or more of the following boundary conditions occur:

- W denotes a wall cell. Distinction is made between:
 - W1 - Solid wall
 - W2 - Free surface
 - D denotes a dead, or inactive, cell. Dead cells were used to define the regions surrounding the inlet and outlet pipes.
 - I denotes an inlet cell. In this problem only I1 inlet cells were used, but cells of type I2, I3, etc., may be used to describe a range of inlet conditions if required.
 - O denotes an outlet cell.
 - . denotes a live cell. Calculations of flow occur in these cells.
- ② The velocity boundary conditions are defined here. The W1 type solid walls have all velocity components set to zero, whilst the I1 inlet cells have a u-velocity component of 0.561 m/s. This is the mean inlet velocity. At the W2 - free

surface - type wall boundary the links are cut. This means that the wall acts as a friction free surface, and the simulation does not assume that all the velocity components must be zero at this boundary.

- ③ The inlet (I1) turbulence conditions were selected such that the turbulence intensity was 5%, and the characteristic length was 0.1 m, i.e., half the inlet diameter.
- ④ The acceleration due to gravity (9.81 m/s^2 in the vertical direction) was defined in this section.
- ⑤ The density and viscosity for water were entered here.
- ⑥ This section refers to the particle tracking. The options presented here are discussed in detail in Chapter 7.
- ⑦ This section lists the boundary conditions used for the particle tracking (see Chapter 7 for details).
- ⑧ The particle properties are listed here. Only the particle density is of relevance to this research project (see Chapter 7)
- ⑨ This section lists the injection points and particle properties for the 68 distributed particles that were used in the particle tracking experiments. The X, Y and Z positions of each particle are listed, followed by the u -, v - and w -velocity components. Note that the particles were spatially distributed across the whole area of the inlet, and that they all entered with a u -velocity component equal to the mean inlet velocity, 0.561 m/s. The particle diameter was constant, at $4.7 \times 10^{-5} \text{ m}$. This is the mean diameter of the crushed olive stone, as determined in laboratory tests (see Chapter 3).
- ⑩ The final section of the LP-file lists the parameters which were used in the numerical solution of the flow field. Guidance on the meaning of the various parameters and the way in which they should be altered may be found in the FLUENT User Manual (1993).

```

I I LICENSED BY AND THE PROPERTY OF FLUENT INC., CENTERRA RESOURCE PARK, 10 CAVENDISH CT., LEBANON, NH 03766. 603-643-2600 I
I
I I FFFFF L U U EEEEE N N TTTTTT I
I I F F L U U E NN N T I
I I FFFF L U U EEEE N N N T I
I I F L U U E N N N T I
I I F LLLL UUU EFLEE N N T I
I I
I I OUTPUT PRODUCED BY VFRSI N 4. 3 I
I I

```

* * * * *

* FLUENT (V4. 3) Fluid Flow Modeling * * * * *

* * * * *

* Copyright (C) 1984, 1989, 1991 by Fluent Inc. * * * * *

* All rights reserved. No part of this code may be * * * * *

* reproduced or otherwise used in any form without express * * * * *

* written permission from Fluent Inc. Unless this code is * * * * *

* subject to terms of the license agreement. * * * * *

* FLUENT, FLUENT BFC, FLUENT PC, and FLUENT/CVD * * * * *

* are registered trademarks of: * * * * *

* * * * *

* Fluent Inc. * * * * *

* Centera Resource Park * * * * *

* 10 Cavendish Court * * * * *

* Lebanon, New Hampshire 03766 USA * * * * *

* (8) 445-4454 * * * * *

* * * * *

* 75000 Cells, 10 Species Equations Available * * * * *

* * * * *

- UNITS SYSTEM -

| INDEX | PROPERTY | UNITS | S.I. CONVERSION FACTOR |
|-------|----------------|----------------|------------------------|
| 1 | DIMENSIONLESS | DIMENSIONLESS | 1.0 E+00 |
| 2 | MASS | KILOGRAMS | 1.0 E+00 |
| 3 | LENGTH | METERS | 1.000E+00 |
| 4 | TIME | SECONDS | 1.00 E+00 |
| 5 | VEL CITY | METERS/SEC | 1. E+00 |
| 6 | FORCE | NFTONS | 1. E+ 0 |
| 7 | ACCELERATION | MFTERS/SEC/SEC | 1. 0E+00 |
| 8 | ENFRGY | JOULES | 1.00 E+0 |
| 9 | POWER | WATTS | 1. 0E+ 0 |
| 10 | MASS FLOW RATE | KILOGRAMS/SEC | 1. E+00 |

| | | | |
|----|------------------|------------------|-----------|
| 11 | TEMPERATURE | KELVIN | 1.000E+00 |
| 12 | ENTHALPY | JOULES/KILOGRAM | 1.000E+00 |
| 13 | PRESSURE | PASCALS | 1.000E+00 |
| 14 | DENSITY | KILOGRAMS/CU.M | 1.000E+00 |
| 15 | VISCOSITY | KG/M-SEC. | 1.0 E+ |
| 16 | K.E. OF TURBLNCE | M.SQ/SEC/SEC | 1.0 E+0 |
| 17 | K.E. DISS. RATE | M.SQ/SEC/SEC/SEC | 1. E+ |
| 18 | SPEC. HEAT CAP. | JOULES/KG-K | 1. E+ |
| 19 | THERMAL CONDUCT. | WATTS/M-K | 1. E+ |
| 20 | DIFFUSIVITY | M.SQ/SEC. | 1.0 E+ |
| 21 | ACTIVATION ENRGY | JOULES/KGMOL | 1. E+ |
| 22 | ANGLE | RADIANS | 1. 0 E+ |
| 23 | HEAT FLUX | WATTS/M.SQ. | 1. E+ |
| 24 | PARTICLE DIAM. | METERS | 1. E+ |
| 25 | MOMENTUM TR RATE | KG.M/SEC SEC | 1. E+ |
| 26 | HEAT TRANSF COEF | WATTS/M.SQ-K | 1. E+ |
| 27 | PERMEABILITY | M.SQ. | 1. E+ |
| 28 | (INTERNAL MISC.) | UNDEFINED | 1. E+ |
| 29 | VOLUME. FLOWRATE | CU.M/SEC. | 1.0 E+ |
| 3 | AREA | M.SQ. | 1. E+ 0 |
| 31 | ARRHENIUS FACTOR | CONSISTENT UNITS | 1. E+ |
| 32 | INERTIAL FACTOR | PER METER | 1.0 OE+ |
| 33 | VOL. HEAT RATE | WATTS/CU.M. | 1. E+ |
| 34 | ABSORB./SCATER. | PER METER | 1.0 E+00 |
| 35 | ANGULAR VELOCITY | RADIANS/SECOND | 1. E+00 |
| 36 | MOL. SIZE PARAM. | ANGSTROMS | 1. E+ 0 |
| 37 | PRESSURE GRAD. | PASCALS/METER | 1. E+ 0 |

① - GEOMETRY -

BOUNDARY FITTED COORDINATES

NI = 82 NJ 14 NK 3

CELL TYPES: K 1 and 32

| | | | | | | | | | | | | | | | | | | | | | | | | | | | | | | |
|----|----|----|----|----|----|----|----|----|----|----|----|----|----|----|----|----|----|----|----|----|----|----|----|----|----|----|----|----|----|----|
| J | I | 2 | 4 | 6 | 8 | 10 | 12 | 14 | 16 | 18 | 20 | 2 | 24 | 6 | 28 | 30 | 32 | 34 | 36 | 38 | 40 | 42 | 44 | 46 | 48 | 50 | 52 | 54 | 56 | |
| 14 | W1 | W1 | W1 | W1 | W1 | W1 | W1 | W1 | W1 | W1 | W1 | W1 | W1 | W1 | W1 | W1 | W1 | W1 | W1 | W1 | W1 | W1 | W1 | W1 | W1 | W1 | W1 | W1 | W1 | 14 |
| 13 | W1 | W1 | W1 | W1 | W1 | W1 | W1 | W1 | W1 | W1 | W1 | W1 | W1 | W1 | W1 | W1 | W1 | W1 | W1 | W1 | W1 | W1 | W1 | W1 | W1 | W1 | W1 | W1 | W1 | 13 |
| 12 | W1 | W1 | W1 | W1 | W1 | W1 | W1 | W1 | W1 | W1 | W1 | W1 | W1 | W1 | W1 | W1 | W1 | W1 | W1 | W1 | W1 | W1 | W1 | W1 | W1 | W1 | W1 | W1 | W1 | 12 |
| 11 | W1 | W1 | W1 | W1 | W1 | W1 | W1 | W1 | W1 | W1 | W1 | W1 | W1 | W1 | W1 | W1 | W1 | W1 | W1 | W1 | W1 | W1 | W1 | W1 | W1 | W1 | W1 | W1 | W1 | 11 |
| 10 | W1 | W1 | W1 | W1 | W1 | W1 | W1 | W1 | W1 | W1 | W1 | W1 | W1 | W1 | W1 | W1 | W1 | W1 | W1 | W1 | W1 | W1 | W1 | W1 | W1 | W1 | W1 | W1 | W1 | 10 |
| 9 | W1 | W1 | W1 | W1 | W1 | W1 | W1 | W1 | W1 | W1 | W1 | W1 | W1 | W1 | W1 | W1 | W1 | W1 | W1 | W1 | W1 | W1 | W1 | W1 | W1 | W1 | W1 | W1 | W1 | 9 |
| 8 | W1 | W1 | W1 | W1 | W1 | W1 | W1 | W1 | W1 | W1 | W1 | W1 | W1 | W1 | W1 | W1 | W1 | W1 | W1 | W1 | W1 | W1 | W1 | W1 | W1 | W1 | W1 | W1 | W1 | 8 |
| 7 | W1 | W1 | W1 | W1 | W1 | W1 | W1 | W1 | W1 | W1 | W1 | W1 | W1 | W1 | W1 | W1 | W1 | W1 | W1 | W1 | W1 | W1 | W1 | W1 | W1 | W1 | W1 | W1 | W1 | 7 |
| 6 | W1 | W1 | W1 | W1 | W1 | W1 | W1 | W1 | W1 | W1 | W1 | W1 | W1 | W1 | W1 | W1 | W1 | W1 | W1 | W1 | W1 | W1 | W1 | W1 | W1 | W1 | W1 | W1 | W1 | 6 |
| 5 | W1 | W1 | W1 | W1 | W1 | W1 | W1 | W1 | W1 | W1 | W1 | W1 | W1 | W1 | W1 | W1 | W1 | W1 | W1 | W1 | W1 | W1 | W1 | W1 | W1 | W1 | W1 | W1 | W1 | 5 |
| 4 | W1 | W1 | W1 | W1 | W1 | W1 | W1 | W1 | W1 | W1 | W1 | W1 | W1 | W1 | W1 | W1 | W1 | W1 | W1 | W1 | W1 | W1 | W1 | W1 | W1 | W1 | W1 | W1 | W1 | 4 |

[illegible][illegible]

| CELL TYPES: | | | K | 2 and 31 | | | | | | | | | | | | | | | | | | | | | | | | | | |
|-------------|----|----|----|----------|----|----|----|----|----|----|----|----|----|----|----|----|----|----|----|----|----|----|----|----|----|----|----|----|----|----|
| J | I= | 2 | 4 | 6 | 8 | 10 | 12 | 14 | 16 | 18 | 20 | 2 | 24 | 26 | 2 | 30 | 32 | 34 | 36 | 38 | 4 | 42 | 44 | 46 | 48 | 50 | 52 | 54 | 56 | |
| 14 | W1 | W1 | W1 | W1 | W1 | W1 | W1 | W1 | W1 | W1 | W1 | W1 | W1 | W1 | W1 | W1 | W1 | W1 | W1 | W1 | W1 | W1 | W1 | W1 | W1 | W1 | W1 | W1 | W1 | W1 |
| 13 | W1 | W1 | W1 | W1 | W1 | W1 | W1 | W1 | W1 | W1 | W1 | W1 | W1 | W1 | W1 | W1 | W1 | W1 | W1 | W1 | W1 | W1 | W1 | W1 | W1 | W1 | W1 | W1 | W1 | W1 |
| 12 | W1 | W1 | W1 | W1 | W1 | W1 | W1 | W1 | W1 | W1 | W1 | W1 | W1 | W1 | W1 | W1 | W1 | W1 | W1 | W1 | W1 | W1 | W1 | W1 | W1 | W1 | W1 | W1 | W1 | W1 |
| 11 | W1 | W1 | W1 | W1 | W1 | W1 | W1 | W1 | W1 | W1 | W1 | W1 | W1 | W1 | W1 | W1 | W1 | W1 | W1 | W1 | W1 | W1 | W1 | W1 | W1 | W1 | W1 | W1 | W1 | W1 |
| 10 | W1 | W1 | W1 | W1 | W1 | W1 | W1 | W1 | W1 | W1 | W1 | W1 | W1 | W1 | W1 | W1 | W1 | W1 | W1 | W1 | W1 | W1 | W1 | W1 | W1 | W1 | W1 | W1 | W1 | W1 |
| 9 | W1 | W1 | W1 | W1 | W1 | W1 | W1 | W1 | W1 | W1 | W1 | W1 | W1 | W1 | W1 | W1 | W1 | W1 | W1 | W1 | W1 | W1 | W1 | W1 | W1 | W1 | W1 | W1 | W1 | W1 |
| 8 | W1 | W1 | W1 | W1 | W1 | W1 | W1 | W1 | W1 | W1 | W1 | W1 | W1 | W1 | W1 | W1 | W1 | W1 | W1 | W1 | W1 | W1 | W1 | W1 | W1 | W1 | W1 | W1 | W1 | W1 |
| 7 | W1 | W1 | W1 | W1 | W1 | W1 | W1 | W1 | W1 | W1 | W1 | W1 | W1 | W1 | W1 | W1 | W1 | W1 | W1 | W1 | W1 | W1 | W1 | W1 | W1 | W1 | W1 | W1 | W1 | W1 |
| 6 | W1 | W1 | W1 | W1 | W1 | W1 | W1 | W1 | W1 | W1 | W1 | W1 | W1 | W1 | W1 | W1 | W1 | W1 | W1 | W1 | W1 | W1 | W1 | W1 | W1 | W1 | W1 | W1 | W1 | W1 |
| 5 | W1 | W1 | W1 | W1 | W1 | W1 | W1 | W1 | W1 | W1 | W1 | W1 | W1 | W1 | W1 | W1 | W1 | W1 | W1 | W1 | W1 | W1 | W1 | W1 | W1 | W1 | W1 | W1 | W1 | W1 |
| 4 | W1 | W1 | W1 | W1 | W1 | W1 | W1 | W1 | W1 | W1 | W1 | W1 | W1 | W1 | W1 | W1 | W1 | W1 | W1 | W1 | W1 | W1 | W1 | W1 | W1 | W1 | W1 | W1 | W1 | W1 |
| 3 | W1 | W1 | W1 | W1 | W1 | W1 | W1 | W1 | W1 | W1 | W1 | W1 | W1 | W1 | W1 | W1 | W1 | W1 | W1 | W1 | W1 | W1 | W1 | W1 | W1 | W1 | W1 | W1 | W1 | W1 |
| 2 | W1 | W1 | W1 | W1 | W1 | W1 | W1 | W1 | W1 | W1 | W1 | W1 | W1 | W1 | W1 | W1 | W1 | W1 | W1 | W1 | W1 | W1 | W1 | W1 | W1 | W1 | W1 | W1 | W1 | W1 |
| 1 | W1 | W1 | W1 | W1 | W1 | W1 | W1 | W1 | W1 | W1 | W1 | W1 | W1 | W1 | W1 | W1 | W1 | W1 | W1 | W1 | W1 | W1 | W1 | W1 | W1 | W1 | W1 | W1 | W1 | W1 |
| J | I | 2 | 4 | 6 | 8 | 1 | 12 | 14 | 16 | 18 | 20 | 22 | 24 | 26 | 28 | 3 | 32 | 34 | 36 | 38 | 40 | 42 | 44 | 46 | 48 | 50 | 52 | 54 | 56 | |

[illegible]

[illegible]

| CELL TYPES: | | K | | | | | | | | | | 3 to 12 and 21 to 30 | | | | | | | | | | | | | | | | | |
|-------------|------|------|------|------|------|------|------|------|------|------|------|----------------------|------|------|------|------|------|------|------|------|------|------|------|------|------|------|------|------|------|
| J | I | 2 | 4 | 6 | 8 | 10 | 12 | 14 | 16 | 18 | 20 | 22 | 24 | 26 | 28 | 3 | 32 | 34 | 36 | 38 | 4 | 42 | 44 | 46 | 48 | 50 | 52 | 54 | 56 |
| 14 | W1W1 | W1W1 | W1W1 | W1W1 | W1W1 | W1W1 | W1W1 | W1W1 | W1W1 | W1W1 | W1W1 | W1W1 | W1W1 | W1W1 | W1W1 | W1W1 | W1W1 | W1W1 | W1W1 | W1W1 | W1W1 | W1W1 | W1W1 | W1W1 | W1W1 | W1W1 | W1W1 | W1W1 | W1W1 |
| 13 | W1W1 | W1W1 | W1W1 | W1W1 | W1W1 | W1W1 | W1W1 | W1W1 | W1W1 | W1W1 | W1W1 | W1W1 | W1W1 | W1W1 | W1W1 | W1W1 | W1W1 | W1W1 | W1W1 | W1W1 | W1W1 | W1W1 | W1W1 | W1W1 | W1W1 | W1W1 | W1W1 | W1W1 | W1W1 |
| 12 | W1W1 | D | D | D | D | D | D | D | D | D | D | D | D | D | D | D | D | D | D | D | D | D | D | D | D | D | D | D | D |
| 11 | W1W1 | D | D | D | D | D | D | D | D | D | D | D | D | D | D | D | D | D | D | D | D | D | D | D | D | D | D | D | D |
| 10 | W1W1 | D | D | D | D | D | D | D | D | D | D | D | D | D | D | D | D | D | D | D | D | D | D | D | D | D | D | D | D |
| 9 | W1W1 | D | D | D | D | D | D | D | D | D | D | D | D | D | D | D | D | D | D | D | D | D | D | D | D | D | D | D | D |
| 8 | W1W1 | D | D | D | D | D | D | D | D | D | D | D | D | D | D | D | D | D | D | D | D | D | D | D | D | D | D | D | D |
| 7 | W1W1 | D | D | D | D | D | D | D | D | D | D | D | D | D | D | D | D | D | D | D | D | D | D | D | D | D | D | D | D |
| 6 | W1W1 | D | D | D | D | D | D | D | D | D | D | D | D | D | D | D | D | D | D | D | D | D | D | D | D | D | D | D | D |
| 5 | W1W1 | D | D | D | D | D | D | D | D | D | D | D | D | D | D | D | D | D | D | D | D | D | D | D | D | D | D | D | D |
| 4 | W1W1 | D | D | D | D | D | D | D | D | D | D | D | D | D | D | D | D | D | D | D | D | D | D | D | D | D | D | D | D |
| 3 | W1W1 | D | D | D | D | D | D | D | D | D | D | D | D | D | D | D | D | D | D | D | D | D | D | D | D | D | D | D | D |
| 2 | W1W1 | W1W1 | W1W1 | W1W1 | W1W1 | W1W1 | W1W1 | W1W1 | W1W1 | W1W1 | W1W1 | W1W1 | W1W1 | W1W1 | W1W1 | W1W1 | W1W1 | W1W1 | W1W1 | W1W1 | W1W1 | W1W1 | W1W1 | W1W1 | W1W1 | W1W1 | W1W1 | W1W1 | W1W1 |
| 1 | W1W1 | W1W1 | W1W1 | W1W1 | W1W1 | W1W1 | W1W1 | W1W1 | W1W1 | W1W1 | W1W1 | W1W1 | W1W1 | W1W1 | W1W1 | W1W1 | W1W1 | W1W1 | W1W1 | W1W1 | W1W1 | W1W1 | W1W1 | W1W1 | W1W1 | W1W1 | W1W1 | W1W1 | W1W1 |
| J | I | 2 | 4 | 6 | 8 | 10 | 12 | 14 | 16 | 18 | 20 | 22 | 24 | 26 | 28 | 3 | 32 | 34 | 36 | 38 | 40 | 44 | 46 | 48 | 50 | 52 | 54 | 56 | |

| CELL TYPES: K | | | | | | | | | | | | | | | | |
|--|------|------|------|------|------|------|------|------|------|------|------|------|------|------|------|----|
| J I= 59 61 63 65 67 69 71 73 75 77 79 81 | | | | | | | | | | | | | | | | |
| 14 | W2W2 | W2W1 | W1W1 | W1W1 | W1W1 | W1W1 | W1W1 | W1W1 | W1W1 | W1W1 | W1W1 | W1W1 | W1W1 | W1W1 | W1W1 | 14 |
| 13 | . | . | . | W1 | W1 | W1 | W1 | W1 | W1 | W1 | W1 | W1 | W1 | W1 | W1 | 13 |
| 12 | . | . | . | W1 | W1 | W1 | W1 | W1 | W1 | W1 | W1 | W1 | W1 | W1 | W1 | 12 |
| 11 | . | . | . | W1 | W1 | W1 | W1 | W1 | W1 | W1 | W1 | W1 | W1 | W1 | W1 | 11 |
| 10 | . | . | . | W1 | W1 | W1 | W1 | W1 | W1 | W1 | W1 | W1 | W1 | W1 | W1 | 1 |
| 9 | . | . | . | W1 | W1 | W1 | W1 | W1 | W1 | W1 | W1 | W1 | W1 | W1 | W1 | 9 |
| 8 | . | . | . | W1 | W1 | W1 | W1 | W1 | W1 | W1 | W1 | W1 | W1 | W1 | W1 | 8 |
| 7 | . | . | . | W1 | W1 | W1 | W1 | W1 | W1 | W1 | W1 | W1 | W1 | W1 | W1 | 7 |
| 6 | . | . | . | W1 | W1 | W1 | W1 | W1 | W1 | W1 | W1 | W1 | W1 | W1 | W1 | 6 |
| 5 | . | . | . | W1 | W1 | W1 | W1 | W1 | W1 | W1 | W1 | W1 | W1 | W1 | W1 | 5 |
| 4 | . | . | . | W1 | W1 | W1 | W1 | W1 | W1 | W1 | W1 | W1 | W1 | W1 | W1 | 4 |
| 3 | . | . | . | W1 | W1 | W1 | W1 | W1 | W1 | W1 | W1 | W1 | W1 | W1 | W1 | 3 |
| 2 | . | . | . | W1 | W1 | W1 | W1 | W1 | W1 | W1 | W1 | W1 | W1 | W1 | W1 | 2 |
| 1 | W1 | W1 | W1 | W1 | W1 | W1 | W1 | W1 | W1 | W1 | W1 | W1 | W1 | W1 | W1 | 1 |
| J I= 59 61 63 65 67 69 71 73 75 77 79 81 | | | | | | | | | | | | | | | | |

CELL TYPES: K - 13 and 20

[illegible]

CELL TYPES: K = 13 and 20

[illegible]

CELL TYPES: K = 14 to 19

[illegible]


```

③ - TURBULENCE BOUNDARY CONDITIONS -
    - TWO EQUATION MODEL -
      ZONE          TURB.-INTEN.  CHAR.-LENGTH
      -----
      W1            SET           SET
      W2            SET           SET
      I1            5.000E+00     1.000E-01

      X = 0.000E+00
      Y =-9.810E+00
      Z = 0.000E+00

    - TURBULENCE MODEL CONSTANTS -
      C1 = 1.4E+00
      C2 = 1.9E+00
      CMU = 9.0E-02

    - WALL FUNCTION TURBULENCE MODEL CONSTANTS -
      WALL ZONE  CAPPA  ELOG
      W1         4.187E-01  9.793E+00
      W2         4.187E-01  9.793E+00

    - USER DEFINED PHYSICAL MODELS -
      NON-NEWTONIAN FLUID - NO
    - USER DEFINED PROPERTIES -
      FLUID VISCOSITY      - NO
      FLUID DENSITY        - NO
      TURBULENT VISCOSITY  - NO
    - USER DEFINED SOURCE TERMS -
      X-MOMENTUM EQUATION  - NO
      Y-MOMENTUM EQUATION  - NO
      Z-MOMENTUM EQUATION  - NO
      PRESSURE CORRECTION EQUATION - NO
      TURBULENT K.E. EQUATION - NO
  
```

```

④ - GRAVITATIONAL ACCELERATIONS -
  
```

```

TURB. K.E. DISSIPATION EQUATION - NO
- USER STARTUP SUBROUTINE IS NOT ACTIVE -
- USER DEFINED ADJUSTMENTS -
  X-MOMENTUM EQUATION - NO
  X-MOMENTUM EQUATION - NO
  X-MOMENTUM EQUATION - NO
- USER DEFINED REAL VARIABLES -
  USER DEFINED REAL VARIABLE, USPAR1 - 0. E+00
  USER DEFINED REAL VARIABLE, USPAR2 - 0. E+0
  USER DEFINED REAL VARIABLE, USPAR3 - 0. E+
  USER DEFINED REAL VARIABLE, USPAR4 - 0. E+
  USER DEFINED REAL VARIABLE, USPAR5 - 0.0 E+
  USER DEFINED REAL VARIABLE, USPAR6 - 0.0 E+0
  USER DEFINED REAL VARIABLE, USPAR7 - 0. E+
  USER DEFINED REAL VARIABLE, USPAR8 - 0. E+0
  USER DEFINED REAL VARIABLE, USPAR9 - 0. E+
- USER DEFINED INTEGER VARIABLES -
  USER DEFINED INTEGER VARIABLE, IUFLG1 - 0
  USER DEFINED INTEGER VARIABLE, IUFLG2 - 0
  USER DEFINED INTEGER VARIABLE, IUFLG3 - 0
  USER DEFINED INTEGER VARIABLE, IUFLG4 - 0
  USER DEFINED INTEGER VARIABLE, IUFLG5 - 0
  USER DEFINED INTEGER VARIABLE, IUFLG6 - 0
  USER DEFINED INTEGER VARIABLE, IUFLG7 - 0
  USER DEFINED INTEGER VARIABLE, IUFLG8 - 0
  USER DEFINED INTEGER VARIABLE, IUFLG9 - 0
- DENSITY DEFINITION -
  DENSITY = 1.000E+03
- VISCOSITY DEFINITION -
  VISCOSITY 9.000E-04
- SECOND PHASE SOLUTION CONTROL PARAMETERS -
  MAXIMUM NUMBER OF STEPS - 99999
  STEP LENGTH FACTOR - 2.0 E+01
  COEFFICIENT OF RESTITUTION FUNCTION OF ANGLE - NO

```

⑤

⑥

```

COEFFICIENT OF RESTITUTION          - 1.000E+00
NUMBER OF WALL REFLECTIONS ALLOWED PER CELL - 25
SELECT RUNGA-KUTTA METHOD            - NO
SELECT DETAILED TRACKING REPORT      - NO
SELECT STEP-BY-STEP TRACKING REPORT  - NO
ALLOW INJECTIONS TO HAVE DIFFERENT PROPERTIES - NO
SECOND PHASE SAMPLING PROBE ENABLED  - NO
THERMOPHORESIS FORCE ENABLED         - NO

NO SECOND PHASE COUPLING

```

⑦ - PARTICLE/DROPLET BOUNDARY CONDITIONS -

```

ZONE      BOUNDARY CONDITION
-----
W1        REFLECT
W2        SALTATION
O         ESCAPE
I1        ESCAPE

```

- PARTICLE LAWS ACTIVATED FOR USER-DEFINED HISTORY -

```

INERT      - NO
VAPORIZE   - YES
BOILING    - YES
DEVOLAT    - YES
BURNOUT    - YES
INERT      - NO

```

⑧ - SECOND PHASE PARTICLE/DROPLET PROPERTIES -

```

PARTICLE DENSITY      2.5 E+03
BOILING POINT         3.73 F+ 2
LATENT HEAT OF VAPORIZATION 1.00 E+03
VAPORIZATION TEMPERATURE 3.73 E+02
FRACTION VOLATILE COMPONENT 1.000E+0

```

- SECOND PHASE INITIAL CONDITIONS -

⑨

| INJECT NO | TYPE | (X) | (Y) | (Z) | (U) | (V) | (W) | (T) | (DIAM) | (MELOW) | |
|-----------|-------------|-----------|-----------|-----------|-----------|-----|--------|-----------|-----------|-----------|-----------|
| 1 | INERT PART. | 3.020E+00 | 9.000E-02 | 3.96 E- 1 | 5.610E-01 | 0. | E+00 | 0.00 E+00 | 2.730E+02 | 4.7 E-05 | 0.00 E+ |
| 2 | INERT PART. | 3.020E+00 | 1.10 E-01 | 3.960E- 1 | 5.610E- 1 | 0. | E+ 0 | 0.00 E+0 | 2.730E+02 | 4.70 E- 5 | 0.000E+00 |
| 3 | INERT PART. | 3.020E+0 | 5.00 E-02 | 4.160E-01 | 5.610E-01 | . | 0 E+ 0 | 0.0 E+ | 2.73 E+02 | 4.7 E- 5 | 0. 00E+ |
| 4 | INERT PART. | 3.020E+00 | 7.000E-02 | 4.16 E-01 | 5.610E-01 | 0. | 00E+00 | 0.0 0E+00 | 2.73 E+02 | 4.70 E- 5 | 0.000E+00 |

| | | | | | | | | | | |
|----|-------------|-----------|-----------|-----------|-----------|-----------|-----------|-----------|-----------|-----------|
| 5 | INERT PART. | 3.020E+00 | 9.000E-02 | 4.160E-01 | 5.610E-01 | 0.000E+00 | 0.000E+00 | 2.730E+02 | 4.700E-05 | 0.000E+00 |
| 6 | INERT PART. | 3.020E+00 | 1.100E-01 | 4.160E-01 | 5.610E-01 | 0.000E+00 | 0.000E+00 | 2.730E+02 | 4.700E-05 | 0.000E+00 |
| 7 | INERT PART. | 3.020E+00 | 1.300E-01 | 4.160E-01 | 5.610E-01 | 0.000E+00 | 0.000E+00 | 2.730E+02 | 4.700E-05 | 0.000E+00 |
| 8 | INERT PART. | 3.020E+00 | 1.500E-01 | 4.160E-01 | 5.610E-01 | 0.000E+00 | 0.000E+00 | 2.730E+02 | 4.700E-05 | 0.000E+00 |
| 9 | INERT PART. | 3.020E+00 | 3.00 E-02 | 4.360E-01 | 5.61 E-01 | 0.000E+00 | 0.000E+00 | 2.73 E+02 | 4.7 E-05 | 0.00E+00 |
| 10 | INERT PART. | 3.020E+00 | 5.000E-02 | 4.360E-01 | 5.61 E-1 | 0.00 E+ | 0.00 E+ | 2.73 E+2 | 4.7 E-5 | 0.00 E+00 |
| 11 | INERT PART. | 3.020E+00 | 7.0 E-02 | 4.36 E-1 | 5.61 E-1 | 0.0 E+ | 0.0 E+ | 2.73 E+2 | 4.7 E-5 | 0.00 E+00 |
| 12 | INERT PART. | 3.02 E+0 | 9.0 E-02 | 4.36 E-1 | 5.61 E-01 | 0.0 E+ | 0.0 E+ | 2.73 E+2 | 4.7 E-5 | 0.00 E+00 |
| 13 | INERT PART. | 3.020E+0 | 1.1 E-01 | 4.36 E-1 | 5.61 E-1 | 0.0 E+ | 0.0 E+ | 2.73 E+2 | 4.7 E-5 | 0.00 E+00 |
| 14 | INERT PART. | 3.02 E+0 | 1.3 E-01 | 4.36 E-1 | 5.61 E-1 | 0.0 E+ | 0.0 E+ | 2.73 E+2 | 4.7 E-5 | 0.00 E+00 |
| 15 | INERT PART. | 3.02 E+00 | 1.5 E-01 | 4.36 E-1 | 5.61 E-1 | 0.0 E+ | 0.0 E+ | 2.73 E+2 | 4.7 E-5 | 0.00 E+00 |
| 16 | INERT PART. | 3.02 E+ | 1.7 E-1 | 4.36 E-1 | 5.61 E-1 | 0.0 E+ | 0.0 E+ | 2.73 E+2 | 4.7 E-5 | 0.00 E+00 |
| 17 | INERT PART. | 3.02 E+ | 3.0 E-2 | 4.56 E-1 | 5.61 E-1 | 0.0 E+ | 0.0 E+ | 2.73 E+2 | 4.7 E-5 | 0.00 E+00 |
| 18 | INERT PART. | 3.02 E+ | 5.0 E- | 4.56 E-1 | 5.61 E-01 | 0.0 E+ | 0.0 E+ | 2.73 E+2 | 4.7 E-5 | 0.00 E+00 |
| 19 | INERT PART. | 3.0 E+00 | 7.0 E-02 | 4.56 E-01 | 5.61 E-1 | 0.0 E+ | 0.0 E+ | 2.73 E+2 | 4.7 E-5 | 0.00 E+00 |
| 20 | INERT PART. | 3.0 E+00 | 9.0 E-2 | 4.56 E-1 | 5.61 E-1 | 0.0 E+ | 0.0 E+ | 2.73 E+2 | 4.7 E-5 | 0.00 E+00 |
| 21 | INERT PART. | 3.02 E+ | 1.10 E-1 | 4.56 E-1 | 5.61 E-1 | 0.0 E+ | 0.0 E+ | 2.73 E+2 | 4.7 E-5 | 0.00 E+00 |
| 22 | INERT PART. | 3.02 E+ | 1.3 E-01 | 4.56 E-01 | 5.61 E-1 | 0.0 E+ | 0.0 E+ | 2.73 E+2 | 4.7 E-5 | 0.00 E+00 |
| 23 | INERT PART. | 3.02 E+00 | 1.5 E-1 | 4.56 E-01 | 5.61 E-1 | 0.0 E+ | 0.0 E+ | 2.73 E+2 | 4.7 E-5 | 0.00 E+00 |
| 24 | INERT PART. | 3.020E+ | 1.7 E-1 | 4.56 E-1 | 5.61 E-1 | 0.0 E+ | 0.0 E+ | 2.73 E+2 | 4.7 E-5 | 0.00 E+00 |
| 25 | INERT PART. | 3.0 E+ | 1.0 E-2 | 4.76 E-1 | 5.61 E-1 | 0.0 E+ | 0.0 E+ | 2.73 E+2 | 4.7 E-5 | 0.00 E+00 |
| 26 | INERT PART. | 3.0 E+ | 3.0 E-2 | 4.760E-01 | 5.61 E-1 | 0.0 E+ | 0.0 E+ | 2.73 E+2 | 4.7 E-5 | 0.00 E+00 |
| 27 | INERT PART. | 3.0 E+0 | 5.0 E- | 4.76 E-1 | 5.610E-1 | 0.0 E+ | 0.0 E+ | 2.73 E+2 | 4.7 E-5 | 0.00 E+00 |
| 28 | INERT PART. | 3.02 E+00 | 7.00 E-02 | 4.760E-1 | 5.61 E-1 | 0.0 E+ | 0.0 E+ | 2.73 E+2 | 4.7 E-5 | 0.00 E+00 |
| 29 | INERT PART. | 3.020E+00 | 9.000E-02 | 4.760E-01 | 5.61 E-01 | 0.0 E+ | 0.0 E+ | 2.73 E+2 | 4.7 E-5 | 0.00 E+00 |
| 30 | INERT PART. | 3.020E+0 | 1.1 E-1 | 4.76 E-1 | 5.61 E-1 | 0.0 E+ | 0.0 E+ | 2.73 E+2 | 4.7 E-5 | 0.00 E+00 |
| 31 | INERT PART. | 3.02 E+0 | 1.3 E-01 | 4.760E-01 | 5.61 E-1 | 0.0 E+ | 0.0 E+ | 2.73 E+2 | 4.7 E-5 | 0.00 E+00 |
| 32 | INERT PART. | 3.0 E+00 | 1.500E-01 | 4.760E-01 | 5.61 E-01 | 0.0 E+ | 0.0 E+ | 2.73 E+2 | 4.7 E-5 | 0.00 E+00 |
| 33 | INERT PART. | 3.020E+00 | 1.70E-01 | 4.760E-01 | 5.61 E-01 | 0.0 E+ | 0.0 E+ | 2.730E+2 | 4.700E-05 | 0.00 E+00 |
| 34 | INERT PART. | 3.02 E+00 | 1.900E-01 | 4.76 E-01 | 5.610E-01 | 0.0 E+ | 0.0 E+ | 2.73 E+2 | 4.700E-5 | 0.00 E+00 |
| 35 | INERT PART. | 3.02 E+00 | 1.00 E-02 | 4.960E-01 | 5.610E-01 | 0.000E+00 | 0.000E+00 | 2.730E+02 | 4.7 E-05 | 0.000E+00 |
| 36 | INERT PART. | 3.020E+00 | 3.000E-02 | 4.960E-01 | 5.610E-01 | 0.0 E+ | 0.000E+0 | 2.73 E+02 | 4.70 E-05 | 0.00 E+00 |
| 37 | INERT PART. | 3.020E+00 | 5.0 E-02 | 4.960E-01 | 5.610E-01 | 0.0 E+ | 0.000E+0 | 2.73 E+02 | 4.70 E-05 | 0.00 E+00 |
| 38 | INERT PART. | 3.020E+00 | 7.0 E-0 | 4.960E-01 | 5.610E-01 | 0.00 E+ | 0.000E+0 | 2.73 E+2 | 4.700E-05 | 0.000E+00 |
| 39 | INERT PART. | 3.00E+00 | 9.00E-2 | 4.960E-01 | 5.61E-01 | 0.000E+ | 0.000E+ | 2.73 E+2 | 4.700E-5 | 0.00 E+00 |
| 40 | INERT PART. | 3.020E+00 | 1.1 E-1 | 4.960E-01 | 5.61 E-01 | 0.00E+0 | 0.000E+0 | 2.730E+2 | 4.700E-5 | 0.000E+00 |
| 41 | INERT PART. | 3.02 E+00 | 1.30 E-01 | 4.960E-01 | 5.610E-01 | 0.0 E+ | 0.0 E+ | 2.73 E+02 | 4.700E-5 | 0.000E+00 |
| 42 | INERT PART. | 3.02 E+00 | 1.50E-01 | 4.960E-01 | 5.61 E-01 | 0.0 E+ | 0.00 E+ | 2.73 E+02 | 4.700E-5 | 0.000E+00 |
| 43 | INERT PART. | 3.02 E+00 | 1.700E-01 | 4.960E-01 | 5.610E-01 | 0.00 E+ | 0.00 E+ | 2.73 E+02 | 4.700E-05 | 0.000E+00 |
| 44 | INERT PART. | 3.020E+00 | 1.90 E-01 | 4.960E-01 | 5.61 E-01 | 0.00 E+ | 0.00 E+ | 2.73 E+2 | 4.700E-05 | 0.000E+00 |
| 45 | INERT PART. | 3.02 E+00 | 3.000E-02 | 5.160E-01 | 5.610E-01 | 0.00E+0 | 0.000E+0 | 2.730E+02 | 4.700E-5 | 0.000E+00 |
| 46 | INERT PART. | 3.020E+00 | 5.00 E-02 | 5.160E-01 | 5.61 E-01 | 0.0 E+ | 0.00E+0 | 2.730E+2 | 4.700E-5 | 0.000E+00 |
| 47 | INERT PART. | 3.02 E+00 | 7.0 E- | 5.160E-1 | 5.61 E-01 | 0.00 E+ | 0.00E+0 | 2.73 E+2 | 4.700E-05 | 0.00E+00 |
| 48 | INERT PART. | 3.020E+00 | 9.0 E-02 | 5.160E-01 | 5.61 E-01 | 0.0 E+ | 0.00E+0 | 2.73 E+2 | 4.700E-5 | 0.00E+00 |
| 49 | INERT PART. | 3.020E+00 | 1.1 E-01 | 5.160E-01 | 5.61 E-01 | 0.00 E+ | 0.00E+0 | 2.73 E+2 | 4.700E-5 | 0.00E+00 |
| 50 | INERT PART. | 3.00E+00 | 1.30 E-01 | 5.160E-01 | 5.61 E-1 | 0.00 E+ | 0.000E+0 | 2.73 E+02 | 4.700E-05 | 0.00E+00 |
| 51 | INERT PART. | 3.020E+00 | 1.50 E-01 | 5.160E-01 | 5.610E-1 | 0.00 E+ | 0.0 E+ | 2.730E+02 | 4.70 E-05 | 0.00E+00 |
| 52 | INERT PART. | 3.020E+00 | 1.70 E-01 | 5.160E-01 | 5.610E-01 | 0.00 E+ | 0.0 E+ | 2.73 E+2 | 4.7 E-05 | 0.000E+00 |

- SOLUTION CONTROL PARAMETERS -

```

- I-DIRECTION
- J-DIRECTION
- YES
- SIMPLE
- NO
- YES
- 1.0 E-3
- 1. E-06
- YES
- YES
- NO
- NO
- NO
- NO
- NO
- NO
- NO
- NO
- NO
- NO

```

DIFFERENCING SCHEME - POWER LAW

REFERENCE PRESSURE LOCATION :

| | | |
|----|---|---|
| I | J | K |
| 22 | 2 | 2 |

| VARIABLE | SOLVED | BLOCK CORRECT | NO. SWEEPS | UNDERRELAX 1 | UNDERRELAX 2 |
|----------|--------|---------------|------------|--------------|--------------|
| 1 | 1 | 1 | 1 | 1 | 1 |
| 2 | 1 | 1 | 1 | 1 | 1 |
| 3 | 1 | 1 | 1 | 1 | 1 |
| 4 | 1 | 1 | 1 | 1 | 1 |
| 5 | 1 | 1 | 1 | 1 | 1 |
| 6 | 1 | 1 | 1 | 1 | 1 |
| 7 | 1 | 1 | 1 | 1 | 1 |
| 8 | 1 | 1 | 1 | 1 | 1 |
| 9 | 1 | 1 | 1 | 1 | 1 |
| 10 | 1 | 1 | 1 | 1 | 1 |
| 11 | 1 | 1 | 1 | 1 | 1 |
| 12 | 1 | 1 | 1 | 1 | 1 |
| 13 | 1 | 1 | 1 | 1 | 1 |
| 14 | 1 | 1 | 1 | 1 | 1 |
| 15 | 1 | 1 | 1 | 1 | 1 |
| 16 | 1 | 1 | 1 | 1 | 1 |
| 17 | 1 | 1 | 1 | 1 | 1 |
| 18 | 1 | 1 | 1 | 1 | 1 |
| 19 | 1 | 1 | 1 | 1 | 1 |
| 20 | 1 | 1 | 1 | 1 | 1 |
| 21 | 1 | 1 | 1 | 1 | 1 |
| 22 | 1 | 1 | 1 | 1 | 1 |
| 23 | 1 | 1 | 1 | 1 | 1 |
| 24 | 1 | 1 | 1 | 1 | 1 |
| 25 | 1 | 1 | 1 | 1 | 1 |
| 26 | 1 | 1 | 1 | 1 | 1 |
| 27 | 1 | 1 | 1 | 1 | 1 |
| 28 | 1 | 1 | 1 | 1 | 1 |
| 29 | 1 | 1 | 1 | 1 | 1 |
| 30 | 1 | 1 | 1 | 1 | 1 |
| 31 | 1 | 1 | 1 | 1 | 1 |
| 32 | 1 | 1 | 1 | 1 | 1 |
| 33 | 1 | 1 | 1 | 1 | 1 |
| 34 | 1 | 1 | 1 | 1 | 1 |
| 35 | 1 | 1 | 1 | 1 | 1 |
| 36 | 1 | 1 | 1 | 1 | 1 |
| 37 | 1 | 1 | 1 | 1 | 1 |
| 38 | 1 | 1 | 1 | 1 | 1 |
| 39 | 1 | 1 | 1 | 1 | 1 |
| 40 | 1 | 1 | 1 | 1 | 1 |
| 41 | 1 | 1 | 1 | 1 | 1 |
| 42 | 1 | 1 | 1 | 1 | 1 |
| 43 | 1 | 1 | 1 | 1 | 1 |
| 44 | 1 | 1 | 1 | 1 | 1 |
| 45 | 1 | 1 | 1 | 1 | 1 |
| 46 | 1 | 1 | 1 | 1 | 1 |
| 47 | 1 | 1 | 1 | 1 | 1 |
| 48 | 1 | 1 | 1 | 1 | 1 |
| 49 | 1 | 1 | 1 | 1 | 1 |
| 50 | 1 | 1 | 1 | 1 | 1 |
| 51 | 1 | 1 | 1 | 1 | 1 |
| 52 | 1 | 1 | 1 | 1 | 1 |
| 53 | 1 | 1 | 1 | 1 | 1 |
| 54 | 1 | 1 | 1 | 1 | 1 |
| 55 | 1 | 1 | 1 | 1 | 1 |
| 56 | 1 | 1 | 1 | 1 | 1 |
| 57 | 1 | 1 | 1 | 1 | 1 |
| 58 | 1 | 1 | 1 | 1 | 1 |
| 59 | 1 | 1 | 1 | 1 | 1 |
| 60 | 1 | 1 | 1 | 1 | 1 |
| 61 | 1 | 1 | 1 | 1 | 1 |
| 62 | 1 | 1 | 1 | 1 | 1 |
| 63 | 1 | 1 | 1 | 1 | 1 |
| 64 | 1 | 1 | 1 | 1 | 1 |
| 65 | 1 | 1 | 1 | 1 | 1 |
| 66 | 1 | 1 | 1 | 1 | 1 |
| 67 | 1 | 1 | 1 | 1 | 1 |
| 68 | 1 | 1 | 1 | 1 | 1 |
| 69 | 1 | 1 | 1 | 1 | 1 |
| 70 | 1 | 1 | 1 | 1 | 1 |
| 71 | 1 | 1 | 1 | 1 | 1 |
| 72 | 1 | 1 | 1 | 1 | 1 |
| 73 | 1 | 1 | 1 | 1 | 1 |
| 74 | 1 | 1 | 1 | 1 | 1 |
| 75 | 1 | 1 | 1 | 1 | 1 |
| 76 | 1 | 1 | 1 | 1 | 1 |
| 77 | 1 | 1 | 1 | 1 | 1 |
| 78 | 1 | 1 | 1 | 1 | 1 |
| 79 | 1 | 1 | 1 | 1 | 1 |
| 80 | 1 | 1 | 1 | 1 | 1 |
| 81 | 1 | 1 | 1 | | |

| | | | | | |
|------------|-----|-----|-----|------------|------------|
| PRESSURE | YES | NO | 5 | 5.0000E-01 | 5.0000E-01 |
| U-VELOCITY | YES | NO | 1 | 4.0000E-01 | 2.000 E-01 |
| V-VELOCITY | YES | NO | 10 | 4.0000E-01 | 2.0000E-01 |
| W-VELOCITY | YES | NO | 10 | 4.0000E-01 | 2.0000E-01 |
| TURB. K.E. | YES | NO | 5 | 2.0000E-01 | 2.0000E-01 |
| K.E. DISS. | YES | NO | 5 | 2.0000E-01 | 2.0000E-01 |
| PROPERTIES | YES | N/A | N/A | N/A | N/A |
| VISCOSITY | N/A | N/A | N/A | 2.0000E-01 | 2.0000E-01 |

APPENDIX B -
Validation of the Fluent Flow Field Simulations

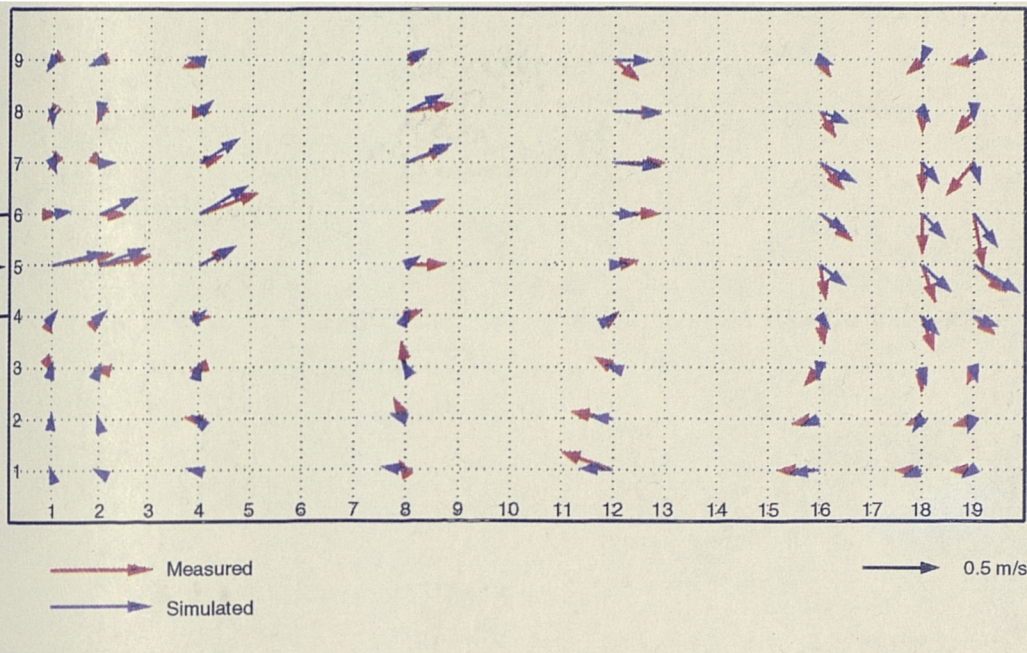
This appendix contains graphical comparisons between measured and simulated flow data for two flow situations. Full details of the flow measurements and the numerical simulation were presented in chapter 6.

For each simulation the data are broken down into two-dimensional slices. In the case of SIM1, for example, there are five horizontal slices and two vertical slices. The first slice presented is for SIM1, and is a horizontal slice located 0.01 m above the chamber bed.

Two plots are presented for each slice:

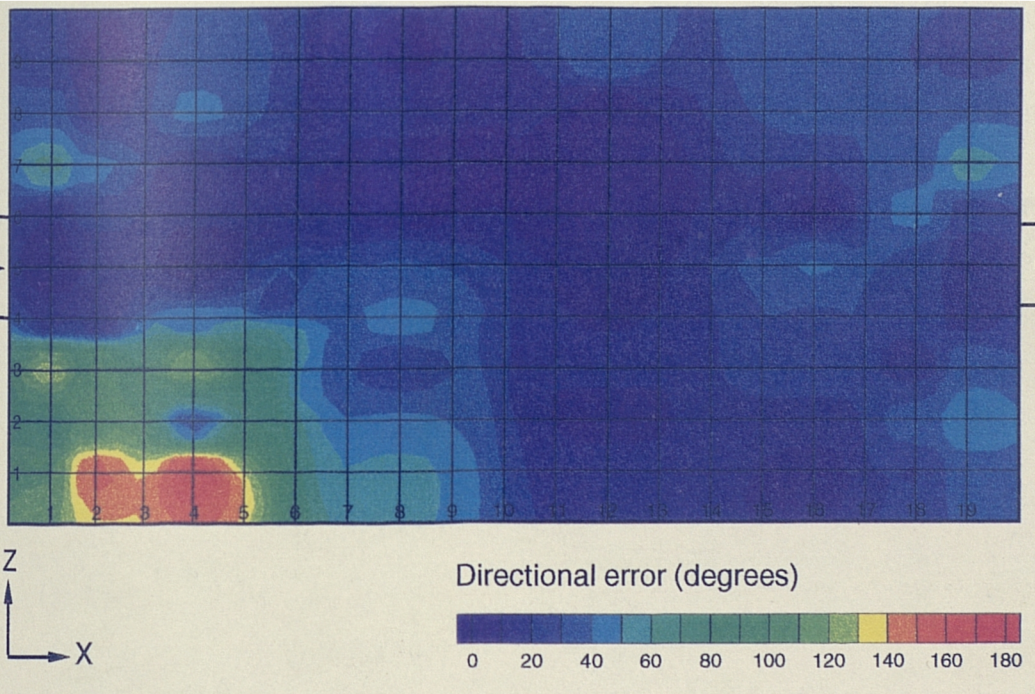
1. a vector plot, with the simulated vectors shown in blue and the measured data shown in red;
2. a contour plot of the directional errors. This plot shows errors in the range 0 (coloured blue) to 180° (coloured red), it is possible to determine whether the errors were clockwise or anticlockwise by reference to the velocity vectors above.

Simulation 1 $Y = 0.01\text{ m}$



(a) Comparison of velocity vectors

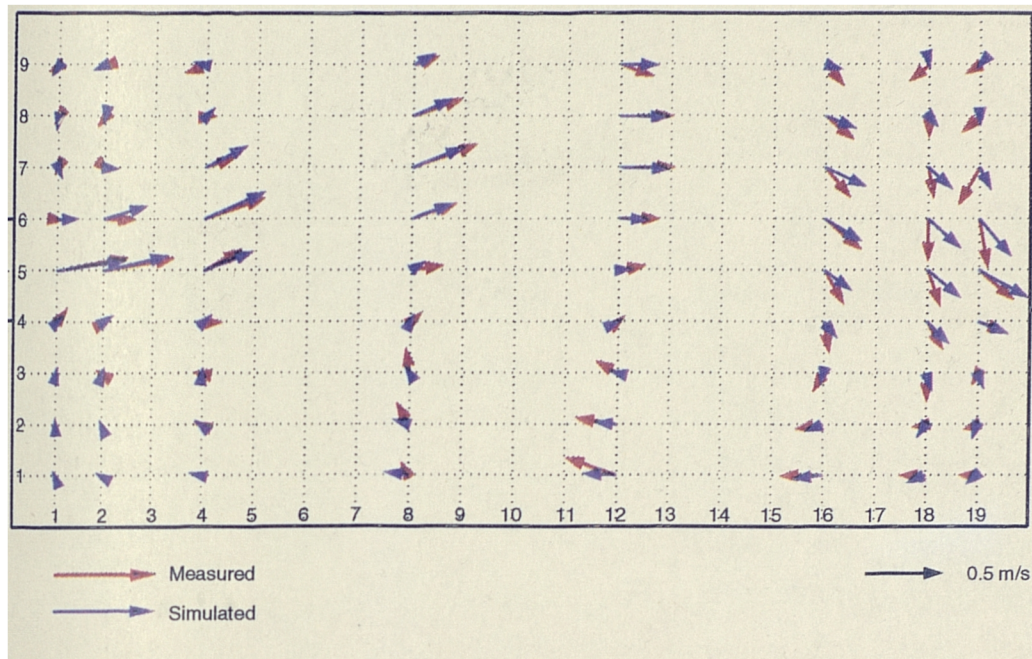
Simulation 1 $Y = 0.01\text{ m}$



(b) Directional errors

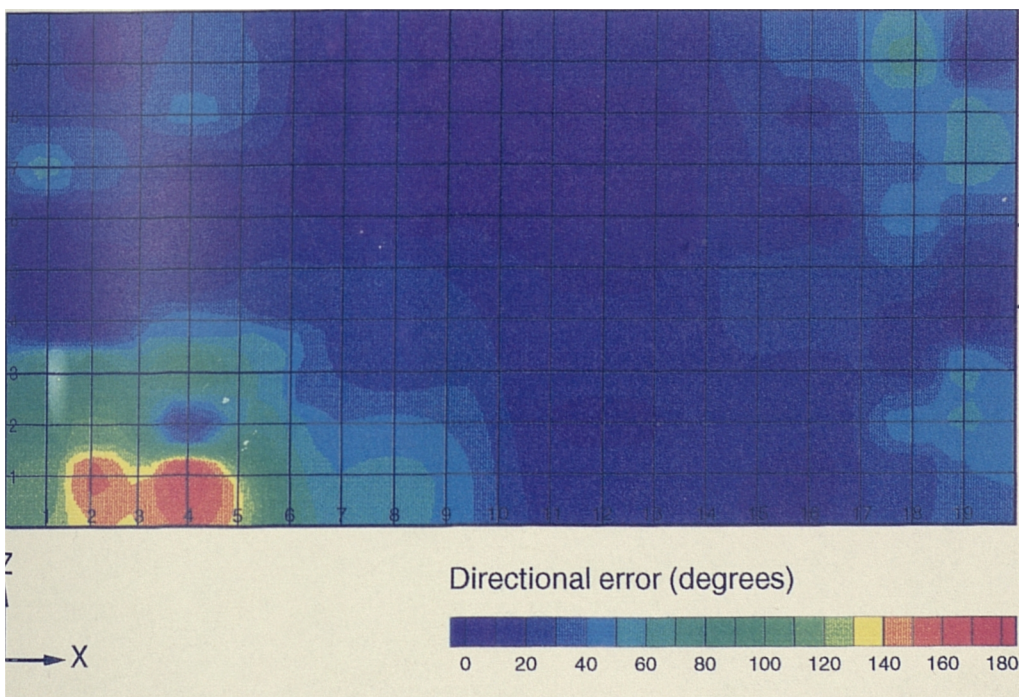
Simulation 1, Horizontal slice through the flow at a depth of 0.01 m above the chamber bed

Simulation 1 $Y = 0.02$ m



(a) Comparison of velocity vectors

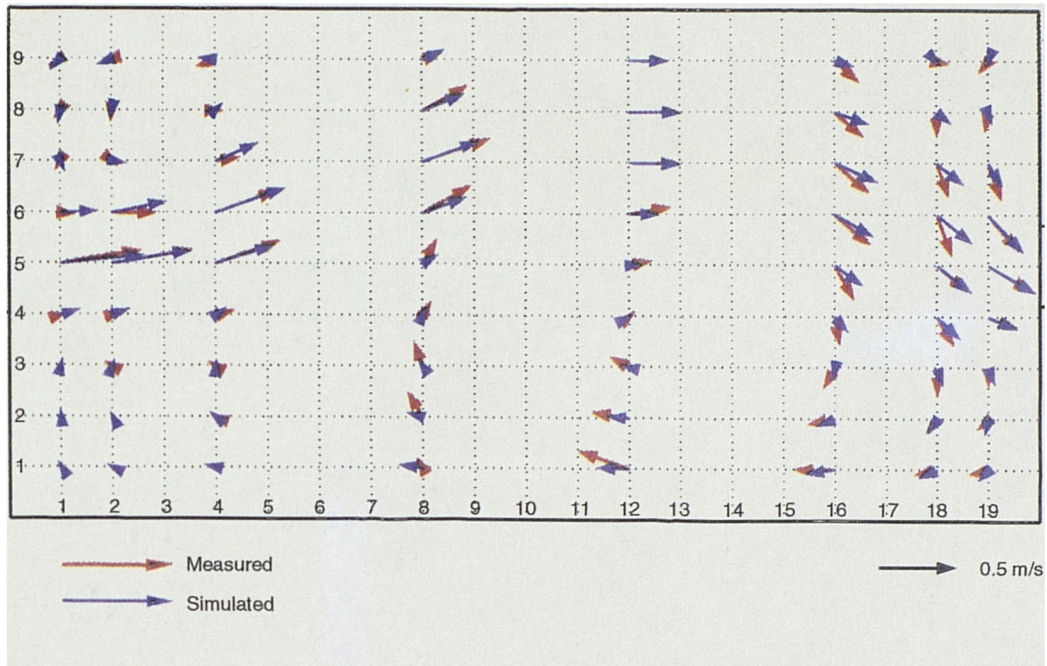
Simulation 1 $Y = 0.02$ m



(b) Directional errors

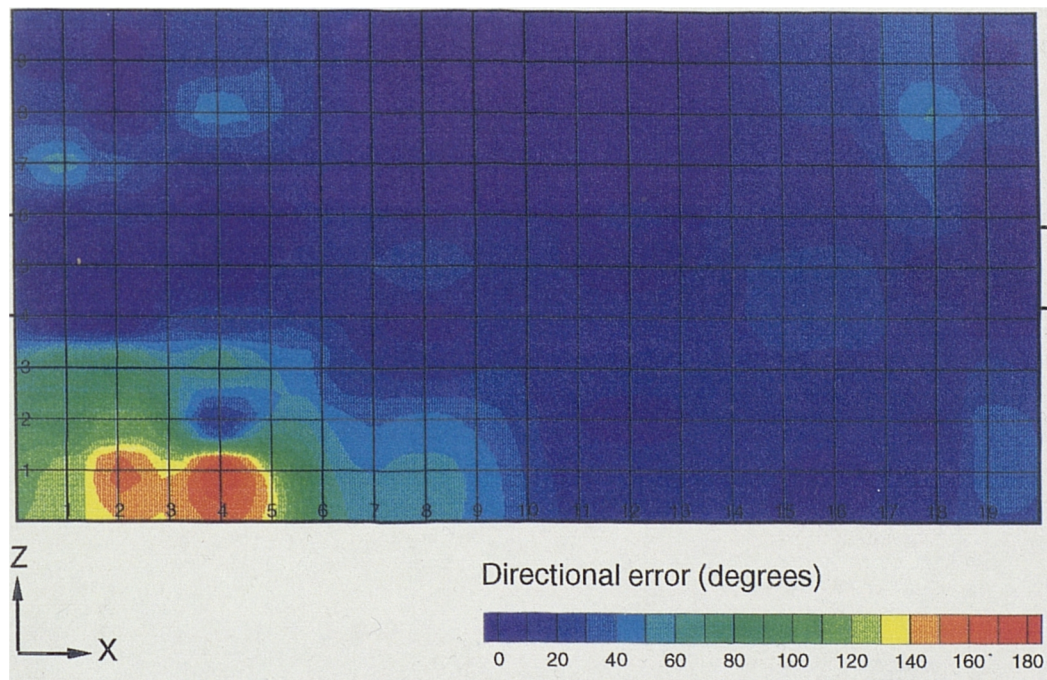
Simulation 1, Horizontal slice through the flow at a depth of 0.02 m above the chamber bed

Simulation 1 $Y = 0.04$ m



(a) Comparison of velocity vectors

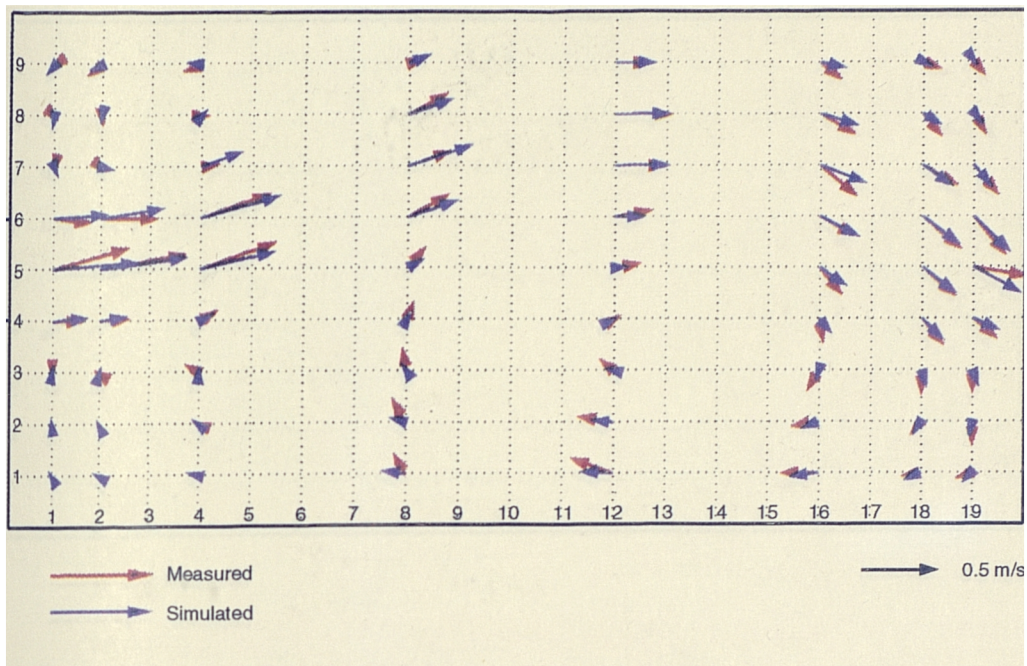
Simulation 1 $Y = 0.04$ m



(b) Directional errors

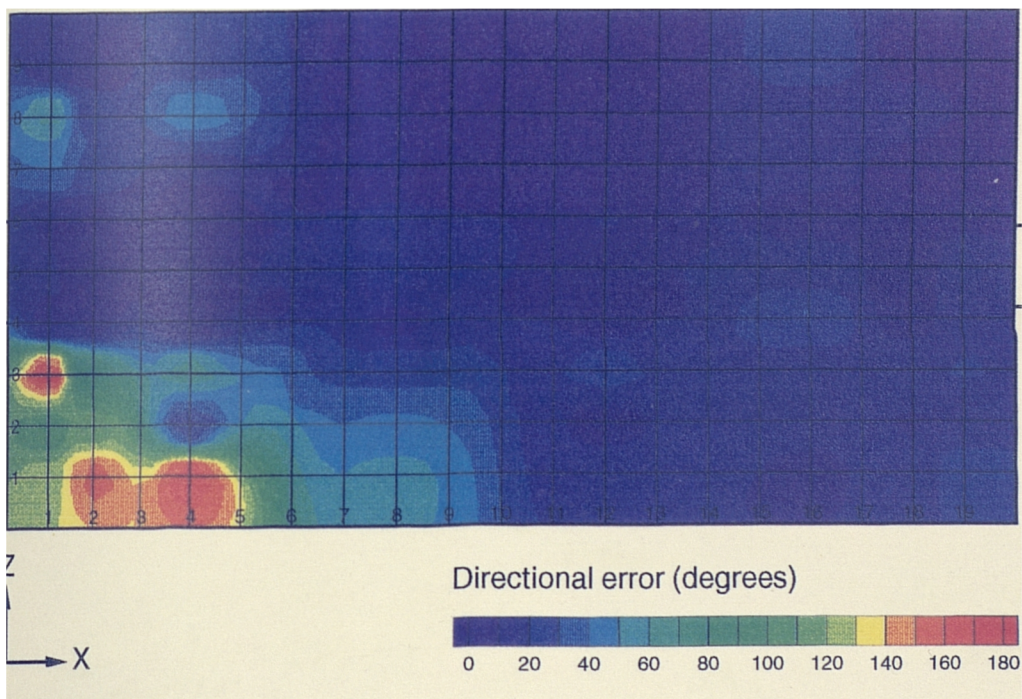
Simulation 1, Horizontal slice through the flow at a depth of 0.04 m above the chamber bed

Simulation 1 $Y = 0.08$ m



(a) Comparison of velocity vectors

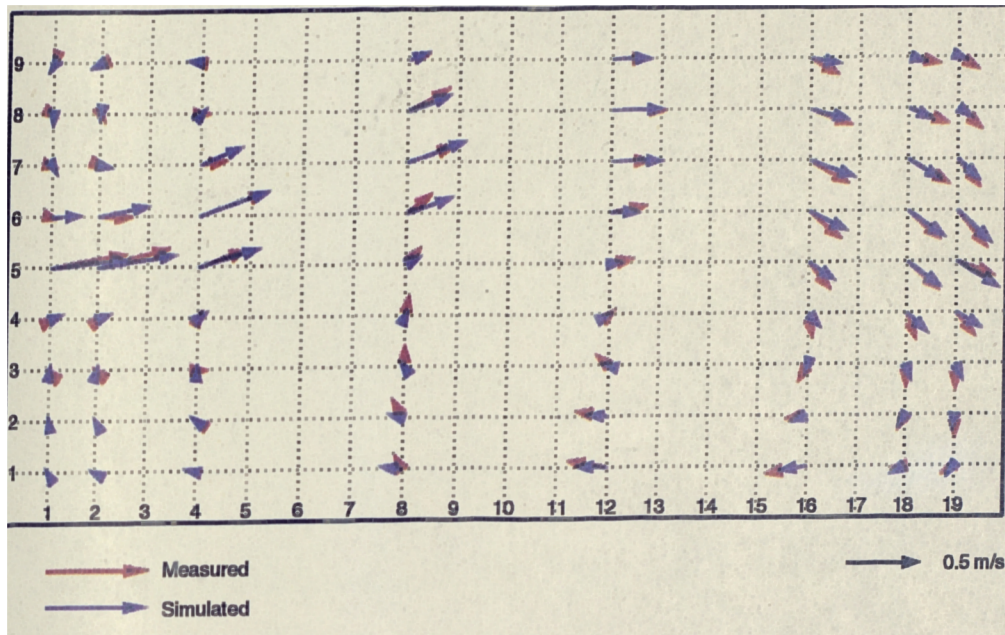
Simulation 1 $Y = 0.08$ m



(b) Directional errors

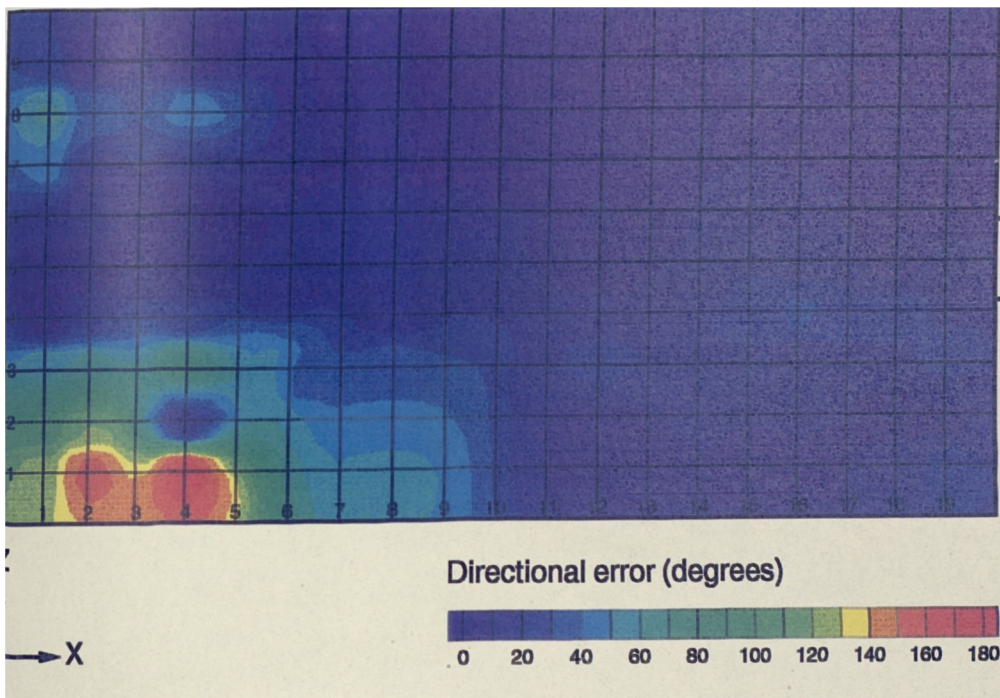
Simulation 1, Horizontal slice through the flow at a depth of 0.08 m above the chamber bed

Simulation 1 $Y = 0.16$ m



(a) Comparison of velocity vectors

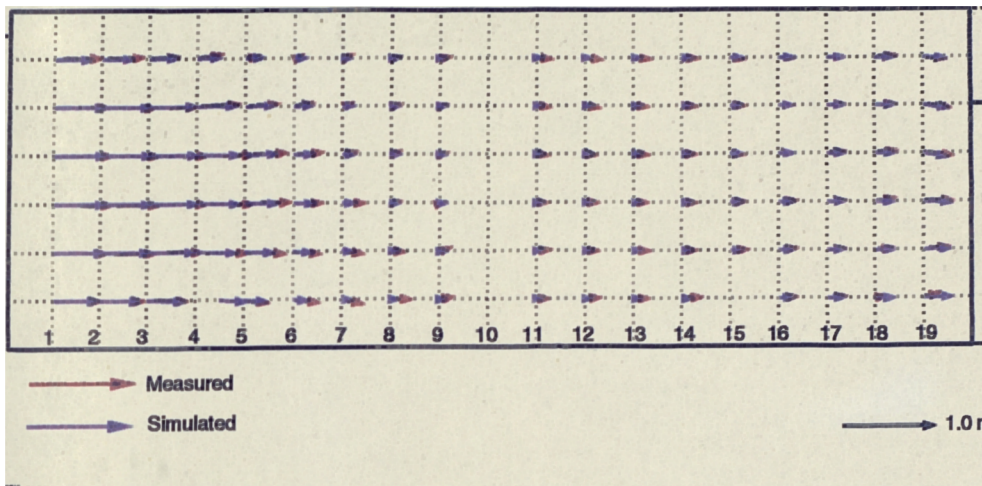
Simulation 1 $Y = 0.16$ m



(b) Directional errors

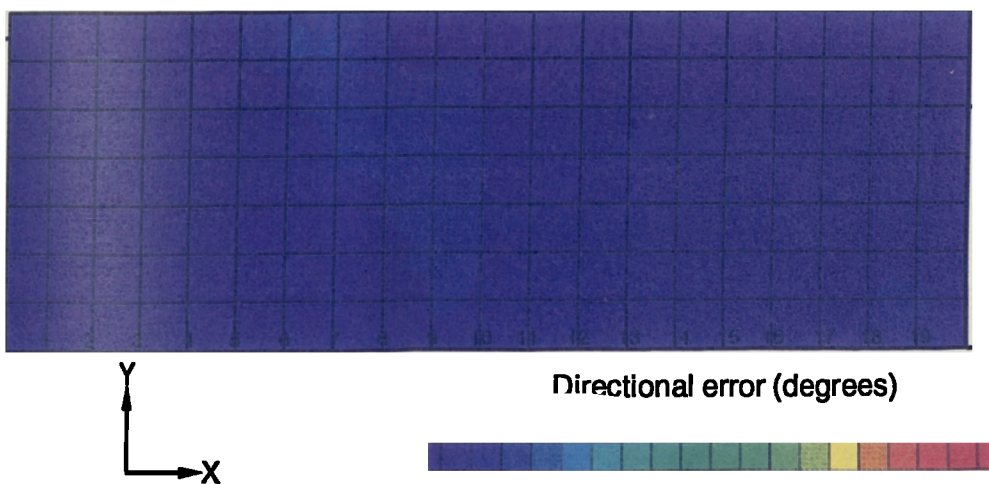
Simulation 1, Horizontal slice through the flow at a depth of 0.16 m above the chamber bed

Simulation 1 $Z = 0.486$ m



(a) Comparison of velocity vectors

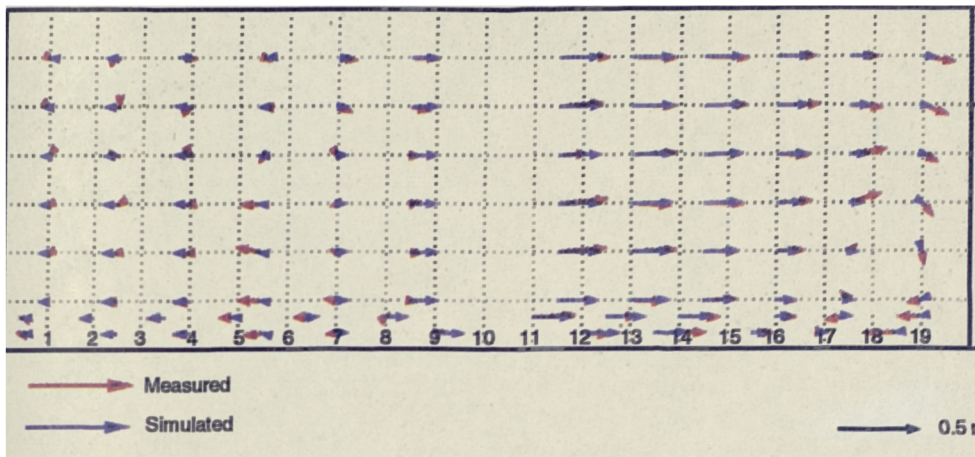
Simulation 1 $Z = 0.486$ m



(b) Directional errors

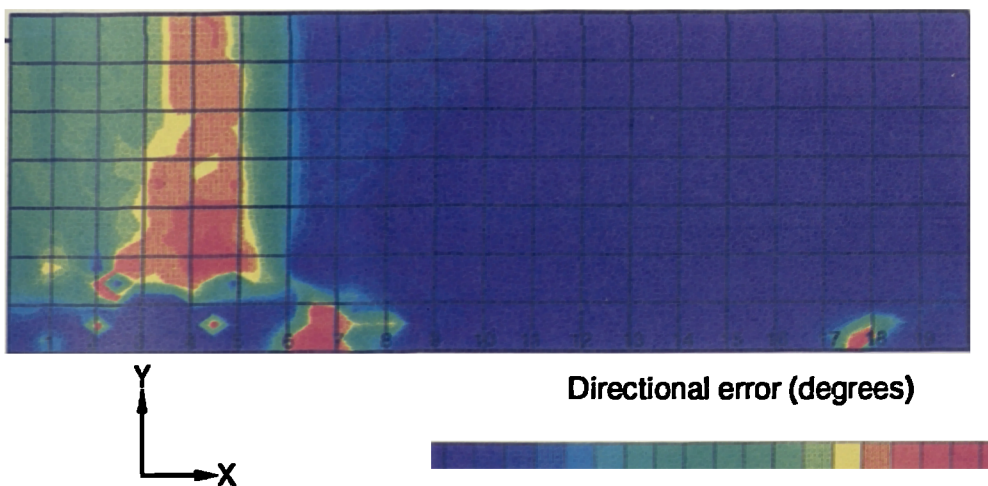
Simulation 1, Vertical slice through the flow at a distance of 0.486 m from the right wall

Simulation 1 $Z = 0.875$ m



(a) Comparison of velocity vectors

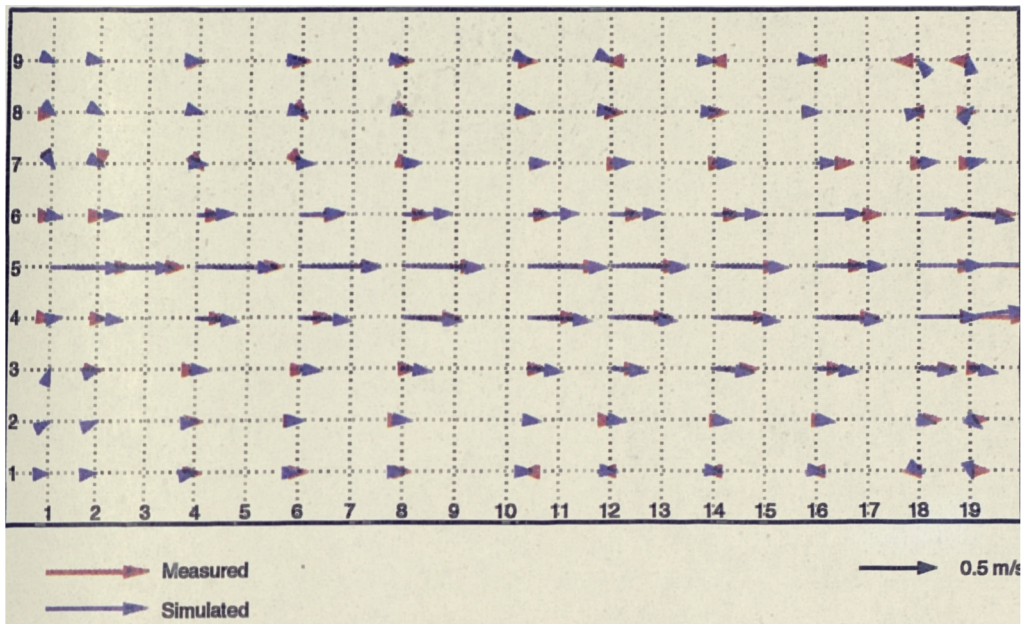
Simulation 1 $Z = 0.875$ m



(b) Directional errors

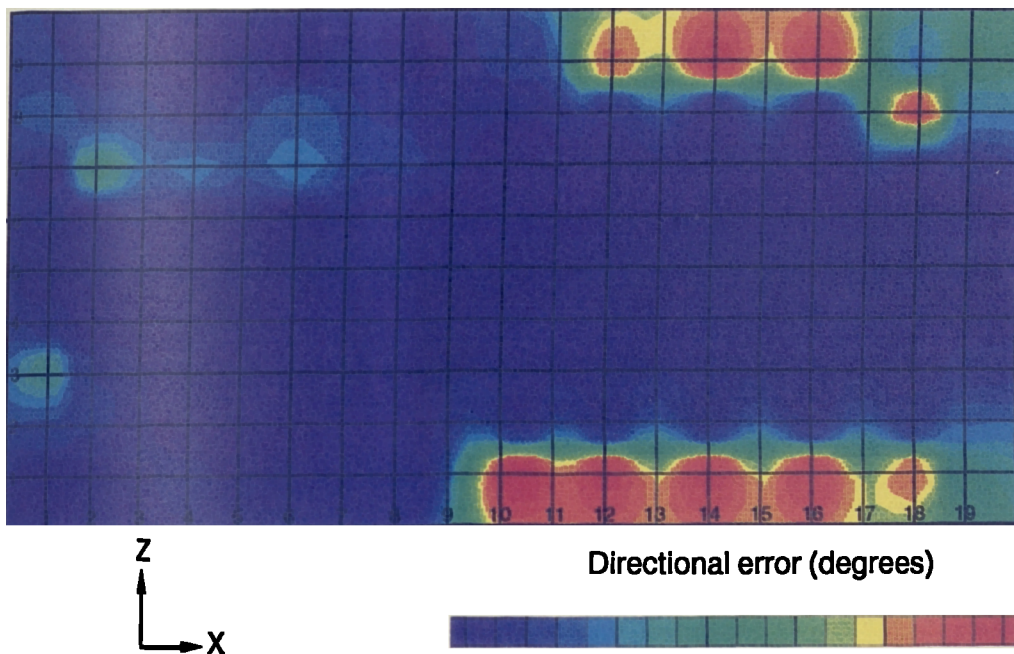
Simulation 1, Vertical slice through the flow at a distance of 0.875 m from the right wall

Simulation 2 $Y = 0.02$ m



(a) Comparison of velocity vectors

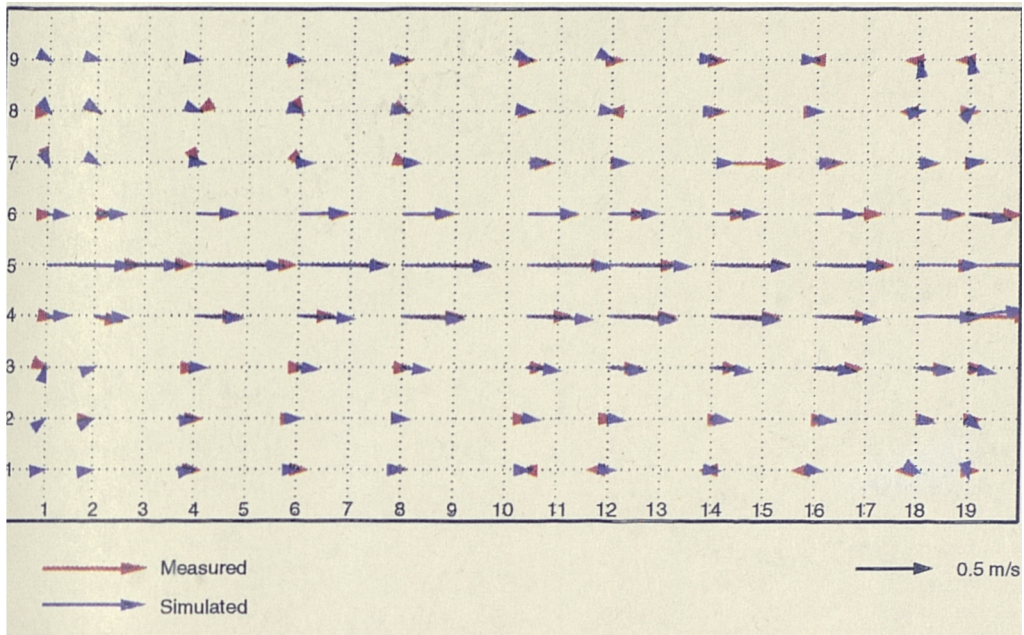
Simulation 2 $Y = 0.02$ m



(b) Directional errors

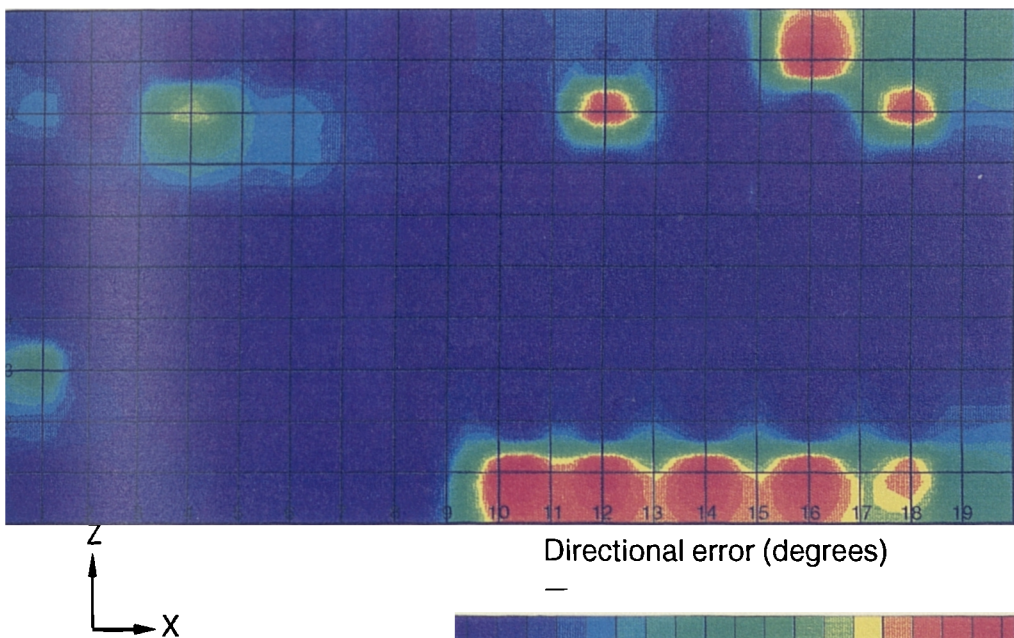
Simulation 2, Horizontal slice through the flow at a depth of 0.02 m above the chamber bed

Simulation 2 $Y = 0.04$ m



(a) Comparison of velocity vectors

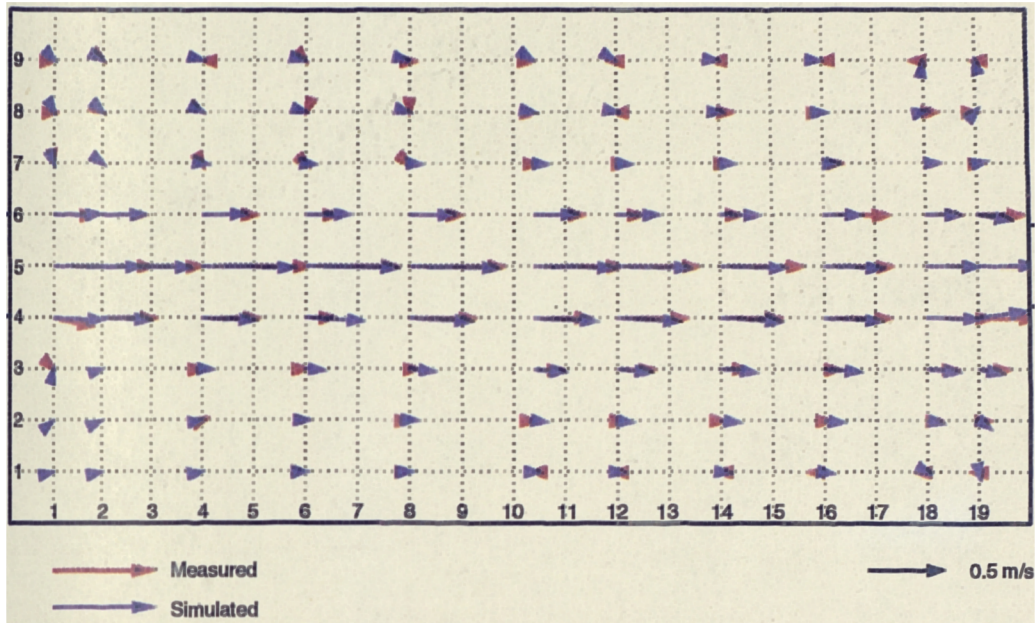
Simulation 2 $Y = 0.04$ m



(b) Directional errors

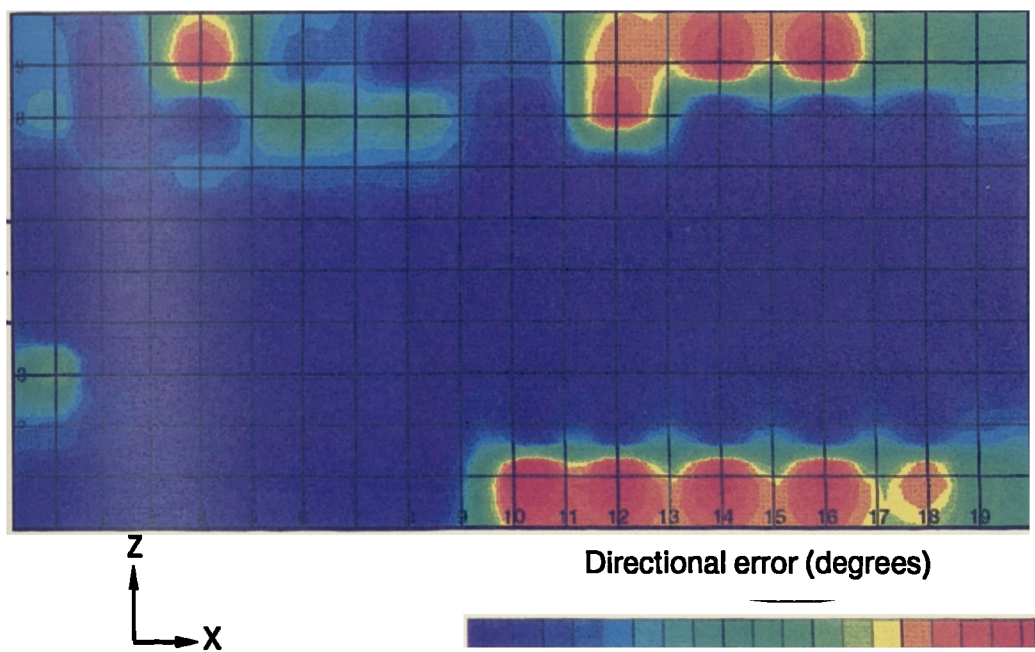
Simulation 2, Horizontal slice through the flow at a depth of 0.04 m above the chamber bed

Simulation 2 $Y = 0.08$ m



(a) Comparison of velocity vectors

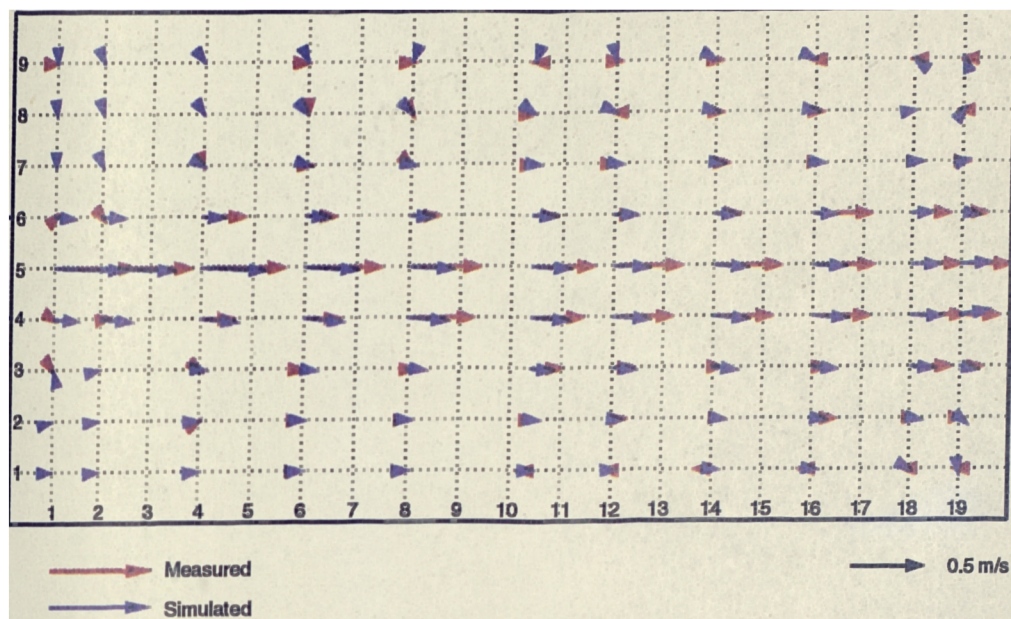
Simulation 2 $Y = 0.08$ m



(b) Directional errors

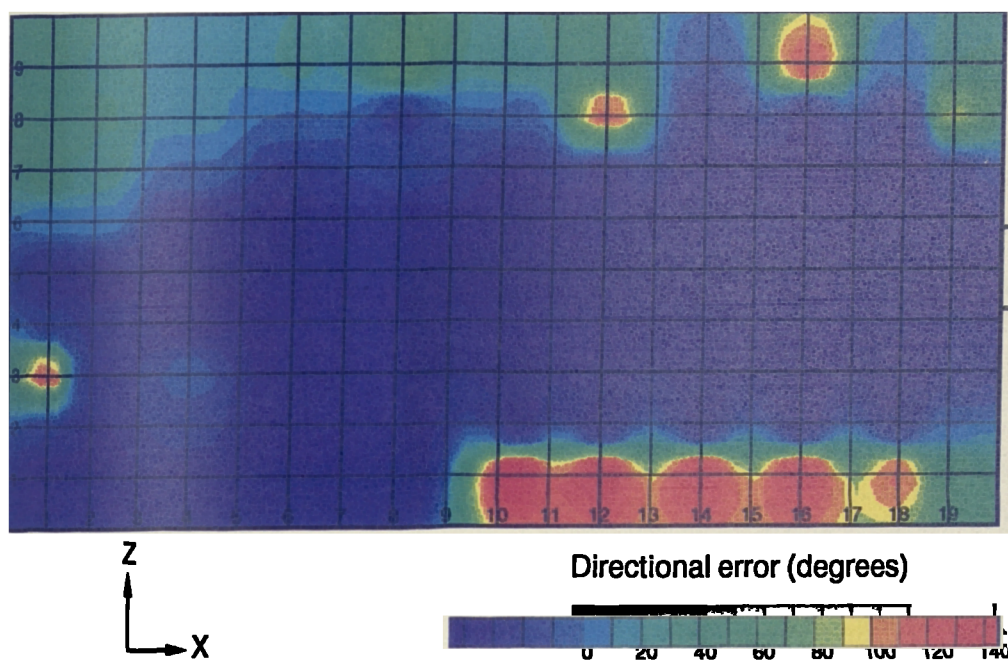
Simulation 2, Horizontal slice through the flow at a depth of 0.08 m above the chamber bed

Simulation 2 $Y = 0.16$ m



(a) Comparison of velocity vectors

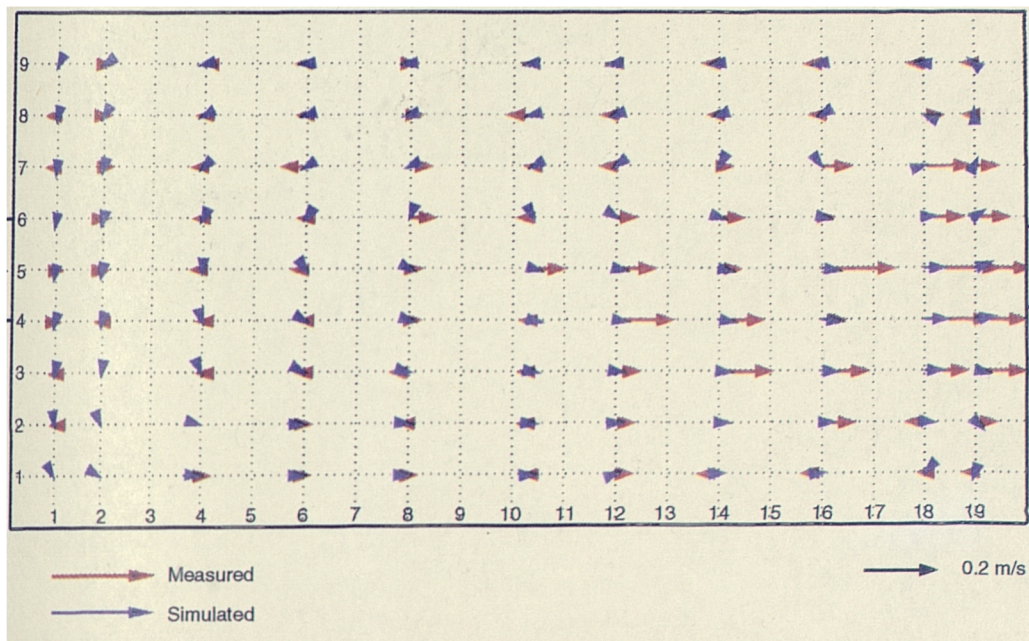
Simulation 2 $Y = 0.16$ m



(b) Directional errors

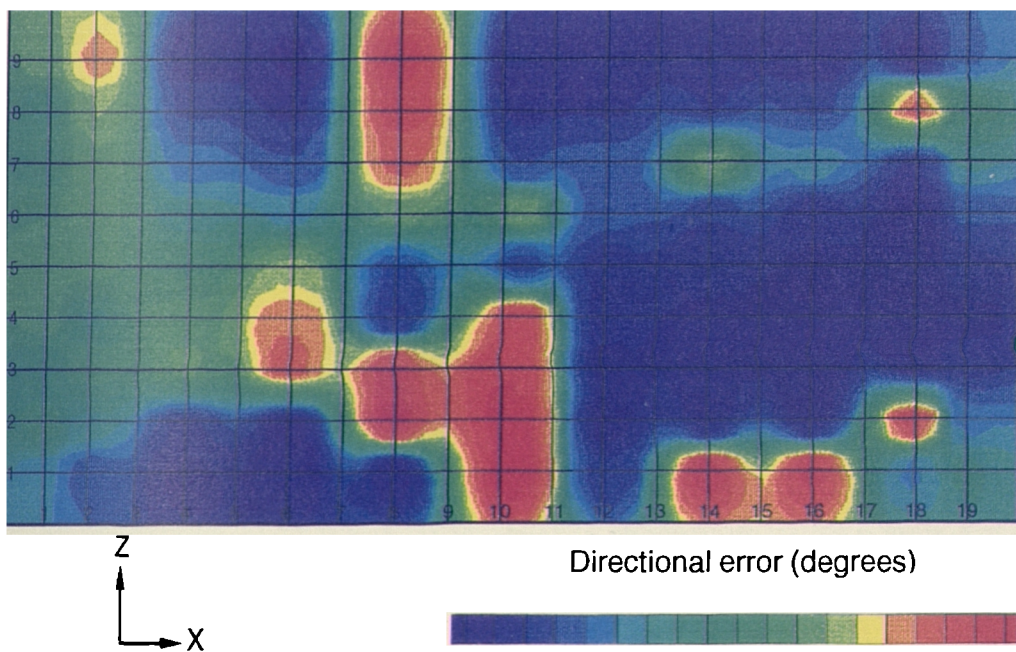
Simulation 2, Horizontal slice through the flow at a depth of 0.16 m above the chamber bed

Simulation 2 $Y = 0.32$ m



(a) Comparison of velocity vectors

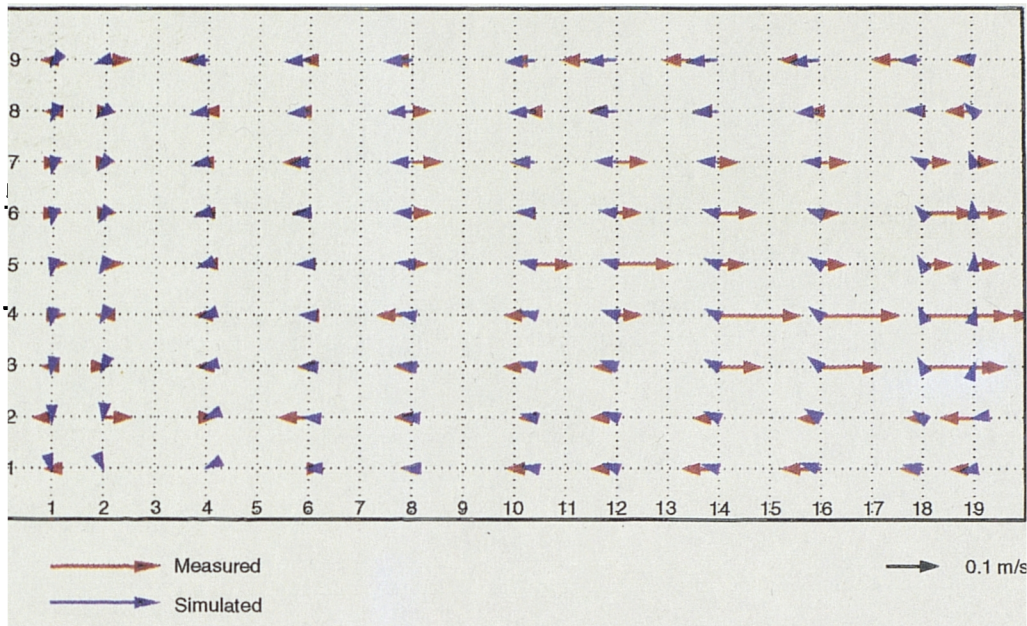
Simulation 2 $Y = 0.32$ m



(b) Directional errors

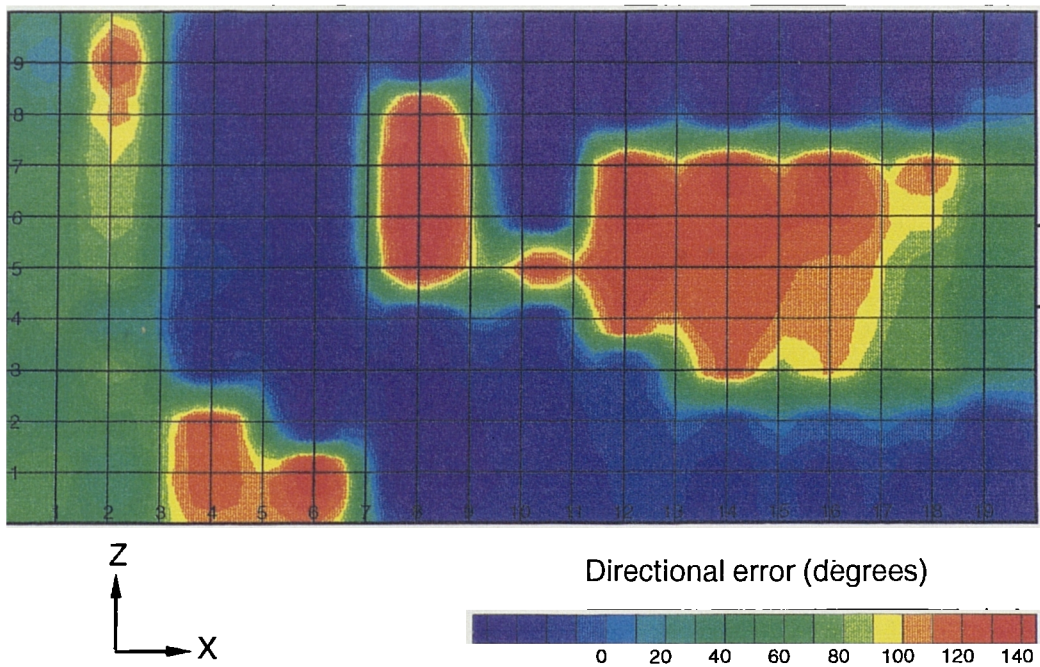
Simulation 2, Horizontal slice through the flow at a depth of 0.32 m above the chamber bed

Simulation 2 $Y = 0.48$ m



(a) Comparison of velocity vectors

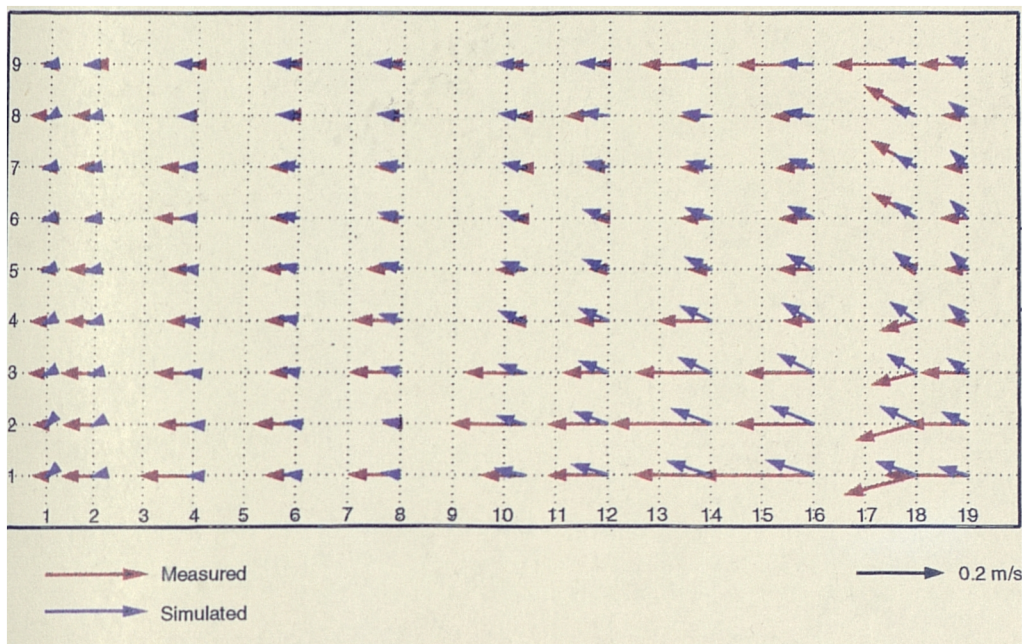
Simulation 2 $Y = 0.48$ m



(b) Directional errors

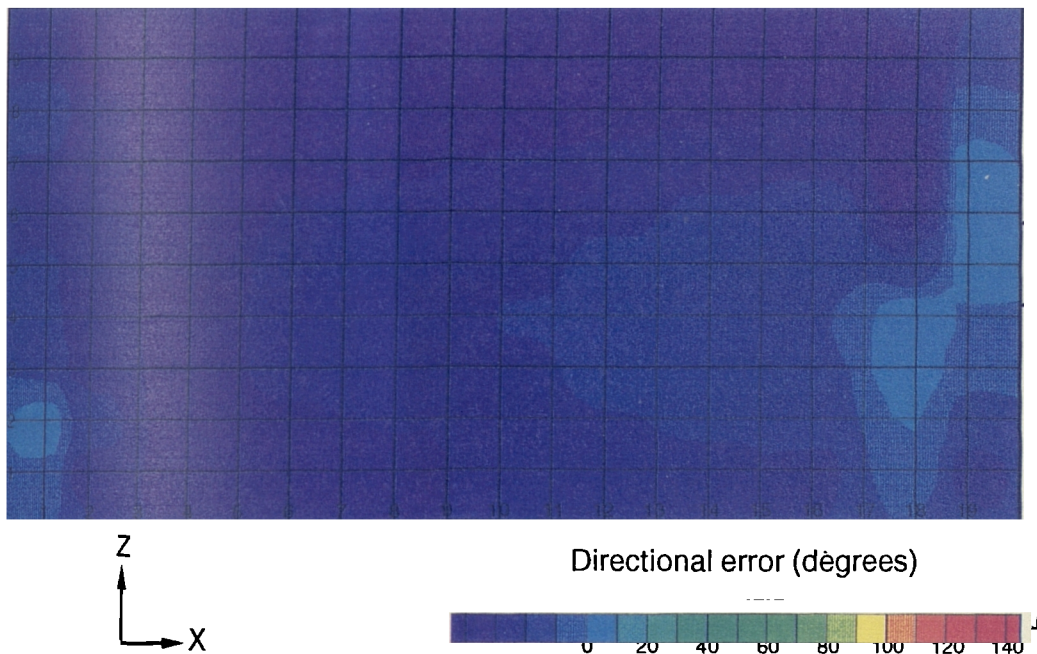
Simulation 2, Horizontal slice through the flow at a depth of 0.48 m above the chamber bed

Simulation 2 $Y = 0.64$ m



(a) Comparison of velocity vectors

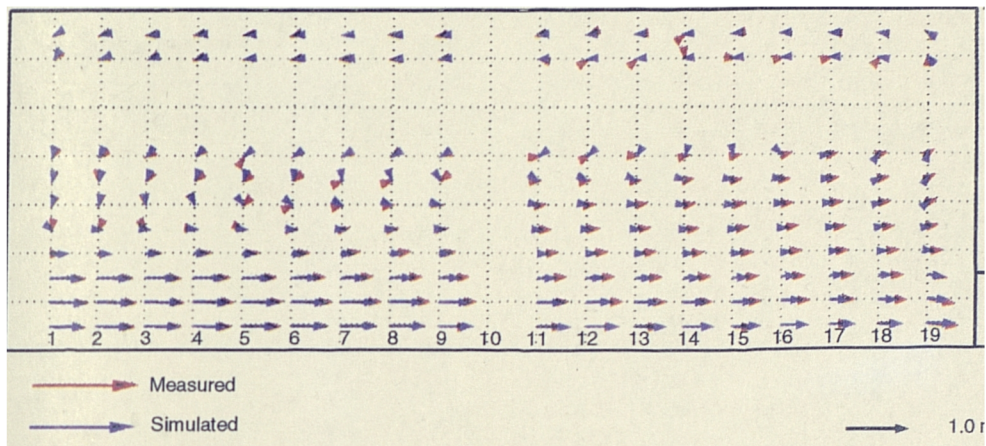
Simulation 2 $Y = 0.64$ m



(b) Directional errors

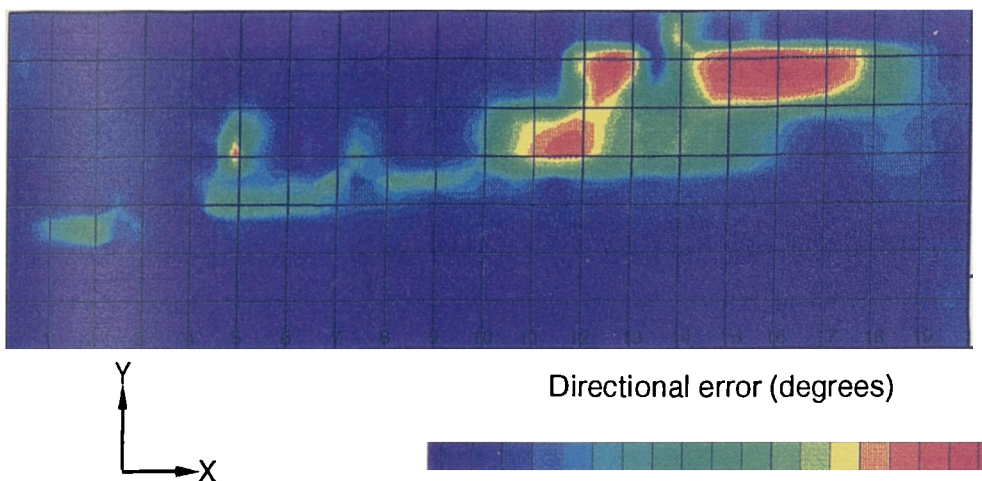
Simulation 2, Horizontal slice through the flow at a depth of 0.64 m above the chamber bed

Simulation 2 $Z = 0.486$ m



(a) Comparison of velocity vectors

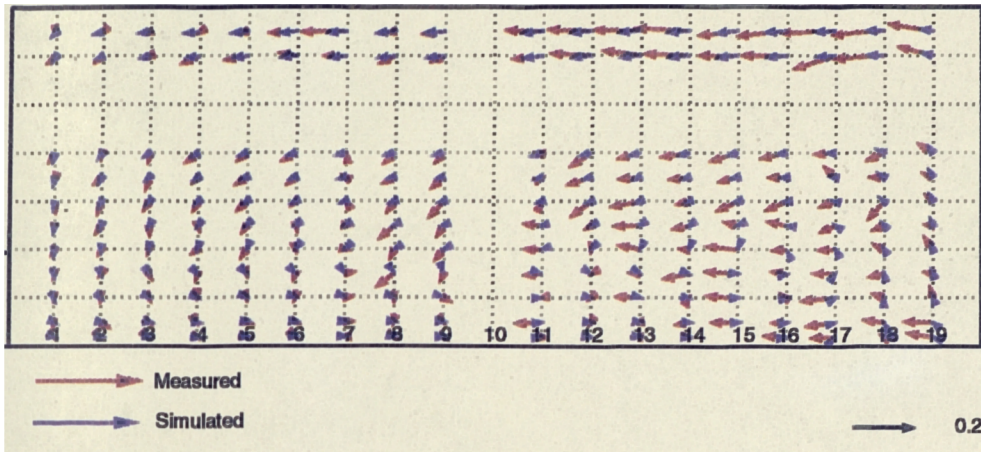
Simulation 2 $Z = 0.486$ m



(b) Directional errors

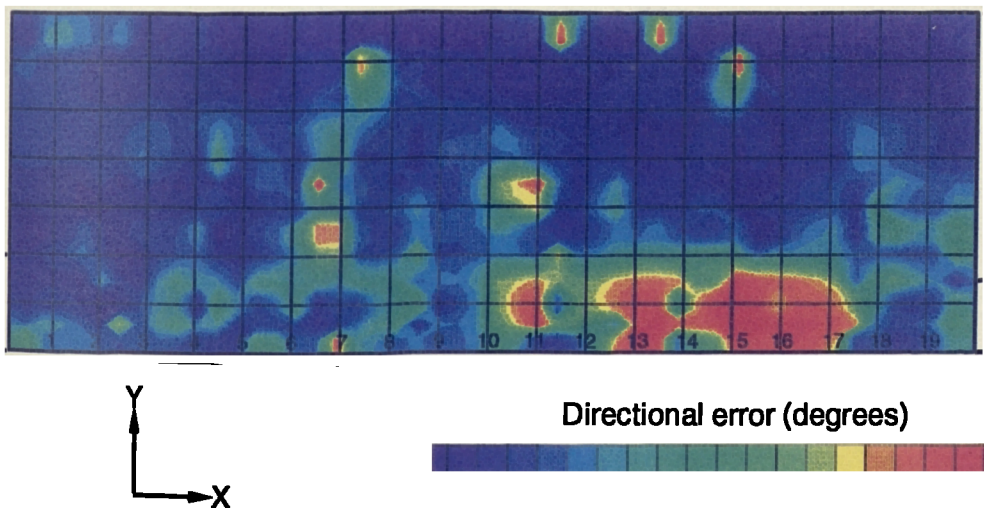
Simulation 2, Vertical slice through the flow at a distance of 0.486 m from the right wall

Simulation 2 $Z = 0.875$ m



(a) Comparison of velocity vectors

Simulation 2 $Z = 0.875$ m



(b) Directional errors

Simulation 2, Vertical slice through the flow at a distance of 0.875 m from the right wall

APPENDIX C -
Laboratory Efficiency Test Data

This Appendix contains the full set of results from the laboratory efficiency tests which were discussed in chapter 4. The results are presented for each chamber in turn. Chamber No. 1 refers to the basic chamber configuration ($L/B = 2.06$, no benching), Chamber No. 2 refers to the chamber with V-shaped benching at a transverse gradient of 1 in 4 and Chamber No. 3 refers to the chamber in which the length to breadth ratio was increased to 2.5. Chamber No. 3 had a flat bed profile.

For each chamber, the test results are ordered sequentially from the minimum mean inlet velocity (\bar{u}) tested up to the highest value of \bar{u} . The calculated sedimentation efficiency, η , is presented for each test, and the date on which the test was carried out is also reported. In most cases three repeat tests were carried out for each configuration. The three tests are each given a test reference of either A, B or C. For each test the graph showing the continuous record of sediment concentration at the inflow to and outflow from the laboratory chamber is also presented.

The test results are summarised in Table C1 and Figure C1, which is a more detailed version of Figure 4.5. The individual test results are represented by hollow symbols, while the mean result for each configuration is depicted with a filled symbol of the same shape and colour. The mean results are also joined with a line.

Table C1 Summary of the Efficiency Test Results

| Configuration | Mean inlet velocity (\bar{u}) | η - Test A | η - Test B | η - Test C | η - Mean |
|---|-----------------------------------|-----------------|-----------------|-----------------|---------------|
| Chamber No. 1 Basic Chamber | 0.151 | 0.594 | 0.646 | 0.698 | 0.646 |
| | 0.192 | 0.481 | 0.483 | 0.501 | 0.488 |
| | 0.227 | 0.167 | 0.204 | 0.275 | 0.215 |
| | 0.254 | 0.252 | 0.185 | 0.240 | 0.226 |
| | 0.334 | 0.185 | 0.111 | 0.142 | 0.146 |
| | 0.361 | 0.203 | 0.264 | 0.080 | 0.182 |
| | 0.406 | -0.068 | 0.097 | 0.074 | 0.035 |
| | 0.495 | 0.208 | 0.175 | 0.132 | 0.171 |
| | 0.565 | 0.096 | 0.090 | 0.083 | 0.090 |
| | 0.619 | -0.009 | -0.057 | 0.040 | -0.009 |
| Chamber No. 2 Benching at 1 in 4 | 0.151 | 0.912 | 0.776 | 0.429 | 0.705 |
| | 0.192 | 0.430 | 0.443 | 0.354 | 0.409 |
| | 0.227 | 0.377 | 0.369 | 0.340 | 0.362 |
| | 0.254 | 0.247 | 0.400 | 0.319 | 0.322 |
| | 0.334 | 0.212 | 0.237 | 0.146 | 0.198 |
| | 0.361 | 0.212 | 0.202 | 0.177 | 0.197 |
| | 0.406 | 0.209 | 0.196 | 0.159 | 0.188 |
| | 0.495 | † | 0.182 | 0.116 | 0.149 |
| | 0.565 | 0.099 | 0.132 | 0.111 | 0.114 |
| | 0.619 | 0.189 | 0.177 | 0.036 | 0.134 |
| Chamber No. 3 L/B = 2.5 | 0.176 | 0.439 | 0.589 | 0.492 | 0.507 |
| | 0.212 | 0.687 | 0.578 | 0.532 | 0.599 |
| | 0.247 | 0.420 | 0.713 | 0.347 | 0.493 |
| | 0.282 | 0.684 | 0.319 | 0.301 | 0.435 |
| | 0.317 | 0.253 | 0.401 | † | 0.327 |
| | 0.388 | 0.025 | -0.052 | 0.085 | 0.019 |
| | 0.459 | 0.150 | 0.029 | † | 0.089 |
| | 0.564 | -0.017 | 0.068 | † | 0.026 |

† Missing data resulted from computer file errors.

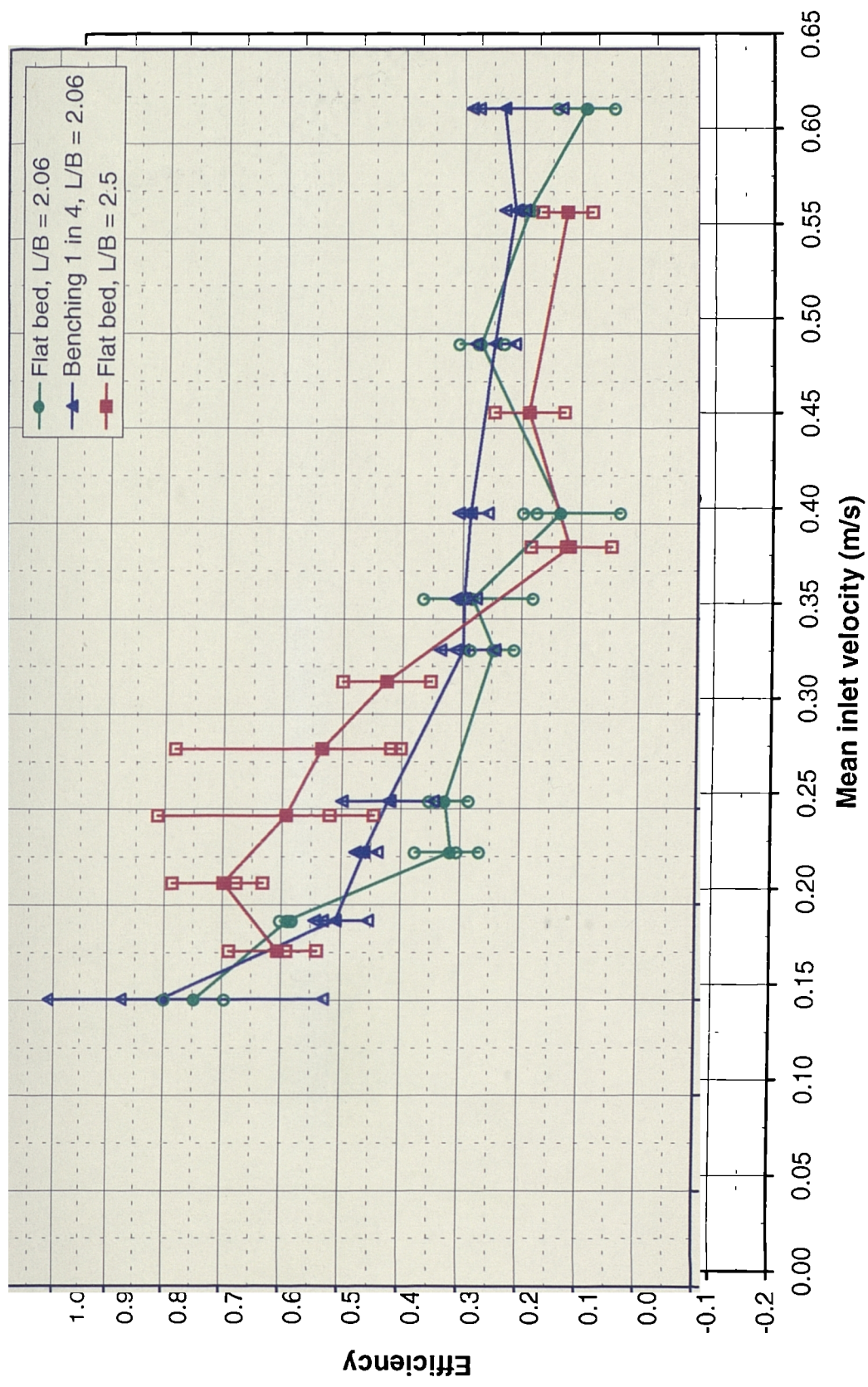
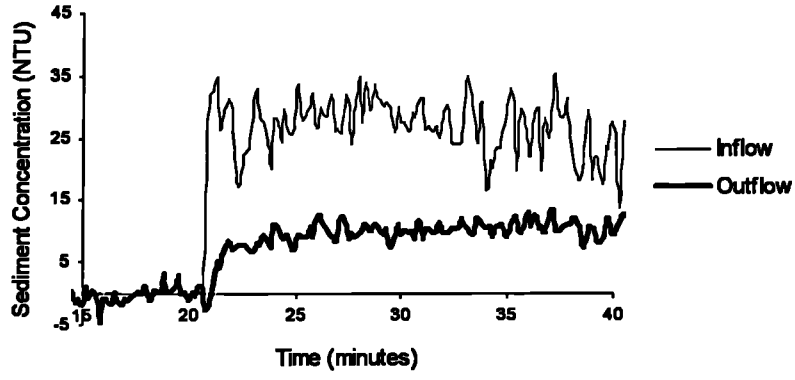
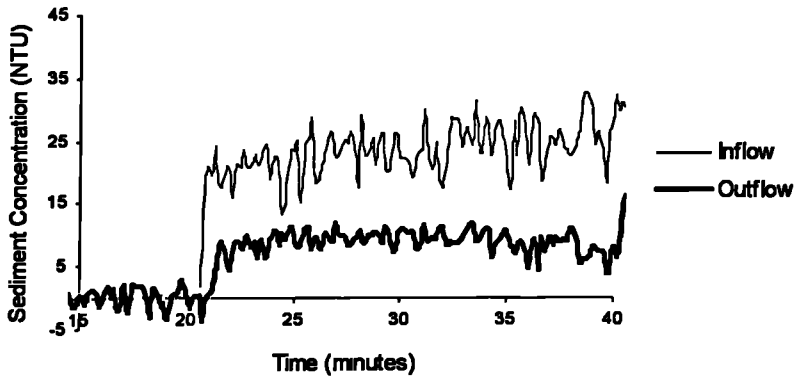
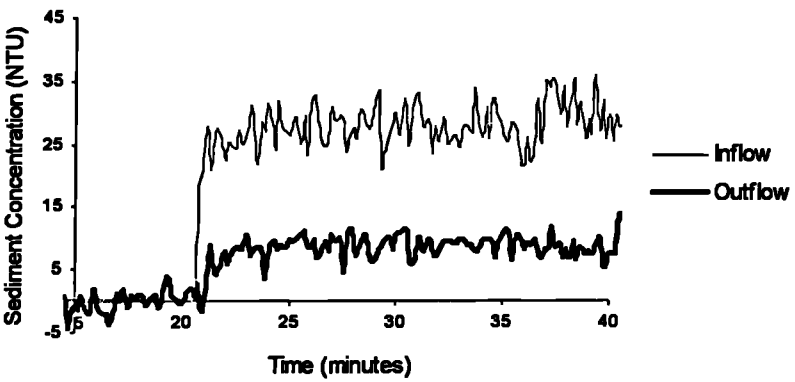
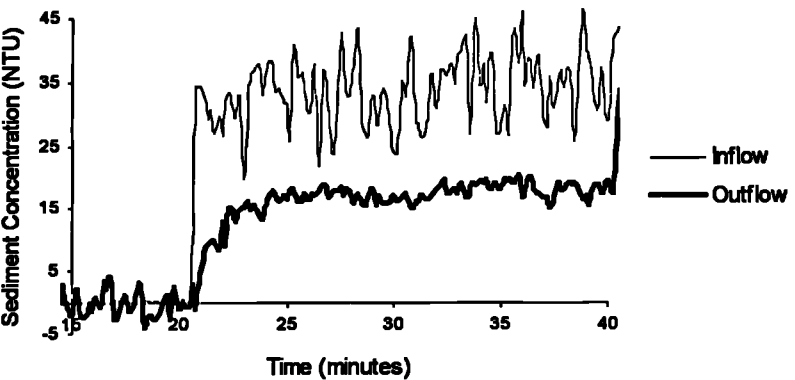
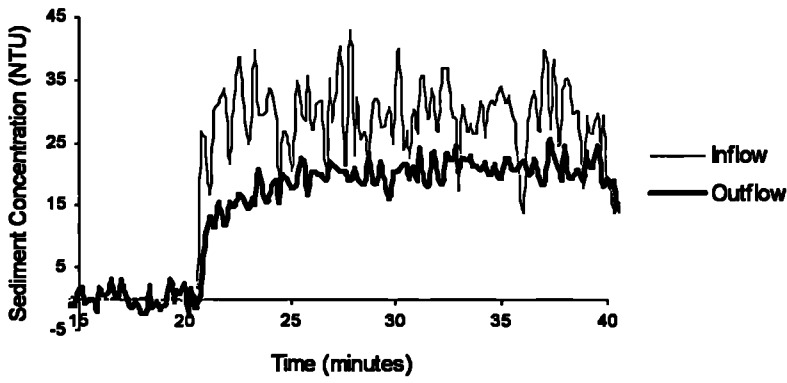
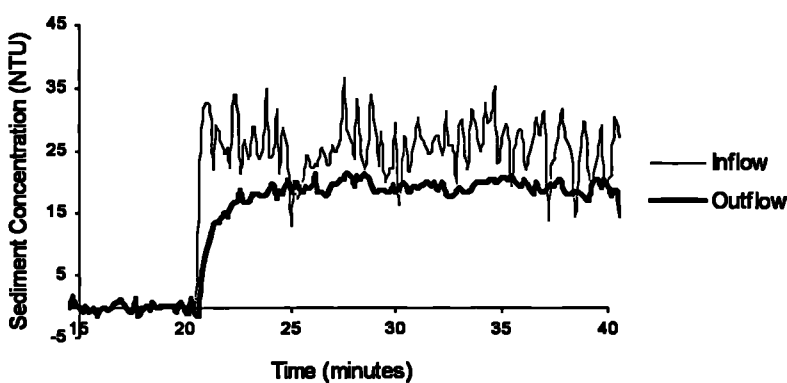
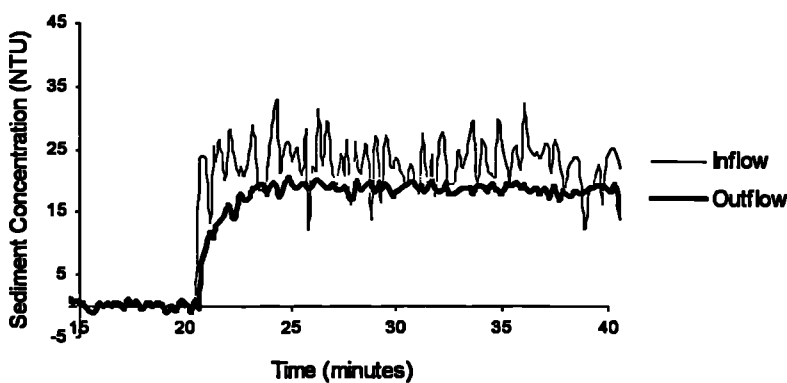
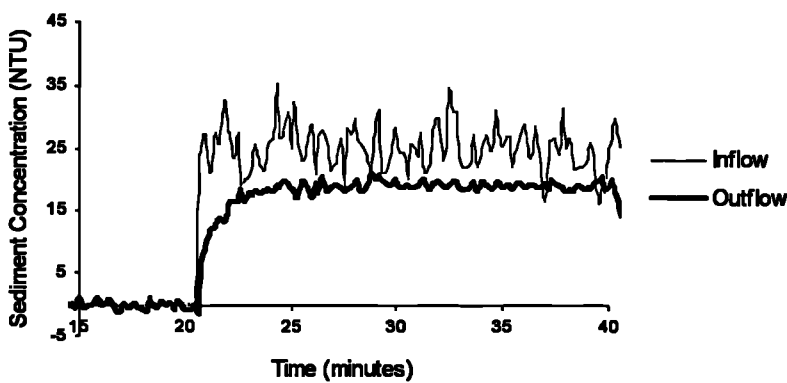


Figure C1 Individual laboratory efficiency results

| | |
|--|--|
| <p>Chamber No. 1</p> <p>$\bar{u} = 0.151 \text{ m/s}$</p> <p>$\eta = 0.594$</p> <p>Date: 02/06/93</p> <p>Test ref. A</p> |  |
| <p>Chamber No. 1</p> <p>$\bar{u} = 0.151 \text{ m/s}$</p> <p>$\eta = 0.646$</p> <p>Date: 07/06/93</p> <p>Test ref. B</p> |  |
| <p>Chamber No. 1</p> <p>$\bar{u} = 0.151 \text{ m/s}$</p> <p>$\eta = 0.698$</p> <p>Date: 08/06/93</p> <p>Test ref. C</p> |  |
| <p>Chamber No. 1</p> <p>$\bar{u} = 0.192 \text{ m/s}$</p> <p>$\eta = 0.481$</p> <p>Date: 06/05/93</p> <p>Test ref. A</p> |  |

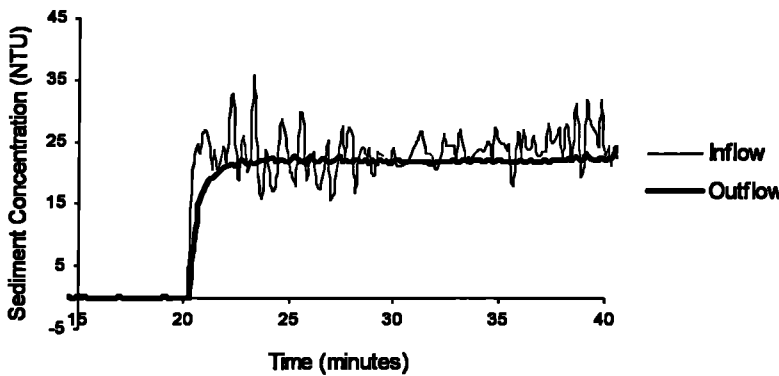
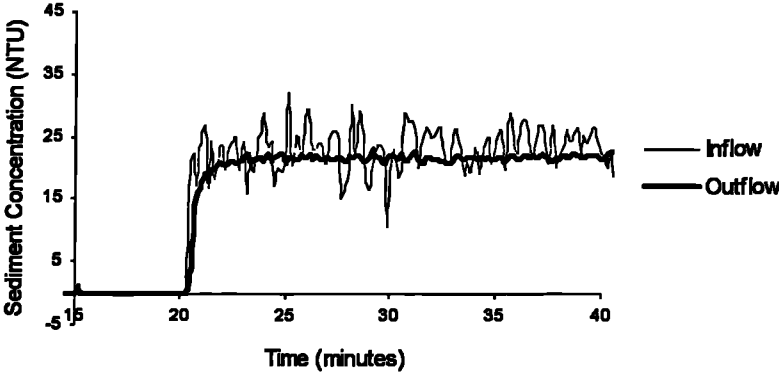
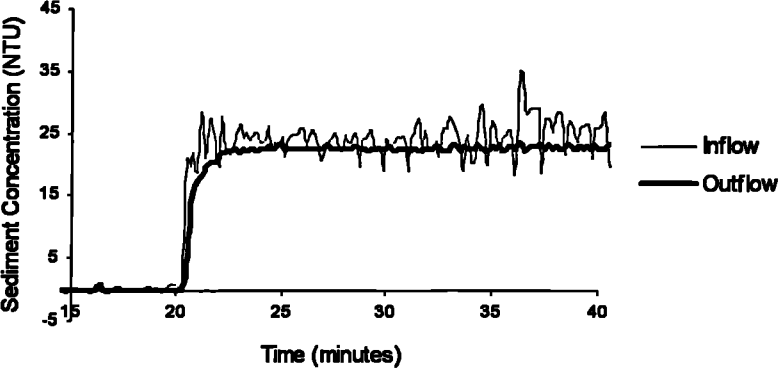
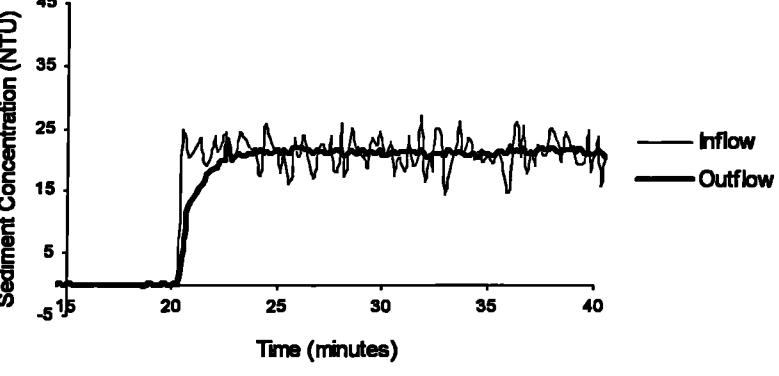
| | |
|--|--|
| <p>Chamber No. 1</p> <p>$\bar{u} = 0.192 \text{ m/s}$</p> <p>$\eta = 0.483$</p> <p>Date: 07/05/93</p> <p>Test ref. B</p> | |
| <p>Chamber No. 1</p> <p>$\bar{u} = 0.192 \text{ m/s}$</p> <p>$\eta = 0.501$</p> <p>Date: 14/05/93</p> <p>Test ref. C</p> | |
| <p>Chamber No. 1</p> <p>$\bar{u} = 0.227 \text{ m/s}$</p> <p>$\eta = 0.167$</p> <p>Date: 02/06/93</p> <p>Test ref. A</p> | |
| <p>Chamber No. 1</p> <p>$\bar{u} = 0.227 \text{ m/s}$</p> <p>$\eta = 0.204$</p> <p>Date: 11/06/93</p> <p>Test ref. B</p> | |

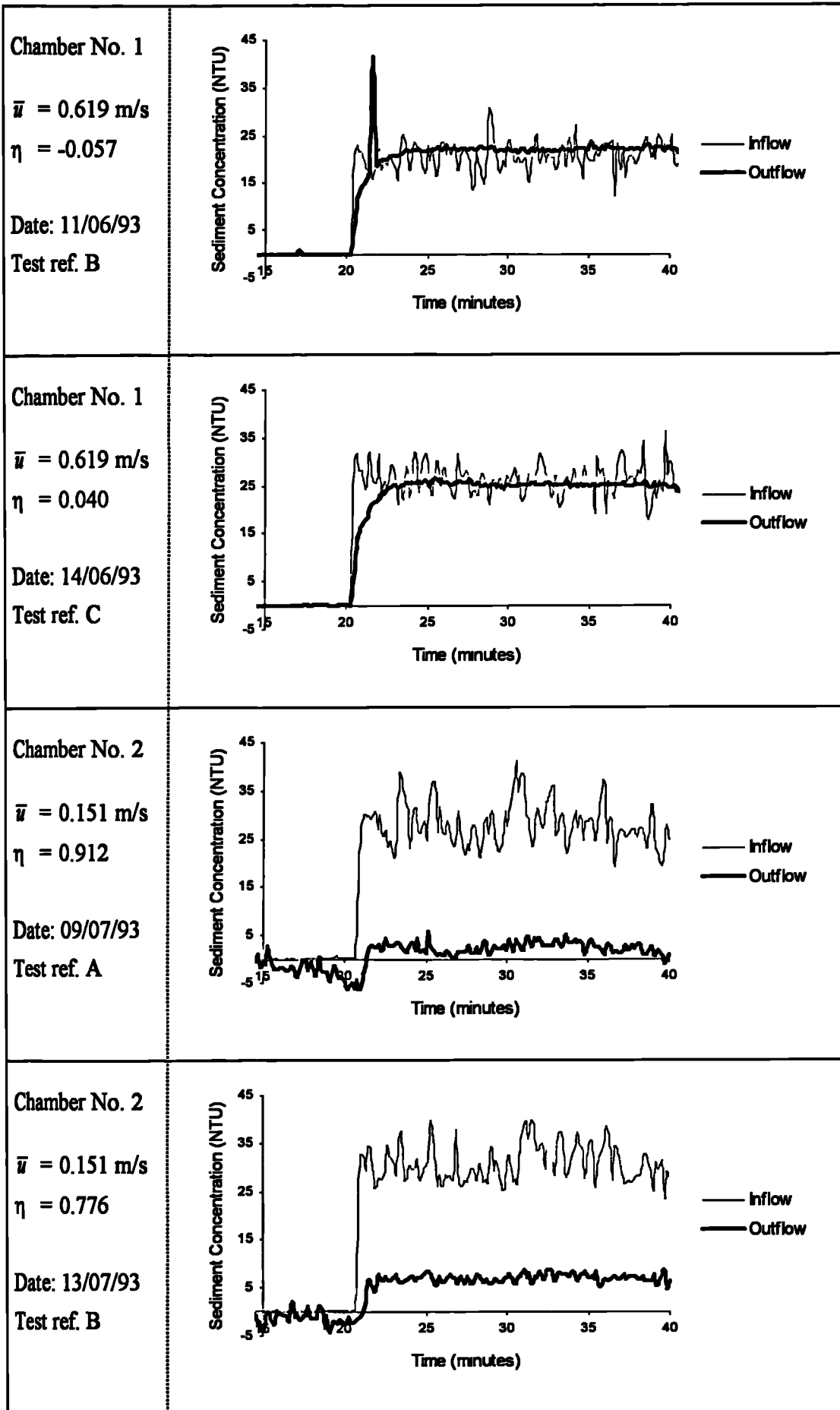
| | |
|--|--|
| <p>Chamber No. 1</p> <p>$\bar{u} = 0.227 \text{ m/s}$</p> <p>$\eta = 0.275$</p> <p>Date: 14/06/93</p> <p>Test ref. C</p> |  |
| <p>Chamber No. 1</p> <p>$\bar{u} = 0.254 \text{ m/s}$</p> <p>$\eta = 0.252$</p> <p>Date: 02/06/93</p> <p>Test ref. A</p> |  |
| <p>Chamber No. 1</p> <p>$\bar{u} = 0.254 \text{ m/s}$</p> <p>$\eta = 0.185$</p> <p>Date: 07/06/93</p> <p>Test ref. B</p> |  |
| <p>Chamber No. 1</p> <p>$\bar{u} = 0.254 \text{ m/s}$</p> <p>$\eta = 0.240$</p> <p>Date: 08/06/93</p> <p>Test ref. C</p> |  |

| | |
|--|--|
| <p>Chamber No. 1</p> <p>$\bar{u} = 0.334 \text{ m/s}$</p> <p>$\eta = 0.185$</p> <p>Date: 06/05/93</p> <p>Test ref. A</p> | |
| <p>Chamber No. 1</p> <p>$\bar{u} = 0.334 \text{ m/s}$</p> <p>$\eta = 0.111$</p> <p>Date: 07/05/93</p> <p>Test ref. B</p> | |
| <p>Chamber No. 1</p> <p>$\bar{u} = 0.334 \text{ m/s}$</p> <p>$\eta = 0.142$</p> <p>Date: 14/05/93</p> <p>Test ref. C</p> | |
| <p>Chamber No. 1</p> <p>$\bar{u} = 0.361 \text{ m/s}$</p> <p>$\eta = 0.203$</p> <p>Date: 02/06/93</p> <p>Test ref. A</p> | |

| | |
|---|--|
| <p>Chamber No. 1</p> <p>$\bar{u} = 0.361 \text{ m/s}$</p> <p>$\eta = 0.264$</p> <p>Date: 07/06/93</p> <p>Test ref. B</p> | |
| <p>Chamber No. 1</p> <p>$\bar{u} = 0.361 \text{ m/s}$</p> <p>$\eta = 0.080$</p> <p>Date: 08/06/93</p> <p>Test ref. C</p> | |
| <p>Chamber No. 1</p> <p>$\bar{u} = 0.406 \text{ m/s}$</p> <p>$\eta = -0.068$</p> <p>Date: 02/06/93</p> <p>Test ref. A</p> | |
| <p>Chamber No. 1</p> <p>$\bar{u} = 0.406 \text{ m/s}$</p> <p>$\eta = 0.097$</p> <p>Date: 11/06/93</p> <p>Test ref. B</p> | |

| | |
|--|--|
| <p>Chamber No. 1</p> <p>$\bar{u} = 0.406 \text{ m/s}$</p> <p>$\eta = 0.074$</p> <p>Date: 14/06/93</p> <p>Test ref. C</p> | <p>Sediment Concentration (NTU)</p> <p>Time (minutes)</p> <p>— Inflow</p> <p>— Outflow</p> |
| <p>Chamber No. 1</p> <p>$\bar{u} = 0.495 \text{ m/s}$</p> <p>$\eta = 0.208$</p> <p>Date: 06/05/93</p> <p>Test ref. A</p> | <p>Sediment Concentration (NTU)</p> <p>Time (minutes)</p> <p>— Inflow</p> <p>— Outflow</p> |
| <p>Chamber No. 1</p> <p>$\bar{u} = 0.495 \text{ m/s}$</p> <p>$\eta = 0.175$</p> <p>Date: 07/05/93</p> <p>Test ref. B</p> | <p>Sediment Concentration (NTU)</p> <p>Time (minutes)</p> <p>— Inflow</p> <p>— Outflow</p> |
| <p>Chamber No. 1</p> <p>$\bar{u} = 0.495 \text{ m/s}$</p> <p>$\eta = 0.132$</p> <p>Date: 14/05/93</p> <p>Test ref. C</p> | <p>Sediment Concentration (NTU)</p> <p>Time (minutes)</p> <p>— Inflow</p> <p>— Outflow</p> |

| | |
|---|--|
| <p>Chamber No. 1</p> <p>$\bar{u} = 0.565 \text{ m/s}$</p> <p>$\eta = 0.096$</p> <p>Date: 02/06/93</p> <p>Test ref. A</p> |  |
| <p>Chamber No. 1</p> <p>$\bar{u} = 0.565 \text{ m/s}$</p> <p>$\eta = 0.090$</p> <p>Date: 07/06/93</p> <p>Test ref. B</p> |  |
| <p>Chamber No. 1</p> <p>$\bar{u} = 0.565 \text{ m/s}$</p> <p>$\eta = 0.083$</p> <p>Date: 08/06/93</p> <p>Test ref. C</p> |  |
| <p>Chamber No. 1</p> <p>$\bar{u} = 0.619 \text{ m/s}$</p> <p>$\eta = -0.009$</p> <p>Date: 02/06/93</p> <p>Test ref. A</p> |  |



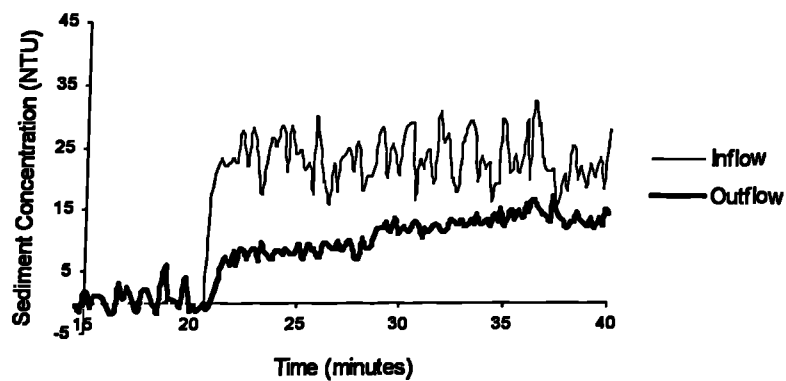
Chamber No. 2

$\bar{u} = 0.151 \text{ m/s}$

$\eta = 0.429$

Date: 10/08/93

Test ref. C



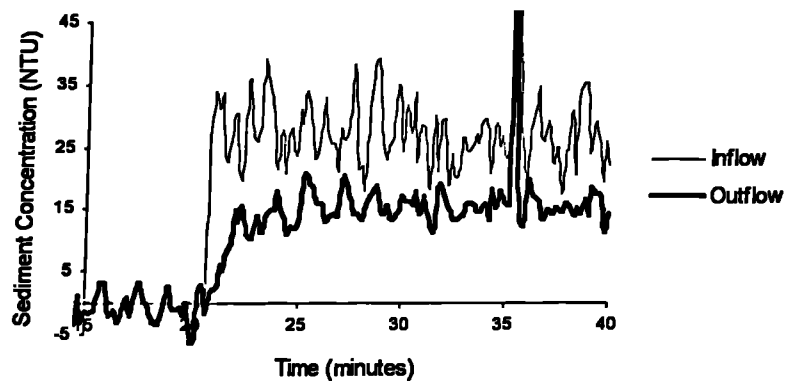
Chamber No. 2

$\bar{u} = 0.192 \text{ m/s}$

$\eta = 0.430$

Date: 12/07/93

Test ref. A



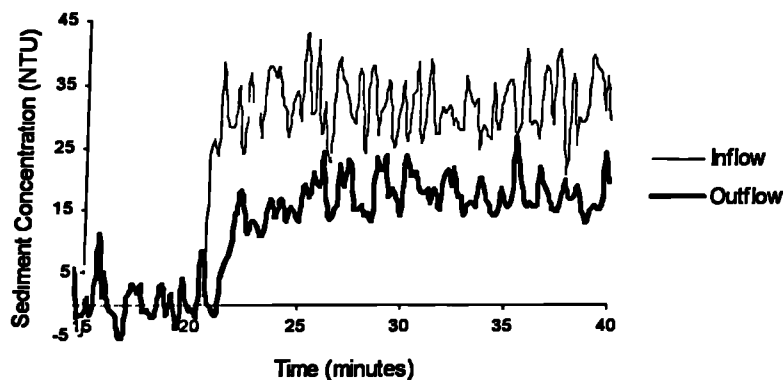
Chamber No. 2

$\bar{u} = 0.192 \text{ m/s}$

$\eta = 0.443$

Date: 13/07/93

Test ref. B



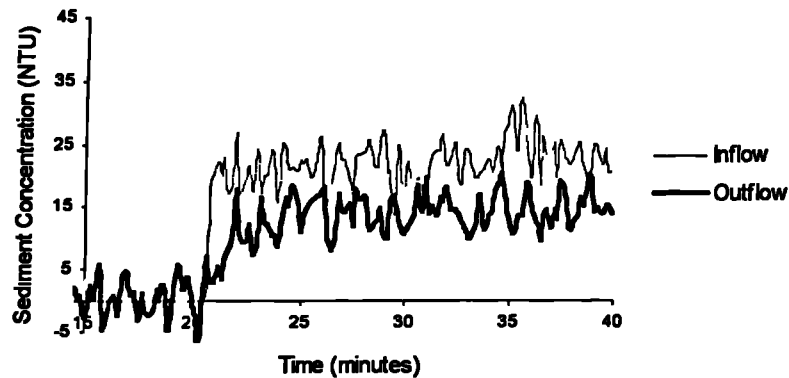
Chamber No. 2

$\bar{u} = 0.192 \text{ m/s}$

$\eta = 0.354$

Date: 10/08/93

Test ref. C



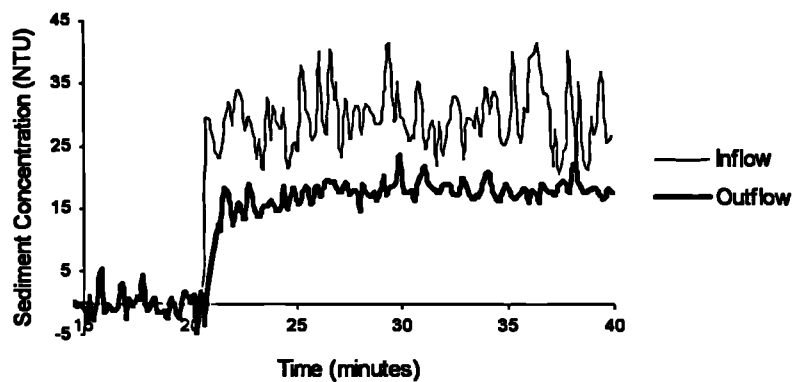
Chamber No. 2

$$\bar{u} = 0.227 \text{ m/s}$$

$$\eta = 0.377$$

Date: 12/07/93

Test ref. A



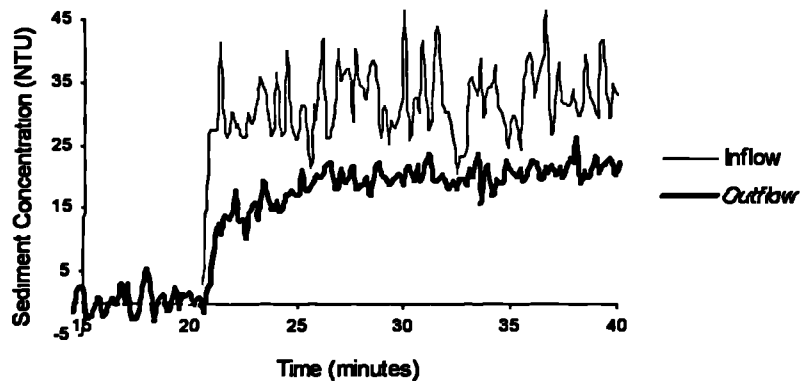
Chamber No. 2

$$\bar{u} = 0.227 \text{ m/s}$$

$$\eta = 0.369$$

Date: 13/07/93

Test ref. B



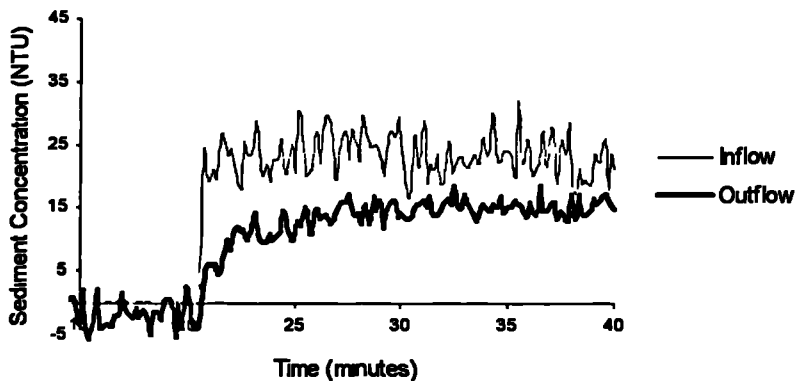
Chamber No. 2

$$\bar{u} = 0.227 \text{ m/s}$$

$$\eta = 0.340$$

Date: 10/08/93

Test ref. C



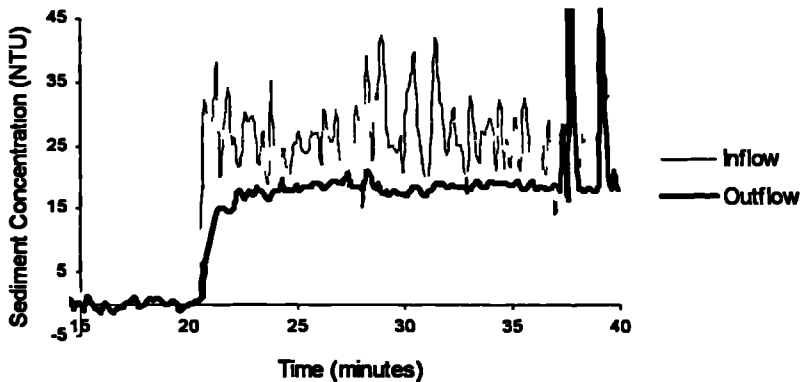
Chamber No. 2

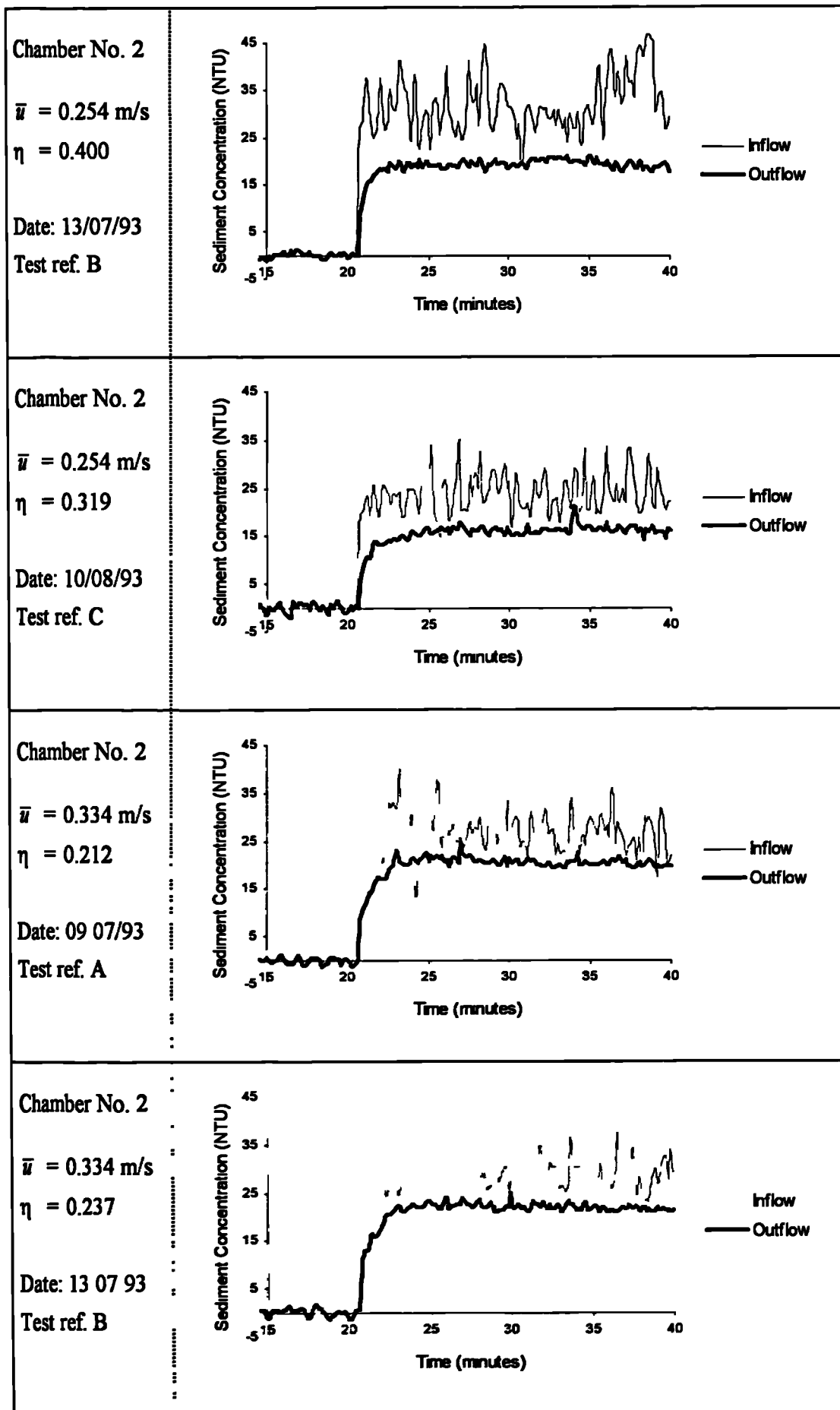
$$\bar{u} = 0.254 \text{ m/s}$$

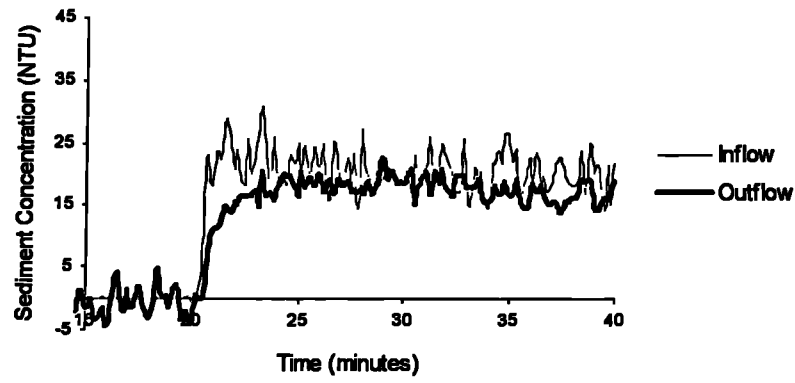
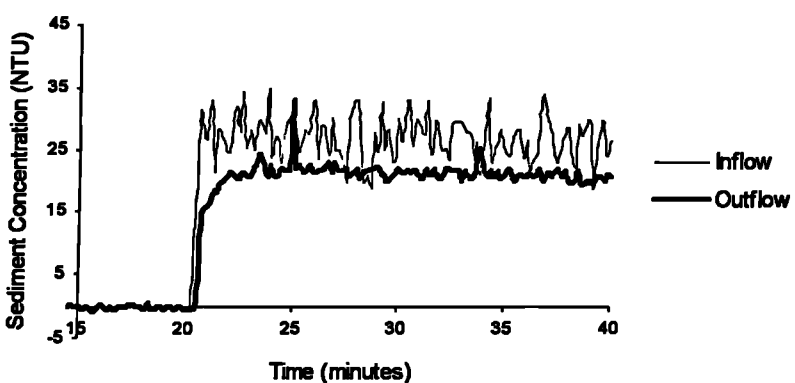
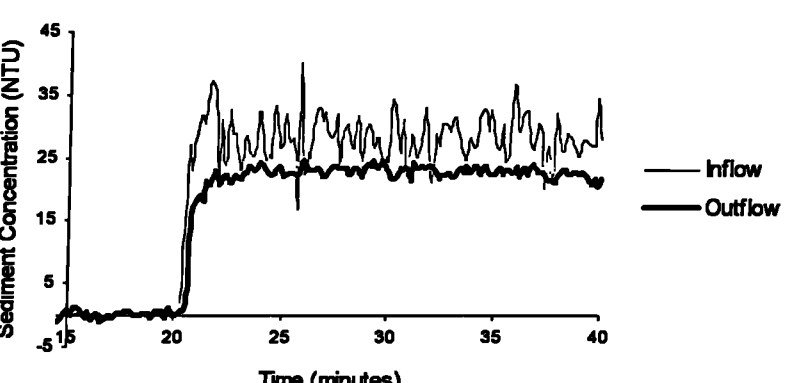
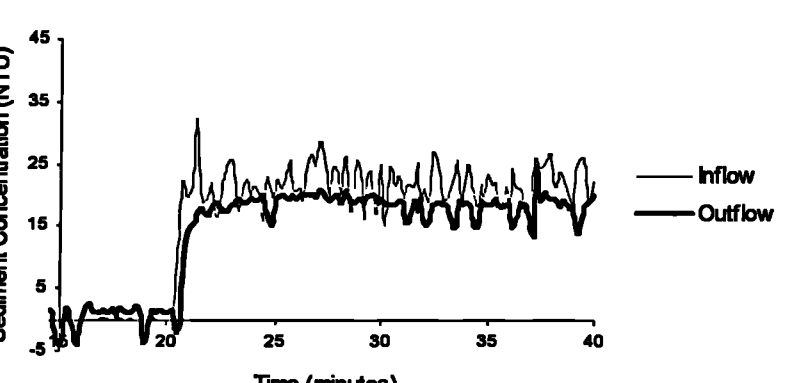
$$\eta = 0.247$$

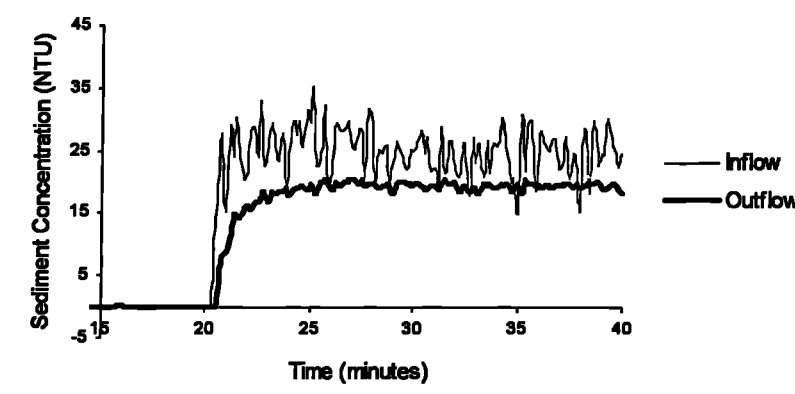
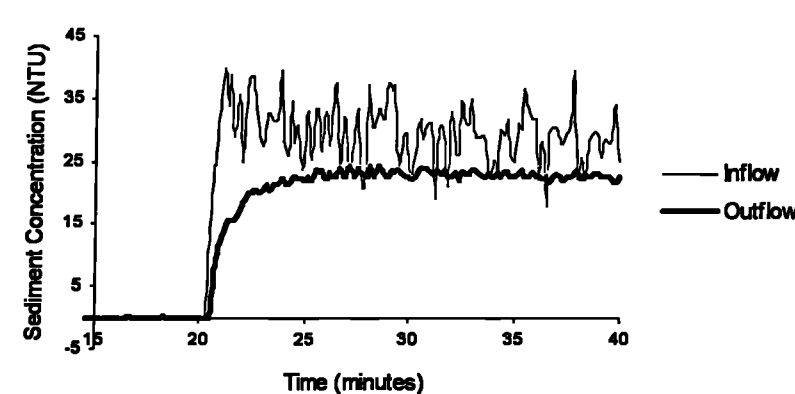
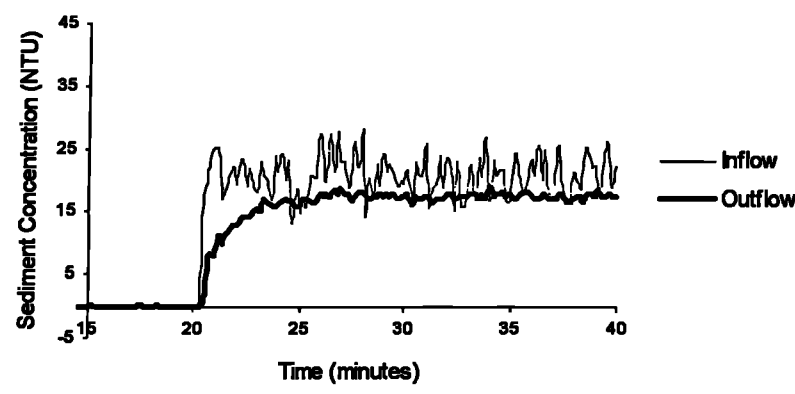
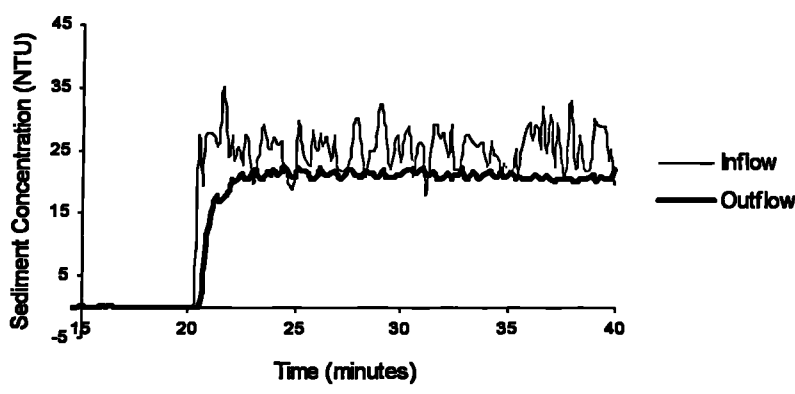
Date: 09/07/93

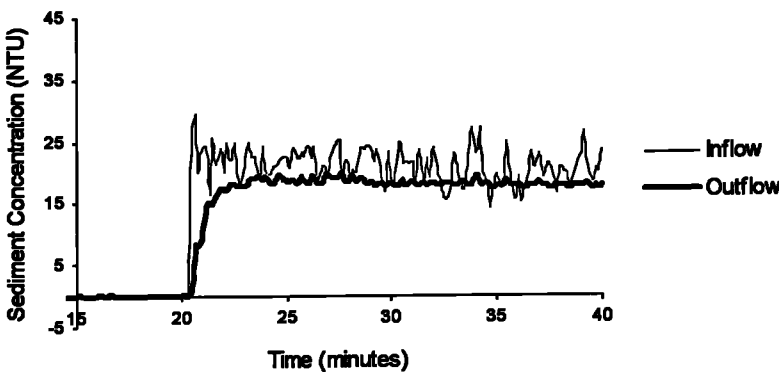
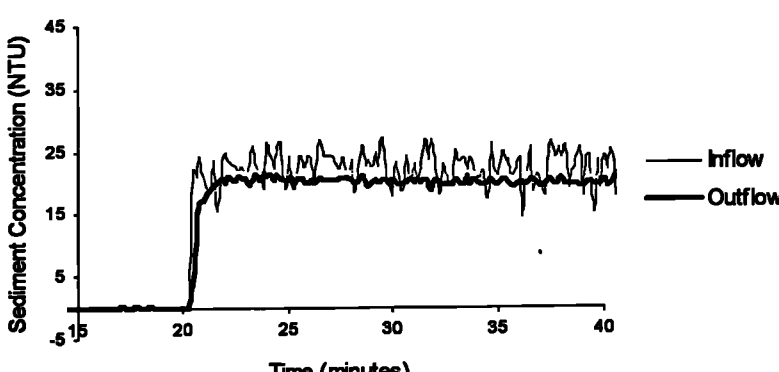
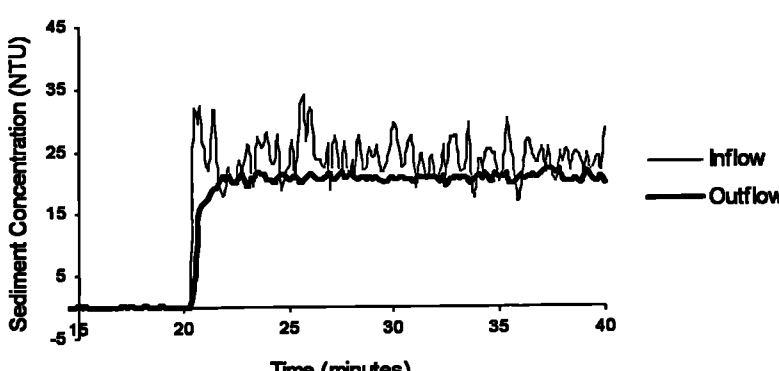
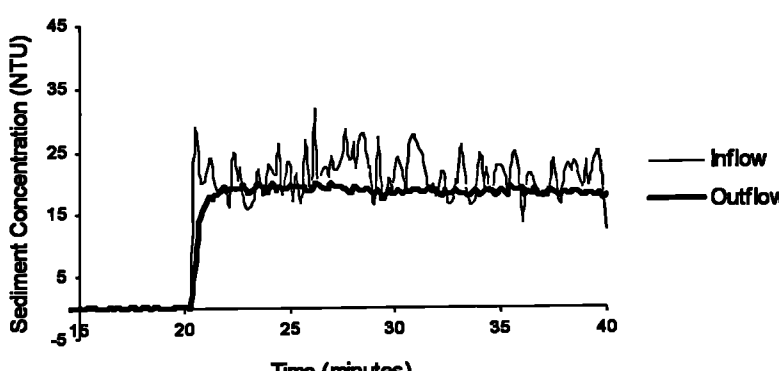
Test ref. A

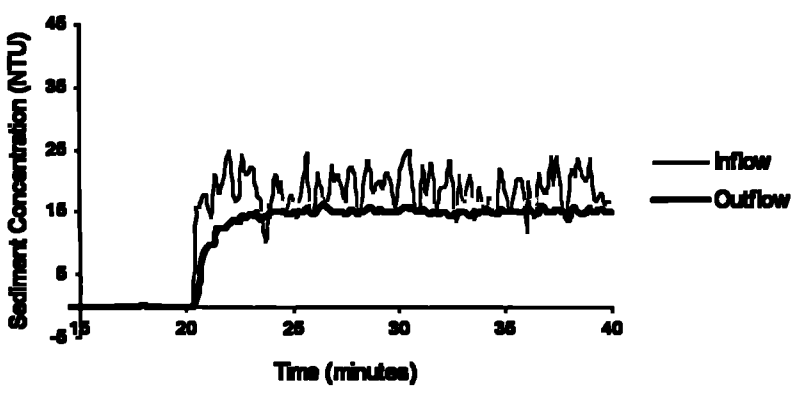
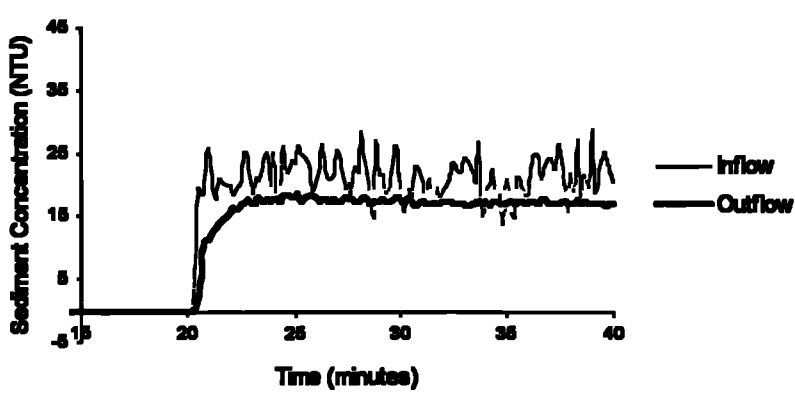
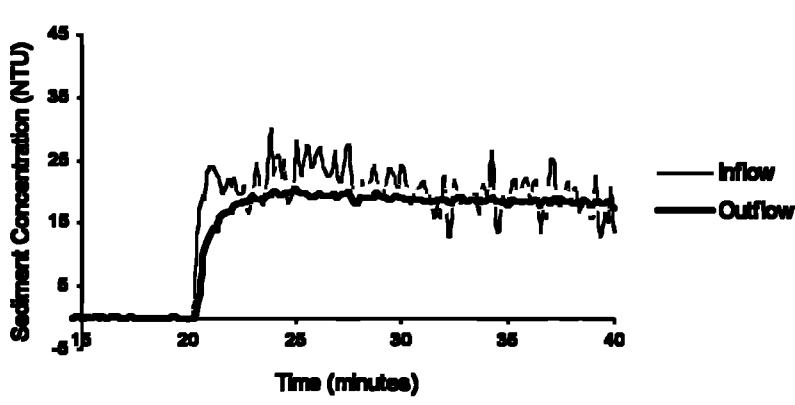
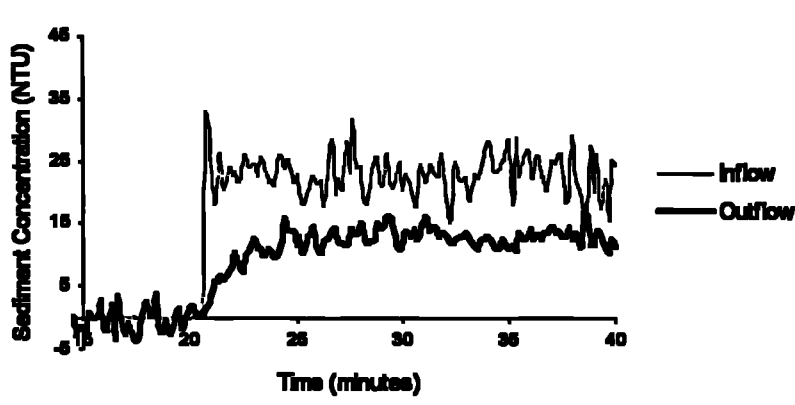


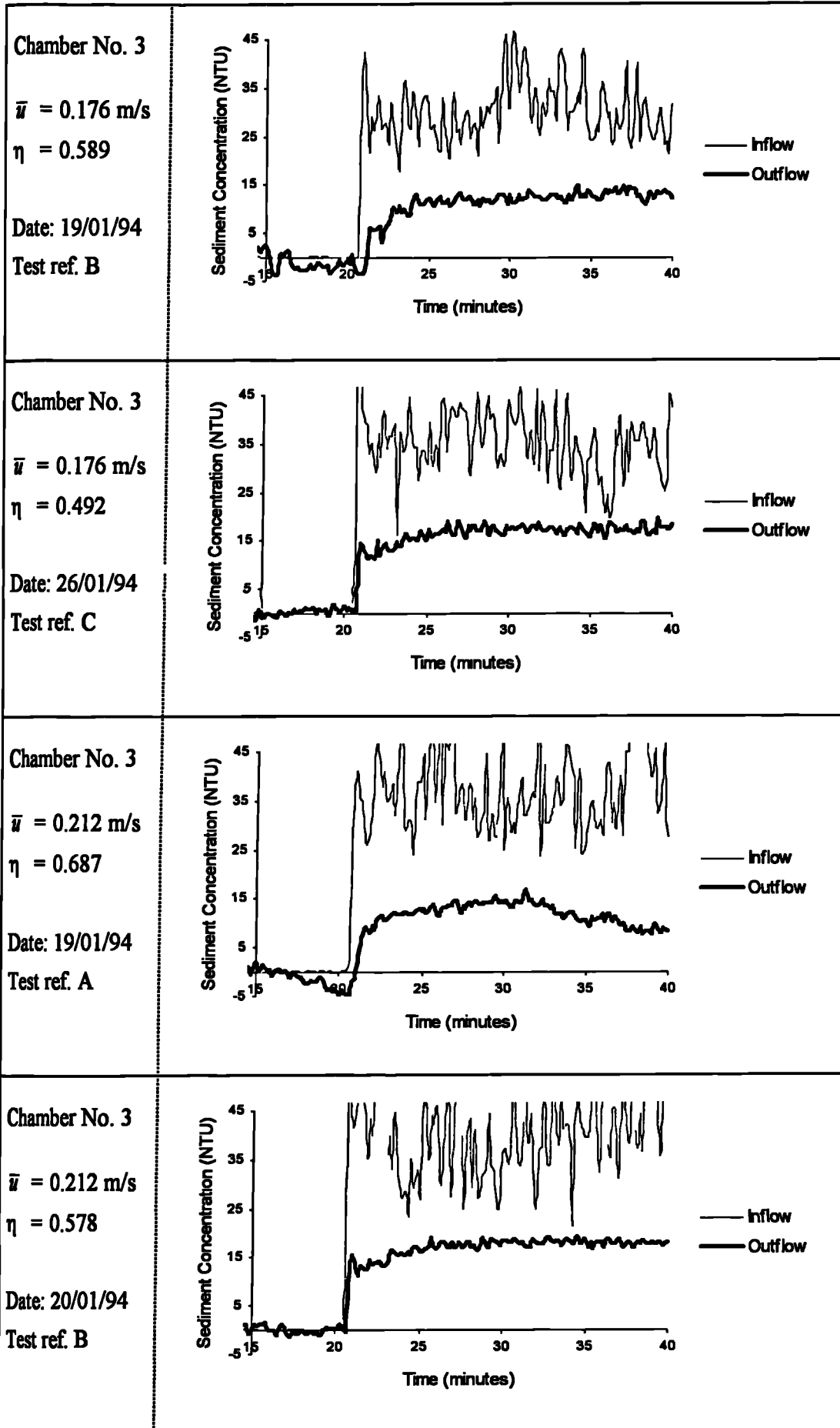


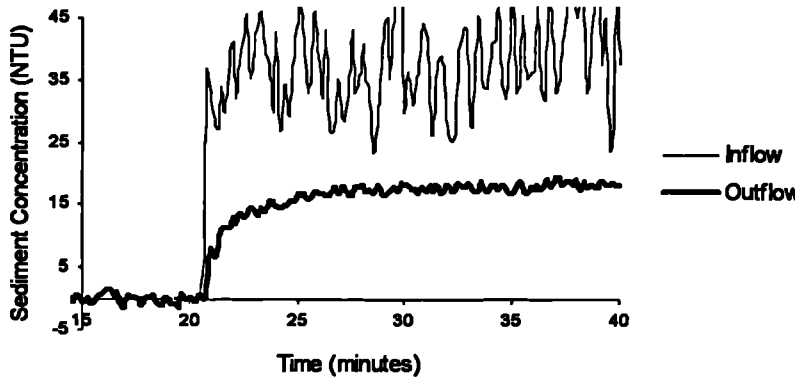
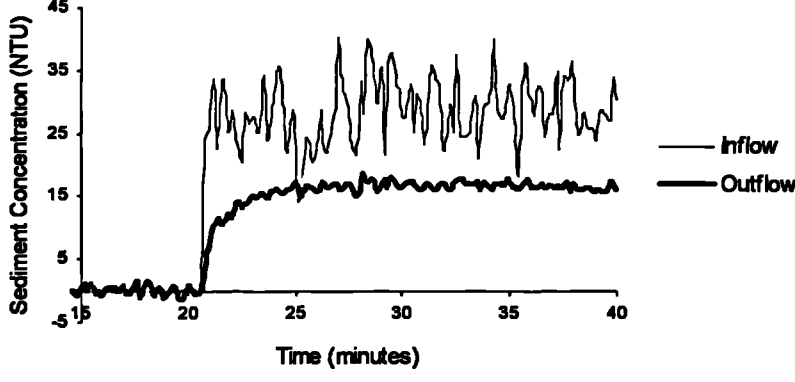
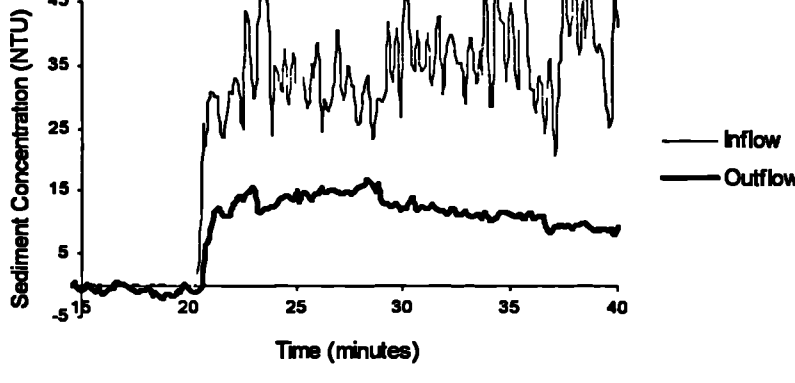
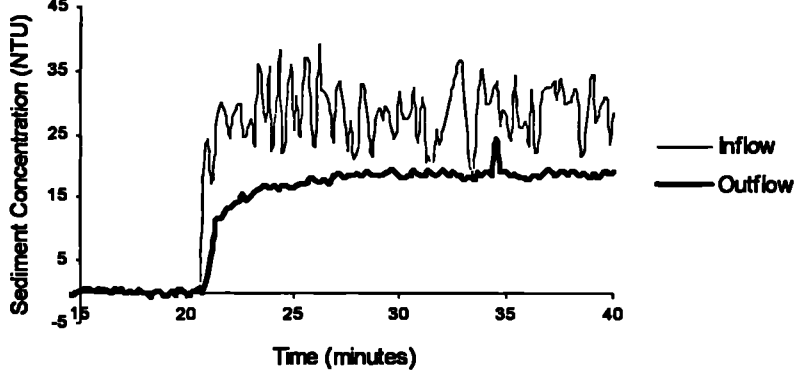
| | |
|--|--|
| <p>Chamber No. 2</p> <p>$\bar{u} = 0.334 \text{ m/s}$</p> <p>$\eta = 0.146$</p> <p>Date: 09/08/93</p> <p>Test ref. C</p> |  |
| <p>Chamber No. 2</p> <p>$\bar{u} = 0.361 \text{ m/s}$</p> <p>$\eta = 0.212$</p> <p>Date: 09/07/93</p> <p>Test ref. A</p> |  |
| <p>Chamber No. 2</p> <p>$\bar{u} = 0.361 \text{ m/s}$</p> <p>$\eta = 0.202$</p> <p>Date: 13/07/93</p> <p>Test ref. B</p> |  |
| <p>Chamber No. 2</p> <p>$\bar{u} = 0.361 \text{ m/s}$</p> <p>$\eta = 0.177$</p> <p>Date: 09/08/93</p> <p>Test ref. C</p> |  |

| | |
|--|--|
| <p>Chamber No. 2</p> <p>$\bar{u} = 0.406 \text{ m/s}$</p> <p>$\eta = 0.209$</p> <p>Date: 12/07/93</p> <p>Test ref. A</p> |  |
| <p>Chamber No. 2</p> <p>$\bar{u} = 0.406 \text{ m/s}$</p> <p>$\eta = 0.196$</p> <p>Date: 13/07/93</p> <p>Test ref. B</p> |  |
| <p>Chamber No. 2</p> <p>$\bar{u} = 0.406 \text{ m/s}$</p> <p>$\eta = 0.159$</p> <p>Date: 10/08/93</p> <p>Test ref. C</p> |  |
| <p>Chamber No. 2</p> <p>$\bar{u} = 0.495 \text{ m/s}$</p> <p>$\eta = 0.182$</p> <p>Date: 13/07/93</p> <p>Test ref. B</p> |  |

| | |
|--|--|
| <p>Chamber No. 2</p> <p>$\bar{u} = 0.495 \text{ m/s}$</p> <p>$\eta = 0.116$</p> <p>Date: 09/08/93</p> <p>Test ref. C</p> |  |
| <p>Chamber No. 2</p> <p>$\bar{u} = 0.565 \text{ m/s}$</p> <p>$\eta = 0.099$</p> <p>Date: 09/07/93</p> <p>Test ref. A</p> |  |
| <p>Chamber No. 2</p> <p>$\bar{u} = 0.565 \text{ m/s}$</p> <p>$\eta = 0.132$</p> <p>Date: 13/07/93</p> <p>Test ref. B</p> |  |
| <p>Chamber No. 2</p> <p>$\bar{u} = 0.565 \text{ m/s}$</p> <p>$\eta = 0.111$</p> <p>Date: 09/08/93</p> <p>Test ref. C</p> |  |

| | |
|--|--|
| <p>Chamber No. 2</p> <p>$\bar{u} = 0.619 \text{ m/s}$</p> <p>$\eta = 0.189$</p> <p>Date: 12/07/93</p> <p>Test ref. A</p> |  |
| <p>Chamber No. 2</p> <p>$\bar{u} = 0.619 \text{ m/s}$</p> <p>$\eta = 0.177$</p> <p>Date: 13/07/93</p> <p>Test ref. B</p> |  |
| <p>Chamber No. 2</p> <p>$\bar{u} = 0.619 \text{ m/s}$</p> <p>$\eta = 0.036$</p> <p>Date: 09/08/93</p> <p>Test ref. C</p> |  |
| <p>Chamber No. 3</p> <p>$\bar{u} = 0.176 \text{ m/s}$</p> <p>$\eta = 0.439$</p> <p>Date: 12/01/94</p> <p>Test ref. A</p> |  |



| | |
|--|--|
| <p>Chamber No. 3</p> <p>$\bar{u} = 0.212 \text{ m/s}$</p> <p>$\eta = 0.532$</p> <p>Date: 26/01/94</p> <p>Test ref. C</p> |  |
| <p>Chamber No. 3</p> <p>$\bar{u} = 0.247 \text{ m/s}$</p> <p>$\eta = 0.420$</p> <p>Date: 12/01/94</p> <p>Test ref. A</p> |  |
| <p>Chamber No. 3</p> <p>$\bar{u} = 0.247 \text{ m/s}$</p> <p>$\eta = 0.713$</p> <p>Date: 19/01/94</p> <p>Test ref. B</p> |  |
| <p>Chamber No. 3</p> <p>$\bar{u} = 0.247 \text{ m/s}$</p> <p>$\eta = 0.347$</p> <p>Date: 26/01/94</p> <p>Test ref. C</p> |  |

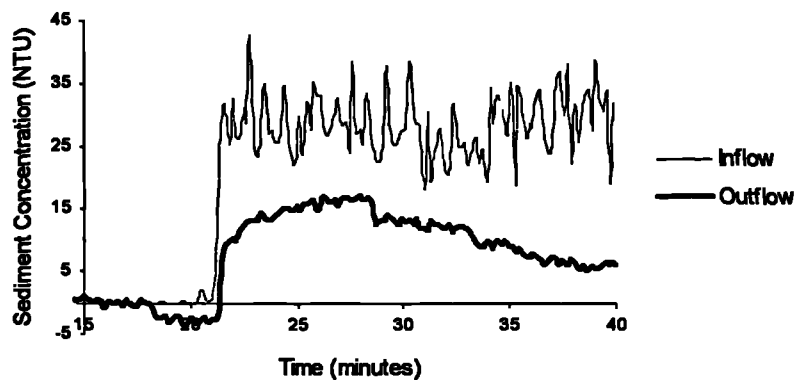
Chamber No. 3

$\bar{u} = 0.282 \text{ m/s}$

$\eta = 0.684$

Date: 19/01/94

Test ref. A



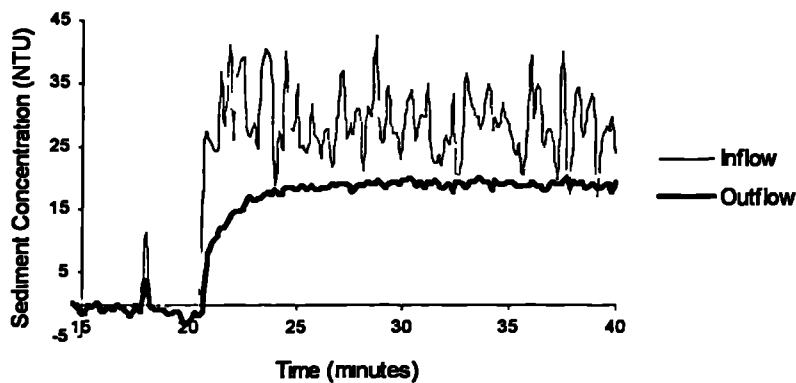
Chamber No. 3

$\bar{u} = 0.282 \text{ m/s}$

$\eta = 0.319$

Date: 20/01/94

Test ref. B



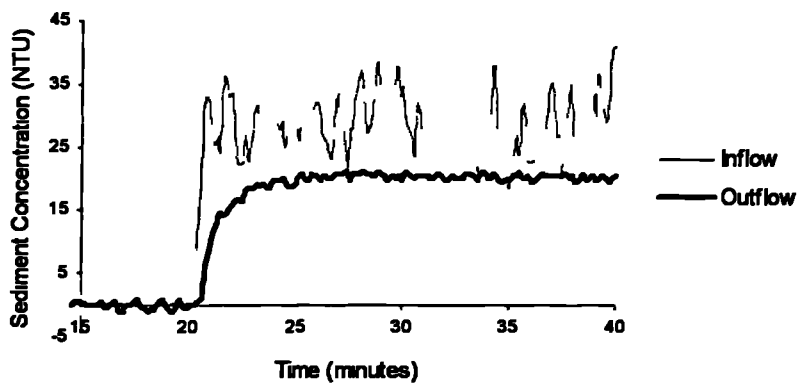
Chamber No. 3

$\bar{u} = 0.282 \text{ m/s}$

$\eta = 0.301$

Date: 26/01/94

Test ref. C



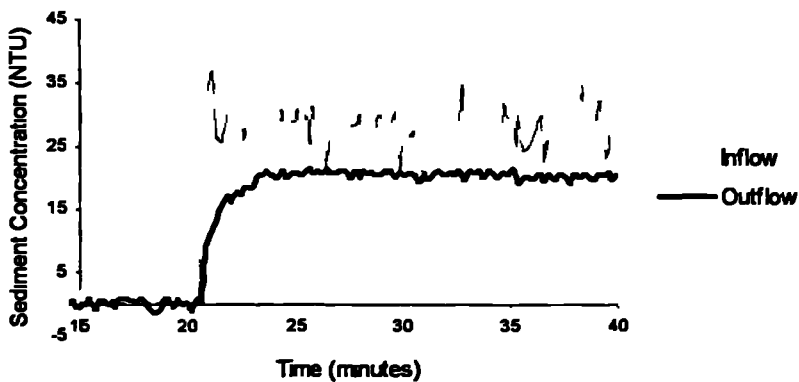
Chamber No. 3

$\bar{u} = 0.317 \text{ m/s}$

$\eta = 0.253$

Date: 12/01 94

Test ref. A



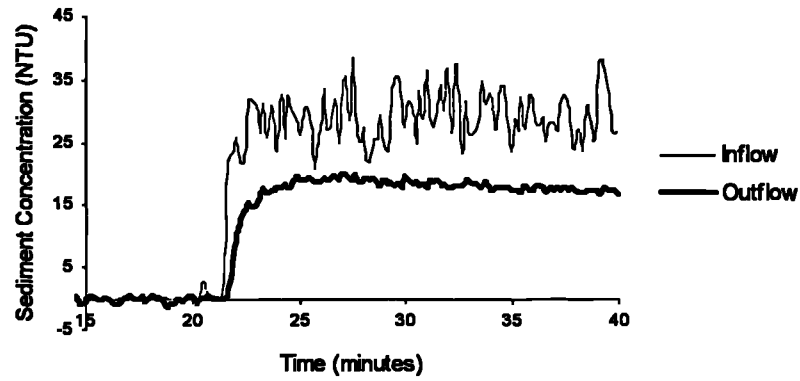
Chamber No. 3

$\bar{u} = 0.317 \text{ m/s}$

$\eta = 0.401$

Date: 19/01/94

Test ref. B



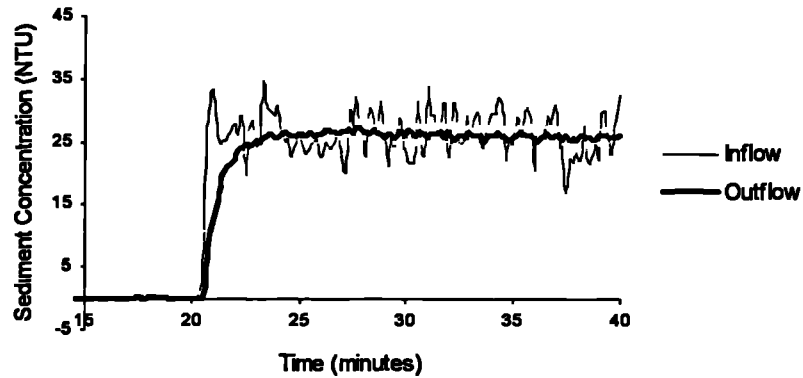
Chamber No. 3

$\bar{u} = 0.388 \text{ m/s}$

$\eta = 0.025$

Date: 11/01/94

Test ref. A



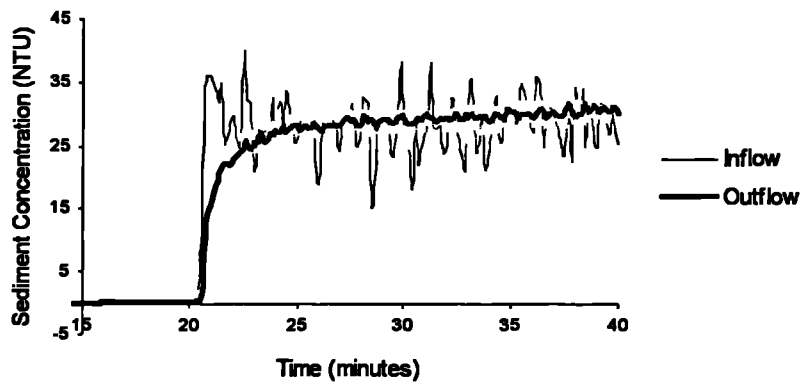
Chamber No. 3

$\bar{u} = 0.388 \text{ m/s}$

$\eta = -0.052$

Date: 20/01/94

Test ref. B



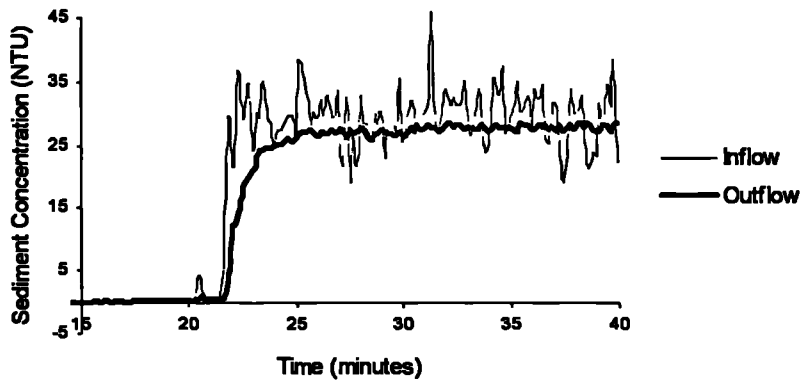
Chamber No. 3

$\bar{u} = 0.388 \text{ m/s}$

$\eta = 0.085$

Date: 26/01/94

Test ref. C



| | |
|---|--|
| <p>Chamber No. 3</p> <p>$\bar{u} = 0.459 \text{ m/s}$</p> <p>$\eta = 0.150$</p> <p>Date: 26/01/94</p> <p>Test ref. A</p> | |
| <p>Chamber No. 3</p> <p>$\bar{u} = 0.459 \text{ m/s}$</p> <p>$\eta = 0.029$</p> <p>Date: 20/01/94</p> <p>Test ref. B</p> | |
| <p>Chamber No. 3</p> <p>$\bar{u} = 0.564 \text{ m/s}$</p> <p>$\eta = -0.017$</p> <p>Date: 12/01/94</p> <p>Test ref. A</p> | |
| <p>Chamber No. 3</p> <p>$\bar{u} = 0.564 \text{ m/s}$</p> <p>$\eta = 0.068$</p> <p>Date: 20/01/94</p> <p>Test ref. B</p> | |